



JOHN ALEXANDER PEREZ SEPULVEDA

LAGRANGIAN-EULERIAN APPROXIMATION METHODS FOR
BALANCE LAWS AND HYPERBOLIC CONSERVATION LAWS

*MÉTODOS DE APROXIMAÇÃO LAGRANGEANO-EULERIANO
PARA LEIS DE BALANÇO E LEIS DE CONSERVAÇÃO
HIPERBÓLICAS*

CAMPINAS
2015



UNIVERSIDADE ESTADUAL DE CAMPINAS

Instituto de Matemática, Estatística
e Computação Científica

JOHN ALEXANDER PEREZ SEPULVEDA

LAGRANGIAN-EULERIAN APPROXIMATION METHODS FOR
BALANCE LAWS AND HYPERBOLIC CONSERVATION LAWS

MÉTODOS DE APROXIMAÇÃO LAGRANGEANO-EULERIANO
PARA LEIS DE BALANÇO E LEIS DE CONSERVAÇÃO
HIPERBÓLICAS

Thesis presented to the Institute of Mathematics, Statistics and Scientific Computing of the University of Campinas in partial fulfillment of the requirements for the degree of Doctor in applied mathematics.

Tese apresentada ao Instituto de Matemática, Estatística e Computação Científica da Universidade Estadual de Campinas como parte dos requisitos exigidos para a obtenção do título de Doutor em matemática aplicada.

Orientador: Eduardo Cardoso de Abreu

ESTE EXEMPLAR CORRESPONDE À VERSÃO FINAL DA TESE DEFENDIDA PELO ALUNO JOHN ALEXANDER PEREZ SEPULVEDA, E ORIENTADA PELO PROF. DR. EDUARDO CARDOSO DE ABREU.

Assinatura do Orientador

Eduardo Cardoso de Abreu

CAMPINAS
2015

Agência de fomento: Capes
Nº processo: 0

Ficha catalográfica
Universidade Estadual de Campinas
Biblioteca do Instituto de Matemática, Estatística e Computação Científica
Maria Fabiana Bezerra Muller - CRB 8/6162

P415L Perez Sepulveda, John Alexander, 1974-
Lagrangian-Eulerian approximation methods for balance laws and hyperbolic conservation laws / John Alexander Perez Sepulveda. – Campinas, SP : [s.n.], 2015.

Orientador: Eduardo Cardoso de Abreu.
Tese (doutorado) – Universidade Estadual de Campinas, Instituto de Matemática, Estatística e Computação Científica.

1. Equações diferenciais hiperbólicas. 2. Leis de conservação (Física). 3. Método dos volumes finitos. 4. Mecânica dos fluídos. I. Abreu, Eduardo Cardoso de, 1974-. II. Universidade Estadual de Campinas. Instituto de Matemática, Estatística e Computação Científica. III. Título.

Informações para Biblioteca Digital

Título em outro idioma: Métodos de aproximação Lagrangeano-Euleriano para leis de balanço e leis de conservação hiperbólicas

Palavras-chave em inglês:

Hyperbolic differential equations

Conservation laws (Physics)

Finite volume method

Fluid mechanics

Área de concentração: Matemática Aplicada

Titulação: Doutor em Matemática Aplicada

Banca examinadora:

Eduardo Cardoso de Abreu [Orientador]

Luis Felipe Feres Pereira

Sandra Mara Cardoso Malta

Fábio Antonio Dorini

Lucas Catão de Freitas Ferreira

Data de defesa: 21-07-2015

Programa de Pós-Graduação: Matemática Aplicada

Tese de Doutorado defendida em 21 de julho de 2015 e aprovada

Pela Banca Examinadora composta pelos Profs. Drs.

Eduardo Cardoso de Abreu

Prof(a). Dr(a). EDUARDO CARDOSO DE ABREU

Luis Felipe Feres Pereira

Prof(a). Dr(a). LUIS FELIPE FERES PEREIRA

Sandra Mara Cardoso Malta

Prof(a). Dr(a). SANDRA MARA CARDOSO MALTA

Fábio Antonio Dorini

Prof(a). Dr(a). FÁBIO ANTONIO DORINI

Lucas Catão de Freitas Ferreira

Prof(a). Dr(a). LUCAS CATÃO DE FREITAS FERREIRA

“To my wife Monica, and my sons Camila and Tomás, because all is very easy when we are together”

Acknowledgement

Foremost, I want to thank God.

I would like to express my sincere gratitude to my wife Monica, and my sons Camila and Tomás for their love and for helping me survive all the stress from these four years and not letting me give up. I would also like to thank my advisor Dr. Eduardo Abreu for his understanding, wisdom, assistance and suggestions throughout my project. To my institution, ITM-Instituto Metropolitano because gave me the space and the time to study. To the Institute of Mathematics, Statistics and Scientific Computing (IMECC) - Graduate Program in Applied Mathematics - for providing me the opportunity to be a student of this prestigious institution. To my evaluating committee, Dr. Felipe Pereira, Dra. Sandra Malta, Dr. Favio Dorini and Dr. Lucas Ferreira for their valuable suggestions. To the discussion group, Abel, Arthur, Paola, Juan, Jardel, Ciro and other that they passed by the seminary, because always their observations they brought a light. I would like to thanks Arthur, Paola and Ciro that they help me with English. And finally, I want to give a sincere gratitude to the institutions that they helped to get the aim. I give my thank to CAPES for the graduate fellowship (2011-2015). In addition, I also give my thank to the financial support FAPESP through grants No. 2011/11897-6 and No. 2014/03204-9 and CNPq through grants No. MCTI/CNPQ/Universal No 445758/2014-7.

Resumo

Neste trabalho, estudamos um volume finito de controle no espaço-tempo local, em um marco Lagrangiano-Euleriano com o objetivo de construir um esquema localmente conservativo que modele o delicado balanço não-linear entre as aproximações numéricas do fluxo hiperbólico e o termo fonte, em problemas de lei de balanço ligados ao caráter puramente hiperbólico da lei de conservação. Efetuamos a análise de estabilidade e de convergência do método para o caso linear da lei de conservação hiperbólica e de problemas de lei de balanço em espaços discretos convenientes. De fato, baseados nesta condição de estabilidade, nós substituímos a equação da lei de conservação escalar dada por uma aproximação de diferenças finitas que dependente dos parâmetros da malha, no espaço e no tempo, a fim construir uma sequência convergente para a única solução entrópica da lei de conservação escalar, pelo menos, para o caso em que a função de fluxo é do tipo convexo. Para o melhor de nosso conhecimento, este trabalho é o primeiro a estabelecer uma prova rigorosa para convergência para da única solução entrópica construída por tubos integrais em um procedimento Lagrangiano-Euleriano, para leis de conservação hiperbólicas em uma dimensão espacial com fluxo convexo. Ressaltamos a importância e a utilidade de identificar equações modificadas, no escopo das diferenças finitas, associada ao método Lagrangiano-Euleriano o qual usamos para dar uma explicação sobre a possibilidade de instabilidade na construção dos tubos integrais longos; tal construção tem sido chamado a atenção de muitos autores na literatura disponível. O esquema construído é livre de Riemann solvers, mas se soluções locais de Riemann estão disponíveis para um determinado problema, estes podem ser incorporados naturalmente no esquema. Um grande conjunto não-trivial, distinto e bem conhecido de experimentos numéricos tanto para problemas unidimensionais, como para problemas bidimensionais não-lineares estão disponíveis na literatura especializada, que inclui leis de conservação escalares hiperbólicas e sistemas escalares de leis de conservação hiperbólicas e de leis de balanço, são discutidos para ilustrar o desempenho do novo método, onde incluímos experimentos numéricos com fluxos convexo, não-convexo e funções de fluxo descontínuos. Os resultados numéricos são comparados com soluções exatas sempre que possível ou soluções aproximadas com malha fina em outros casos.

Palavras-chave: Enfoque Lagrangiano-Euleriano, Volume Finito, Leis de balanço, Leis de conservação hiperbólicas, Mecânica dos fluidos, Problemas de fluxo em meios porosos.

Abstract

In this work, we study a local space-time finite control volume in a Lagrangian-Eulerian framework in order to design a locally conservative scheme to account the delicate nonlinear balance between the numerical approximations of the hyperbolic flux and the source term for balance law problems linked to the purely hyperbolic character of conservation laws. We have performed stability and convergence analysis of the method for linear differential hyperbolic and balance law problems in convenient discrete spaces. Indeed, based on this stability condition, we replace the given scalar conservation law equation by a finite difference approximation depending on mesh parameters in space and in time in order to construct a sequence that is convergent to the unique entropy solution to the scalar conservation law, at least for the case where flux function is of convex type. To the best of our knowledge, this work is the first to establish a rigorous convergence proof for the uniqueness of the entropy solution constructed integral tubes by a Lagrangian-Eulerian procedure for hyperbolic conservation laws in one-space dimension with convex flux. We also add some meaningful comments on the usefulness of identifying modified equations, which models the behavior of the analogue difference scheme associated to the Lagrangian-Eulerian method and use it to give a possible explanation on the possibility of instability in construction of long integral tubes; such construction has been called the attention of many authors in the available literature. The designed scheme is also free of Riemann solvers, but if local Riemann solutions are available for a particular problem it is natural to incorporate such feature into the scheme. Furthermore, by combining ideas of the new approach, we give a formal construction of a new algorithm for solving several nonlinear hyperbolic conservation laws in two space dimensions. A set of nontrivial and distinct well-known one-dimensional as well as two-dimensional numerical experiments for nonlinear problems available in the specialized literature - scalar and system - of hyperbolic conservation law and balance law types are discussed to illustrate the performance of the new method, including numerical experiments with convex, non-convex and discontinuous flux functions. The numerical results are compared with accurate approximate solutions or exact solutions whenever possible.

Keywords: Lagrangian-Eulerian approach, Finite volume, Balance laws, Hyperbolic conservation laws, fluid mechanics, porous media flow problems

Contents

Dedicatória	5
Acknowledgement	6
1 Introduction	11
1.1 Motivation and significance of the research work	11
1.2 Aims and objectives	15
1.3 Preliminary results and ongoing work	16
1.4 Organization of the thesis	18
2 The revisited Lagrangian-Eulerian scheme for linear hyperbolic conservation laws	19
2.1 Formal construction: statement of the Lagrangian-Eulerian formulation and notations	19
2.1.1 The local Lagrangian-Eulerian conservation relation	20
2.1.2 The Lagrangian-Eulerian scheme for linear hyperbolic conservation laws and its mathematical properties	22
2.2 A multiple time-step formulation for the Lagrangian-Eulerian scheme	29
3 The conservative finite difference Lagrangian-Eulerian scheme for nonlinear scalar conservation laws	33
3.1 Preliminary concepts	33
3.2 On the construction of a unique entropy solution based on the Lagrangian-Eulerian scheme for convex scalar conservation law	38
3.3 The finite difference Lagrangian-Eulerian scheme in conservative form	48
3.4 Numerical experiments for hyperbolic problems with convex and nonconvex fluxes	49
3.5 Numerical experiments with discontinuous flux functions, model problems Adimurthi, J. Jaffré and V. Gowda §3.5.1 and R. Burger, K. H. Karlsen and J. D. Towers §3.5.2	51
4 The Lagrangian-Eulerian approach to nonlinear hyperbolic conservation laws	59
4.1 The Lagrangian-Eulerian scheme in conservative form	59
4.2 A Lipschitz condition to the Lagrangian-Eulerian numerical flux function	61
4.3 Monotonicity and TVD properties for the Lagrangian-Eulerian scheme	64
4.4 Equivalence between finite difference and finite volume Lagrangian-Eulerian formulations	65
4.5 Numerical experiments for hyperbolic problems with convex and non-convex fluxes	66

5	The Lagrangian-Eulerian scheme for hyperbolic balance laws	70
5.1	Linear case for balance laws	71
5.1.1	Midpoint rule	74
5.1.2	The trapezoidal rule	76
5.1.3	Stability and convergence for Lagrangian-Eulerian scheme for linear balance laws	76
5.2	Nonlinear balance law	78
5.2.1	Predictor-corrector method	80
5.2.2	Midpoint method	81
5.2.3	Trapezoidal method	81
5.3	Stability of the Lagrangian Eulerian scheme to nonlinear balance law	82
5.3.1	Predictor corrector approximation	83
5.3.2	An approximation of the source term by the Midpoint quadrature rule	84
5.3.3	An approximation of the source term by the Trapezoidal quadrature rule	84
5.4	Numerical experiments for nonlinear scalar balance laws	85
6	The Lagrangian-Eulerian scheme for systems of hyperbolic conservation laws and balance laws	98
6.1	Extension to systems of hyperbolic conservation laws and balance laws	98
6.2	Numerical experiments for systems of nonlinear balance laws	101
6.3	Numerical experiments for systems of nonlinear hyperbolic conservation laws	107
7	The extension of the Lagrangian-Eulerian scheme for hyperbolic conservation laws in two-space dimensions	112
7.1	The Lagrangian-Eulerian relation for hyperbolic conservation laws linked to balance laws	115
7.1.1	The locally conservative Lagrangian-Eulerian relation for scalar multidimensional hyperbolic conservation laws linked to one-dimensional system of balance laws	120
7.2	Numerical experiments for nonlinear hyperbolic law em 2D	125
8	Concluding remarks and perspectives for the future	160
8.1	Concluding remarks	161
8.2	Perspectives for future work	163
8.3	Final Considerations	163
	Bibliography	165
A	Uniqueness of the Entropy Solution	177
B	Licença	184
B.1	Sobre a licença dessa obra	184

Chapter 1

Introduction

In this work we explore a locally conservative and divergence space-time finite control volume in a Lagrangian-Eulerian framework (see [50, 52, 57, 121, 137]), first developed in the context of purely hyperbolic conservation laws, in order to design a locally conservative scheme to account the balance between numerical approximations of the hyperbolic flux function and the source term linked to steady solutions. Our new Lagrangian-Eulerian scheme is aimed to be not dependent on a particular structure of the source term. The designed scheme is Riemann solver-free for the resolution of (local) Riemann problems, but, if Riemann solutions are available for a particular problem it is somewhat natural to incorporate such information into the procedure and thus yielding flexibility to the development of distinct numerical strategies upon the specific model under consideration. Indeed, the flexibility of our Lagrangian-Eulerian scheme allows its extension for constructing balance laws systems solution approximations, hyperbolic laws systems solution approximations and multidimensional hyperbolic conservation laws solution approximations.

A set of representative numerical experiments for nonlinear balance law (scalar and systems in one-space dimensions, hyperbolic conservation laws, scalar and systems in one-space dimensions and scalar problems in two-space dimensions) are presented in order to illustrate the method's performance. The numerical results are compared with accurate approximate solutions or exact solutions whenever possible.

1.1 Motivation and significance of the research work

We are interested in numerically solving balance law problems linked to the homogeneous purely hyperbolic conservation law counterpart. In this work, we aim to present a Lagrangian-Eulerian scheme in a cell-centered framework devoted to this task. This scheme consists on one more tentative to deal with the difficult issue of the well-balancing between the computation of the numerical flux function and the source term by means of a natural *unbiased* upwind approach, which in turn is Riemann-solver-free and it seems to be able to handle nonlinear scalar and system problems.

A variety of efficient numerical schemes for hyperbolic systems of conservation laws has been developed in the recent past for different problem settings. These schemes evolved following the natural understanding of fundamental concepts from the theory of nonlinear hyperbolic conservation laws concerning the characteristic surfaces properties, existence, uniqueness, and solution of the Riemann problem; see, e.g., Dafermos [43], LeFloch [107], Bressan [27] and

Liu [38, 117, 118] and many others [40, 60, 65, 67, 82, 83, 102, 103, 109, 127, 128, 139]. In addition, for a scalar balance law, the solution strongly depend on certain properties of the source term (see [27, 38, 43, 67, 107, 117, 118]). For example, when the source term is a non-increasing function, the total variation of the exact solution of the scalar balance law is also a non-increasing function, as in the homogeneous case (see, e.g., [67, 43]). In general, however, the source term might not be decreasing (see [36, 45, 115, 130]) and some semi-implicit and fully implicit scheme are not applicable, at least in a straightforward manner [36, 45]. Additionally, it is possible to design well-balanced schemes which are also asymptotically consistent for a particular system of parabolic equations (e.g., diffusive-dispersive character) [67, 68], but the resulting scheme is stable under a very restrictive parabolic-like CFL condition $\Delta t < \mathcal{C}(\Delta x)^2$. For instance, the width of the shock layer, in light of a parabolic equation in the spirit of convection-diffusion transport problems of the form, $u = u(x, t)$, $u_t + f_x(u) = (\epsilon u_x)_x$, $\epsilon > 0$, is $O(\epsilon)$ (see [90, 92]). Using a splitting fractional time step Δt for such equations the width of the numerical shock layer will be $O(\sqrt{\Delta t \epsilon})$ because the nonlinear self-sharpening mechanisms of the fractional flow function $f(u)$ is thrown away by the unphysical entropy loss due to Oleinik's convexification [127, 128] introduced in the convective step by the hyperbolic scheme for $u_t + f_x(u) = 0$. Thus, in order to not overestimate the shock layer (the nonlinear balance between purely hyperbolic/parabolic terms), the splitting step should not be (significantly) larger than ϵ [90, 92]. Indeed, in constructing Riemann solutions (approximate Riemann solvers), Liu [116] introduced a shock wave admissibility criterion that encompasses both the Lax criterion (see [43, 105]) and the Oleinik criterion [127, 128]. It is well known that the Liu criterion is not general. If one wants to construct approximate solutions of a conservation/balance laws, then, such solutions must respect the continuous counterparts as well as its properties. For instance, the only fully satisfactory admissibility criterion for the shock waves occurring in convection-diffusion immiscible three-phase flow transport problems is the viscous (parabolic) profile criterion introduced by Gel'fand [60]; see also Courant and Friedrichs [40]. Furthermore, the solution of Riemann problems is greatly facilitated by using so-called Riemann invariants [43, 139]. However, such invariants are guaranteed to exist only for strictly hyperbolic systems of no more than two equations (see e.g., [43, 139]). Indeed, the presence of an umbilical point or an elliptic region almost always prohibits the existence of Riemann invariants. This fact is at the root of the complexity of construction of exact and approximate solutions when strict hyperbolicity fails (see, e.g., [1, 2, 15, 24, 25, 31, 82, 83, 84, 102, 103, 113] and references therein). From the view point of the design of constructive algorithms, there seems to be some evidence of why some numerical formulations are not well suited in order to capture the correct qualitative approximate solutions. For instance, in [98] the authors showed that a semi-discrete central scheme may fail to converge to the unique entropy solution of a non-convex conservation law. On the other hand, the use of the finite element method for the numerical solution of hyperbolic, or "nearly hyperbolic" problems and other strongly non-self-adjoint PDE problems is, generally speaking, not satisfactory. These problems do not arise naturally in a variational setting, namely, they do not arise naturally from minimization of an energy norm in L^2 -spaces. It is worth mentioning that finite element methods for hyperbolic problems such as the discontinuous Galerkin finite element method are based on semi-discrete approximations along with assumptions of (local) variable separation in order to write the appropriate basis functions in the space variable. Moreover, solutions for nonlinear hyperbolic conservation laws admits discontinuities (shocks) in L^1 [28, 73, 85]; see also [91, 93]. Tveito and Winther [151] provide numerical examples where methods based on 2×2 Riemann solvers may fail since

the entropy non-classical solution of non-strictly hyperbolic conservation laws is quite difficult to compute (see also [1, 2]). Splitting strategies to the case of balance law problems of the form $u = u(x, t)$, $u_t + f_x(u) = \epsilon^{-1}g(u)$, $\epsilon > 0$, typically rely on composition of exact and approximate solutions to the purely hyperbolic part (Riemann solutions) $u_t + f_x(u) = 0$ and steady (well-balanced) solutions to $u_t = \epsilon^{-1}g(u)$, see, e.g., [32, 58, 65, 67, 68, 106, 115, 131, 148].

We notice that Karlsen and Towers [94] gave a convergence proof for the Lax-Friedrichs finite difference scheme for non-convex genuinely nonlinear scalar conservation laws of the form $u_t + f(u, k(x, t))_x = 0$, $u = u(x, t)$, where the coefficient $k(x, t)$ is allowed to be discontinuous along curves in the (x, t) -plane. These authors also proved stability, and uniqueness, for an extended Kruzhkov entropy solution, provided that the flux function satisfies a so-called crossing condition, and that strong traces of the solution exist along the curves where $k(x, t)$ is discontinuous. In this direction, they were able to show that a convergent subsequence of approximations produced by the Lax-Friedrichs scheme to the above equation converges to such an entropy solution [94]. On the other hand, the celebrated central scheme introduced by Nessyahu and Tadmor [124] is also based on the classical Lax-Friedrichs scheme in a staggered grid. Nessyahu and Tadmor proved that the resulting scalar scheme, under a CFL requirement, satisfies both the Total Variation Diminishing property and a local cell entropy inequality, in order to get convergence to the unique entropy solution, at least in the genuinely nonlinear scalar case. Indeed, in [93] was proposed a Kruzhkov-type entropy condition for scalar nonlinear degenerate parabolic equations with discontinuous coefficients $u_t + f(\gamma(x), u)_x = A(u)_{xx}$. They establish L^1 stability, and thus uniqueness, for weak solutions satisfying the entropy condition, provided that the flux function satisfies a so-called “crossing condition” and the solution satisfies a technical condition regarding the existence of traces at the jump points in the coefficients. Furthermore, [91] analyzed a class of semi-discrete monotone difference schemes for scalar degenerate convection-diffusion equations in one spatial dimension of the form $u_t + f(u)_x = [A(u)]_{xx}$. These nonlinear equations are well-posed within a class of (discontinuous) entropy solutions. Moreover, it was proved [91] that the L^1 error between the approximate solutions and the unique entropy solution is $\mathcal{O}(\Delta x^{1/3})$, where Δx denotes the spatial discretization parameter; see also [26, 89, 101] for more details. These works are related to the priori (L^1, L^∞, BV) estimates discussed in [78, 153]. Therefore, supported on these previous arguments, we developed our scheme based on a Eulerian central scheme finite volume formulation, but in a space-time Lagrangian-Eulerian framework.

Additionally, in a splitting approach for balanced laws the most standard way is to treat the associated purely hyperbolic conservation law with a locally conservative finite volume scheme, and then the related system of ODE associated to the purely source term with a robust solver as such as Runge-Kutta or predictor-corrector procedures. These algorithms employed a splitting technique by means of first integrating the purely hyperbolic terms of balance conservation law [27, 38, 43, 102, 103, 107, 117, 118] (see also [32, 58, 67]) and then integrating the appropriate ODE for the source term in an intermediate step (see [45, 111]). Of course, the overall accuracy of the full approach rely on the mathematical properties for each one of these sub-steps. Indeed, first-order splittings and Strang splittings lead to global schemes that are neither well-balanced nor asymptotically consistent because the local balance linked between the numerical hyperbolic flux and the numerical source only occurs through the initial condition of each sub-step [30, 45, 67, 87, 160]. It is worth mentioning that the high-order splitting scheme proposed in [131] is asymptotically consistent with the stiff limit and can also reach high order of accuracy in the stiff limit, but it is not uniformly accurate

in the whole possible range of the stiffness parameter. On the other hand, recently developed Runge-Kutta schemes overcome these difficulties, providing basically the same advantages of the splitting schemes, without some of the drawback of the order restriction (see [32, 45, 58, 67]). The development of efficient numerical schemes for such systems is challenging, since in many applications the relaxation time varies from values of order one to very small values if compared to the time scale determined by the characteristic speeds of the system. In this second case the hyperbolic system with relaxation is said to be stiff and typically its solutions are well approximated by solutions of a suitable reduced set of conservation laws called equilibrium system (see [38, 102, 103, 117, 118]). Usually it is extremely difficult, if not impossible, to split the problem in separate regimes and to use different solvers in the stiff and non stiff regions. Thus one has to use the original relaxation system in the whole computational domain. The construction of schemes that work for all ranges of the relaxation time, using coarse grids that do not resolve the small relaxation time, has been studied mainly in the context of upwind methods using a method of lines approach combined with suitable operator splitting techniques [30] and more recently in the context of central schemes [130, 115].

Non-splitting methods (or unsplitting schemes), however, have some advantages and are sometimes preferred. Nevertheless, when a time-dependent PDE involves terms that need a different numerical treatment, it is natural to employ alternative discrete strategies for each one of them. An example of this kind of situation is provided by PDEs of convection-diffusion type. Another one is the case of balance law problems.

Many other approaches to solve balance laws by means of constructive numerical algorithms have been proposed up to date, but with no general framework (see, e.g., [27, 38, 43, 65, 67, 102, 103, 106, 107, 117, 118, 148]) since it is a very hard problem. For some other approach, we have, based on *generalized Riemann problems* [65, 106, 148], semidiscrete methods discontinuous Galerkin [119] and semidiscrete central-upwind schemes [97]. However, these methods are not robust enough in general to deal with stiff source terms. Indeed, it has been shown [97, 98] (see also [94]) that using semi-discrete central-upwind schemes may fail to converge to the unique entropy solution of non-convex purely hyperbolic conservation laws, and thus may fail to recover the Kruzhkov solution (see, e.g., [38, 43, 65, 117, 118]) or the convergence may be so slow that achieving a proper accuracy would require the use of impractically fine meshes [94, 97, 98]. Other semidiscrete-like recent results on the development of high order methods for balance law problems can be found in [23, 45, 67, 111, 131, 160] such as IMEX Runge-Kutta schemes and IMEX schemes up to order 3 that are strong-stability-preserving (see, e.g, [69, 131]).

On the other hand, in [19, 50, 52, 57, 80, 121, 137, 154] the authors present distinct Lagrangian-Eulerian formulations to the case of linear [18, 17, 80] and nonlinear [17, 19, 49, 51, 56, 57, 154] transport flow problems; to the purely linear transport problem the space-time integral curves coincide with characteristic equations [19, 80] (see also [27]). Such Lagrangian-Eulerian approach provides a very accurate solution to purely advection problems, virtually free of numerical diffusion. These schemes are derived from the divergence forms of the equations. It is the use of the divergence form of a parabolic equation that allows relatively easy localization of desired conservation principles in a form amenable to the application of finite element or finite volume approaches in a locally conservative fashion. Essentially, this formulation evolves from the efforts to develop fast, accurate, and stable versions of *Modified Method of Characteristics* (see [19, 49, 51, 56, 57] and also [19, 80, 154] and references therein) to numerical methods for transport-dominated diffusive systems, with the primary objective of incorporating changes in these procedures to obtain the preservation of desired conservation principles. Here we want to

follow such idea for balance laws cases. Instead of consider the balance laws in non-divergence form (see, e.g., [34, 58, 107, 129]) and make use of the characteristics associated with the first-order purely hyperbolic transport part of the system in a fractional step procedure that splits the transport from the source part of the balance law system, the authors, in [57] (see also [18, 17, 52, 53, 81, 121, 137]), identified the region in space-time domains where the mass flux for two-phase flow problems takes place, working with a nonlinear advection equation in integral form. This point of view produces a new class of numerical methods that locally conserve the mass, and are very competitive computationally. In contrast, the Lagrangian-Eulerian method discussed here relates the divergence form (locally conservative) with the full balance equation. It is the use of the divergence form that allows the localization of the transport so that the desired conservation property can also be localized. This means that the conservative paths is treated by a characteristic tracing algorithm from a fixed Eulerian space-time control volume over each time step for evolution. In connection to [33, 44], the choice of the paths family is important because it determines the speed of propagation of discontinuities. Although it should be based on the physical aspects of the problem, it is natural from the mathematical point of view, to require this family to satisfy some hypotheses concerning the relationship of the paths with the integral curves of the characteristic fields, but with no requirement of exact or approximate solutions of (local) Riemann problems. Our approach is also distinct from Lagrangian-Eulerian hydrodynamics methods [120] since we do not use any Riemann solutions for the computation of the numerical fluxes at interfaces, but they both share similar ideas such as cell-centered moving mesh control volumes (see, e.g., [120]).

1.2 Aims and objectives

This thesis focus in developing a numerical method, which is based in the work of Jim Douglas Jr, Felipe Pereira et al. [52, 57, 121, 137]. Our aim is to construct a numerical method to hyperbolic conservation laws in two dimensional variables. In the spirit of above works, we get a way to reach our aim,

- We use the ideas of Douglas Jr, Felipe Pereira et al. in [52, 57, 121, 137] to construct a numerical scheme in finite difference form to solve linear conservation law and utilize the finite difference theory to prove consistence, stability and convergence of this scheme by using the Lax theorem.
- We use the theory of finite difference, and the fundamental concepts in [57, 121, 137], of the locally conservative and divergence space-time finite control volume, in a Lagrangian-Eulerian framework, to extend the numerical scheme constructed in the item above to linear balance laws.
- We define, using the finite difference theory, the CFL-condition and the stability interval in the linear case which will be extended to our Lagrangian-Eulerian scheme to solve nonlinear conservation law and will allow the use of the Harten theory in [76, 75], the Smoller theory in [138, 139] and the Majda and Crandall theory in [42] to prove the convergence to entropic solution of the nonlinear hyperbolic law of the approximate solutions of our Lagrangian-Eulerian scheme, at least when flux is convex. In chapter 16 of the Smoller book [138, 139] it was proved the convergence to the entropic solution for the Lax-Friedrichs finite difference scheme. The first version of this convergence proof appear

in 1983 (see [138]), for the finite difference scheme of Lax-Friedrichs. We use this same approach to prove that our Lagrangian-Eulerian scheme converges to the entropic solution. There are other mathematically different approaches to the existence problem for a scalar conservation law, along with its pertinent stringent requirements [138, 139]. We have decided to give a proof via the finite differences approach for several reasons. For instance, the other methods require several more restrictive hypothesis and a more theoretical treatment than we would like to treat, namely, finite difference, or finite volume, methods are more capable of being generalized to the case of systems of conservation laws. Indeed, the convergence proof proposed by Smoller [138] will be used here to give a comprehensive presentation of the key issues embedded in the seminal works of Harten [75, 76] as well as the theory Majda and Crandall [42] to prove the convergence to entropic solution of the nonlinear hyperbolic problems.

- We extend the numerical scheme to solve hyperbolic linear conservation laws and the finite control volume of [57, 121, 137], which in turn now describes a balance law into a nonlinear balance law, in the same way we work in the linear case. In principle the source term can be treated as in the linear case, but the integral over the control volume will be approximated with some basic quadrature rules as such: midpoint rule, trapezoidal rule and predictor-corrector.
- We extend the Lagrangian-Eulerian scheme for each equation of the scalar balance law system and scalar hyperbolic law system, we use one finite control volume to each equation, which represent the conservation law or the balance law in the corresponding case. In this approach, we use our Lagrangian-Eulerian scheme, for balance law (or conservation law) in each equation and then we solve each equation explicitly with Δt time step. At this point it is very important to highlight that we are not using a splitting technique, our scheme is a explicit method and it refreshes every variable in each time step Δt .
- Finally, we consider the hyperbolic conservation law

$$\frac{\partial u}{\partial t} + \frac{\partial f(u)}{\partial x} + \frac{\partial g(u)}{\partial y} = 0,$$

which we write in the convenient form of balance law system,

$$\begin{cases} \frac{\partial u}{\partial t} + \frac{\partial f(u)}{\partial x} = -\frac{\partial g(u)}{\partial y}, \\ \frac{\partial u}{\partial t} + \frac{\partial g(u)}{\partial y} = -\frac{\partial f(u)}{\partial x}. \end{cases}$$

Here, we consider one finite control volume for each equation with $\Delta t/2$, where Δt is defined by the CFL-condition. Then we solve each balance law sequentially in each dimensional direction, x and y or y and x , using the Lagrangian-Eulerian scheme to solve hyperbolic balance law.

1.3 Preliminary results and ongoing work

Although some mathematical formalism in the construction of Lagrangian-Eulerian methods for hyperbolic problems can be found in [18, 17, 19, 49, 51, 52, 56, 57, 80, 154], no results in

the sense of Lax equivalence theorem in ℓ^2 -spaces consistency, stability and convergence for linear problems was discussed in these works. Such a discussion is presented here for the linear hyperbolic case, which is further extended to the case of linear balance laws. Furthermore, as opposed in [20, 21, 22, 80], our Lagrangian-Eulerian framework are explicit schemes designed on a fixed Eulerian grid (staggered mesh grid to use a conservative cell-centered discretization) along with a (CFL) time step stability restriction (it is possible to derive semi-implicit schemes naturally from the proposed formulation but this will not be discussed here). Indeed, we do not make use of any high-order reconstruction in the time and the space discretization or splitting of the differential equation (see [20, 21, 22, 32, 58, 80]). This class of method follows the ELLAM-formalism “Eulerian-Lagrangian Localized Adjoint Method” (see e.g., [35, 134]) as the original Modified Method of Characteristics (MMOC) does [50], to discretize the time along the characteristic curves associated to the hyperbolic term of the advection diffusion equation. It is worth mentioning that ELLAM schemes are locally (and global) mass balance conservative, although extension to nonlinear equations is not easily straightforward. For a comprehensive review of this approach see papers [20, 21, 22, 35, 80, 134]. As indicated, it was first done a formal approach for the numerical analysis of the new method in the linear case via an interpretation (or somewhat reinterpretation) of the scheme discussed for a parabolic modified equation [52] of the new method in a finite difference approximation spaces via Fourier ℓ^p -space (see [62, 109, 142]), although it is possible to show that the resulting method satisfies a conservative version where the numerical flux function is consistent with the flux function of the hyperbolic equation and it also satisfies a Lipschitz continuity condition. Furthermore, it was possible to obtain a modified equation associated to the method which is useful to perform an analysis of the dissipation - dispersion relation of the announced method. Indeed, a simple geometric interpretation of the method was also made to understand the effect of numerical dissipation at each time step.

Some preliminary results were shown in the following scientific events:

- Lagrangian Approximation Schemes for Balance Laws (Apresentação de Trabalho). In: VII Encontro Nacional de Matemática e Aplicações (VII ENAMA), 2013, Rio de Janeiro. see [9, 12].
- Design of a well balanced Lagrangian approximation scheme for balance laws (Apresentação de Trabalho). In: 29^o Colóquio Brasileiro de Matemática IMPA, Rio de Janeiro, 21 de julho a 02 de agosto de 2013. see [8, 12].
- A Lagrangian-Eulerian algorithm scheme for Hyperbolic Conservation Laws and Balance Laws (Apresentação de Trabalho). In: HYP2014- XV International Conference on Hyperbolic Problems, 2014, Rio de Janeiro, see [11, 6, 12].
- A new locally Conservative Lagrangian Eulerian method for hyperbolic and Balance laws (Apresentação de Trabalho). In: VIII Pan-American Workshop Applied and Computational Mathematics, 2014, Barranquilla-Colombia, see [13, 12].
- Design, analysis, and implementation of a Lagrangian-Eulerian approximation scheme for hyperbolic conservation laws and balance laws (Apresentação de Trabalho), International Congress of Mathematicians, August 13 - 21, 2014 Coex , Seoul , Korea. 2014, see [7, 12].
- A Lagrangian-Eulerian algorithm for solving hyperbolic problems and balance laws / Um método Lagrangiano-Euleriano para aproximação de leis de balanço e de leis de

conservação hiperbólica (Apresentação de Trabalho/Congresso); I Brazilian Congress of Young Researchers in Pure and Applied Mathematics (10-12, December 2014); IME/USP. 2014, see [10, 12].

- A Lagrangian-Eulerian algorithm for solving hyperbolic conservation laws with applications, 6th International Conference on Approximation Methods and Numerical Modelling in Environment and Natural Resources. Pau, France 2015. Editorial Universidad de Granada (2015) 600-617 [5, 12]

1.4 Organization of the thesis

We introduced and discussed a motivation, along with the significance of the current research work. The rest of the thesis is organized as follows. In chapter 2 we will discuss the Lagrangian-Eulerian scheme for hyperbolic conservation laws. In particular, we will present some properties of the Lagrangian-Eulerian scheme for linear hyperbolic conservation laws, namely, consistency, stability and convergence by means of the Lax equivalence theorem. Moreover, we will also derive the associated modified equation for the Lagrangian-Eulerian scheme and describe the dispersive-dissipative relation to explain the one-dimensional numerical experiments results. We will be able to write the Lagrangian-Eulerian scheme in conservative form for nonlinear hyperbolic conservation laws, this is explained in chapter 3 and in chapter 4. In chapter 3 we will include the Lagrangian-Eulerian scheme written in finite difference form, the proof of convergence for entropic solution in sense of Smoller and the proof in the sense of Harten, Crandall and Majda, while in chapter 4 we will include the Lagrangian-eulerian scheme that arises of the direct construction proposal in [57, 121, 137]. The numerical fluxes in both methods are consistent with the hyperbolic equation and satisfy a Lipschitz continuity condition. Furthermore, numerical experiments for hyperbolic conservation laws with convex and non-convex flux functions will be performed in order to illustrate the qualities of the new scheme. In chapter 5 we will discuss the Lagrangian-Eulerian scheme for hyperbolic balance laws. In particular, we will also discuss stability and convergence properties for the Lagrangian-Eulerian scheme for linear balance laws. Moreover in chapter 6, we will perform and discuss some numerical experiments for nonlinear scalar balance laws and nonlinear systems of balance laws. Finally, in chapter 7 we will discuss the extension of the Lagrangian-Eulerian scheme for systems of balance laws in one-space dimension for hyperbolic conservation laws in two-space dimensions, along with numerical experiments. As an attempt to make our Eulerian-Lagrangian scheme attractive for the user we decided to implement the full algorithm in the Matlab language programming.

Also, it is easy to understand for engineers and users from industry with maybe less training in programming. Of course, we naturally expect the Eulerian-Lagrangian code to be considerable slower when programmed in Matlab than the analogue codes in C, C++ or Fortran.

Thus, the purpose of this work is to provide another approach to tackle the above mentioned class of differential equations. In addition, we do not use any special nonlinear reconstruction ([20, 21, 22, 32, 39, 58, 69, 80, 98, 124]) since our main objective is to show a Lagrangian-Eulerian based on previous works [19, 27, 57, 80, 154] in a simple setting description. This will be further addressed in the future. Indeed, several examples for scalar conservation laws with *convex* and *non-convex* flux functions are discussed to illustrate the viability of the method. We also perform numerical experiments for representative systems of balance law available in the literature.

Chapter 2

The revisited Lagrangian-Eulerian scheme for linear hyperbolic conservation laws

In this section we will define an equivalent finite difference of an Lagrangian-Eulerian approach based on locally conservative finite volume method and to the hyperbolic linear constant-coefficient case we will indeed prove its consistency, stability and convergence in the sense of classical Lax stability (see e.g., [62, 109, 142]). This analysis is not discussed in [18, 17, 19, 49, 51, 52, 56, 57, 80, 154], First, a locally space-time conservation relation based on a form of the divergence theorem will be derived (see, e.g., [18, 43, 52, 57, 67]), in terms where local flux balance takes place. The method is suitable for the purely convection by considering two-level or multilevel time steps for a constant-coefficient difference schemes. Latter on it will be extended for the case of a balance law equation in the variable space. In addition, we also address on the usefulness of identifying modified equations which model the behavior of the difference scheme in connection to the original equation taking into account the regularity of the initial data. The balance law finite difference analogue based on the locally conservative Lagrangian-Eulerian will be discussed next.

2.1 Formal construction: statement of the Lagrangian-Eulerian formulation and notations

Consider the initial value problem for single conservation laws as follows:

$$\frac{\partial u}{\partial t} + \frac{\partial H(u)}{\partial x} = 0, \quad t > 0, \quad -\infty < x < \infty, \quad (2.1.1)$$

$$u(x, 0) = \eta(x), \quad -\infty < x < \infty, \quad (2.1.2)$$

where $H(u)$ is a smooth function of u , $u = u(x, t)$. For the construction of the Lagrangian-Eulerian procedure, we first consider the equation (2.1.1) written in locally conservative space-time generalized divergence form, along with $u(x, 0) = \eta(x)$,

$$\nabla_{t,x} \left[\begin{array}{c} u \\ H(u) \end{array} \right] = 0, \quad t > 0, \quad -\infty < x < \infty. \quad (2.1.3)$$

In order to set the finite dimensional function spaces relying on solving the approximate problem by the Lagrangian-Eulerian method for (2.1.1)-(2.1.2), we now introduce some notation. The plane region $\mathbb{R} \times \overline{\mathbb{R}} = \{(x, t); -\infty < x < \infty; t \geq 0\}$ will be replaced by the lattice $\mathbb{N} \times \mathbb{Z} = \{(j, n); j = 0, \pm 1, \pm 2, \dots; n = 0, 1, 2, \dots\}$, and instead of functions $u(\cdot, t) \in L^p(\mathbb{R})$ for $t \geq 0$, we will consider the sequences $U^n = (U^n)_j$, $j \in \mathbb{Z}$ for $n = 0, 1, 2, \dots$, for a given mesh $h > 0$ and a time level

$$t^n = \sum_{i=0}^n \Delta t^i, \quad (2.1.4)$$

with $t^0 = 0$, for non-constant time step Δt^i . In the time level t^n , we have $x_j^n = jh$, $x_{j+\frac{1}{2}}^n = jh + \frac{h}{2}$ on the uniform local grid or original grid, here $h_j^n = \Delta x^n = x_{j+\frac{1}{2}}^n - x_{j-\frac{1}{2}}^n = h$, $j \in \mathbb{Z}$, where $x_{j\pm\frac{1}{2}}^n$ are endpoint of the cell. For the non-uniform grid we have $h_j^{n+1} = \overline{\Delta x}^{n+1} = \overline{x}_{j+\frac{1}{2}}^{n+1} - \overline{x}_{j-\frac{1}{2}}^{n+1}$, in the time level t^{n+1} . Here x_j^n and \overline{x}_j^{n+1} are the centers of the cells $[x_{j-\frac{1}{2}}^n, x_{j+\frac{1}{2}}^n]$ and $[\overline{x}_{j-\frac{1}{2}}^{n+1}, \overline{x}_{j+\frac{1}{2}}^{n+1}]$ respectively, and the numerical approximation of the solution u in these cells are defined by,

$$U(x_j, t^n) = U_j^n = \frac{1}{h} \int_{x_{j-\frac{1}{2}}^n}^{x_{j+\frac{1}{2}}^n} u(x, t^n) dx, \quad \text{and} \quad \overline{U}_j^{n+1} = \frac{1}{h_j^{n+1}} \int_{\overline{x}_{j-\frac{1}{2}}^{n+1}}^{\overline{x}_{j+\frac{1}{2}}^{n+1}} u(x, t^{n+1}) dx \quad j \in \mathbb{Z}, \quad (2.1.5)$$

respectively, and the initial condition is $U(x_j^0, t^0) = U_j^0$ in the cells $[x_{j-\frac{1}{2}}^0, x_{j+\frac{1}{2}}^0]$, $j \in \mathbb{Z}$. Notice, in the equations (2.1.5), the quantity $u(x, t)$ is a solution of (2.1.1). The discrete counterpart of the space $L^p(\mathbb{R})$ is l_h^p , the space of sequences $U = (U_j)$, with $j \in \mathbb{Z}$, such that $\|U\|_{l_h^p} = \left(h \sum_{j \in \mathbb{Z}} |U_j|^p\right)^{\frac{1}{p}}$, $1 \leq p < \infty$ or $\|U\|_{l_h^\infty} = \sup_{j \in \mathbb{Z}} |U_j|$ where U is defined in the appropriate l_p -space (see, e.g., [142]).

2.1.1 The local Lagrangian-Eulerian conservation relation

Following similar ideas in [17, 52, 57], we consider cell-centered finite-volume in a Lagrangian framework (see left picture in Figure 2.1) and it reads:

$$D_j^n = \{(t, x) / t^n \leq t \leq t^{n+1}, \sigma_j^n(t) \leq x \leq \sigma_{j+1}^n(t)\}, \quad (2.1.6)$$

where $\sigma_j^n(t)$ is a parameterized curve such that $\sigma_j^n(t^n) = x_j^n$; i.e., define the space-time local control volume D_j^n (see left picture in Figure 2.1) to be the set contained between $[x_j^n, x_{j+1}^n]$ and $[\overline{x}_{j-\frac{1}{2}}^{n+1}, \overline{x}_{j+\frac{1}{2}}^{n+1}]$, and two integral curves given by $\sigma_j^n(t)$ and $\sigma_{j+1}^n(t)$, $t \in [t^n, t^{n+1}]$. From the basic calculus we know the divergence theorem states that the outward flux of a vector field through a closed surface is equal to the volume integral of the divergence over the region inside the surface. Thus, from the conservation law (2.1.3) we get:

$$\iint_{D_j^n} \nabla_{t,x} \begin{bmatrix} u \\ H(u) \end{bmatrix} dV = 0 \quad \Leftrightarrow \quad \oint_{\partial D_j^n} \begin{bmatrix} u \\ H(u) \end{bmatrix} \cdot \vec{n} ds = 0. \quad (2.1.7)$$

Thus, by naturally enforcing a discrete local conservation over control volumes D_j^n , which in turn ‘‘fill-up’’ the space-time domain, the scheme then satisfies global conservation in space-time.

Equations (2.1.7) implies that the parameterized curves $\sigma_j^n(t)$ and $\sigma_{j+1}^n(t)$ are naturally impervious zero-flux boundaries. Indeed, in order to construct such ‘‘impervious zero-flux’’

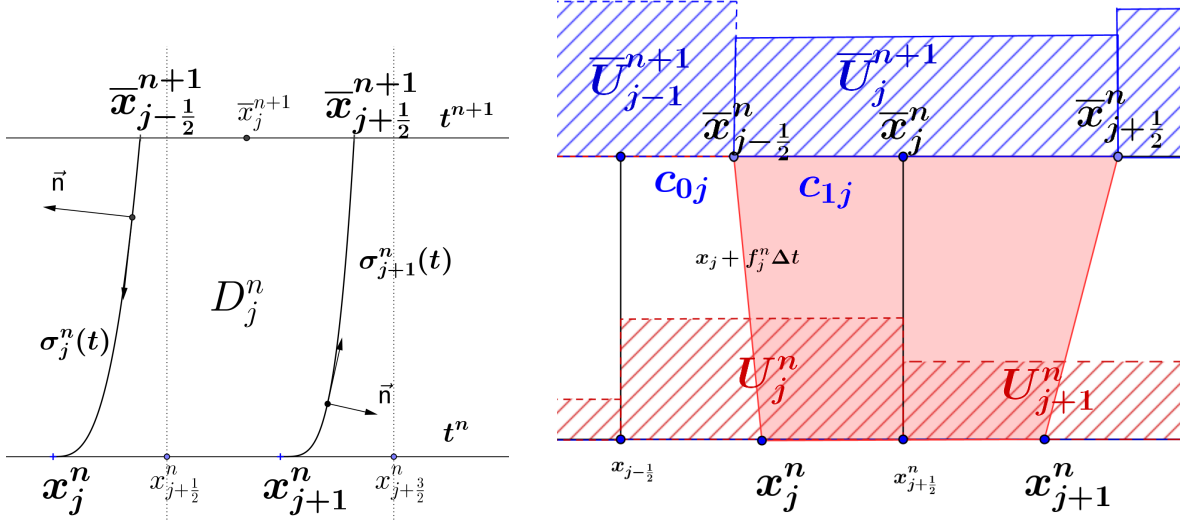


Figure 2.1: Geometric design of the local Lagrangian-Eulerian space-time control-volume D_j^n (left) and its first order approximation (right).

family of parameterized curves $\sigma_j^n(t)$ governing the space-time D_j^n , consider $\gamma^n(\xi) = (x(\xi), t(\xi))$ with respect to the oriented left picture Figure 2.1. That is to say, we might formally write down $\frac{d\gamma^n(\xi)}{d\xi} = \left(\frac{dx(\xi)}{d\xi}, \frac{dt(\xi)}{d\xi}\right)$. From this follows that for $t^n \leq t \leq t^{n+1}$ we get $\frac{d\gamma_j^n(\xi)}{d\xi} \perp \vec{n}$ and $\frac{d\gamma_{j+1}^n(\xi)}{d\xi} \perp \vec{n}$ since the slope $\left(\frac{dx(\xi)}{d\xi}, \frac{dt(\xi)}{d\xi}\right)$ agrees to the slope the vector $[H(u), u]^\top$ over curves $\sigma_j^n(t)$ and $\sigma_{j+1}^n(t)$, for $j \in \mathbb{Z}$, which we have assuming the fact $[H(u), u]^\top \cdot \vec{n} = 0$ from (2.1.7). Of course, for any real number $\varpi \neq 0$ we write $\frac{dx(\xi)}{d\xi} = \varpi H(u)$ and $\frac{dt(\xi)}{d\xi} = \varpi u$. For the sake of simplicity of presentation we shall suppose $u \neq 0$ (this assumption can be suppressed by introducing some extra notation in the analysis to define the endpoints $[\bar{x}_{j-\frac{1}{2}}^{n+1}, \bar{x}_{j+\frac{1}{2}}^{n+1}]$ by analytical straight lines). Now, consider the suitable change of variable $\sigma(t) = x(\xi(t))$, along with the chain rule $\frac{d\sigma(t)}{dt} = \frac{dx(\xi)}{d\xi} \frac{d\xi}{dt}$, to define the following system of ordinary differential equations:

$$\frac{d\sigma_j^n(t)}{dt} = \frac{H(u)}{u}, \quad \sigma_j^n(t^n) = x_j^n, \quad t^n \leq t \leq t^{n+1}, \quad (2.1.8)$$

From this fact, the region D_j^n will be called ‘‘Integral tube’’ (see, e.g., [52, 57]). As a natural consequence of (2.1.7)-(2.1.8), the integrals over the curves $\sigma_j^n(t)$ vanish and then the line integral over the boundary of the region ∂D_j^n in (2.1.7) leads to the (natural) local conservation,

$$\int_{\bar{x}_{j-\frac{1}{2}}^{n+1}}^{\bar{x}_{j+\frac{1}{2}}^{n+1}} u(x, t^{n+1}) dx = \int_{x_j^n}^{x_{j+1}^n} u(x, t^n) dx, \quad (2.1.9)$$

where we define $\bar{x}_{j-\frac{1}{2}}^{n+1} = \sigma_j^n(t^{n+1})$ and $\bar{x}_{j+\frac{1}{2}}^{n+1} = \sigma_{j+1}^n(t^{n+1})$. Next, we use (2.1.5) with the conser-

vation law (2.1.9) to get:

$$\begin{aligned}
\bar{U}_j^{n+1} &= \frac{1}{h_j^{n+1}} \int_{\bar{x}_{j-\frac{1}{2}}^{n+1}}^{\bar{x}_{j+\frac{1}{2}}^{n+1}} u(x, t^{n+1}) dx \\
&= \frac{1}{h_j^{n+1}} \int_{x_j^n}^{x_{j+1}^n} u(x, t^n) dx \\
&= \frac{h}{h_j^{n+1}} \left[\frac{1}{h} \int_{x_j^n}^{x_{j+\frac{1}{2}}^n} u(x, t^n) dx + \frac{1}{h} \int_{x_{j+\frac{1}{2}}^n}^{x_{j+1}^n} u(x, t^n) dx \right] \\
&= \frac{h}{h_j^{n+1}} \left[\frac{1}{2} U_j^n + \frac{1}{2} U_{j+1}^n \right].
\end{aligned} \tag{2.1.10}$$

The resulting local approximations U_j^{n+1} , $j \in \mathbb{Z}$, are defined over the original grid as

$$U_j^{n+1} = \frac{1}{h} [c_{0j} \bar{U}_{j-1}^{n+1} + c_{1j} \bar{U}_j^{n+1}]. \tag{2.1.11}$$

Here $c_{0j} = (\frac{h}{2} + f_j^n k^n)$, $c_{1j} = h - c_{0j} = (\frac{h}{2} - f_j^n k^n)$ and we use, in the ordinary differential system 2.1.8, the approximation $f_j^n = \frac{H(U_j^n)}{U_j^n} \approx \frac{H(u)}{u}$ and notice that the approximated curve $\sigma_j^n(t) = x_j^n + f_j^n k^n$ is a straight line for f_j^n along with $k^n = \Delta t^n = t^{n+1} - t^n$ (see right picture in Figure 2.1).

Notice that the nonlinear quantity $H(u)/u$ is related to the unknown solution u , and so one cannot find the exact trace lines of the fluid particles. Although simple at first glance, is not well understood how to define a good, robust and efficient approximations to $H(u)/u$ by means of nonlinear reconstructions (see [17, 19, 20, 21, 22, 52, 80]). Here we use a quite simple explicit approximation $f_j^n \approx \frac{H(u)}{u}$ (but with quite good results), for both hyperbolic and balance equations, which is advantageous to the numerical analysis. Indeed, all machinery developed for implicit strategies for source terms to the case of balance laws (see [23, 45, 67, 69, 111, 131, 160]) can be used to the family of problems involving ODEs in (2.1.8). Finally, combining equations (2.1.8) and (2.1.11) produces the basic building block of the new Lagrangian-Eulerian scheme of approximate solutions to hyperbolic conservation laws and balance laws.

2.1.2 The Lagrangian-Eulerian scheme for linear hyperbolic conservation laws and its mathematical properties

Now we will define a equivalent finite difference of an Lagrangian-Eulerian approach based on locally conservative finite volume method and to the hyperbolic linear constant-coefficient case we will indeed prove its consistency, stability and convergence in the sense of classical Lax stability (see e.g., [62, 109, 142]).

Consider the linear flux function $H(u) = a u$, $a \in \mathbb{R}$ to the conservation law (2.1.3), along with the Lagrangian-Eulerian approach (2.1.8)-(2.1.11), whose exact well-known solution is $u(x, t) = \eta(x - at)$. Therefore, we set $f_j = a$ with $h_j^{n+1} = h$, $j \in \mathbb{Z}$. Thus, the solutions of the family of initial value problem:

$$\frac{d\sigma_j^n(t)}{dt} = a, \quad \sigma_j^n(t^n) = x_j^n, \tag{2.1.12}$$

is precisely $\sigma_j^n(t) = a(t - t^n) + x_j^n$ and, in connection with the definitions above, also reads that $\bar{x}_{j-\frac{1}{2}}^{n+1} = \sigma_j^n(t^{n+1}) = ak + x_j^n$. Moreover, using a simple mathematical reasoning the above construction can be viewed as an analogue of finite difference scheme for linear hyperbolic conservation laws. The procedure for balance laws is quite straightforward. In addition, such construction for finite difference schemes is distinct to that Lagrangian-Eulerian method based on mixed finite elements as discussed in [52] for a parabolic equation. Then, we notice from equations (2.1.9) and (2.1.10) that:

$$\bar{U}_j^{n+1} = \frac{1}{h_j^{n+1}} \int_{\bar{x}_{j-\frac{1}{2}}^{n+1}}^{\bar{x}_{j+\frac{1}{2}}^{n+1}} u(x, t^{n+1}) dx = \frac{1}{h_j^{n+1}} \int_{x_j^n}^{x_{j+1}^n} u(x, t^n) dx = \frac{1}{h_j^{n+1}} \frac{1}{2} h [U_j^n + U_{j+1}^n] = \frac{1}{2} [U_j^n + U_{j+1}^n], \quad (2.1.13)$$

and replacing (2.1.13) into (2.1.11) reads (the one-step or *the two-level* finite difference scheme):

$$U_j^{n+1} = \frac{1}{4} [U_{j-1}^n + 2U_j^n + U_{j+1}^n] - \frac{ak^n}{2h} [U_{j+1}^n - U_{j-1}^n], \quad (2.1.14)$$

then, with fixed $k = k^n$, we get the equivalent difference finite scheme to the linear conservation laws:

$$U_j^{n+1} = \frac{1}{4} [U_{j-1}^n + 2U_j^n + U_{j+1}^n] - \frac{ak}{2h} [U_{j+1}^n - U_{j-1}^n]. \quad (2.1.15)$$

It was found [18, 19] by only geometrical arguments (see left picture in Figure 2.1) based on numerical domain of influence and domain of dependence for (2.1.15) the following Courant-Friedrichs-Lewy CFL-like stability condition $ak/h < 1/2$. For linear PDEs however, the fact that consistency (for a linear scheme) plus stability is equivalent to convergence is known as the Lax equivalence theorem (Lax-Richtmyer stability [109, 142]) in the sense of classical stability of difference schemes in ℓ^p - spaces (see, e.g., [62, 109, 142]). Thus, to prove convergence we need consistency and a suitable form of stability. The linear Lagrangian-Eulerian scheme (2.1.15) is designed to a straightforward application of Lax equivalence theory.

Consistency

In order to prove the consistency for the Lagrangian-Eulerian approximation scheme (2.1.15), we consider the Linear differential equation $Pu = 0$, where the operator $P = \frac{\partial}{\partial t} + a\frac{\partial}{\partial x}$, $a > 0$ and the difference finite scheme $P_{h,k}U = 0$, where:

$$P_{h,k}\phi = \frac{\phi_j^n - \frac{1}{4} \left([\phi_{j-1}^n + \phi_j^n] + [\phi_j^n + \phi_{j+1}^n] \right)}{k} + a \frac{\phi_{j+1}^n - \phi_{j-1}^n}{2h}. \quad (2.1.16)$$

Here $\phi(x, t)$ is any smooth function and $\phi_j^n = \phi(jh, nk)$. Thus, the linear difference finite scheme (2.1.15) is consistent with the Linear PDE $Pu = 0$ (in the classical sense of Lax [62, 109, 142]) when (point-wise convergence in ℓ^2 - space),

$$\tau_{h,k} \equiv P\phi - P_{h,k}\phi \rightarrow 0 \quad \text{as} \quad h, k \rightarrow 0. \quad (2.1.17)$$

In this case, we have (by Taylor series expansions directly on the local truncation error $\tau_{h,k}$):

$$\begin{aligned}\tau_{h,k} &= P\phi - P_{h,k}\phi \\ &= \frac{1}{k} \left[\phi_j^{n+1} - \frac{1}{4} (\phi_{j-1}^n + 2\phi_j^n + \phi_{j+1}^n) + \frac{ak}{2h} (\phi_{j+1}^n - \phi_{j-1}^n) \right] \\ &= \left[\frac{a^2k}{2} - \frac{h}{k} \frac{h}{4} \right] \phi_{xx} + O(k^2) + O(h^2).\end{aligned}\tag{2.1.18}$$

In (2.1.18) it was used that $u_{tt} = a^2 u_{xx} + O(k^2)$. Indeed, keeping the ratio h/k fixed we might write:

$$\tau_{h,k} = O(k + h),\tag{2.1.19}$$

and then $\tau_{h,k} \rightarrow 0$ as $h, k \rightarrow 0$; *i.e.*, the analogue finite difference scheme (2.1.15) based on the locally conservative Lagrangian-Eulerian procedure (2.1.8)-(2.1.11) is consistent.

Stability (Convergence)

By means of the Fourier analysis every one-step like (2.1.15) (or two-level scheme from t^n to t^{n+1}) can be recast in a recurrence relation, given by (from the Fourier inversion formula):

$$\widehat{U}^{n+1} = (g(h\xi))\widehat{U}^n, \quad \text{with} \quad \widehat{U}^n = (g(h\xi))^n \widehat{U}^0,\tag{2.1.20}$$

where \widehat{U}^n is the Fourier transform of a grid function U^n , defined at grid points $x_j = jh$ for $j = 0, \pm 1, \pm 2, \dots$ and all crucial information about a scheme is embedded in its amplification factor *or characteristic function* $g(h\xi)$ for the scheme at wave number ξ . Therefore, replacing U_j^n by $g^n e^{i\xi jh}$ and plugging this into the Lagrangian-Eulerian scheme (2.1.15) and matching coefficients reads (with $\omega \equiv h\xi$ for convenience of notation):

$$g(\omega)^{n+1} e^{i\xi jh} = \frac{1}{4} \left(g(\omega)^n e^{i\xi(j-1)h} + 2g(\omega)^n e^{i\xi jh} + g(\omega)^n e^{i\xi(j+1)h} \right) - \frac{ak}{2h} \left(g(\omega)^n e^{i\xi(j+1)h} - g(\omega)^n e^{i\xi(j-1)h} \right).\tag{2.1.21}$$

From (2.1.21) one easily find that,

$$g(\omega) = \frac{1}{4} \left(e^{-i\xi h} + 2 + e^{i\xi h} \right) - \frac{ak}{2h} \left(e^{i\xi h} - e^{-i\xi h} \right) = \frac{1}{2} (1 + \cos(\xi h)) - v \sin(\xi h),\tag{2.1.22}$$

where $v = akh^{-1}$ is the Courant number. Thus, the Lagrangian-Eulerian finite difference scheme is stable if there is a positive constant K (independent of ξ, h, k , but h, k are in the stability region) such that, $|g(\omega, k, h)| \leq 1 + Kk$. If amplification factor does not depend of h and k , then $g(\omega, k, h)$ can be replaced with the restricted stability condition $|g(\omega)| \leq 1$ (in the classical sense, see, e.g., [62, 142]). Thus, the amplification factor of the Lagrangian-Eulerian scheme (2.1.15) is given by,

$$|g(\xi)|^2 = \frac{1}{4} (1 + \cos(\xi h))^2 + v^2 \sin^2(\xi h).\tag{2.1.23}$$

Notice that the restriction $|g(\omega)| \leq 1$ is also true if $v^2 \leq \frac{1}{4}$, and then we get,

$$|v| \leq \frac{1}{2}.\tag{2.1.24}$$

This now gives a support to what was used in [18, 19]. Additionally, a more detailed analysis of the amplification factor (2.1.22) shows that the bound in the equation (2.1.24) can be greater. We consider now the function from (2.1.23),

$$t(\omega, v) = |g(\omega)|^2 = \frac{1}{4} (1 + \cos(\omega))^2 + v^2 \sin^2(\omega). \quad (2.1.25)$$

Differentiation of $t(\omega, v)$ with respect to ω and setting $t_\omega(\omega, v) = 0$ reads,

$$\cos(\omega) = \frac{\frac{1}{2}}{2v^2 - \frac{1}{2}}, \quad (2.1.26)$$

from which we get the following constraint for $v \neq \frac{1}{2}$:

$$\left| \frac{\frac{1}{2}}{2v^2 - \frac{1}{2}} \right| \leq 1. \quad (2.1.27)$$

Therefore $0 < v < \frac{1}{2}$ or $\frac{\sqrt{2}}{2} < v$; more about the nature of approximations given by Lagrangian-Eulerian scheme (2.1.15) within these stability intervals will be addressed further in the next Section 2.1.2 by using the modified equation framework. Indeed, this function $t(\omega, v)$ has no critical points on the interval $\frac{1}{2} < v < \frac{\sqrt{2}}{2}$, but $t_\omega(\omega, v) \equiv 0$ in this interval is zero. This implies that function $t(\omega, v)$ is constant there (see left picture in Figure 2.2), but the function is still limited by one for $v \in]\frac{1}{2}, \frac{\sqrt{2}}{2}[$. The right picture in Figure 2.2 shows the stability region with $v = \frac{1}{2}$ and the corresponding stability region to the function $t(\omega, v)$ along with the interval where the ω is constant. Now, notice that the function $t(\omega, v)$ (2.1.27) associated to the analogue linear Lagrangian-Eulerian scheme (2.1.15) is continuous, even smooth with respect to the variable v . Therefore, stability condition for the linear Lagrangian-Eulerian scheme (2.1.15) is (see also the right picture in Figure 2.2, where it is shown the continuous and smooth enlargement of the stability region of the scheme (2.1.15)),

$$|v| < \frac{\sqrt{2}}{2}, \quad v = \frac{ak}{h}, \quad a \in \mathbb{R}, \quad h, k > 0. \quad (2.1.28)$$

We now are ready to invoke the fundamental theorem of numerical analysis (the Lax-Richtmyer equivalence theorem). A consistent linear difference finite scheme of the form (2.1.15) for a linear conservation law of the form (2.1.3), with $H(u) = au$, $a \in \mathbb{R}$ is convergent if and only if it is Lax-Richtmyer stable. Therefore, by the results discussed in Sections 2.1.2 and 2.1.2 we have convergence for scheme (2.1.15) in ℓ^2 -space.

The modified equation for the Lagrangian-Eulerian scheme

Insights in the qualitative behavior (see numerical experiments from Figure 2.3 to Figure 2.5) can be obtained by regarding the so-called modified equations of the discretization. It is worth mentioning that here we will use modified equations aiming the understanding of qualitative behavior of approximations (related to the two-level Lagrangian-Eulerian scheme (2.1.15)) in the spirit of critical work of [37] (see also [72, 155]), that related it with the Fourier-Von Neumann method for the linear stability analysis of the linear initial-value problem (Lax stability in PDEs as before) of two-level linear difference schemes. Let $\phi(x, t)$ in C^∞ , with

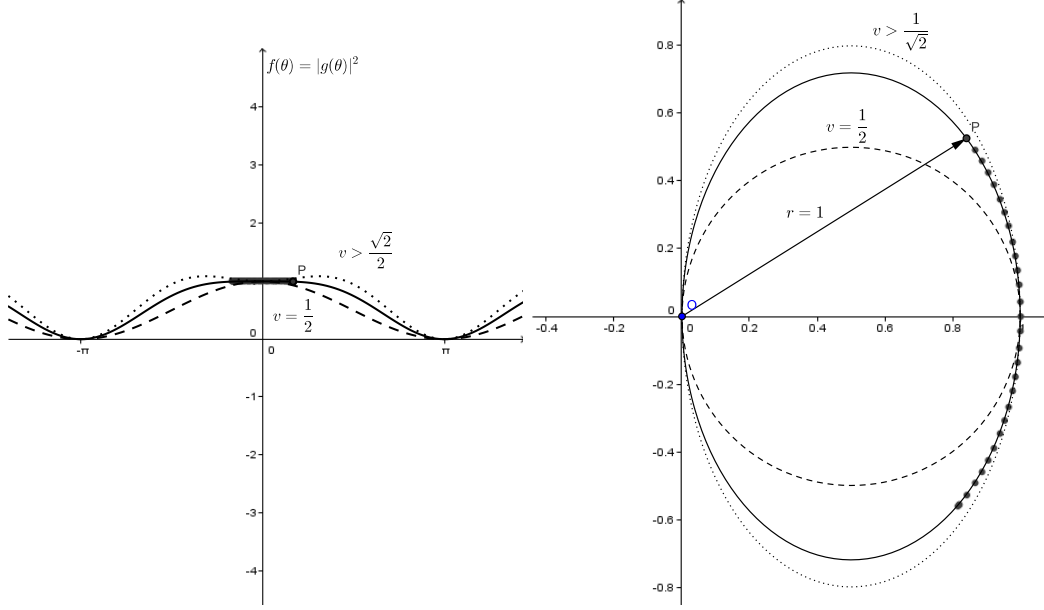


Figure 2.2: It is shown (left) the amplification factor function $t_\omega(\omega, v)$ and (right) the set of image points of the locus of $g(\omega)$ for the Lagrangian-Eulerian scheme (2.1.15), as for both cases ω varies along with the limiting Courant number $v = \sqrt{2}/2$.

all bounded derivatives with respect to x and t , in the setting of modified equations and plug this into (2.1.15) along with the stability results pointed out in the previous sections. Further Taylor series expansion in (2.1.15) gives,

$$\phi_t + a\phi_x = \frac{h^2}{2k} \left(\frac{1}{2} - \frac{a^2 k^2}{h^2} \right) \phi_{xx} - \frac{ah^2}{3} \left(1 - \frac{a^2 k^2}{h^2} \right) \phi_{xxx} + O(k^3). \quad (2.1.29)$$

or in a more convenient form (keep in mind $v = \frac{ak}{h}$ with ratio k/h fixed),

$$\phi_t + a\phi_x = \frac{ah}{2v} \left(\frac{1}{2} - \frac{a^2 k^2}{h^2} \right) \phi_{xx} - \frac{ah^2}{3} \left(1 - \frac{a^2 k^2}{h^2} \right) \phi_{xxx} + O(k^3). \quad (2.1.30)$$

Stability (2.1.28) of the discrete Lagrangian-Eulerian scheme (2.1.15) being analyzed holds as $h \rightarrow 0$. This ensure that any derivatives appearing in the remainder are bounded as $h \rightarrow 0$ and it means that modified equation (2.1.30) is a suitable candidate to verify that its solution satisfies the discrete equation (2.1.15) for an $O(k^3)$ remainder to approximate the *exact* linear hyperbolic PDE (2.1.1) with $H(u) = au$. Equation of the form (2.1.30) arise in fluid dynamics when both diffusion (viscosity term ϕ_{xx}) and dispersion (capillarity term ϕ_{xxx}) play a role. The diffusion smooths out the discontinuous solutions of (2.1.1) while the dispersion causes high-frequency oscillations. The dispersion process is an example of combined convection and diffusion. Thus, from equation (2.1.30) one might expect numerical solutions by scheme (2.1.15) to the purely linear hyperbolic PDE be contaminated by both spurious dispersion and diffusion effects. Thus, let us consider the numerical experiments related to a linear hyperbolic conservation law to the Lagrangian-Eulerian scheme (2.1.15), which in turn will be the building block to the analogue Lagrangian-Eulerian balance law approximate scheme. In the linear case, the complicated behaviors exhibited by the Fourier series sums would serve as a good testing ground for the

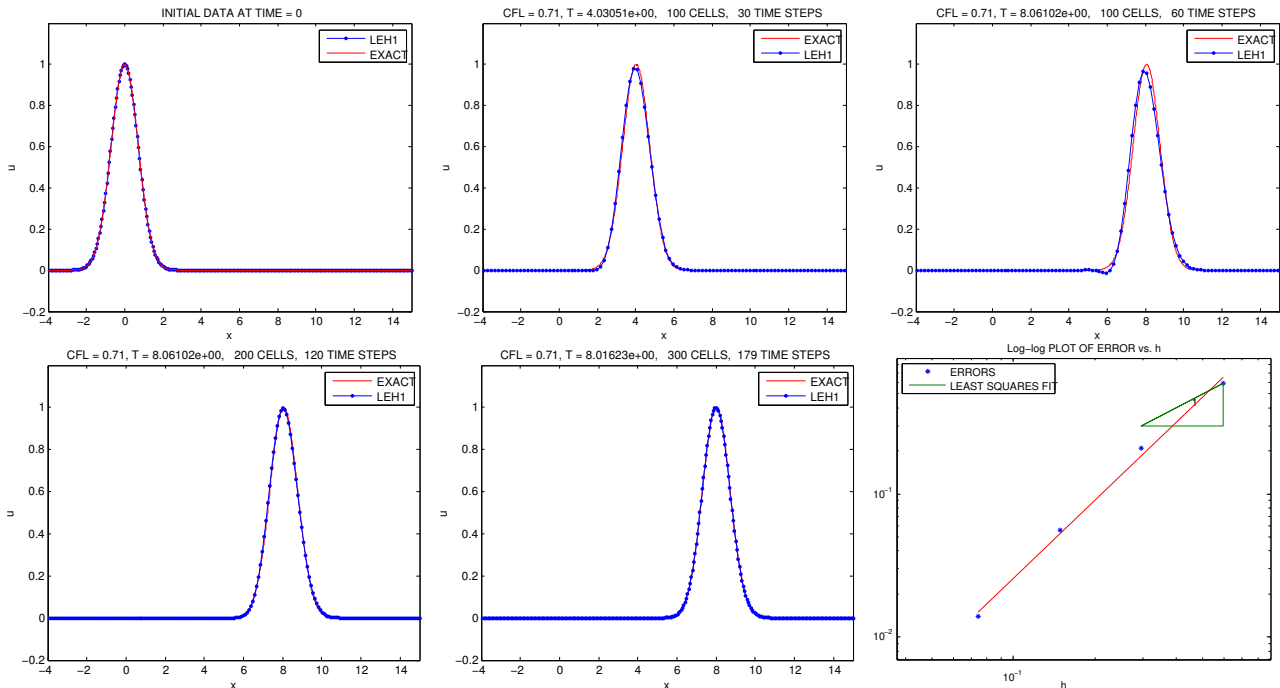


Figure 2.3: Approximate numerical solutions with **smooth** Gaussian initial condition.

application of numerical methods for diffusive/dispersive waves to rough data. Thus, let us discuss the application of the Lagrangian scheme (2.1.15) with *three type* of initial data:

\mathcal{C}^∞ **smooth data** (see Figure 2.3). It is shown the smooth initial condition $u(x, 0) \equiv \eta(x) = e^{-x^2}$ (top left) and computed solutions at $t = 4$ (top middle) and $t = 8$ (top right) with CFL number $v = \sqrt{2}/2$. As expected from the modified equation analysis the solutions start to exhibit dispersion since the range of the *dominant dispersion regime* is controlled by $1/2 < v < \sqrt{2}/2$ which is improved with refinement (see Figure 2.3 bottom).

In Section 2.1.2 we establish a convergence proof in ℓ^2 -space by means of von Neumann analysis for the Lagrangian-Eulerian scheme 2.1.15. Although the CFL number is in the range $1/2 < v < \sqrt{2}/2$ where the diffusion are in balance or dominates the dispersion, the above numerical experiments related to those in Figure 2.3 bottom, illustrate the fact of entire truncation error vanishing (see right picture) at all grid points under grid refinement, as expected from previous theoretical analysis. At this point (left and right picture) notice the excellent resemblance between the exact and approximate solutions computed by the Lagrangian-Eulerian scheme with any reminiscence of the spurious effects from the numerical dispersion/diffusion artifacts.

The following numerical experiment with a **Lipschitz initial data** illustrates again (see Figure 2.4) both cases where the diffusion are in balance, or dominates the dispersion as $h \rightarrow 0$ with ratio k/h fixed corresponding essentially to what is shown in Figure 2.3. The **Lipschitz** initial condition in this experiment is $\eta(x) = x + 1$, $-1 < x < 0$, $\eta(x) = -x + 1$, $0 < x < 1$ and $\eta(x) = 0$ elsewhere.

The following numerical experiment with a **discontinuous initial data** (see Figure 2.5) also illustrates both cases above mentioned as $h \rightarrow 0$ with ratio k/h . Here, a **discontinuous** initial condition is $\eta(x) = 1$, $-2 < x < 2$ and $\eta(x) = 0$ elsewhere.

In other words, the classical convergence (consistency + stability) property of a numerical

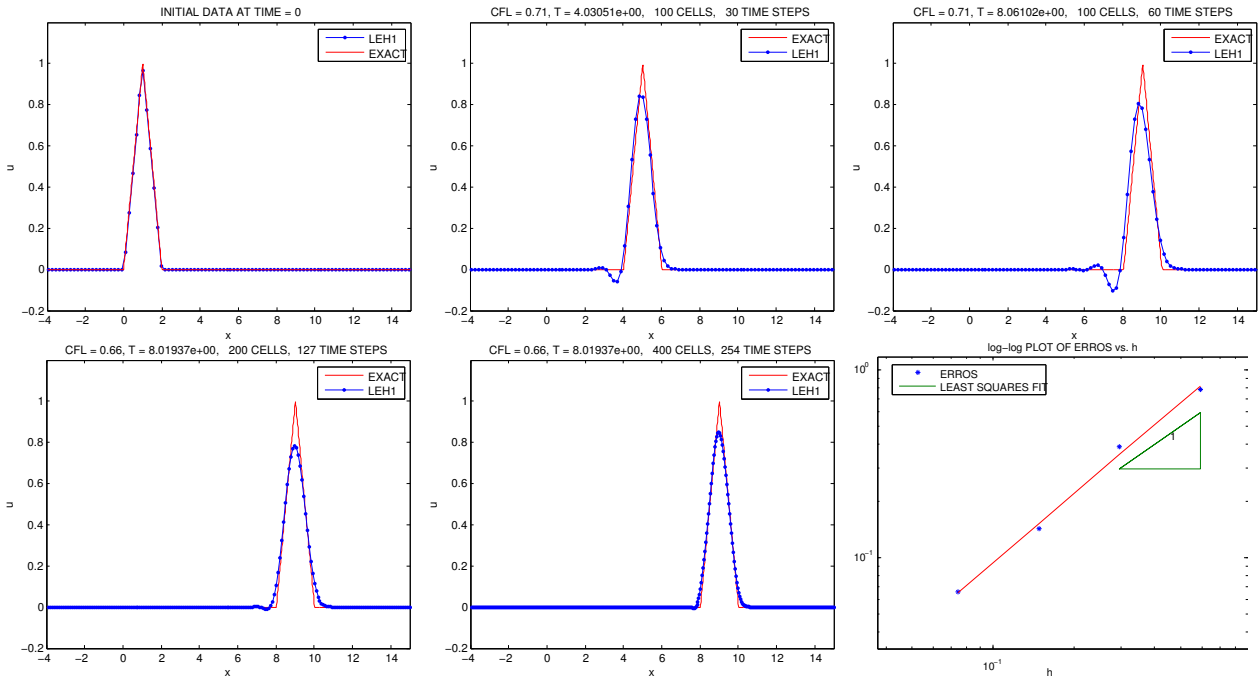


Figure 2.4: Numerical experiment with a **Lipschitz** initial condition

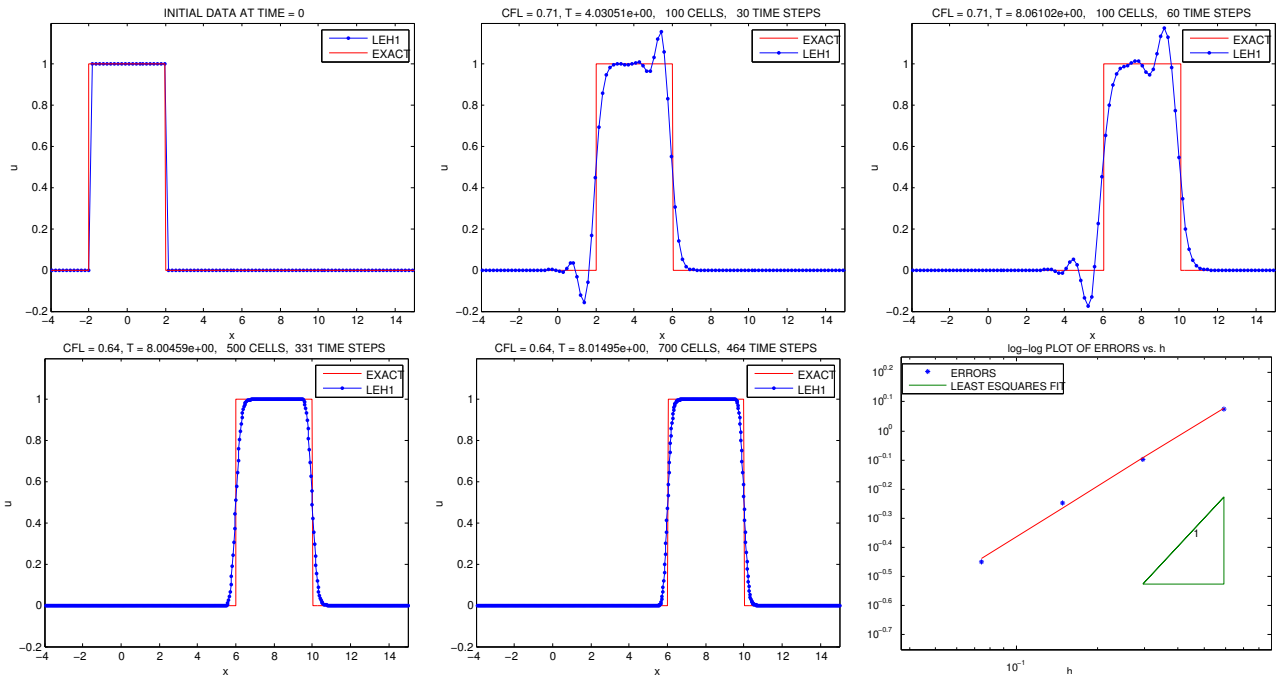


Figure 2.5: Numerical experiment with a **discontinuous** initial condition

scheme does not suffice to guarantee its suitability for providing good approximations to the controls that might be needed in applications. Such nice properties may be lost under numerical discretization as the mesh size tends to zero due to the existence of high-frequency spurious solutions for which the group velocity vanishes not fast enough. We will not suggest any specialized remedies since we are primarily interested in discuss the properties (we have found) in the most simple framework, which is conducive to analysis and verification by representative numerical tests as follow. Furthermore, we can also write the modified equation (2.1.30) for the Lagrangian-Eulerian scheme as,

$$u_t + au_x = \mu(v)_{dif}u_{xx} + \mu(v)_{disp}u_{xxx}, \quad (2.1.31)$$

where $\mu(v)_{dif} = \frac{ah}{2v}(\frac{1}{2} - v^2)$ and $\mu(v)_{disp} = -\frac{ah^2}{3}(1 - v^2)$, $v = \frac{ak}{h}$. Now, set $u(x, t) = e^{i(\xi x - c(\xi)t)}$ and plug this into the modified equation (2.1.31) to get,

$$-ic(\xi)e^{i(\xi x - c(\xi)t)} + (a(i\xi))e^{i(\xi x - c(\xi)t)} = \mu_{dif}(v)(a(i\xi)^2e^{i(\xi x - c(\xi)t)}) + \mu_{dis}(v)(a(i\xi)^3e^{i(\xi x - c(\xi)t)}). \quad (2.1.32)$$

After a bit of calculation and canceling out common factors reads,

$$-ic(\xi) + i(a(\xi)) = -\mu_{dif}(v)(a(\xi)^2) - i\mu_{disp}(v)(a(\xi)^3). \quad (2.1.33)$$

Thus, setting $v = \sqrt{2}/2$ one can see that $\mu(v)_{dif} = 0$. This reveals us that the modified equation has the only influence of the dispersion term, which in turn is given by $c(\xi) = a\xi + \mu_{disp}(v)(a(\xi)^3)$. Moreover, the group velocity is defined by $c_g(\xi) = c'(\xi)$, and we formally get $c_g(\xi) = a + 3a\mu_{disp}\xi^2$, where $\mu_{disp} < 0$. Then $c_g < a$, as it was verified in the numerical experiments from Figure 2.3 to Figure 2.5.

Cells	Smooth ($\ u - U\ _{l_h^1}(\ u - U\ _{l_h^2})$)	Continuos ($\ u - U\ _{l_h^1}(\ u - U\ _{l_h^2})$)	NonContinuos ($\ u - U\ _{l_h^1}(\ u - U\ _{l_h^2})$)
32	$5.921 \times 10^{-1}(2.980 \times 10^{-1})$	$7.834 \times 10^{-1}(4.521 \times 10^{-1})$	$1.192 \times 10^{-1}(5.454 \times 10^{-1})$
64	$2.082 \times 10^{-1}(1.146 \times 10^{-1})$	$3.898 \times 10^{-1}(2.267 \times 10^{-1})$	$7.984 \times 10^{-1}(4.458 \times 10^{-1})$
128	$5.571 \times 10^{-2}(3.171 \times 10^{-2})$	$1.428 \times 10^{-1}(9.095 \times 10^{-2})$	$5.639 \times 10^{-1}(4.374 \times 10^{-1})$
256	$1.399 \times 10^{-2}(8.006 \times 10^{-3})$	$6.541 \times 10^{-2}(4.869 \times 10^{-2})$	$3.552 \times 10^{-1}(2.887 \times 10^{-1})$
$E(h)$	$1.673 * h^{1.811}(0.835 * h^{1.75})$	$1.550 * h^{1.219}(0.808 * h^{1.096})$	$1.679 * h^{0.574}(0.646 * h^{0.27})$

Table 2.1: Errors between the numerical approximations (U) and exact solutions (u) in $l_h^1(l_h^2)$ ($\|u - U\|_{l_h^1}(\|u - U\|_{l_h^2})$) by problem $u_t + u_x = 0$ with smooth, continuos and noncontinuos initial condition at time frame $T = 2$ and CFL condition equal to $\sqrt{2}/2$.

2.2 A multiple time-step formulation for the Lagrangian-Eulerian scheme

In order to argue to the use of multiple steps in the nonlinear Lagrangian-Eulerian scheme for both hyperbolic conservation laws and balance laws we will first revisit the linear case. It is well known [37] that the connection between an amplification factor $g(\omega)$ and the corresponding modified equation is only partially valid for schemes involving more than two time levels.

In view of the von Neumann analysis this connection reveals (see also [72, 155]) that the amplification factor associated with a wave number generally has $(r - 1)$ roots for an $r - 1$ level

scheme. On the other hand, the procedure specified in Warming and Hyett's interpretation provides information for only the principal root; indeed, this is all what we needed to the three-level Leap-Frog scheme). Thus, we will construct a modified equation (2.2.13) for the three-level Lagrangian-Eulerian scheme (2.2.9) following Warming and Hyett's interpretation [72, 155] in a heuristic framework in order to get some insight of the relation between the numerical dissipation and the CFL condition to argue potential advantages/disadvantages to the use of multiple steps (see left picture in Figure 2.6). The multiple time step procedure for Lagrangian-Eulerian scheme is as follows. The first time step of the Lagrangian-Eulerian scheme is well known; see (2.1.15). In the time t^{n+1} , before of the projection, we have the approximation in the cell $\left[\bar{x}_{j-\frac{1}{2}}^{n+1}, \bar{x}_{j+\frac{1}{2}}^{n+1}\right]$,

$$\bar{U}_j^{n+1} = \frac{h}{2h_j^{n+1}} [U_j^n + U_{j+1}^n], \quad (2.2.1)$$

where $h_j^{n+1} = h + (f_{j+1}^n - f_j^n)k$, $k = \Delta t^n$ and $f_j^n = f(U_j^n) / U_j^n$. Thus, from (2.2.1) reads:

$$\bar{\bar{U}}_j^{n+2} = \frac{1}{2h_j^{n+2}} [h_j^{n+1}\bar{U}_j^{n+1} + h_{j+1}^{n+1}\bar{U}_{j+1}^{n+1}]. \quad (2.2.2)$$

The second step in time is given by plugging equation (2.2.1) into (2.2.2) and after standard algebraic manipulation follows the three-level Lagrangian-Eulerian scheme:

$$\bar{\bar{U}}_j^{n+2} = \frac{h}{4h_j^{n+2}} [U_j^n + 2U_{j+1}^n + U_{j+2}^n], \quad (2.2.3)$$

which in turn is defined over the cell $[\bar{\bar{x}}_{j-\frac{1}{2}}^{n+2}, \bar{\bar{x}}_{j+\frac{1}{2}}^{n+2}]$ where, $h_j^{n+2} = \bar{\bar{x}}_{j+\frac{1}{2}}^{n+2} - \bar{\bar{x}}_{j-\frac{1}{2}}^{n+2}$ and set,

$$\begin{aligned} h_j^{n+2} &= \frac{1}{2}[h_j^{n+1} + h_{j+1}^{n+1}] + (f_{j+1}^n - f_j^n)k^n + (f_{j+1}^{n+1} - f_j^{n+1})k^{n+1} \\ &= h + \frac{1}{2}(f_{j+2}^n - f_j^n)k^n + (f_{j+1}^{n+1} - f_j^{n+1})k^{n+1}. \end{aligned}$$

Next, the approximation (2.2.3) is then projected over the original grid to get,

$$U_j^{n+2} = \frac{1}{h} [c_{1j}\bar{\bar{U}}_{j-2}^{n+2} + c_{2j}\bar{\bar{U}}_{j-1}^{n+2} + c_{3j}\bar{\bar{U}}_j^{n+2}], \quad (2.2.4)$$

where the coefficients c_{1j} , c_{2j} , c_{3j} are defined as follows

$$c_{1j} = \frac{C^-}{2} (1 + \text{sgn}(C^-)), \quad c_{2j} = h - c_{1j} - c_{3j}, \quad c_{3j} = \frac{|C^+|}{2} (1 - \text{sgn}(C^+)), \quad (2.2.5)$$

where

$$C^+ = \frac{h}{2} + f_{j+1}^n k^n - \frac{h_j^{n+1}}{2} + f_j^{n+1} k^{n+1}, \quad C^- = -\frac{h}{2} + f_{j-1}^n k^n + \frac{h_{j-1}^{n+1}}{2} + f_{j-1}^{n+1} k^{n+1}. \quad (2.2.6)$$

The three-level time step Lagrangian-Eulerian procedure is as follows. For simplicity of pre-

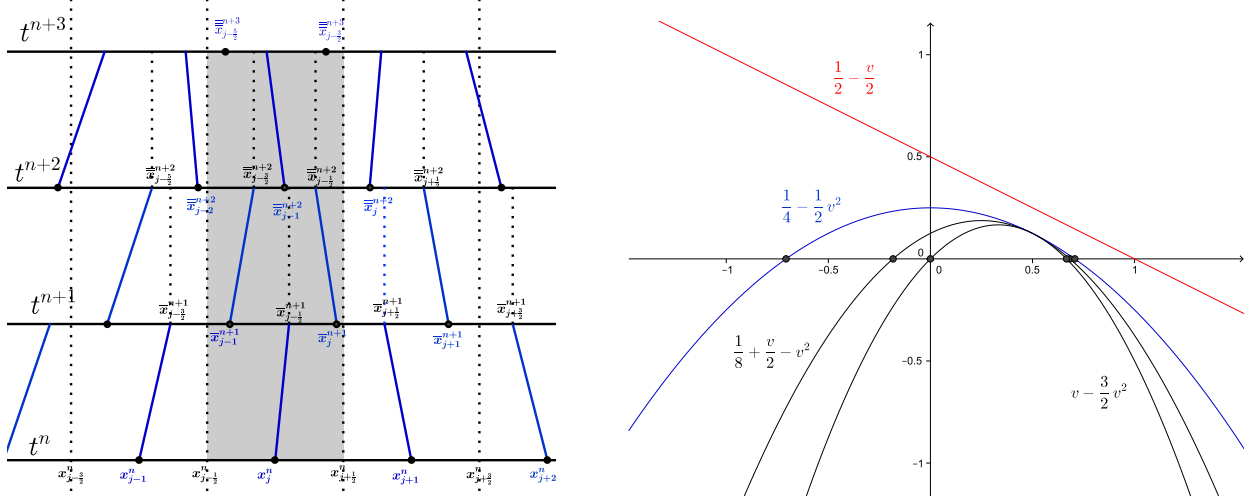


Figure 2.6: Three-level time step Lagrangian-Eulerian procedure.

sensation, let us consider the linear hyperbolic PDE $\frac{\partial u}{\partial t} + \frac{\partial(au)}{\partial x} = 0$, $a > 0$, when $f_j^n = a$, for each n and each j this condition means that the curves σ_j^n are parallels straight lines, therefore $h_j^n = h_j^{n+1} = h$ and we can take $k^n = k$ with this the equation (2.2.6) can be write as,

$$C^+ = \frac{h}{2} + ak - \frac{h}{2} + ak = 2ak, \quad C^- = -\frac{h}{2} + ak + \frac{h}{2} + ak = 2ak. \quad (2.2.7)$$

Notice C^+ and C^- are strictly positive and thus $c_{1j} = 2ak$, $c_{3j} = 0$, $c_{2j} = h - 2ak$ and finally the equation (2.2.3) to the linear case give,

$$\overline{\overline{U}}_j^{n+2} = \frac{1}{4}[U_j^n + 2U_{j+1}^n + U_{j+2}^n]. \quad (2.2.8)$$

Therefore, with the substitution of (2.2.7) in (2.2.4) we get,

$$\begin{aligned} U_j^{n+2} &= \frac{1}{h}[2ak\overline{\overline{U}}_{j-2}^{n+2} + (h - 2ak)\overline{\overline{U}}_{j-1}^{n+2}] \\ &= \frac{1}{4}[U_{j-1}^n + 2U_j^n + U_{j+1}^n] - \frac{ak}{2h}[(U_{j+1}^n - U_{j-1}^n) + (U_j^n - U_{j-2}^n)], \end{aligned} \quad (2.2.9)$$

whose such Lagrangian-Eulerian numerical scheme (2.2.9) has modified equation,

$$\phi_t + a\phi_x = \frac{h^2}{k} \left(\frac{1}{8} + \frac{1}{2}v - v^2 \right) \phi_{xx} - \frac{5}{12}ah^2\phi_{xxx} + O(k^2) + O(h^3). \quad (2.2.10)$$

To the numerical scheme with three time steps, we have,

$$\overline{\overline{\overline{U}}}_j^{n+3} = \frac{1}{2} \left(\overline{\overline{U}}_j^{n+2} + \overline{\overline{U}}_{j+1}^{n+2} \right), \quad (2.2.11)$$

then, the numerical scheme by three time level is,

$$\begin{aligned} U_j^{n+3} &= (3ak - \frac{h}{2})\overline{\overline{\overline{U}}}_{j-3}^{n+3} + (\frac{3}{2}h - 3ak)\overline{\overline{\overline{U}}}_{j-2}^{n+3} \\ &= \frac{1}{8} \left(-\frac{1}{2}U_{j-3}^n + 3U_{j-1}^n + 4U_j^n + \frac{3}{2}U_{j+1}^n \right) + \frac{ak}{8h} [3U_{j-3}^n + 6U_{j-2}^n - 6U_j^n - 3U_{j+1}^n], \end{aligned} \quad (2.2.12)$$

the modified equation by this Lagrangian-Eulerian scheme,

$$\phi_t + a\phi_x = \frac{h^2}{k} \left(v - \frac{3}{2}v^2 \right) \phi_{xx} - \frac{3}{2}k^2\phi_{ttt} - \frac{11}{12}ah^2\phi_{xxx}. \quad (2.2.13)$$

On the left picture of Figure 2.6 is shown the stencil of the multiple time step version of the time step Lagrangian-Eulerian scheme. On the right is shown the real stability interval associated to the diffusion terms of the modified equations to (i) the one step Lagrangian-Eulerian (2.1.15), the parabolic curve $\frac{1}{4} - \frac{1}{2}\mathbf{v}^2$, and for the two and the three-level time step Lagrangian-Eulerian scheme (2.2.9) (black), the parabolic curves (ii) two-step $\frac{1}{8} + \frac{1}{2}\mathbf{v} - \mathbf{v}^2$ and (ii) three-step $\mathbf{v} - \frac{3}{2}\mathbf{v}^2$. For comparison purposes it is shown in red the diffusive coefficients of the associated modified equation $\frac{\partial\phi}{\partial t} + a\frac{\partial\phi}{\partial x} = \frac{ah}{2}[1 - \frac{ak}{h}]\phi_{xx} + O(k^2)$ to the upwind difference scheme $U_j^{n+1} = U_j^n - \frac{ak}{h}[U_j^n - U_{j-1}^n]$.

The diffusive term in the above modified equation (2.2.13) seems to be less dominant than diffusive term in the equation (2.1.15), which in turn the projection step is performed after evolution of one time step (see right picture in Figure 2.6. This justify delaying the projection step further as possible in order to reduce spurious numerical dissipation. On the other hand (see also right picture in Figure 2.6) the modified equation analysis shows that the CFL interval is more restrictive, which in turn may affect the stability of the three-level Lagrangian-Eulerian scheme (2.2.12). Our somewhat naive observation may give some light on the issue of an optimal CFL regime by means of balance between the relative sizes of the diffusion and the dispersion numerical parameters (see also numerical experiments from Figure 2.3 to Figure 2.5).

The analysis suggests that increasing the number of time levels of the method at hand without projection on a fixed grid leads the stability region to decrease. Moreover, it also helps to understand how it is not trivial to build long integral tubes as well as discussed in [18, 17, 20, 21, 22, 57, 80, 159]. This analysis seems to suggest that such construction of the computational point of view can be infeasible due to the inherent difficulty of predicting a priori the interaction of the characteristic curves, particularly in the case of systems of conservation laws. Even in the scalar case, the situation can be very difficult in the case of flux functions that may exhibit discontinuities in their arguments [91, 94].

Chapter 3

The conservative finite difference Lagrangian-Eulerian scheme for nonlinear scalar conservation laws

3.1 Preliminary concepts

In this section we will treat some concepts of convergence to entropic approximate solutions of finite difference methods, which can be written in conservative form. Some concepts will be discussed to give a better understanding of our proposed scheme. For that, we will use some theoretical results from [42, 75, 76, 108, 139].

We consider the following initial data problem

$$\frac{\partial u}{\partial t} + \frac{\partial(H(u))}{\partial x} = 0, \quad u(x, 0) = u_0(x) \quad x \in \mathbb{R}. \quad (3.1.1)$$

A solution of (3.1.1), in the weak sense, see [108, 147], is a u function in $L_{loc}^\infty(\mathbb{R} \times \mathbb{R}^+)$ such that for all $\phi \in C_{loc}^\infty(\mathbb{R} \times \overline{\mathbb{R}^+})$,

$$\int_{-\infty}^{\infty} \int_0^{\infty} \left(u \frac{\partial \phi}{\partial t} + H(u) \frac{\partial \phi}{\partial x} \right) dt dx + \int_{-\infty}^{\infty} u_0(x) \phi(x, 0) dx = 0. \quad (3.1.2)$$

There are situations in which the weak solution is not unique, and one way of choosing the correct solution is to choose the solutions that are limits of an associated viscous problem as the viscosity vanishes (which we shall call vanishing viscosity solutions). There are various reasons to "want" this solution as our solution. One of the most physically appealing reasons is that many of the equations that we are solving approximate a physical situation that includes some sort of dissipation (a sufficiently small amount, which the modeler assumed was negligible). Hence, the solution that we choose will approximate a solution with a small amount of dissipation. One of the very important attributes of the vanishing viscosity solution is the following result, see [108, 147] for more details.

Proposição 3.1.1. (Thomas [147]) If a vanishing viscosity solution of 3.1.1 exists, it is a weak solution.

Note that, if we consider the viscous equation

$$\frac{\partial u^\epsilon}{\partial t} + \frac{\partial H(u^\epsilon)}{\partial x} = \epsilon \frac{\partial^2 u^\epsilon}{\partial x^2}. \quad (3.1.3)$$

If we multiply the above equation by a C_0^∞ test function ϕ (where ϕ and ϕ_x will be zero outside some closed rectangle $[a, b] \times [0, T_n]$) and perform the integrations plus integration by parts

$$-\int_0^\infty \int_{-\infty}^\infty [u^\epsilon \phi_t + H(u^\epsilon) \phi_x] dx dt - \int_{-\infty}^\infty u_0^\infty \phi_0 dx = \epsilon \int_0^\infty \int_{-\infty}^\infty u^\epsilon \phi_{xx} dx dt \quad (3.1.4)$$

and we let $\epsilon \rightarrow 0$, then $u^\epsilon \rightarrow u$, $H(u^\epsilon) \rightarrow H(u)$ and the viscous term tend to zero, and we can see that the viscous solution is a weak solution to equation (3.1.1).

An additional condition is required to pick out the physically relevant vanishing viscosity solution, see [108]. The condition which defines this solution is that it should be the limiting solution of the viscous equation as $\epsilon \rightarrow 0$. but this is not easy to work with. We want to find simpler conditions. In words of [147], before we proceed to decide how to choose the correct solutions, we introduce two common entropy conditions. It is not clear whether and/or how the first condition mimics the physical entropy argument. However, the second condition is truly taking an approach that finds a new variable that is to act like the “entropy” for the given system and the condition is designed to imitate the entropy condition of gas dynamics. We start with the following entropy condition written in Leveque book form.

Definição 3.1.1. (Leveque [108]) **Entropy Condition I:** The solution to equation (3.1.1), $u = u(x, t)$, containing a discontinuity propagating with speed s is said to satisfy Entropy Condition I if

$$H'(u_L) > s > H'(u_R) \quad (3.1.5)$$

where u_L and u_R are the solution values to the left and right of the discontinuity, respectively.

Note that $H'(u)$ is the characteristic speed. For convex H , the Rankine-Hugoniot speed s must lie between $H'(u_L)$ and $H'(u_R)$, so (3.1.1) reduces to simply the requirement that $H'(u_L) > H'(u_R)$, which again by convexity requires $u_L > u_R$ is.

A more general form of this condition, due to Oleinik, applies also to non-convex scalar flux functions H :

Definição 3.1.2. (Leveque [108]) **(Entropic Condition II):** $u(x, t)$ is the entropy solution if all discontinuities have the property that

$$\frac{H(u) - H(u_L)}{u - u_L} \leq s \leq \frac{H(u) - H(u_R)}{u - u_R} \quad (3.1.6)$$

for all u between u_L and u_R .

For convex H , this requirement reduces to (3.1.5). Another form of the entropy condition is based on the spreading of characteristics in a rarefaction fan. If $u(x, t)$ is an increasing function of x in some region, then characteristics spread out if $H'' > 0$. The rate of spreading can be quantified, and gives the following condition, also due to Oleinik.

Definição 3.1.3. (Leveque [108]) **(Entropic Condition III)** $u(x, t)$ is the entropy solution if there is a constant $E > 0$ such that for all $a > 0$, $t > 0$ and $x \in \mathbb{R}$,

$$\frac{u(x + a, t) - u(x, t)}{a} < \frac{E}{t}. \quad (3.1.7)$$

The importance of the latter is well justified in [108].

Note that for a discontinuity propagating with constant left and right states u_L and u_R , this can be satisfied only if $u_R - u_L < 0$, so this agrees with (3.1.5). The form of (3.1.7) may seem unnecessarily complicated, but it turns out to be easier to apply in some contexts. In particular, this formulation has advantages in studying numerical methods. One problem we face in developing numerical methods is guaranteeing that they converge to the correct solution. Some numerical methods are known to converge to the wrong weak solution in some instances. The criterion (3.1.5) is hard to apply to discrete solutions - a discrete approximation defined only at grid points is in some sense discontinuous everywhere. If $U_j < U_{j+1}$ at some grid point, how do we determine whether this is a jump that violates the entropy condition, or is merely part of a smooth approximation of a rarefaction wave? Intuitively, we know the answer: it is part of a smooth approximation, and therefore acceptable, if the size of this jump is $O(\Delta x)$ as we refine the grid and $\Delta x \rightarrow 0$. To turn this into a proof that some method converges to the correct solution, we must quantify this requirement and (3.1.7) gives what we need. Taking $a = \Delta x$, we must ensure that there is a constant $E > 0$ such that

$$U_{j+1}(t) - U_j(t) < \left(\frac{E}{t}\right) \Delta x$$

for all $t > 0$ as $\Delta x \rightarrow 0$. This inequality can often be established for discrete methods. In fact, Oleinik's original proof that an entropy solution to (3.1.1) satisfying (3.1.7) always exists proceeds by defining such a discrete approximation and then taking limits. This is also presented in Theorem 16.1 of Smoller [138, 139].

We shall discuss numerical approximations to weak entropic solutions of (3.1.1) using schemes such that can be write in conservative form

$$\begin{aligned} U_j^{n+1} &= \mathcal{H}(U_{j-q}^n, \dots, U_{j+q}^n) \\ &= U_j^n - \frac{\Delta t}{\Delta x} [F_{j+\frac{1}{2}} - F_{j-\frac{1}{2}}] \end{aligned} \tag{3.1.8}$$

where $F_{j+\frac{1}{2}} = F(U_{j-q+1}^n, \dots, U_{j+q}^n)$ is the numerical flux and satisfies the consistent condition $F(\bar{u}, \dots, \bar{u}) = H(\bar{u})$. If $q = 1$, then F is a function of only two variables and (3.1.8) becomes

$$U_j^{n+1} = U_j^n - \frac{\Delta t}{\Delta x} [F(U_j^n, U_{j+1}^n) - F(U_{j-1}^n, U_j^n)], \tag{3.1.9}$$

which is very natural if we view U_j^n as cell average defined by (2.1.5). We know that the weak solution $u(x, t)$ satisfies the integral form of the conservation law,

$$\int_{x_{j-\frac{1}{2}}}^{x_{j+\frac{1}{2}}} u(x, t^{n+1}) dx = \int_{x_{j-\frac{1}{2}}}^{x_{j+\frac{1}{2}}} u(x, t^n) dx - \left[\int_{t^n}^{t^{n+1}} H(u(x_{j+\frac{1}{2}}^n, t)) dt - \int_{t^n}^{t^{n+1}} H(u(x_{j-\frac{1}{2}}^n, t)) dt \right]. \tag{3.1.10}$$

Dividing by h and using the cell averages defined in (2.1.5), this gives

$$U_j^{n+1} = U_j^n - \frac{1}{\Delta x} \left[\int_{t^n}^{t^{n+1}} H(u(x_{j+\frac{1}{2}}^n, t)) dt - \int_{t^n}^{t^{n+1}} H(u(x_{j-\frac{1}{2}}^n, t)) dt \right]. \tag{3.1.11}$$

By comparing the above equation with (3.1.9), we note that $F(U_j^n, U_{j+1}^n)$ is the following average flux through $x_{j+\frac{1}{2}}$ over the interval $[t^n, t^{n+1}]$,

$$F(U_j^n, U_{j+1}^n) = \frac{1}{\Delta t} \int_{t^n}^{t^{n+1}} H(u(x_{j+\frac{1}{2}}^n, t)) dt.$$

Definição 3.1.4. (Harten, Hyman and Lax [76]) A finite difference scheme (3.1.8) is said to be monotone if \mathcal{H} is a monotone increasing function of each of its arguments.

Is well known [76], that solutions of hyperbolic conservation laws are not uniquely determined by their initial values; an entropy condition is needed to pick out the physically relevant solution. The question arises whether finite-difference approximations converge to this particular solution, the following result of [76] clarify this done.

Theorem 3.1.1. (Harten, Hyman and Lax, [76]) Let

$$\begin{aligned} U_j^{n+1} &= \mathcal{H}(U_{j-q}^n, \dots, U_{j+q}^n) \\ &= U_j^n - \frac{\Delta t}{\Delta x} [F_{j+\frac{1}{2}} - F_{j-\frac{1}{2}}] \end{aligned} \quad (3.1.12)$$

be a finite-difference approximation of (3.1.1) in conservation form, i.e., $F(\bar{u}, \dots, \bar{u}) = H(\bar{u})$, which is monotone:

$$\frac{\partial \mathcal{H}}{\partial U_i^n}(U_{j-q}^n, \dots, U_{j+q}^n) \geq 0, \quad j - q \leq i \leq j + q \quad (3.1.13)$$

Assume that, as Δt and Δx tend to zero, $\Delta t / \Delta x = \text{const.}$, U^n converges boundedly almost everywhere to some function $u(x, t)$. Then according to the theorem of Lax and Wendroff, $u(x, t)$ is a weak solution of (3.1.1), and the Oleinik entropy condition,

$$\frac{H(u) - H(u_L)}{u - u_L} \leq S \leq \frac{H(u) - H(u_R)}{u - u_R} \quad (3.1.14)$$

is satisfied for all discontinuities of u . Here S is the velocity obtained by the Rankine-Hugoniot relation.

Other important concept is Total Variation, of this and using compactness arguments one can deduce the existence of convergent subsequence, we define this concept in follow. Give a function $u = u(x)$, the total variation is defined by

$$TV(u) = \limsup_{\delta \rightarrow 0} \frac{1}{\delta} \int_{-\infty}^{\infty} |u(x + \delta) - u(x)| dx \quad (3.1.15)$$

If u is a smooth function then

$$TV(u) = \int_{-\infty}^{\infty} |u'(x)| dx \quad (3.1.16)$$

- To $u = u(x, t)$ the definition can be to extend to $TV(u(t))$.
- If $U^n = \{U_j^n\}_j$ is a grid function, then

$$TV(U_j^n) = \sum_{i=-\infty}^{\infty} |U_{i+1}^n - U_i^n|. \quad (3.1.17)$$

- When $TV(u_0) < \infty$, then

$$TV(u(t_2)) \leq TV(u(t_1)), \quad t_2 \geq t_1. \quad (3.1.18)$$

Definição 3.1.5. (Harten [75]) Scheme (3.1.8) is said to be a Total Variation Diminishing (TVD) scheme, or Total Variation Non-Increasing (TVNI) scheme, if

$$TV(U^{n+1}) \leq TV(U^n).$$

A consequence of the above definition is that

$$TV(U^n) \leq TV(U^{n-1}) \dots \leq TV(U^0) < \infty \quad (3.1.19)$$

where $\{U_i^0\}$ is data at time $t = 0$. Next we define another class of numerical methods.

Theorem 3.1.2. (Harten [75]) Schemes of the form (3.1.8) for the scalar, nonlinear conservation law (3.1.1) are said to be Monotonicity Preserving Schemes if whenever the data $\{U_i^n\}$ is monotone the solution set $\{U_i^{n+1}\}$ is monotone in the same sense. That is, if U_i^n is monotone increasing so is $\{U_i^{n+1}\}$ and if $\{U_i^n\}$ is monotone decreasing so is $\{U_i^{n+1}\}$.

Theorem 3.1.3. (Harten [75]) In general, the set S_{mon} of monotone schemes is contained in the set S_{tvd} of TVD schemes and this in turn is contained in the set S_{mpr} of monotonicity preserving schemes, that is

$$S_{mon} \subseteq S_{tvd} \subseteq S_{mpr}.$$

For linear schemes (2.1.15) to solve the linear advection equation $\partial u / \partial t + a \partial u / \partial x = 0$ it can be proved that monotone schemes are equivalent to monotonicity preserving schemes.

In 1980 Crandall and Majda (see [42]), proved that general monotone difference schemes always converge and that they converge to the physical weak solution satisfying the entropy condition. Rigorous convergence results follow for dimensional splitting algorithms when each step is approximated by a monotone difference scheme. The main result of this work establishes the convergence of general conservation-form, monotone difference approximations to the unique generalized solution which satisfies the entropy condition. The result is following, which is presented in scalar version. Consider the problem,

$$\begin{cases} \frac{\partial u}{\partial t} + \frac{\partial(H(u))}{\partial x} = 0 \\ u(x, 0) = u_0(x), \quad x \in \mathbb{R}, \end{cases} \quad (3.1.20)$$

where H , is a smooth real-value functions and u is a scalar function. The difference approximations of (3.1.1) of interest here are explicit marching schemes of the form,

$$\begin{aligned} U_{j,k}^{n+1} &= \mathcal{H}(U_{j-p}^n, \dots, U_{j+q+1}^n) \\ &= U_j^n - \lambda^x \Delta_+^x g(U_{j-p}^n, \dots, U_{j+q+1}^n). \end{aligned} \quad (3.1.21)$$

In order to the above equation be consistent with (3.1.1), it must have

$$g(u, u, \dots, u) = H(u), \quad u \in \mathbb{R}. \quad (3.1.22)$$

The functions g is the numerical flux of the approximation. The difference approximation is monotone on the interval $[a, b]$ if \mathcal{G} a nondecreasing function of each argument U_j^n so long as all arguments lie in $[a, b]$. Write $u(x, t) = (S(t)u_0)(x)$, where $S(t) : L^1(\mathbb{R}) \cap L^\infty(\mathbb{R}) \rightarrow L^1(\mathbb{R}) \cap L^\infty(\mathbb{R})$ for each $t \geq 0$ and $t \rightarrow S(t)u_0$ is continuous into $L^1(\mathbb{R})$. To compute this solution numerically we set

$$U_j^0 = \frac{1}{\Delta x} \int_{R_j} u_0(x) dx \quad (3.1.23)$$

here $R_j = \left[(j - \frac{1}{2}) \Delta x, (j + \frac{1}{2}) \Delta x \right]$ and define U^{n+1} from U^n by (3.1.1). And finally, put \mathcal{X}_j^n the characteristic function of $R_j \times [n \Delta t, (n+1) \Delta t)$ and

$$u^{\Delta t} = \sum_{n=0}^{\infty} \sum_{j=-\infty}^{\infty} U_j^n \mathcal{X}_j^n \quad (3.1.24)$$

The main result in [42] is

Theorem 3.1.4. Suppose $u_0 \in L^1(\mathbb{R}) \cap L^\infty(\mathbb{R})$ and $a < u_0 < b$ a.e. Let (3.1.21) be a consistent conservation-form difference approximation to (3.1.1) which is monotone on $[a, b]$ and which has Lipschitz continuous numerical flux g . Let $u^{\Delta t}$ be given by (3.1.21), (3.1.23), (3.1.24). Then as $\Delta t \rightarrow 0$ with $\Delta t / \Delta x$ fixed, $u^{\Delta t}$ converges to $S(t)u_0$ in $L^1(\mathbb{R})$ uniformly for bounded $t \geq 0$. More precisely,

$$\lim_{\Delta t \rightarrow 0} \sup_{0 \leq t \leq T} \int_{\mathbb{R}} |u^{\Delta t}(x, t) - S(t)u_0(x)| dx = 0 \quad (3.1.25)$$

for each $T > 0$.

Reviewing the definitions, (3.1.25) can also be restated as

$$\lim_{\Delta t \rightarrow 0} \sup_{\substack{0 \leq t \leq T \\ n \Delta t \leq t \leq (n+1) \Delta t}} \sum_j \int_{R_j} |U_j^n - S(t)u_0(x)| dx = 0. \quad (3.1.26)$$

3.2 On the construction of a unique entropy solution based on the Lagrangian-Eulerian scheme for convex scalar conservation law

A numerical formulation of the Lagrangian-Eulerian scheme model for the nonlinear case, which we present as a generalization of the Lagrangian-Eulerian scheme (2.1.15), is called in this work as LEH2 (Lagrangian Eulerian Finite Difference scheme) as the follow scheme,

$$U_j^{n+1} = \frac{1}{4}(U_{j-1}^n + 2U_j^n + U_{j+1}^n) - \frac{k}{2h}(H(U_{j+1}^n) - H(U_{j-1}^n)), \quad (3.2.1)$$

where $k = k^n$ and with CFL condition

$$\max_j \left| H'(U_j^n) \frac{k}{h} \right| \leq \frac{\sqrt{2}}{2} \quad (3.2.2)$$

This method results to be conservative, i.e, the scheme (3.2.1) can be written in the conservative form

$$U_j^{n+1} = U_j^n - \frac{k}{h}(\bar{F}(U_j^n, U_{j+1}^n) - \bar{F}(U_{j-1}^n, U_j^n)), \quad (3.2.3)$$

where

$$\bar{F}(U_j^n, U_{j+1}^n) = \frac{1}{4} \left[\frac{h}{k}(U_j^n - U_{j+1}^n) + 2(H(U_{j+1}^n) + H(U_j^n)) \right]. \quad (3.2.4)$$

and also, this numerical method can be written as,

$$\frac{U_j^{n+1} - (U_{j+1}^n + 2U_j^n + U_{j-1}^n)/4}{k} + \frac{H(U_{j+1}^n) - H(U_{j-1}^n)}{2h} = 0. \quad (3.2.5)$$

A convergence proof follows in the spirit on the same approach as discussed in the work of Joel A. Smoller to Lax-Friedrichs scheme. Thus, our result is then similar of that presented in [139]:

Theorem 3.2.1. Let $\eta(x) \in L_\infty(\mathbb{R})$, and let $H \in C^2(\mathbb{R})$ with $H''(u) > 0$ on $\{u : |u| \leq \|\eta(x)\|_\infty\}$. Then there exists a solution u of (3.1.1) with the following properties,

- 1) $|u(x, t)| \leq \|\eta(x)\|_\infty \equiv M, (x, t) \in \mathbb{R} \times \mathbb{R}_+$.
- 2) There is a constant $E > 0$, depending only on $M, \varphi = \min\{H''(u) : |u(x, t)| \leq \|\eta(x)\|_\infty\}$ and $A = \max\{H'(u) : |u(x, t)| \leq \|\eta(x)\|_\infty\}$, such that for every $a > 0, t > 0$, and $x \in \mathbb{R}$,

$$\frac{u(x+a, t) - u(x, t)}{a} < \frac{E}{t}. \quad (3.2.6)$$

- 3) u is stable and depends continuously on $\eta(x)$ in the following sense: If $\eta(x), \xi(x) \in L_\infty(\mathbb{R}) \cap L_1(\mathbb{R})$ with $|\eta(x)| \leq \|\xi(x)\|_\infty$, and $v(x)$ is the corresponding constructed solution of (3.1.1) with initial data $\xi(x)$, then for every $x_1, x_2 \in \mathbb{R}$, with $x_1 < x_2$, and every $t > 0$,

$$\int_{x_1}^{x_2} |u(x, t) - v(x, t)| dx \leq \int_{x_1 - At}^{x_2 + At} |\eta(x) - \xi(x)| dx. \quad (3.2.7)$$

We start the proof by considering the Lagrangian-Eulerian scheme (3.2.1) in the finite difference form (3.2.5). Based on the stability condition (2.1.28), see [11], established to scheme (3.2.1), notice that both holds $A > 0$ and $\varphi > 0$, with k and h :

$$\frac{Ak}{h} \leq \frac{1}{2}. \quad (3.2.8)$$

Following [139], we establish first the finite difference scheme analogue of item (1) that appears in Theorem 3.2.1. Next, we will highlight the pertinent modifications to accommodate the proof to our Lagrangian-Eulerian scheme (3.2.1).

Lemma 3.2.1. For every $n \in \mathbb{Z}, k \in \mathbb{Z}_+, |U_j^n| \leq M$

Proof. Write (3.2.1) as

$$\begin{aligned} U_j^{n+1} &= \frac{1}{4} (U_{j-1}^n + 2U_j^n + U_{j+1}^n) - \frac{k}{2h} (H(U_{j+1}^n) - H(U_{j-1}^n)) \\ &= \frac{1}{4} (U_{j-1}^n + 2U_j^n + U_{j+1}^n) - \frac{k}{2h} H'(\theta_j^n) (U_{j+1}^n - U_{j-1}^n) \\ &= \left(\frac{1}{4} + \frac{k}{2h} H'(\theta_j^n) \right) U_{j-1}^n + \frac{1}{2} U_j^n + \left(\frac{1}{4} - \frac{k}{2h} H'(\theta_j^n) \right) U_{j+1}^n \end{aligned} \quad (3.2.9)$$

where θ_j^n is between U_{j+1}^n and U_{j-1}^n . We assume inductively that $|U_j^n| \leq M$ for all $j \in \mathbb{Z}$, $n \in \mathbb{Z}_+$, and that the CFL condition (3.2.8) holds, then $\frac{1}{4} \pm \frac{k}{2h} H'(\theta_j^n) \geq 0$, and thus

$$|U_j^{n+1}| \leq \left(\frac{1}{4} + \frac{k}{2h} H'(\theta_j^n)\right) M + \frac{1}{2} M + \left(\frac{1}{4} - \frac{k}{2h} H'(\theta_j^n)\right) M \leq M \quad (3.2.10)$$

We now turn our attention to establish a discrete version of the entropy condition (3.2.6) associated to our nonlinear Lagrangian-Eulerian scheme (3.2.1). It is worth mentioning that here we used a different stencil with respect to the spatial grid with length h instead of $2h$ as used in [139].

Lemma 3.2.2. (Entropy Condition). If $c = \min\{\varphi/2, A/4M\}$, then for $j \in \mathbb{Z}$, $n \in \mathbb{Z}_+$,

$$\frac{U_j^n - U_{j-1}^n}{h} \leq \frac{E}{nk}, \text{ where } E = \frac{1}{c}. \quad (3.2.11)$$

Proof. Let

$$z_j^n = \frac{U_j^n - U_{j-1}^n}{h} \quad (3.2.12)$$

Then, from the Lagrangian-Eulerian scheme follows:

$$\begin{aligned} z_j^{n+1} &= \frac{1}{4} z_{j-1}^n + \frac{1}{2} z_j^n + \frac{1}{4} z_{j+1}^n - \frac{k}{2h^2} \left(H'(U_j^n)(U_{j+1}^n - U_j^n) + \frac{1}{2} H''(\theta_1)(U_{j+1}^n - U_j^n)^2 \right) \\ &\quad - \frac{k}{2h^2} \left(H'(U_{j-1}^n)(U_j^n - U_{j-1}^n) + \frac{1}{2} H''(\theta_2)(U_j^n - U_{j-1}^n)^2 \right) \\ &\quad - \frac{k}{2h^2} \left(H'(U_j^n)(U_{j-1}^n - U_j^n) + \frac{1}{2} H''(\theta_3)(U_{j-1}^n - U_j^n)^2 \right) \\ &\quad - \frac{k}{2h^2} \left(H'(U_{j-1}^n)(U_{j-2}^n - U_{j-1}^n) + \frac{1}{2} H''(\theta_4)(U_{j-2}^n - U_{j-1}^n)^2 \right), \end{aligned}$$

where θ_1 is between U_{j+1}^n and U_j^n , θ_2 and θ_3 is between U_j^n and U_{j-1}^n , and θ_4 is between U_{j-2}^n and U_{j-1}^n . Write (3.2) as:

$$\begin{aligned} z_j^{n+1} &= \left(\frac{1}{4} + \frac{k}{2h} H'(U_{j-1}^n)\right) z_{j-1}^n + \left(\frac{1}{2} + \frac{k}{2h} H'(U_j^n) - \frac{k}{2h} H'(U_{j-1}^n)\right) z_j^n \\ &\quad + \left(\frac{1}{4} - \frac{k}{2h} H'(U_j^n)\right) z_{j+1}^n \\ &\quad - \frac{k}{4} \left(H''(\theta_1)(z_{j+1}^n)^2 + (H''(\theta_2) + H''(\theta_3))(z_j^n)^2 + H''(\theta_4)(z_{j-1}^n)^2 \right) \end{aligned} \quad (3.2.13)$$

Now, define $\hat{z}_j^n = \max\{z_{j-1}^n, z_j^n, z_{j+1}^n, 0\}$. Take $\hat{z}_j^n = 0$. Then estimate (3.2.2) holds, since $z_j^n \leq \hat{z}_j^n \leq E/nk$. Suppose now that $\hat{z}_j^n \neq 0$ with $\hat{z}_j^n = z_{j+1}^n$. As in [139], the other possibilities can be analyzed by means of the same techniques. Using the Lagrangian-Eulerian CFL condition written as $Ak/h \leq 1/2$ (see (2.1.28)) we have,

$$\begin{aligned} z_j^{n+1} &\leq \left(\frac{1}{4} + \frac{k}{2h} H'(U_{j-1}^n)\right) \hat{z}_j^n + \left(\frac{1}{2} + \frac{k}{2h} H'(U_j^n) - \frac{k}{2h} H'(U_{j-1}^n)\right) \hat{z}_j^n \\ &\quad + \left(\frac{1}{4} - \frac{k}{2h} H'(U_j^n)\right) \hat{z}_j^n - \frac{ck}{4} (4(z_{j+1}^n)^2) \\ &\leq \hat{z}_j^n - ck(\hat{z}_j^n)^2. \end{aligned} \quad (3.2.14)$$

By Lemma 3.2.1 we see $|U_j^n| \leq M$. This plus CFL condition (3.2.8) for scheme (3.2.5) and the fact $c \leq A/4M$ reads,

$$z_j^n \leq |z_j^n| \leq \frac{M}{h} \leq \frac{M}{2Ak} \leq \left(\frac{M}{k}\right) \left(\frac{1}{2A}\right) \leq \left(\frac{M}{k}\right) \left(\frac{1}{8cM}\right) = \frac{1}{8kc}. \quad (3.2.15)$$

Take $M^n = \max_j \{\hat{z}_j^n\}$ and notice that $M^n \geq 0$. Next, define $\phi(y) = y - cky^2$ to perform the calculation $\phi' = 1 - 2cky$ to see that it is an increasing function if $y < \frac{1}{2ck}$. From (3.2.15) follows that $\hat{z}_j^n \leq M^n \leq (8kc)^{-1} < (2ck)^{-1}$ such that,

$$\phi(\hat{z}_j^n) \leq \phi(M^n), \quad \text{which in turn gives } \hat{z}_j^n - ck(\hat{z}_j^n)^2 \leq M^n - ck(M^n)^2. \quad (3.2.16)$$

Again, following [139] we use (3.2.14) to conclude that $z_j^{n+1} \leq M^k - ch(M^n)^2$ for all $j \in \mathbb{Z}$, and furthermore that,

$$M^{n+1} \leq M^n - ck(M^n)^2. \quad (3.2.17)$$

We suppose¹ that for all n ,

$$M^n \leq w(nk), \quad (3.2.18)$$

then we get $z_j^n \leq M^n \leq w(nk) \leq \frac{1}{cnk + \frac{1}{M^0}} \leq \frac{1}{cnk} = \frac{E}{nk}$. with this, the Lemma is proved. It thus remains to prove (3.2.18). This is done by induction. Note that the case $n = 0$ is trivial. Suppose that (3.2.18) holds for n ; in order to show it for $n + 1$, we need a Lemma.

Lemma 3.2.3. If J is a constant, and

$$\frac{J - w(nk)}{k} \leq w'(nk), \quad (3.2.19)$$

then $J \leq w(nk + k)$.

Proof. First we note that $w(t) > 0$ if $t > 0$, therefore $w'(t) < 0$ and $w''(t) > 0$ on $t \leq 0$. then

$$\frac{w(nk + k) - w(nk)}{k} \geq w'(nk) \geq \frac{J - w(nk)}{k} \quad (3.2.20)$$

so that $w(nk + k) \geq J$. With this the lemma is proved.

Completing now the proof of Lemma (3.2.2), we have from (3.2.17) $M^{n+1} \leq M^n - ck(M^n)^2$, but also

$$M^n \leq w(nk) = \frac{1}{cnk + 1/M^0} \leq \frac{1}{cnk + ck} \leq \frac{1}{2ck} \quad (3.2.21)$$

since (3.2.18) holds and $n \geq 1$. Since ϕ is monotone on this interval, $\phi(M^n) \leq \phi(w(nk))$, then

$$M^{n+1} \leq M^n - ck(M^n)^2 \leq w(nk) - ck(w(nk))^2. \quad (3.2.22)$$

With this

$$\frac{M^{n+1} - w(nk)}{k} \leq -ck(w(nk))^2 = w'(nk), \quad (3.2.23)$$

with the Lemma 3.2.3 gives $M^{n+1} \leq w(nk + k)$. This completes the proof.

¹Here we also include the hint used in [139]: consider the following ordinary differential equation $\frac{dw}{dt} = -cw^2$, $t > 0$, with initial condition is $w(0) = M^0$, whose solution is given by $w(t) = \frac{1}{ct + \frac{1}{M^0}}$.

Lemma 3.2.4. (Space Estimate). For any $X > 0$ and $nk \geq \alpha > 0$, there is a constant C depending on X and α , but independent of k and h , such that,

$$\sum_{|j| \leq \frac{X}{h}} |U_{j+1}^n - U_j^n| \leq C. \quad (3.2.24)$$

Proof. Let $V_j^n = U_j^n - C_1 j h$, where C_1 is kept as large as needed to hold true $\frac{E}{\alpha} < C_1$. Thus using Lemma 3.2.2 (with a modified stencil to the entropy condition (3.2.6) and (3.2.2) to our Lagrangian-Eulerian scheme (3.2.5) reads,

$$\begin{aligned} V_{j+1}^n - V_j^n &= U_{j+1}^n - C_1(j+1)h - U_j^n + C_1 j h \\ &= U_{j+1}^n - U_j^n - C_1 h \leq \frac{hE}{nk} - C_1 h = h \left(\frac{E}{nk} - C_1 \right) \leq h \left(\frac{E}{\alpha} - C_1 \right) < 0, \end{aligned}$$

and

$$\begin{aligned} \sum_{|j| \leq \frac{X}{h}} |U_{j+1}^n - U_j^n| &\leq \sum_{|j| \leq \frac{X}{h}} |V_{j+1}^n - V_j^n| + \sum_{|j| \leq \frac{X}{h}} C_1 h - \sum_{|j| \leq \frac{X}{h}} (V_{j+1}^n - V_j^n) + C_1 h \left(\frac{2X}{h} \right) \\ &\leq 2 \max_{|j| \leq |V_j^n|} + 2C_1 X \leq 2M + 2C_1 X, \end{aligned}$$

and the desired result is proved. In [139], it was shown that the finite difference approximations to the entropy solution of the initial value problem (3.1.1) converge to all upper-half plane $-\infty < x < \infty$, $t > 0$. Due to the nature of the stencil of the Lax-Friedrichs scheme, two cases with respect to the discrete time level were computed independently, namely when $n - p > 0$ is even and when $n - p > 0$ is odd. Here we will use the same Lagrangian-Eulerian scheme (3.2.5) with a pertinent change in the proof to account both situations simultaneously, as performed in the entropy condition (3.2.6) – see also (3.2.2) – as well as in the previous Space Estimate Lemma 3.2.4.

Lemma 3.2.5. (Time Estimate). If $\frac{k}{h} \leq \delta < 0$, and $h, k \leq 1$, then there exist an $L > 0$, independent of k and h such that if $n > p$, $pk \geq \alpha > 0$,

$$\sum_{|j| \leq \frac{X}{h}} |U_j^n - U_j^p| \leq L(n - p)k. \quad (3.2.25)$$

Proof. Let

$$A = \frac{1}{4} + \frac{h}{2k} H'(\theta_j), \quad B = \frac{1}{2}, \quad C = \frac{1}{4} - \frac{h}{2k} H'(\theta_j). \quad (3.2.26)$$

We point out that under CFL condition for stability of finite difference Lagrangian-Eulerian scheme (3.2.5) given by $Ak/h \leq 1/2$ – see (2.1.28) – that A , B and C are non-negative numbers and satisfy that $A + B + C = 1$, i.e., the convexity of the flux function. We now write the Lagrangian-Eulerian scheme (3.2.5) as,

$$U_j^{n+1} = AU_{j-1}^n + BU_j^n + CU_{j+1}^n, \quad (3.2.27)$$

and then using the fact that $A + B + C = 1$ reads,

$$|U_j^n - U_j^{n-1}| \leq A|U_{j-1}^{n-1} - U_j^{n-1}| + B|U_{j+1}^{n-1} - U_j^{n-1}|. \quad (3.2.28)$$

Multiplying by h , by summing, and using Lemma (3.2.4)

$$\sum_{|j| \leq \frac{X}{h}} |U_j^n - U_j^{n-1}| h \leq A \sum_{|j| \leq \frac{X}{h}} |U_{j-1}^{n-1} - U_j^{n-1}| h + B \sum_{|j| \leq \frac{X}{h}} |U_{j+1}^{n-1} - U_j^{n-1}| h \leq ch. \quad (3.2.29)$$

If $(n - p) \in \mathbb{N}$, the systematic use of the triangle inequality gives,

$$\begin{aligned} \sum_{|j| \leq \frac{X}{h}} |U_j^n - U_j^p| h &\leq \sum_{|j| \leq \frac{X}{h}} |U_j^n - U_j^{n-1} + U_j^{n-1} + \dots + U_j^{p-1} - U_j^p| h \\ &\leq \sum_{|j| \leq \frac{X}{h}} \sum_{i=p}^{n-1} |U_j^i - U_j^{i+1}| h \leq \sum_{i=p}^{n-1} \sum_{|j| \leq \frac{X}{h}} |U_j^i - U_j^{i+1}| h \\ &\leq \sum_{i=p}^{n-1} ch = ch(n - p) = \frac{c}{\delta}(n - p). \end{aligned} \quad (3.2.30)$$

The desired proof gives us that the solution of the finite difference Lagrangian-Eulerian scheme has a finite speed of propagation with Lipschitz constant $L = \frac{c}{\delta}$ in t , namely saying that under the pertinent stability condition $h/k \geq \delta > 0$ that the discrete values U_j^n produced by the finite difference scheme from the values of U_j^0 for a bounded set of values for all involved j 's.

As in [139] we were also able to show that the difference approximations are L_1 locally Lipschitz continuous in t .

Lemma 3.2.6. (Stability) Let $\{U_j^n\}$ and $\{V_j^n\}$ be solution of the finite difference Lagrangian-Eulerian scheme (3.2.5), corresponding to the initial values U_j^0 and V_j^0 , respectively, where $\sup_j \{|U_j^0|\} < M$ and $\sup_j \{|V_j^0|\} < M$. Then if $n > 0$,

$$\sum_{|j| \leq N} |U_j^n - V_j^n| h \leq \sum_{|j| \leq N+k} |U_j^0 - V_j^0| h. \quad (3.2.31)$$

Proof. Let $W_j^n = U_j^n - V_j^n$. Thus from the corresponding Lagrangian-Eulerian scheme (3.2.5) reads,

$$W_j^{n+1} = \frac{1}{4}W_{j-1}^n + \frac{1}{2}W_j^n + \frac{1}{4}W_{j+1}^n - \frac{k}{2h}H'(\theta_{j+1})(U_{j+1}^n - V_{j+1}^n) + \frac{k}{2h}H'(\theta_{j-1})(U_{j-1}^n - V_{j-1}^n), \quad (3.2.32)$$

where θ_{j+1} (resp. θ_{j-1}) is between U_{j+1}^n and V_{j+1}^n (resp. U_{j-1}^n and V_{j-1}^n). Therefore,

$$W_j^{n+1} = \left(\frac{1}{4} + \frac{k}{2h}H'(\theta_{j-1}) \right) W_{j-1}^n + \frac{1}{2}W_j^n + \left(\frac{1}{4} - \frac{k}{2h}H'(\theta_{j+1}) \right) W_{j+1}^n. \quad (3.2.33)$$

The coefficients of the scheme (3.2.33) W_{j-1}^n , W_j^n and W_{j+1}^n are non-negative numbers under the CFL condition (2.1.28); see also the Time Estimate Lemma 3.2.5. Thus,

$$|W_j^{n+1}| \leq \left(\frac{1}{4} + \frac{k}{2h}H'(\theta_{j-1}) \right) |W_{j-1}^n| + \frac{1}{2}|W_j^n| + \left(\frac{1}{4} - \frac{k}{2h}H'(\theta_{j+1}) \right) |W_{j+1}^n|. \quad (3.2.34)$$

If we sum up for all $|j| \leq N$,

$$\sum_{|j| \leq N} |W_j^{n+1}| \leq \sum_{|j| \leq N} \left[\frac{1}{4} + \frac{k}{2h} H'(\theta_{j-1}) \right] |W_{j-1}^n| + \frac{1}{2} \sum_{|j| \leq N} |W_j^n| + \sum_{|j| \leq N} \left[\frac{1}{4} - \frac{k}{2h} H'(\theta_{j+1}) \right] |W_{j+1}^n|,$$

or rearranged the index of the sum in convenient form,

$$\sum_{|j| \leq N} |W_j^{n+1}| \leq \sum_{|j| \leq N+1} \left(\frac{1}{4} + \frac{k}{2h} H'(\theta_j) + \frac{1}{2} + \frac{1}{4} - \frac{k}{2h} H'(\theta_j) \right) |W_j^n| = \sum_{|j| \leq N+1} |W_j^n|.$$

Thus, by induction arguments (for n) plus the CFL condition for stability of finite difference Lagrangian-Eulerian scheme (3.2.5) essentially to assure the convexity, the result of Lemma 3.2.6 is then established. Next, to investigate the convergence of the Lagrangian-Eulerian approximations we will follow very closely the constructive strategy developed by J. Smoller [139] (Chapter 16, Lemmas 16.7, 16.8 and 16.9) thanks to an unexpected observation to put (3.2.1) into the form (3.2.5). For convenience of the reader we recall the key arguments in what follows, but highlighting the pertinent modifications to accommodate the proofs to our Lagrangian-Eulerian finite difference scheme (3.2.5). Thus, following the same constructive approach, we wish to consider the approximations as functions defined in the upper-half plane, i.e., $-\infty < x < \infty$ and $t \geq 0$. To this end, we will construct a family of functions $\{U_{k,h}\}$ extracted from the $\{U_j^n\}$ by defining,

$$U_{k,h}(x, t) = U_j^n, \quad (x, t) \in R, \quad (3.2.35)$$

where $R = \{(x, t) : jh \leq x \leq (j+1)h, nk \leq t \leq (n+1)k\}$, thus the value of $U_{k,h}$ in the rectangle R is the value of the difference approximation at the point (nh, jh) .

Lemma 3.2.7. (Lemma 16.7, Chapter 16 at [139]) There exist a sequence $U_{k_i, h_i} \subseteq U_{k,h}$ which converge to a measurable function $u(x, t)$ in the sense that for any $X > 0$, $t > 0$, and $T > 0$, both

$$\int_{|x| \leq X} |U_{k_i, h_i}(x, t) - u(x, t)| dx \longrightarrow 0, \quad (3.2.36)$$

$$\int_{0 \leq t \leq T} \int_{|x| \leq X} |U_{k_i, h_i}(x, t) - u(x, t)| dx dt \longrightarrow 0, \quad (3.2.37)$$

as $i \longrightarrow \infty$ (i.e., $(k_i, h_i) \longrightarrow (0, 0)$). Furthermore, the limit function satisfies $\sup_{\substack{x \in \mathbb{R} \\ t > 0}} |u(x, t)| \leq M$ and the stability inequality (3.2.7).

The proof start from Lemmas 3.2.1 and 3.2.4, which in turn we were successful in establishing the set of functions $U_{k,h}$ as functions of x that are uniformly bounded, and have uniformly bounded total variation on each bounded interval on any line $t = \text{const.} > 0$, with respect to the finite difference computational mesh grid k and h . The remaining of the proof is kept unchanged by invoking Helly's theorem to construct a subsequence $U'_{k,h}$ which in turn converges at each point on any bounded interval, but for all time lines $t = \text{const.} > 0$ in the upper-half plane. We recall that we have used a different stencil with respect to the spatial grid with length; see the finite difference form (3.2.5). Thus, Lemma 3.2.8 and Lemma 3.2.41 are our analogue versions of Lemma 16.8 and Lemma 16.9 of Chapter 16 proved in [139]. It will be shown that the limit function $u(x, t)$ satisfies the entropy inequality (3.2.6), by using the spatial distance $(x_1 - x_2) > h_i$ (instead of $(x_1 - x_2) > 2h_i$ in the very beginning) and $(U_j^n - U_{j-1}^n)$ (instead of $(U_j^n - U_{j-2}^n)$ in the r.h.s of (3.2.40)).

Lemma 3.2.8. The function $u(x, t)$ constructed in Lemma 3.2.7 satisfies an entropic inequality of the form (2.1.3).

Proof. It suffices to show that if $(x_1 - x_2) > h_i$ and $t > k_i$ that,

$$\frac{U_i(x_1, t) - U_i(x_2, t)}{x_1 - x_2} < \frac{E}{t - h_i}, \quad (3.2.38)$$

where the U_i 's are defined as in the proof of Lemma 3.2.7, and the constant E is defined in Lemma 3.2.2. This is so because if (3.2.38) holds, we get our desired result by passing to the limit as $i \rightarrow \infty$. Thus, let $x_1 > x_2$, and note that,

$$U_i(x_j, t) = U_i\left(x_j - \varepsilon_j, \left[\frac{t}{k_i}k_i\right]\right), \quad j = 1, 2, \quad (3.2.39)$$

for some ε_i , where $0 \leq \varepsilon_j \leq h_i$ thus,

$$\frac{U_i(x_1, t) - U_i(x_2, t)}{x_1 - x_2} = \frac{1}{x_1 - x_2} \sum (U_j^n - U_{j-1}^n), \quad (3.2.40)$$

where $n = [t/k_i]k_i$ and the sum over all integer in the interval $[x_2 - \varepsilon_2, x_1 - \varepsilon_1]$. Using Lemma 3.2.2, we have:

$$\begin{aligned} \frac{U_i(x_1, t) - U_i(x_2, t)}{x_1 - x_2} &\leq \frac{E(x_1 - \varepsilon_1 - x_2 + \varepsilon_2)}{[(t/k_i)]k_i(x_1 - x_2)} \\ &\leq \frac{E(x_1 - \varepsilon_1 - x_2 + \varepsilon_2)}{(t - k_i)(x_1 - x_2)} \\ &\leq \frac{E}{(t - k_i)} + \frac{E(\varepsilon_2 - \varepsilon_1)}{(t - k_i)(x_1 - x_2)} \\ &\leq \frac{2E}{(t - k_i)}. \end{aligned}$$

since $\varepsilon_2 - \varepsilon_1 \leq h_i \leq 1$, for i large, and thus the desired result of the Lemma 3.2.8 is established.

In the next Lemma 3.2.41 we make a direct use of the form Lagrangian-Eulerian finite difference scheme (3.2.5).

Lemma 3.2.9. Let $h_i \rightarrow 0$ as $i \rightarrow \infty$, and suppose that for $\phi \in C_0^3$,

$$\lim_{i \rightarrow \infty} \int_{-\infty}^{\infty} [U_i(x, 0) - u_0(x)] \phi(x, 0) dx = 0. \quad (3.2.41)$$

Then u satisfies

$$\iint_{t>0} (u\phi_t + H(u)\phi_x) dx dt + \int_{t=0} u_0(x) dx = 0, \quad (3.2.42)$$

for every test function $\phi \in C_0^1$ (associated with the initial value problem (3.1.1)).

Proof. Since ϕ is bounded and measurable, (3.2.41) holds if for every $X > 0$,

$$\lim_{i \rightarrow \infty} \int_{-X}^X |U_i(x, 0) - u_0(x)| dx = 0. \quad (3.2.43)$$

However, since u_0 is bounded and measurable, there exist step functions $U_h(x, 0)$, constant on intervals $jh \leq (j+1)h$, $j \in \mathbb{Z}$, which converge locally in L_1 to u_0 satisfying (3.2.43). As in [139], we take these functions to define the initial values of our Lagrangian-Eulerian scheme (3.2.5). We also note that this scheme can be written in the form,

$$\frac{U_j^{n+1} - U_j^n}{k} - \frac{U_{j-1}^n - 2U_j^n + U_{j+1}^n}{4k} + \frac{H(U_{j+1}^n) - H(U_{j-1}^n)}{2h} = 0. \quad (3.2.44)$$

Multiplying (3.2.44) by $\phi_j^n = \phi(jh, nk)$ reads,

$$\begin{aligned} & \frac{\phi_j^{n+1} U_j^{n+1} - \phi_j^n U_j^n}{k} - \frac{\phi_j^{n+1} - \phi_j^n}{k} U_j^{n+1} + \frac{h^2}{4k} \frac{2\phi_j^n - \phi_{j+1}^n - \phi_{j-1}^n}{h^2} U_j^n \\ & + \frac{\phi_{j+1}^n U_j^n - \phi_j^n U_{j-1}^n}{4k} + \frac{\phi_{j-1}^n U_j^n - \phi_j^n U_{j+1}^n}{4k} + \frac{\phi_{j+1}^n H(U_{j+1}^n) - \phi_{j-1}^n H(U_{j-1}^n)}{2h} \\ & - H(U_{j+1}^n) \frac{\phi_{j+1}^n - \phi_j^n}{2h} - H(U_{j-1}^n) \frac{\phi_j^n - \phi_{j-1}^n}{2h} = 0. \end{aligned}$$

The test function ϕ has compact support and $\phi_j^n = 0$ if $n \geq [T/k]$. Multiply (3.2) by hk and sum up for all $j \in \mathbb{Z}$, $n \in \mathbb{Z}_+$. Using the telescopic property at the first and fourth to sixth they cancel out, except for the first term with $k = 0$. Thus,

$$\begin{aligned} & -h \sum_j U_j^0 \phi_j^0 + hk \left(\sum_{j,k} \left[-U_j^{n+1} \frac{\phi_j^{n+1} - \phi_j^n}{k} - \frac{h^2}{4k} \frac{\phi_{j+1}^n - 2\phi_j^n + \phi_{j-1}^n}{h^2} U_j^n \right] \right) \\ & - hk \sum_{j,k} H(U_{j+1}^n) \frac{\phi_{j+1}^n - \phi_j^n}{2h} - hk \sum_{j,k} H(U_{j-1}^n) \frac{\phi_j^n - \phi_{j-1}^n}{2h} = 0. \end{aligned}$$

Since $U_{k,h}$ is piecewise constant, ϕ is smooth, and the integrals are limits of step functions, we can write:

$$\begin{aligned} & - \sum_j U_j^0 \phi_j^0 h = - \int_{t=0} U_{k,h} \phi + \delta_1, \\ & - \sum_{j,k} \frac{h^2}{4k} \frac{\phi_{j+1}^n - 2\phi_j^n + \phi_{j-1}^n}{h^2} U_j^n hk = - \frac{h^2}{4k} \iint_{t \geq 0} U_{k,h} \phi_{xx} + \delta_3, \\ & - \sum_{j,k} \left[U_j^{n+1} \frac{\phi_j^{n+1} - \phi_j^n}{k} \right] hk = - \iint_{t \geq 0} U_{k,h} \phi_t + \delta_2, \\ & - hk \sum_{j,k} H(U_{j+1}^n) \frac{\phi_{j+1}^n - \phi_j^n}{2h} = - \frac{1}{2} \iint_{t \geq 0} H(U_{k,h}) \phi_x + \hat{\delta}_4. \end{aligned}$$

With the above four identities we can write the immediately previous equation in weak form above as,

$$- \int_{t=0} U_{k,h} \phi + \delta_1 - \iint_{t \geq 0} U_{k,h} \phi_t + \delta_2 - \frac{h^2}{4k} \iint_{t \geq 0} U_{k,h} \phi_{xx} + \delta_3 - \iint_{t \geq 0} H(U_{k,h}) \phi_x + \delta_4 = 0,$$

where $\delta_i \rightarrow 0$ uniformly, as $h, k \rightarrow 0$. We replace $U_{k,h}$ by $U_i = U_{k_i, h_i}$ to get:

$$\iint_{t \geq 0} (U_i \phi_t + H(U_i) \phi_x) + \frac{h_i^2}{4k_i} \iint_{t \geq 0} U_i \phi_{xx} + \int_{t=0} U_i \phi = \delta(k_i, h_i). \quad (3.2.45)$$

Notice that $\delta(k_i, h_i) \rightarrow 0$ as $i \rightarrow \infty$. Thus, if $i \rightarrow \infty$, $U_i \rightarrow u$ locally in L_1 (Lemma 3.2.8), and $h_i \rightarrow 0$, $h_i^2/k_i \rightarrow 0$ (since h_i/k_i is bounded), so that, by choice of the initial data, we have

$$\frac{h_i^2}{4k_i} \iint_{t \geq 0} U_i \phi_{xx} \rightarrow 0, \quad \int_{t=0} U_i \phi \rightarrow \int_{t=0} u \phi, \quad \iint_{t \geq 0} U_i \phi_t \rightarrow \iint_{t \geq 0} u \phi_t,$$

and it finally reads,

$$\left| \iint_{t \geq 0} [H(U_i) - H(u)] \phi_x \right| \leq \|\phi_x\|_{L^\infty} \iint_{spt \phi} |H(U_i) - H(u)| \leq \|\phi_x\|_{L^\infty} \iint_{spt \phi} |H'(\xi)| |U_i - u|,$$

where ξ is some point in spt of ϕ , and there is a constant C independent of i so that,

$$\left| \iint_{t \geq 0} [H(U_i) - H(u)] \phi_x \right| \leq C \iint_{spt \phi} |U_i - u|, \quad (3.2.46)$$

Thus, we conclude that

$$\iint_{t \geq 0} H(U_i) \phi_x \rightarrow \iint_{t \geq 0} f(u) \phi_x. \quad (3.2.47)$$

With this, as $i \rightarrow \infty$,

$$\iint_{t > 0} (u \phi_t + H(u) \phi_x) dx dt + \int_{t=0} u_0(x) dx = 0, \quad (3.2.48)$$

and the proof of the Lemma 3.2.9 is now finished.

Thanks to the constructive strategy designed by J. Smoller in [139], we are ready to accomplish the final part of Theorem 3.2.1 we recall that (3.2.43) holds, and thus, so does (3.2.44). Notice that we have used our Lagrangian-Eulerian finite difference scheme (3.2.5) as a building block in all steps of the proof. But since C_0^3 is dense in C_0^1 it is also true we get that (3.2.44) holds for all $\phi \in C_0^1$. Thus u is indeed solution of our initial value problem (3.1.1) – in the sense of (3.2.42) – and, of course, u satisfies (3.2.6) and (3.2.7), and $|u| \leq \|u_0\|_{L^\infty}$.

Additionally, we mention the uniqueness of the entropy solution u to (3.1.1) with respect to the entropy condition (3.2.6) constructed by means of the Lagrangian-Eulerian finite difference scheme (3.2.5) also holds as it is described in details in appendix A. The demonstration of the uniqueness of the Lagrangian-Eulerian scheme follows the steps of the demonstration at [139] for the Lax-Friedrichs scheme. By means of the Theorem 3.2.1 and similar results it is also possible to benefit from the same results concerning the asymptotic behavior of the entropy solution to an N-wave; see [139], Chapter 16 Sections B and C for further details. Namely, that our scheme is able to numerically reproduce the expected asymptotic behavior of the entropy solution for long time simulations, e.g., to the initial value problem with respect to the inviscid Burgers equation. To conclude, we point out some further additional advantages of the similarity of structure of the Lagrangian-Eulerian scheme (3.2.5) with respect to the Lax-Friedrichs scheme to get further convergence proofs based on the very relevant works for conservation laws for construction of high order schemes [91, 124, 125, 143] and for discontinuous flux functions [16, 29, 94]. Indeed, central differencing based numerical schemes for hyperbolic with staggered-like control volumes

seems to benefit from a natural structure to capture approximate entropy shock solutions (e.g., [94, 124, 151]), which have already been successfully applied to balance laws problems [115] and to the case of numerical simulation of non-classical waves in three-phase problems in porous media problems [1, 2]. Thus, [124, 125] is viewed as a high-order sequel to the celebrated first-order Lax-Friedrichs on a staggered grid, which in turn also exhibit good shock capturing entropy properties [16, 29, 91, 94, 124, 125, 143, 151].

3.3 The finite difference Lagrangian-Eulerian scheme in conservative form

We recall that a numerical formulation of the type Lagrangian-Eulerian scheme for nonlinear case, which we presented as a generalization of the Lagrangian-Eulerian scheme (2.1.15),

$$U_j^{n+1} = \frac{1}{4}(U_{j-1}^n + 2U_j^n + U_{j+1}^n) - \frac{k}{2h}(H(U_{j+1}^n) - H(U_{j-1}^n)), \quad (3.3.1)$$

where $k = k^n$ and with CFL condition

$$\max_j \left| H'(U_j^n) \frac{k}{h} \right| \leq \frac{\sqrt{2}}{2} \quad (3.3.2)$$

with conservative form

$$U_j^{n+1} = U_j^n - \frac{k}{h}(\bar{F}(U_j^n, U_{j+1}^n) - \bar{F}(U_{j-1}^n, U_j^n)), \quad (3.3.3)$$

where

$$\bar{F}(U_j^n, U_{j+1}^n) = \frac{1}{4} \left[\frac{h}{k}(U_j^n - U_{j+1}^n) + 2(H(U_{j+1}^n) + H(U_j^n)) \right]. \quad (3.3.4)$$

We note that the flux in the above expression satisfies a consistency condition $\bar{F}(\bar{u}, \bar{u}) = H(\bar{u})$ and to make the numerical scheme is consistent with the original conservation law (2.1.1) some smoothness is also required and it is possible to prove that the flux (3.3.4) satisfies one the Lipschitz continuous condition as

$$|\bar{F}(v, w) - H(\bar{u})| \leq K \max(|v - \bar{u}|, |w - \bar{u}|), \quad (3.3.5)$$

for all v, w with $|v - \bar{u}|$ and $|w - \bar{u}|$ sufficiently small. The above observation about the nonlinear Lagrangian-Eulerian scheme (3.3.3) is that it satisfies a consistency condition which is necessary in order to apply the Lax-Wendroff theorem [147], ensuring the convergence for the weak solution.

Another important observation is that when we write the scheme in explicit form (3.3.1), and directly calculate,

$$\begin{aligned} \frac{\partial U_j^{n+1}}{\partial U_i^n} &= 0, \quad i \neq j-1, j, j+1, \\ \frac{\partial U_j^{n+1}}{\partial U_{j-1}^n} &= \frac{1}{2} \left[\frac{1}{2} + \frac{k}{h} H'(U_{j-1}^n) \right], \quad \frac{\partial U_j^{n+1}}{\partial U_j^n} = \frac{1}{2}, \quad \frac{\partial U_j^{n+1}}{\partial U_{j+1}^n} = \frac{1}{2} \left[\frac{1}{2} - \frac{k}{h} H'(U_{j+1}^n) \right] \end{aligned} \quad (3.3.6)$$

then, we see that all these right-hand sides are nonnegative, therefore the scheme is monotone and TVD [42, 75, 76], whenever the CFL condition

$$\max_j \left| H'(U_j) \frac{k}{h} \right| \leq \frac{1}{2} \quad (3.3.7)$$

is satisfied. And it is well known that for monotone schemes automatically satisfy a Kružkov-type discrete entropy inequality, and therefore approximations converge to an entropy solution

Numerical experiments reveal that the scheme (3.3.1) converge for the weak solution, however this numerical method cannot be derived with what was performed in the linear case.

3.4 Numerical experiments for hyperbolic problems with convex and nonconvex fluxes

Relaxation is known to provide a subtle dissipative mechanism for discontinuities against the destabilizing effect of nonlinear response (see e.g., [38, 67] and references therein).

For any given system of conservation laws, we will construct a corresponding linear hyperbolic system with a stiff source term that approximates the original system with a small dissipative correction [38, 143]. The relaxation approximation to balance law problems can also be used to construct numerical approximations to the equilibrium purely hyperbolic conservation law problems. In [88], Jin and Xin developed a class of first- and second-order nonoscillatory numerical schemes for the conservation laws based on this approach without the need to use a computational grid within the order of the relaxation parameter.

A general convergence theory for one dimensional scalar convex conservation laws was developed by Tadmor and coauthors. The central schemes are simple, efficient and numerically stable with good entropy properties [69, 99, 124, 125, 126, 143] (see also [94, 151]). Additionally, in the one dimensional case the limiting relaxed numerical flux function bears some similarity with the second-order non-oscillatory central differencing scheme developed by Nessyahu and Tadmor [124], in the sense that they both are not Riemann-solver based schemes and then avoiding the costly upwinding on this approach [39, 124, 143]. with applications to correct approximations of balance laws (see [115, 130]).

Central differencing based numerical schemes for hyperbolic with staggered-like control volumes seem to benefit of a natural structure to capture approximate entropy shock solutions (e.g., [94, 124, 151]), which have already been successfully applied to balance laws problems [115, 130] and to the case of numerical simulation of non-classical waves in three-phase problems in porous media problems [1, 2]. Thus, we use classical Nessyahu and Tadmor [124] for comparison purposes. This is a high-order sequel to the celebrated first-order Lax-Friedrichs on a staggered grid, which in turn also exhibit good shock capturing entropy properties [1, 2, 94, 151].

In order to give a somewhat concrete evidence we are computing “good approximations” to correct entropy solutions, we will illustrate the viability of the proposed Lagrangian-Eulerian scheme for the numerical simulation of initial value problems for convex and non-convex flux-type functions.

Example 3.4.1. Inviscid Burgers’ equation with smooth initial data.

We consider inviscid Burgers’ equation, numerical approximate solutions with scheme LEH2 (3.2.1) are shown in Figure (3.1) to the Cauchy Problem (Initial Value Problem with convex

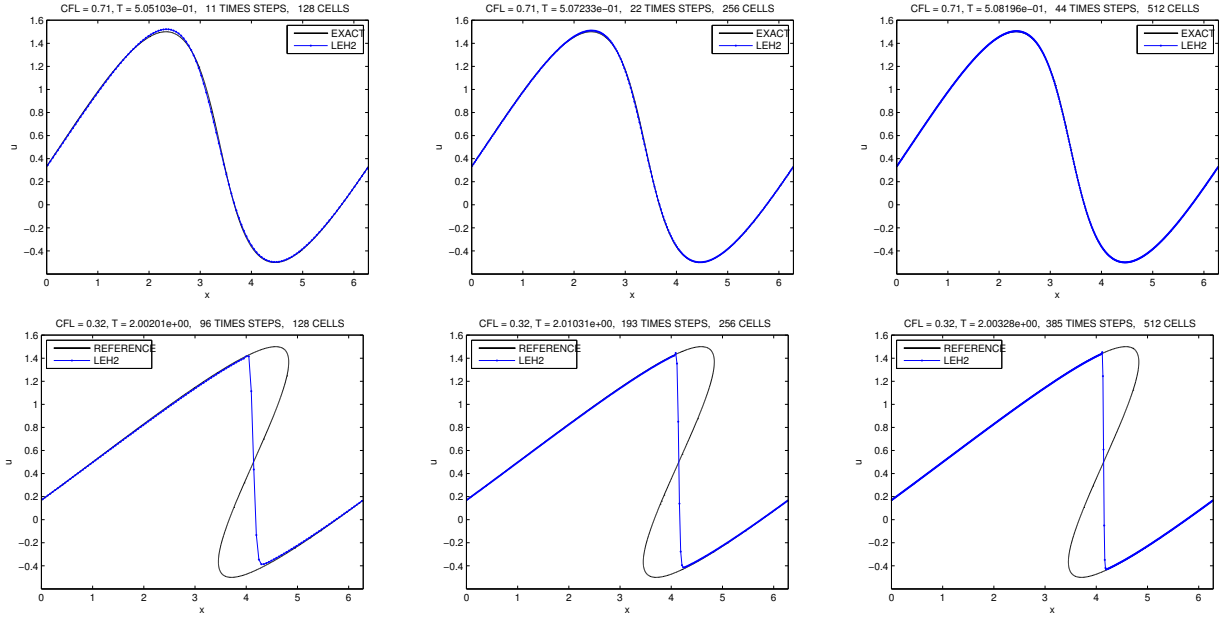


Figure 3.1: **Pre-shock** and **post-shock** solutions computed with LEH2 scheme (3.2.1).

flux function): $u_t + \left(\frac{u^2}{2}\right)_x = 0$, along with smooth initial data $u(x, 0) = 0.5 + \sin(x)$ (see, e.g., [99]). It is well-known the solution of this problem develops a shock discontinuity at the critical time $T_c = 1$, and then it exhibits pre-shock solution for $T_c < 1$ and post-shock solution to $T_c > 1$. In top pictures of Figures 3.1 are shown the pre-shock solutions and in bottom pictures are shown post-shock solutions computed with LEH2 scheme (3.2.1) at time simulation $t = 2$ for 128 cells (left), 256 cells (middle) and 512 (right).

Example 3.4.2. Inviscid Burgers' equation with discontinuous initial data.

We have also conducted similar numerical experiments to that reported in Figure 3.1, but to problem $u_t + \left(\frac{u^2}{2}\right)_x = 0$ along with discontinuous initial data $u(x, 0) = \eta(x) = 1, x < 0$ and $u(x, 0) = \eta(x) = 0, x > 0$. In top pictures are shown snapshot graphs at time $t = 2.4$ of simulation a shock wave moving from left to right. We get a very nice looking numerical approximate solution with scheme LEH2 (3.2.1) propagating at entirely entropy-correct Rankine-Hugoniot speed. We have also considered Burgers' problem $u_t + \left(\frac{u^2}{2}\right)_x = 0$ along with data $u(x, 0) = \eta(x) = 0, x < 0$ and $u(x, 0) = \eta(x) = 1, x > 0$. In Figure 3.2, bottom pictures are shown snapshot graphs at time $t = 1$ of simulation for a moving rarefaction wave from left to right, where the rarefaction wave is spreading out correctly and matching with the exact solution there.

Example 3.4.3. Buckley-Leverett equation

Numerical approximate solutions with scheme LEH2 (3.2.1) are shown to the Riemann Problem (Initial Value Problem with non-convex flux function): $u_t + f_x(u) = 0$, along with Riemann initial data $u(x, 0) \equiv \eta(x) = 1, x < 0$ and $u(x, 0) \equiv \eta(x) = 0, x > 0$. On physical grounds, such initial data corresponds to waterflooding of an oil reservoir. The well known solution for this model comprises a leading shock wave (an oil bank) followed by an attached rarefaction wave. The smoothing of the saturation profile observed at the trailing edge of the

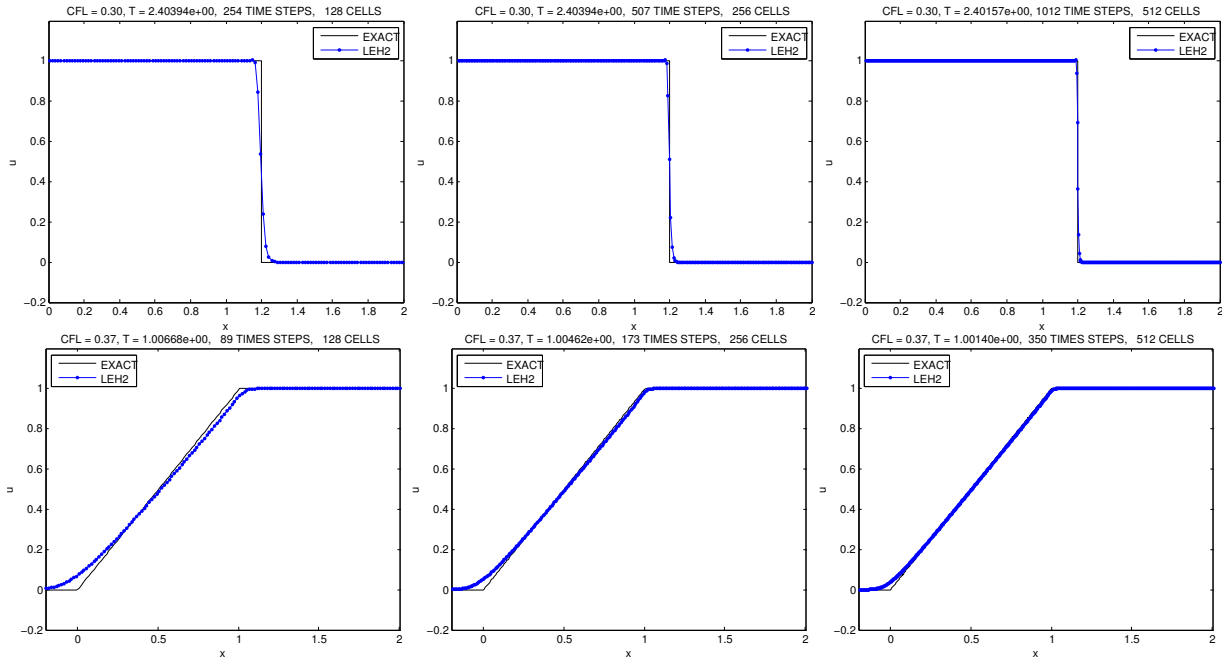


Figure 3.2: Numerical approximation with **discontinuous** initial data.

rarefaction wave where $u = 0.8$, is solely the effect of numerical dissipation. The weak solution satisfying the Oleinik entropy condition is in very good agreement, along with the LEH1 and LEH2 schemes, propagating at entirely entropy-correct Rankine-Hugoniot speed and with the precisely post-shock value. In Figure 3.3 are shown numerical solutions with 128 cells (top) and 256 cells (bottom) advanced at times $t = 0.3$ (left), $t = 0.6$ (middle) and $t = 1$ (right).

Example 3.4.4. Other non-convex flux

We have also considered another non-convex flux function, approximated with scheme LEH2 (3.2.1), to the scalar conservation law $u_t + f_x(u) = 0$, namely $f(u) = 0.5(e^{-25(u-0.5)^2} + 8(u - 0.5)^2)$, and with same Riemann data. Again, the numerical solutions is in agreement with Oleinik entropy condition, whose approximate left and right shock waves are propagating with correct Rankine-Hugoniot speed and entropy-correct post-shock values. In Figure 3.4 are shown numerical approximations with 256 cells (top) and 512 cells (bottom). Snapshot graphs at simulation times $t = 0.3$ (left), $t = 0.6$ (middle) and $t = 1$ (right).

3.5 Numerical experiments with discontinuous flux functions, model problems Adimurthi, J. Jaffré and V. Gowda §3.5.1 and R. Burger, K. H. Karlsen and J. D. Towers §3.5.2

We turn our attention to consider examples for scalar conservation laws with discontinuous flux function as discussed in [14] and [29], which in turn was numerically handled by a Godunov method and by a Engquist-Osher type scheme, respectively. Here we were able to successfully reproduce the same qualitative solutions and features with the aid of our Lagrangian-Eulerian

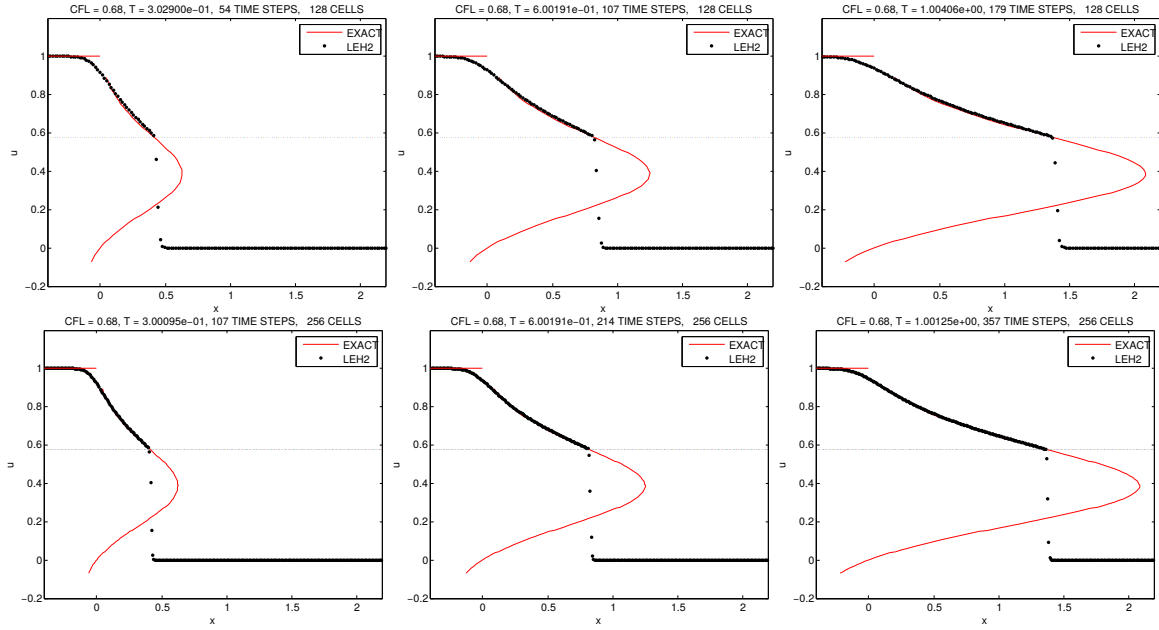


Figure 3.3: Buckley-Leverett with discontinuous initial data.

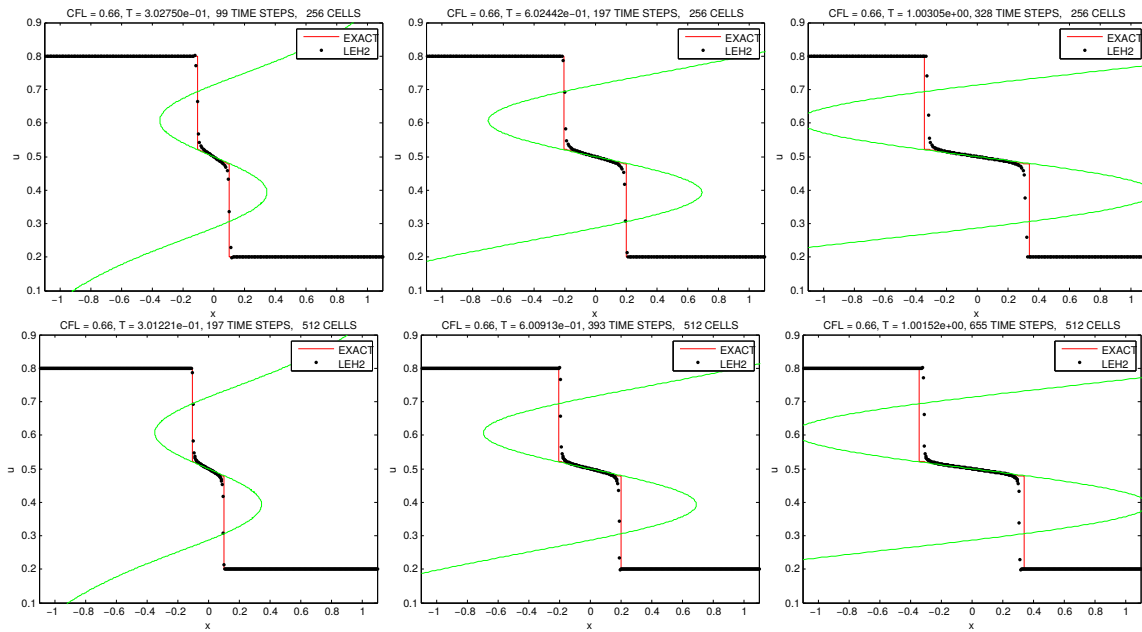


Figure 3.4: Numerical approximation with other non-convex flux

scheme with a convenient Ranking-Hugoniot compatibility condition at the discontinuity. In order to demonstrate the algorithm behavior and its applicability Although with a higher number of computational grid cells, the new numerical scheme is very easy to code and very fast to run on basic laptop as a serial code in a single core for the 1D and 2D numerical experiments. Our interest specifically is over the IVP,

$$\frac{\partial u}{\partial t} + \frac{\partial F(x, u)}{\partial x} = 0, \quad (x, t) \in \mathbb{R} \times (0, T), \quad u(x, 0) = u_0(x), \quad x \in \mathbb{R}, \quad (3.5.1)$$

$$F(x, u) = H(x)f(u) + (1 - H(x))g(u) = f(u), \quad x \geq 0 \quad (3.5.2)$$

or

$$F(x, u) = H(x)f(u) + (1 - H(x))g(u) = g(u), \quad x < 0, \quad (3.5.3)$$

here (as in [14] and [29]) $H(x)$ is the Heaviside function, and the functions g and f are taken as smooth functions on an interval $I \subseteq \mathbb{R}$, with the same endpoints s and S , with $s < S$. Notice, the flux function $F(x, u)$ into this problem has a spatial dependence of the discontinuous point $x = 0$. As discussed in details in [14], a solution of (3.5.1) – in the weak sense – is a u function in $L_{loc}^\infty(\mathbb{R} \times \mathbb{R}^+)$ such that for all $\phi \in C_{loc}^\infty(\mathbb{R} \times \overline{\mathbb{R}^+})$,

$$\int_{-\infty}^{\infty} \int_0^{\infty} \left(u \frac{\partial \phi}{\partial t} + F(x, t) \frac{\partial \phi}{\partial x} \right) dt dx + \int_{-\infty}^{\infty} u_0(x) \phi(x, 0) dx = 0, \quad (3.5.4)$$

then u satisfies (3.5.1) if and only if in the weak sense u satisfies,

$$\frac{\partial u}{\partial t} + \frac{\partial g(u)}{\partial x} = 0, \quad x < 0, \quad t > 0, \quad \frac{\partial u}{\partial t} + \frac{\partial f(u)}{\partial x} = 0, \quad x > 0, \quad t > 0, \quad (3.5.5)$$

By the examples here treated it is assumed, as in [29], that $f, g \in Lip([0, 1])$, $f(u) = g(u)$ for $u = 0, 1$, f has a single maximum at $u_f^* \in [0, 1]$, and g has a single maximum at $u_g^* \in [0, 1]$. The function f is strictly increasing on $(0, u_f^*)$, and strictly decreasing on $(u_f^*, 1)$, and likewise, g is strictly increasing on $(0, u_g^*)$, and strictly decreasing on $(u_g^*, 1)$, and we assume that f and g are genuinely nonlinear in the sense that f and g are nonlinear on any non-degenerate interval. We also assumed that there is at most one $u_\chi \in (0, 1)$, where $f(u_\chi) = g(u_\chi)$, and if there is such an intersection point u_χ , then the graphs of f and g are assumed to intersect transversally at u_χ (a flux crossing), see e.g [14, 29]. For the initial data, it is assumed that $u_0 \in L^\infty$ such that $u_0(x) \in [0, 1]$ for a.e. $x \in \mathbb{R}$. Indeed, when fixed $t \in (0, T)$, it is defined $u_\pm := u(0\pm, t)$. Any weak solution of (3.5.1) will satisfy the Rankine-Hugoniot condition,

$$g(u_-) = f(u_+). \quad (3.5.6)$$

In [14, 29] are imposed the following requirements, which in turn we reproduce here for the sake of completeness.

Definição 3.5.1. (strong characteristic condition). Assume that the pair (u_-, u_+) satisfies (3.5.6). We say that (u_-, u_+) satisfies the strong characteristic condition if,

$$\min\{0, g'(u_-)\} \max\{0, f'(u_+)\} = 0. \quad (3.5.7)$$

Definição 3.5.2. (connection (A, B)). Assume that the functions f and g satisfy all assumptions stated so far. Then a pair of states (A, B) is called a connection if,

$$g(A) = f(B), \quad u_g^* \leq A \leq 1, \quad 0 \leq B \leq u_f^*. \quad (3.5.8)$$

Definição 3.5.3. ((A, B)-characteristic condition). If (u_-, u_+) satisfies (3.5.6) and (A, B) is a connection, then (u_-, u_+) is said to satisfy the (A, B) -characteristic condition if,

$$\min\{0, g'(u_-)\} \max\{0, f'(u_+)\} = 0, \quad \text{if } (u_-, u_+) \neq (A, B). \quad (3.5.9)$$

The Lagrangian-Eulerian scheme for discontinuous flux function. The straightforward extension of our scheme LEH2 (3.2.1) is given by,

$$U_j^{n+1} = \frac{1}{4} [U_{j-1}^n + 2U_j^n + U_{j+1}^n] - \frac{k}{2h} [F(x_{j+1}, U_{j+1}^n) - F(x_{j-1}, U_{j-1}^n)], \quad (3.5.10)$$

where $F(x_{j-1}, U_{j-1}^n)$ and $F(x_{j+1}, U_{j+1}^n)$ are the discontinuous flux function described in (3.5.1) and (3.5.3), which in turn the associated consistent numerical flux related to the conservative form of (2.1.14), can be written as:

$$\bar{F}(U_j^n, U_{j+1}^n) = \frac{1}{4} \left\{ \frac{h}{k} (U_j^n - U_{j+1}^n) + 2 [F(x_{j+1}, U_{j+1}^n) + F(x_j, U_j^n)] \right\}. \quad (3.5.11)$$

Model Problem 3.5.1. Adimurthi, Jaffré & V. Gowda, (SINUM, 2004), Flow in porous media with two rocks types [14].

In the first numerical experiment, we consider, as [14], an idealized flow in which two phases of different densities are flowing in a vertical closed core, in which the porous media is composed by two different rock types creating a discontinuity, mathematically in $x = 0$. Thus, the core is made of two rocks types where the upper part is related with g function, and the down part is related with f function. Such functions are defined as,

$$\begin{aligned} f(u) &= \frac{1}{\phi} \frac{\lambda_1}{\lambda_1 + \lambda_2} (q + (c_1 - c_2) \lambda_2) = \frac{10u^2 (20(1-u)^2)}{10u^2 + 20(1-u)^2}, \quad x > 0, \\ g(u) &= \frac{1}{\phi} \frac{\mu_1}{\mu_1 + \mu_2} (q + (c_1 - c_2) \mu_2) = \frac{50u^2 (5(1-u)^2)}{50u^2 + 5(1-u)^2}, \quad x < 0, \end{aligned} \quad (3.5.12)$$

where are associated the following porous media data; $\phi = 1$, $q = 0$, $c_1 = 2$, $c_2 = 1$, $s = 0$, $S = 1$, $\lambda_1 = 10u^2$, $\lambda_2 = 20(1-u)^2$, $\mu_1 = 50u^2$ and $\mu_2 = 5(1-u)^2$. Note that here, $f(s) = g(s) = 0$ and $f(S) = g(S) = 0$. In this problem, we will use the Lagrangian-Eulerian scheme along with the associated numerical flux (3.5.10). The $F_j^n = F(x_j, U_j^n)$ approximation is in concordance with (3.5.5) and (3.5.6) as follows,

$$F_j^n = \begin{cases} g(U_j^n), & j < 0, \\ \frac{1}{2} [g(U_j^n) + f(U_j^n)] + \frac{1}{2} \min\{f_{\max}, g_{\min}\}, & j = 0, \\ f(U_j^n), & j > 0, \end{cases} \quad (3.5.13)$$

where $f_{\max} = f(\max\{u_f^*, U_1^n\})$ and $g_{\min} = g(\min\{u_g^*, U_{-1}^n\})$. We take the index $j = 0$ as corresponding to the point $x = 0$ in the mesh grid. The resulting approximate solutions are shown in Figure 3.5, which in turn shows the numerical solutions at times $t = 0.5, 1, 2$, and with initial data $u_0(x) = 1$, $x < 0$, $u_0(x) = 0$, $x > 0$. In physical grounds this represent two flows, one heavy fluid (say phase 1) on the left side of $x = 0$ and one light fluid (say

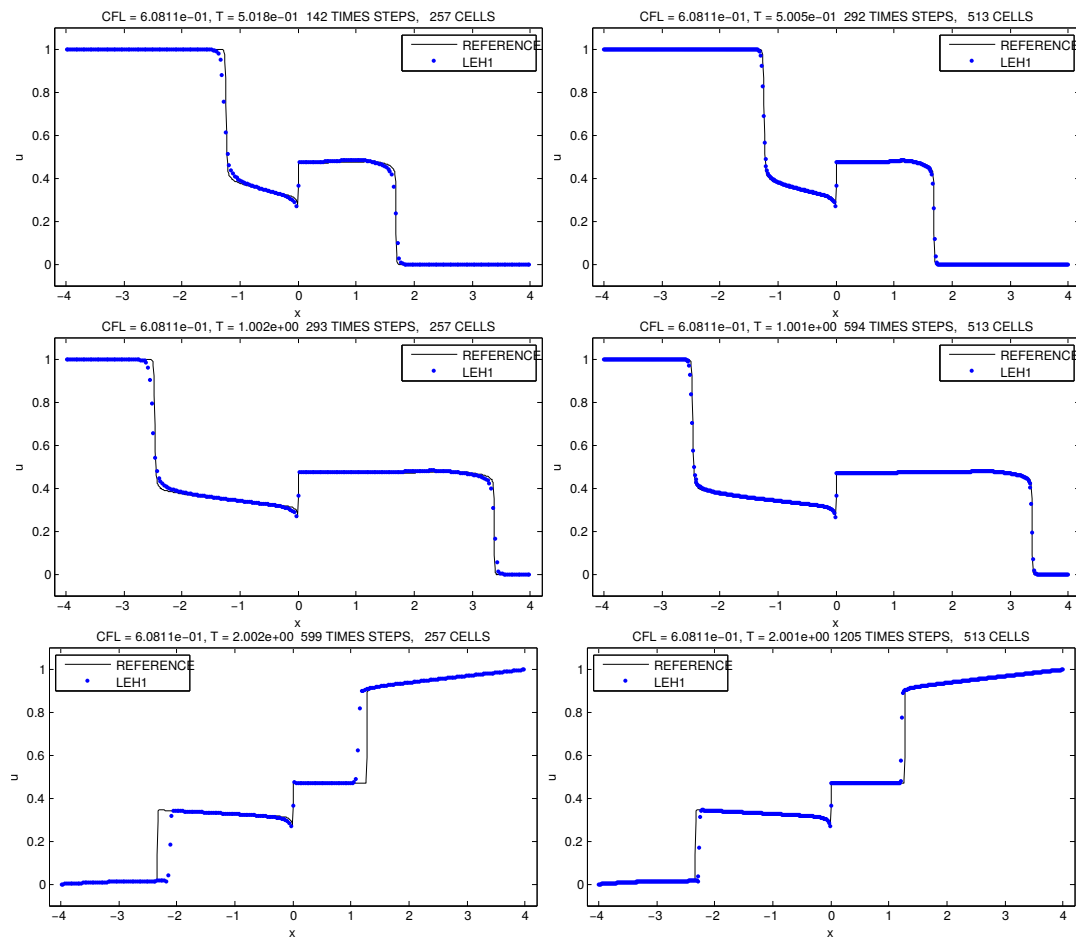


Figure 3.5: Numerical approximation with initial data $u_0(x) = 1, x < 0, u_0(x) = 0, x > 0$

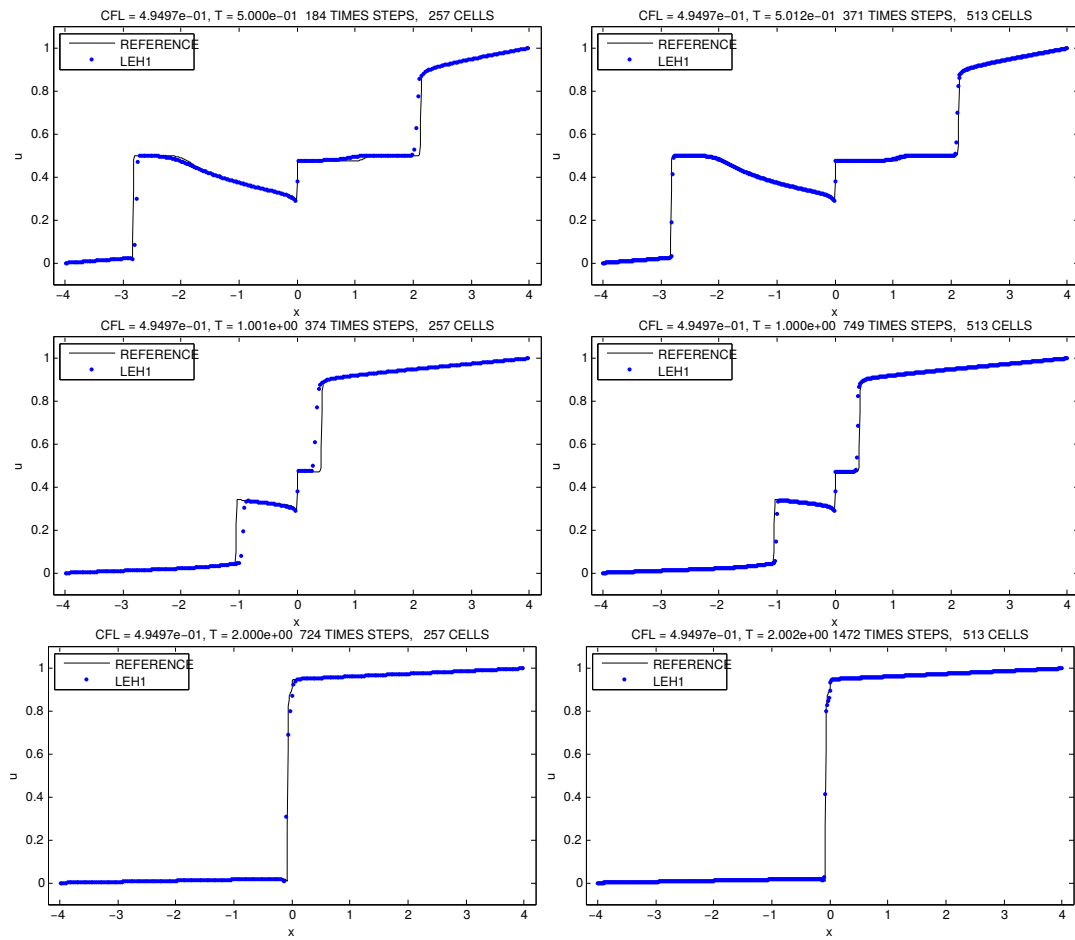


Figure 3.6: Lagrangian-Eulerian solutions calculated with numerical flux (3.5.10) to initial data $u_0(x) = 0.5$.

phase 2) on the right side of $x = 0$. Thus, as the time goes from $t > 0$, the heavy fluid will go to occupy bottom (right) region of the repository as well as the light fluid will go to occupy the top (left) region of the same repository, showing agreement with [14]. In Figure 3.5 are shown computed solutions with our scheme (3.5.10) for this problem, approximate solutions are using a mesh size of 257 cells (left) and 513 cell (right), these approximations were compared with an approximate reference solution, which was calculated with a mesh size of 1025 cells with the same numerical, and in a very good qualitative resemblance as in [14] scheme. The approximations were advanced at times $t = 0.5, 1, 2$ being shown in the top frame, the approximation at $t = 0.5$, in meddle frame to time $t = 1$ and finally in bottom frame at $t = 2$. In addition, we included the elapsed computation times which are as follows: 0.241466 secs (top left), 0.576391 secs (top right), 0.833043 secs (meddle left), 1.359240 secs (meddle right), 2.010356 secs (bottom left) and 4.164250 secs (bottom right). In Figure 3.6 are shown Lagrangian- Eulerian approximation calculated with the same flux (3.5.10) and with initial data $u_0(x) = 0.5$. In the approximations were used a mesh grid of 257 cells (left) and of 513 cells (right), and again numerical approximations were compared with an reference approximated solution calculated with 1025 cells and the same numerical scheme.

Model Problem 3.5.2. Burger, Karlsen & Towers, (SINUM, 2009), Lagrangian-Eulerian scheme with discontinuous flux adapted to flux connections [29].

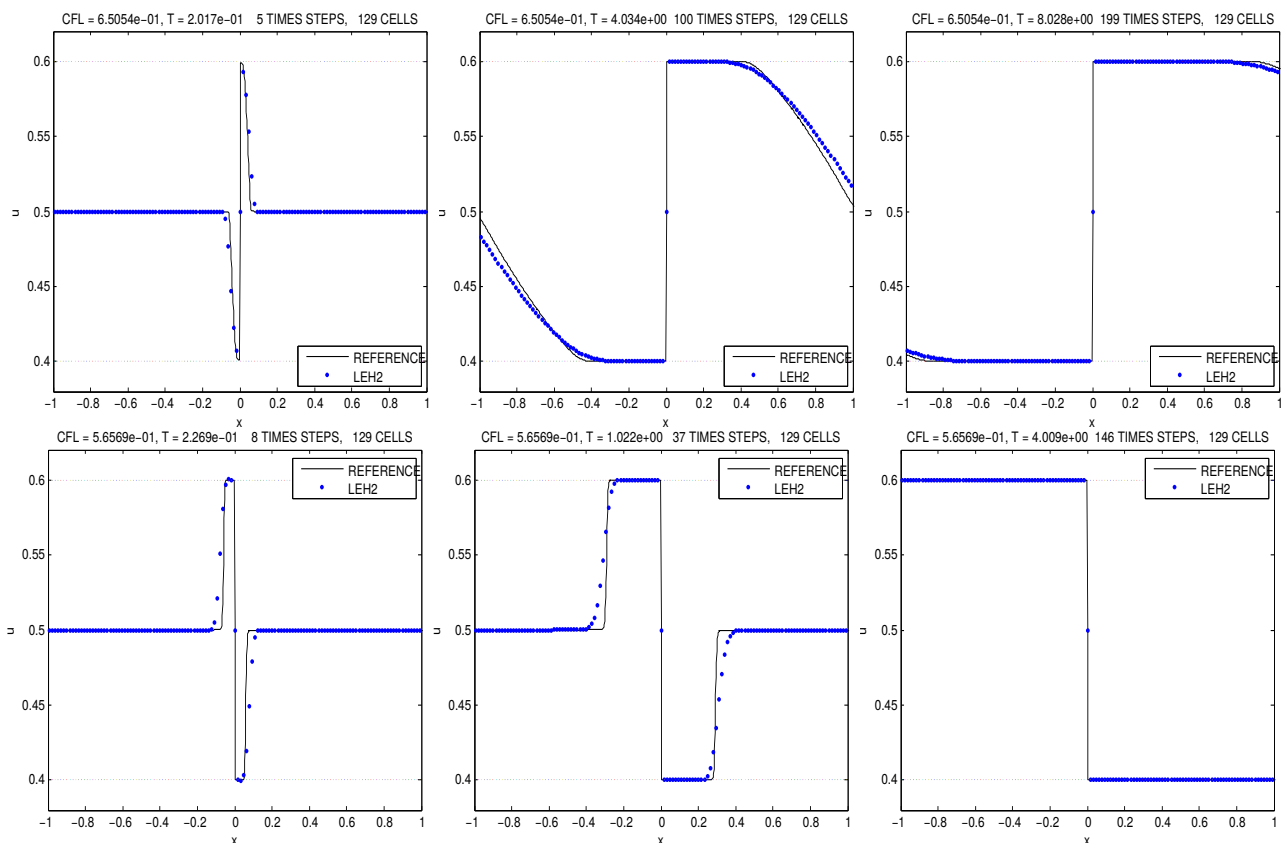


Figure 3.7: Numerical approximation with discontinuous flux adapted to flux connections.

Based in the numerical results obtained with our new Lagrangian-Eulerian scheme, we can say that the new method is very efficient computationally because the computational time is

small given the difficult characteristic of the problem, which have a discontinuous flux and, in addition with very good numerical solutions compared with the obtained in [14] with a Godunov-type method.

We now consider (3.5.1) and (3.5.3), but following the model problem as considered in [29]; see [14, 29] for more details and relevant mathematical theory to the underlying model. As before, we used our Lagrangian-Eulerian scheme (3.5.10), where the discontinuous flux approximation is now given by,

$$F_j^n = F(x_j, U_j^n) = \begin{cases} g(U_j^n), & j < 0, \\ C(A, B), & j = 0 \\ f(U_j^n), & j > 0, \end{cases} \quad (3.5.14)$$

where

$$C(A, B) = \frac{1}{2} (f(A) + g(B)) - \frac{1}{2} \left[\int_B^{U_1} |f'(w)| dw - \int_A^{U_{-1}} |g'(w)| dw \right] \quad (3.5.15)$$

and we define the connection (A, B) as being $u_L = U_{-1}$ and $u_R = U_1$, with initial data $u_0 = 0.5$ along with $\mu_\chi = 0.5$. Notice that in the considered examples $A < \mu_\chi < B$ with $g(A) = f(B)$, the Rankine-Hugoniot condition. Figure 3.7 shows approximations with the Lagrangian-Eulerian scheme (3.5.10), but based in the numerical flux function as proposed in [29] of Engquist-Osher-Type scheme. The approximate solutions were computed in a mesh size of 129 cells at times $t = 0.2, 4, 8$ for the same flux functions $f(u) = u^2(1 - u)$, $g(u) = u(1 - u)^2$ and initial data $u_0 = u_\chi = 0.5$, but for two distinct connections: connection $(A, B) = (0.4, 0.6)$ at top frames and connection $(A, B) = (0.6, 0.4)$ at bottom frames. To better knowledge of our numerical scheme we also include the computational times to each simulated example, the computational times are respectively: 0.020912 secs (top left), 0.404522 secs (top middle), 0.878328 secs (top right), 0.028541 secs (bottom left), 0.554558 secs (bottom middle) and 0.893478 secs (bottom right). Again, the qualitative solutions achieved by our Lagrangian-Eulerian scheme is comparable with those reported in [29]. Again in this numerical example our Lagrangian-Eulerian scheme should be very efficient computationally and with good qualitative properties in its approximations.

Chapter 4

The Lagrangian-Eulerian approach to nonlinear hyperbolic conservation laws

In the previous section we studied the Lagrangian-Eulerian scheme for linear and nonlinear conservation laws of the type (2.1.1 and 2.1.1). Here we will provide a formal construction to analogue Lagrangian-Eulerian scheme to the nonlinear case. We also will present some representative numerical experiments, computed by a Lagrangian-Eulerian scheme version for the nonlinear scalar conservation law along with discontinuous initial data, with **convex** and **non-convex** nonlinear flux functions, such as Burger's and Buckley-Leverett Equation in order to give some numerical evidence we are computing "good approximations" to the true entropy solutions to these problems. To prove the convergence of this scheme, we use some results of the classical theory, which will be discussed in the next section.

4.1 The Lagrangian-Eulerian scheme in conservative form

We essentially mimic the procedure of the linear case, but now notice that the curves $\sigma_j^n(t)$ are not straight lines in general but rather solutions of the differential equations system (2.1.8); we write here again for clarity of presentation:

$$\frac{d\sigma_j^n(t)}{dt} = \frac{H(u)}{u}, \quad t^n < t \leq t^{n+1},$$

with the initial condition $\sigma_j^n(t^n) = x_j^n$, related to the differential problem:

$$\frac{\partial u}{\partial t} + \frac{\partial H(u)}{\partial x} = 0, \quad u(x, 0) = \eta(x). \quad (4.1.1)$$

The idea here is to use the linear Lagrangian-Eulerian scheme as building block to construct *local* approximations with the natural first choice to develop a fully explicit scheme $f_j^n = \frac{H(U_j^n)}{U_j^n} \approx \frac{H(u)}{u}$ with the initial condition $\sigma_j^n(t^n) = x_j^n$ (see Figure 4.1). Now, the solutions $\sigma_j^n(t)$ of the differential equations (2.1.8) system are (local) straight lines, but they are not parallel as in the linear case. In order to start the procedure let us first revisit the coefficients in the linear case,

$$c_{0j} = \frac{h}{2} + f_j^n k^n \quad \text{and} \quad c_{1j} = \frac{h}{2} - f_j^n k^n, \quad \text{with} \quad \max_j \left| \frac{f_j \Delta t^n}{h} \right| < \frac{\sqrt{2}}{2} \quad \text{and} \quad k^n = \min_n \Delta t^n, \quad (4.1.2)$$

where the stability CFL condition in (4.1.2) is given by the construction of the Lagrangian-Eulerian scheme. Thus, we use equations (2.1.9)-(2.1.10) to write:

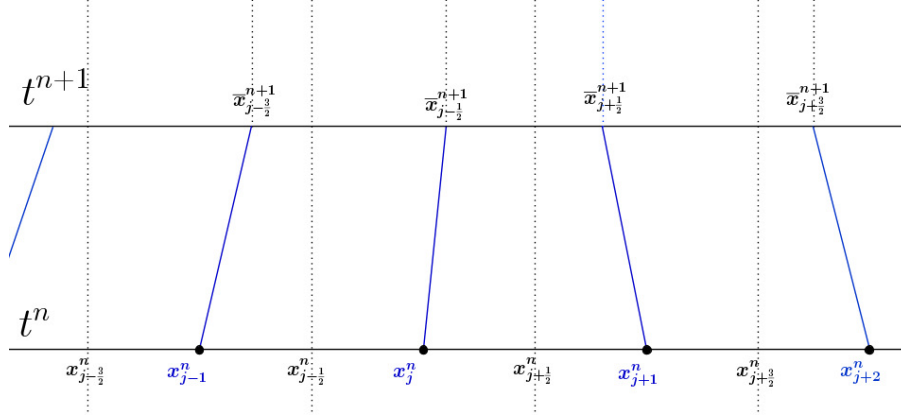


Figure 4.1: Lagrangian-Eulerian scheme nonlinear case

$$\bar{U}_j^{n+1} = \frac{1}{h_j^{n+1}} \frac{1}{2} h [U_j^n + U_{j+1}^n], \quad (4.1.3)$$

and plugging this into (2.1.11) reads,

$$\begin{aligned} U_j^{n+1} &= \frac{1}{h} \left[c_{0j} \frac{1}{h_{j-1}^{n+1}} \frac{h}{2} (U_{j-1}^n + U_j^n) + c_{1j} \frac{1}{h_j^{n+1}} \frac{h}{2} (U_j^n + U_{j+1}^n) \right] \\ &= \frac{c_{0j}}{2} \frac{1}{h_{j-1}^{n+1}} (U_{j-1}^n + U_j^n) + \frac{c_{1j}}{2} \frac{1}{h_j^{n+1}} (U_j^n + U_{j+1}^n). \end{aligned} \quad (4.1.4)$$

Now, notice that for each $j \in \mathbb{Z}$,

$$h_j^{n+1} = \bar{x}_{j+\frac{1}{2}}^{n+1} - \bar{x}_{j-\frac{1}{2}}^{n+1} = x_{j+1}^n + f_{j+1}^n k^n - (x_j^n + f_j^n k^n) = h + (f_{j+1}^n - f_j^n) k^n, \quad (4.1.5)$$

and, also that:

$$h_j^{n+1} = h + (f_{j+1}^n - f_j^n) k^n = \left(\frac{h}{2} + f_{j+1}^n k^n \right) + \left(\frac{h}{2} - f_j^n k^n \right) = c_{0j+1} + c_{1j}. \quad (4.1.6)$$

On the other hand we have,

$$c_{0j} = h_{j-1}^{n+1} - c_{1j-1} \quad \text{and} \quad c_{1j} = h_j^{n+1} - c_{0j+1} \quad (4.1.7)$$

along with,

$$\begin{aligned} c_{1j-1} &= \frac{h}{2} - f_{j-1}^n k^n & c_{0j+1} &= \frac{h}{2} + f_{j+1}^n k^n \\ &= \frac{1}{2} (h_{j-1}^{n+1} - f_{j-1}^n k^n - f_j^n k^n) & &= \frac{1}{2} (h_{j+1}^{n+1} + f_{j+1}^n k^n + f_j^n k^n). \end{aligned}$$

Finally, plugging (4.1.7) into (4.1.4) we get, along with $\mathbb{W}(U_j^n, U_{j+1}^n) \equiv \frac{f_j^n + f_{j+1}^n}{h_j^{n+1}} (U_j^n + U_{j+1}^n)$,

$$U_j^{n+1} = \frac{1}{4} [U_{j-1}^n + 2U_j^n + U_{j+1}^n] - \frac{k^n}{4} (\mathbb{W}(U_{j+1}^n, U_j^n) - \mathbb{W}(U_{j-1}^n, U_j^n)). \quad (4.1.8)$$

The finite difference scheme (4.1.8) is the *new Lagrangian-Eulerian scheme* for the nonlinear problem (4.1.1). Hereafter this numerical scheme will be called LEH1 (Lagrangian Eulerian Hyperbolic scheme 1). Notice, if we set $f_j^n = a$ and plug it into (4.1.8) we recover the linear Lagrangian-Eulerian scheme (2.1.15). Moreover, the scheme (4.1.8) can also be written in conservative form,

$$U_j^{n+1} = U_j^n - \frac{k^n}{h} [F(U_j^n, U_{j+1}^n) - F(U_{j-1}^n, U_j^n)], \quad (4.1.9)$$

where the *Lagrangian-Eulerian numerical flux function* is defined by,

$$F(U_j^n, U_{j+1}^n) = \frac{1}{4} \left[\frac{h}{k^n} (U_j^n - U_{j+1}^n) + h \mathbb{W}(U_j^n, U_{j+1}^n) \right]. \quad (4.1.10)$$

We will next observe that this Lagrangian-Eulerian numerical flux function satisfies a Lipschitz continuous consistency, which in turn is a nice property for *conservative numerical methods* for nonlinear conservation law problems.

4.2 A Lipschitz condition to the Lagrangian-Eulerian numerical flux function

Following again the classical theory of conservation (see elsewhere, e.g., [109]) there is a very simple and natural requirement we can impose on our Lagrangian-Eulerian method which will guarantee that we do not converge to non-solutions (i.e., non-entropy weak solutions). In other words, we need an appropriate form of *consistency* with the weak form of the conservation law, required if we hope to converge to weak solutions. Therefore, the proposed Lagrangian-Eulerian method must be *consistent* with the original conservation law if the *numerical flux function* F reduces to the *true flux function* H for the case of constant flow $F(\bar{u}, \bar{u}) = H(\bar{u})$. Essentially, for consistency, it suffices to have numerical flux function a *Lipschitz continuous function* of each variable. The basic principle underlying such consistency with respect to a conservation law is that the total quantity of a conserved variable in any region changes only due to flux through the (local) boundaries (a locally conservative principle on the level of the control volumes over the computational mesh grid. Indeed, Lax-Wendroff Theorem shall light *only* that we can hope to correctly approximate discontinuous weak solutions to the conservation law by using a conservative method, at least in the sense that if we converge to some function $u(x, t)$ as the grid is refined, through some sequence $k, h \rightarrow 0$, then this function will in fact be a weak solution of the underlying conservation law. The Lax-Wendroff Theorem needs a sequence of discrete solutions (given by a conservative method) that is convergent (weak sense) to start with. Roughly speaking, if this solution looks reasonable and has well-resolved discontinuities (an indication that the method is stable and our grid is sufficiently fine), then we can believe that it is in fact a good approximation to *some weak solution*. Thus, it is important to show that the Lagrangian-Eulerian scheme satisfies a *consistency condition*, meaning the existence of a numerical flux function that is *Lipschitz continuous*. Notice that for the nonlinear hyperbolic conservation law (and balance law) problems, unlike the linear advection hyperbolic equation, the “upwind” direction depends on the initial and then it may vary from point to point in the mesh to resemble the original differential problem. Thus, even in the scalar case we want to avoid the use of a somewhat switch of the directional bias based on the data like upwind schemes do.

To prove that the Lagrangian-Eulerian numerical flux satisfies a Lipschitz condition, we will need first to prove the following two auxiliary Lemmas.

Lemma 4.2.1. If

$$|f_j^n k^n| < \frac{h}{2} - \frac{h}{p}, \quad j, p \in \mathbb{Z}, \quad k, h > 0, \quad \text{and } p > 2 \quad \text{then} \quad |f_{j+1}^n - f_j^n| k^n < \frac{p-2}{p} h. \quad (4.2.1)$$

Proof. From hypothesis of Lemma (4.2.1) we have,

$$-\frac{p-2}{2p} h < f_{j+1}^n k^n < \frac{p-2}{2p} h \quad \text{and} \quad -\frac{p-2}{2p} h < -f_j^n k^n < \frac{p-2}{2p} h. \quad (4.2.2)$$

From (4.2.2) follows,

$$-2\frac{p-2}{2p} h < f_{j+1}^n k^n - f_j^n k^n < 2\frac{p-2}{2p} h \quad \text{or} \quad |f_{j+1}^n k^n - f_j^n k^n| < \frac{p-2}{p} h. \quad (4.2.3)$$

Corollary 4.2.1. With the same hypothesis of the Lemma (4.2.1), then inequality

$$\frac{p}{2(p-1)} < \frac{h}{h_j^{n+1}} < \frac{p}{2}, \quad (4.2.4)$$

also holds, where p is fixed.

Proof. The next inequality follows straightforward from (4.2.3) by adding h ,

$$h - \frac{p-2}{p} h < h + f_{j+1}^n k^n - f_j^n k^n < h + \frac{p-2}{p} h. \quad (4.2.5)$$

Thus,

$$h - \frac{p-2}{p} h < h_j^{n+1} < h + \frac{p-2}{p} h \quad \text{and} \quad \frac{2}{p} < \frac{h_j^{n+1}}{h} < \frac{2p-2}{p}, \quad (4.2.6)$$

then

$$\frac{p}{2(p-1)} < \frac{h}{h_j^{n+1}} < \frac{p}{2}. \quad (4.2.7)$$

Theorem 4.2.1. The numerical flux function is defined by (4.1.10) is consistent with the differential equation (4.1.1).

Proof. First, for $v \neq 0$ we get,

$$F(v, v) = \frac{1}{4} \left[\frac{h}{k^n} (v - v) + \frac{h}{h + \left(\frac{H(v)}{v} - \frac{H(v)}{v}\right)} \left(\frac{H(v)}{v} + \frac{H(v)}{v} \right) (v + v) \right] = H(v). \quad (4.2.8)$$

The Lipschitz condition is proved as follow.

Proof. Let us assume $U_j^n \neq 0$, $j \in \mathbb{Z}$, such that we have,

$$r = j, j + 1, \quad U_r^n = \frac{1}{h} \int_{x_{r-\frac{1}{2}}^n}^{x_{r+\frac{1}{2}}^n} u(x, t^n) dx < \infty \quad \Rightarrow \quad \left| \frac{U_j^n}{U_{j+1}^n} \right| = M_n < \infty. \quad (4.2.9)$$

For U_j, U_{j+1} sufficiently close to \bar{u} , we have $|F(U_j, U_{j+1}) - H(\bar{u})| =$

$$\begin{aligned}
&= \frac{1}{4} \left| \frac{h}{k^n} (U_j - U_{j+1}) + \frac{h}{h_j^{n+1}} (f_{j+1} + f_j) (U_{j+1} + U_j) - 4H(\bar{u}) \right| \\
&\leq \frac{1}{4} \left| \frac{h}{k^n} (U_j - \bar{u} + \bar{u} - U_{j+1}) \right| + \\
&\quad \frac{1}{4} \left| \frac{h}{h_j^{n+1}} \left(H(U_{j+1}) + \frac{H(U_{j+1})}{U_{j+1}} U_j + H(U_j) + \frac{H(U_j)}{U_j} U_{j+1} \right) - 4H(\bar{u}) \right| \\
&\leq \frac{1}{4} \frac{h}{k^n} |U_j - \bar{u}| + \frac{1}{4} \frac{h}{k^n} |\bar{u} - U_{j+1}| + \\
&\quad \frac{1}{4} \left| \frac{h}{h_j^{n+1}} \left(H(U_{j+1}) + \frac{H(U_{j+1})}{U_{j+1}} U_j + H(U_j) + \frac{H(U_j)}{U_j} U_{j+1} \right) - 4H(\bar{u}) \right| \\
&\leq \frac{1}{4} \frac{h}{k^n} |U_j - \bar{u}| + \frac{1}{4} \frac{h}{k^n} |\bar{u} - U_{j+1}| + \frac{1}{4} \left| \frac{h}{h_j^{n+1}} H(U_{j+1}) - H(\bar{u}) \right| + \\
&\quad \frac{1}{4} \left| \frac{h}{h_j^{n+1}} \frac{U_j}{U_{j+1}} H(U_{j+1}) - H(\bar{u}) \right| + \frac{1}{4} \left| \frac{h}{h_j^{n+1}} H(U_j) - H(\bar{u}) \right| + \frac{1}{4} \left| \frac{h}{h_j^{n+1}} \frac{U_{j+1}}{U_j} H(U_j) - H(\bar{u}) \right|.
\end{aligned} \tag{4.2.10}$$

From (4.2.7) and (4.2.9), and the fact that whether $H(x) \neq H(y)$, there is $M > 0$, such that $|\alpha H(x) - H(y)| \leq M |H(x) - H(y)|$ for $\alpha \in \mathbb{R}$. Thus,

$$\begin{aligned}
|F(U_j, U_{j+1}) - H(\bar{u})| &\leq \frac{1}{4} \frac{h}{k^n} |U_j - \bar{u}| + \frac{1}{4} \frac{h}{k^n} |\bar{u} - U_{j+1}| + \\
&\quad \frac{1}{4} M_1 |H(U_{j+1}) - H(\bar{u})| + \frac{1}{4} M_2 |H(U_{j+1}) - H(\bar{u})| + \\
&\quad \frac{1}{4} M_3 |H(U_j) - H(\bar{u})| + \frac{1}{4} + M_4 |H(U_j) - H(\bar{u})|.
\end{aligned} \tag{4.2.11}$$

Indeed, H is differentiable we set $H' \equiv \partial H(u)/\partial u$. Then, by the mean value theorem reads,

$$\begin{aligned}
|F(U_j, U_{j+1}) - H(\bar{u})| &\leq \frac{1}{4} \frac{h}{k^n} |U_j - \bar{u}| + \frac{1}{4} \frac{h}{k^n} |\bar{u} - U_{j+1}| + \\
&\quad \frac{1}{4} M_1 M_d |U_{j+1} - \bar{u}| + \frac{1}{4} M_2 M_d |U_{j+1} - \bar{u}| + \\
&\quad \frac{1}{4} M_3 M_d |U_j - \bar{u}| + \frac{1}{4} M_4 M_d |U_j - \bar{u}|,
\end{aligned} \tag{4.2.12}$$

along with $M_d = \max(|H'(c_1)|, |H'(c_2)|)$. Thus, we finally we get the Lipschitz condition as follows,

$$|F(U_j, U_{j+1}) - H(\bar{u})| \leq K \max(|U_j - \bar{u}|, |U_{j+1} - \bar{u}|), \tag{4.2.13}$$

where $K = \max\left(\frac{1}{4} \left(\frac{h}{k^n} + (M_1 + M_2)M_d\right), \frac{1}{4} \left(\frac{h}{k^n} + (M_3 + M_4)M_d\right)\right)$.

On the other hand, for x sufficiently close to y and $H(x) = H(y)$ we have,

$$|aH(x) - H(y)| \leq |a - 1||H(x)| \leq \frac{|a - 1|}{|x - y|} \max_{z \in [x, y]} |H(z)||x - y|. \quad (4.2.14)$$

The continuity of H allows us to write:

$$|aH(x) - H(y)| \leq C|x - y|, \text{ where } C = \frac{|a - 1|}{|x - y|} \max_{z \in [x, y]} |H(z)|. \quad (4.2.15)$$

Then, from equations (4.2.10) and (4.2.14)-(4.2.15) one might write,

$$\begin{aligned} |F(U_j, U_{j+1}) - H(\bar{u})| &\leq \frac{1}{4} \frac{h}{k^n} |U_j - \bar{u}| + \frac{1}{4} \frac{h}{k^n} |\bar{u} - U_{j+1}| + \frac{1}{4} \left| \frac{h}{h_j^{n+1}} H(U_{j+1}) - H(\bar{u}) \right| \\ &+ \frac{1}{4} \left| \frac{h}{h_j^{n+1}} \frac{U_j}{U_{j+1}} H(U_{j+1}) - H(\bar{u}) \right| + \frac{1}{4} \left| \frac{h}{h_j^{n+1}} H(U_j) - H(\bar{u}) \right| \\ &+ \frac{1}{4} \left| \frac{h}{h_j^{n+1}} \frac{U_{j+1}}{U_j} H(U_j) - H(\bar{u}) \right| \\ &\leq \frac{1}{4} \left(\frac{h}{k^n} + C_1 + C_2 \right) |U_{j+1} - \bar{u}| + \frac{1}{4} \left(\frac{h}{k^n} + C_3 + C_4 \right) |U_j - \bar{u}| \\ &\leq \frac{1}{4} \left(2 \frac{h}{k^n} + C_1 + C_2 + C_3 + C_4 \right) \max \{ |U_{j+1} - \bar{u}|, |U_j - \bar{u}| \}, \end{aligned} \quad (4.2.16)$$

where

$$\begin{aligned} C_1 &= \frac{\left| \frac{h}{h_j^{n+1}} - 1 \right|}{|U_{j+1} - \bar{u}|} \max_{z \in [\bar{u}, U_{j+1}]} |H(z)|, & C_2 &= \frac{\left| \frac{h}{h_j^{n+1}} \frac{U_j}{U_{j+1}} - 1 \right|}{|U_{j+1} - \bar{u}|} \max_{z \in [\bar{u}, U_{j+1}]} |H(z)| \\ C_3 &= \frac{\left| \frac{h}{h_j^{n+1}} - 1 \right|}{|U_j - \bar{u}|} \max_{z \in [\bar{u}, U_{j+1}]} |H(z)|, & C_4 &= \frac{\left| \frac{h}{h_j^{n+1}} \frac{U_{j+1}}{U_j} - 1 \right|}{|U_j - \bar{u}|} \max_{z \in [\bar{u}, U_j]} |H(z)| \end{aligned} \quad (4.2.17)$$

Therefore the numerical flux function $F(U_j, U_{j+1})$ (4.1.10) is consistent.

4.3 Monotonicity and TVD properties for the Lagrangian-Eulerian scheme

Harten [75] showed that the *set of monotone schemes* S_{mon} is contained in the *set of TVD schemes* S_{tvd} , which in turn is contained in the *set of monotonicity preserving schemes* S_{mpr} , i.e., $S_{mon} \subseteq S_{tvd} \subseteq S_{mpr}$. For explicit linear schemes [75],

$$u_j^{n+1} = \sum_{k=-k_l}^{k=k_r} \beta_k u_{i+k}^n, \quad (4.3.1)$$

to solve the linear hyperbolic equation one can prove that *monotone schemes* are equivalent to *monotonicity preserving schemes*. Indeed, Harten [76] has proved that nonlinear solutions for hyperbolic conservation laws obtained by monotone finite-difference schemes do satisfy an

entropy condition. Following with the hypothesis of the Lax-Wendroff theorem, we know that if a finite difference method in conservative form is convergent, then it converges to a weak solution. In the previous sections, it was shown that the numerical flux of our Lagrangian-Eulerian scheme, written in a conservative form, satisfy both a consistency and a Lipschitz continuity condition. Here we will see that the Lagrangian-Eulerian method will indeed satisfies a monotonicity condition under a proper CFL condition interval. To this end, let us first start writing the left hand side of scheme (5.1.2) in the convenient form,

$$U_j^{n+1} = L(U_{j-1}^n, U_j^n, U_{j+1}^n) = \beta_{-1}U_{j-1}^n + \beta_0U_j^n + \beta_1U_{j+1}^n, \quad (4.3.2)$$

where $\beta_{-1} = \frac{1}{2} \left(\frac{1}{2} - v \right)$, $\beta_0 = \frac{1}{2}$ and $\beta_1 = \frac{1}{2} \left(\frac{1}{2} + v \right)$ are nonnegative coefficients for $0 \leq v \leq \frac{1}{2}$, so that our Lagrangian-Eulerian is monotone in the CFL interval of monotonicity $0 \leq v \leq \frac{1}{2}$ and non-monotone for $\frac{1}{2} < v \leq \frac{\sqrt{2}}{2}$. The previous facts do not exclude the possibility of having nonlinear monotonicity-preserving and total variation non-increasing schemes with order higher than one [76, 75]. It is worth mentioning that by means of the above arguments scheme (4.1.9)-(4.1.10) is also monotonicity-preserving scheme and therefore a TVD linear scheme. Therefore, whether our Lagrangian-Eulerian algorithm converges to a weak solution, this solution is the entropic solution to CFL interval $0 \leq v_j^n \leq \frac{1}{2}$. A similar argument can be used to the approximation scheme (4.1.9)-(4.1.10) linked to a scalar nonlinear problem,

$$U_j^{n+1} = L^n(U_{j-1}^n, U_j^n, U_{j+1}^n) = \beta_{-1}^n U_{j-1}^n + \beta_0^n U_j^n + \beta_1^n U_{j+1}^n, \quad (4.3.3)$$

where

$$\beta_{-1}^n = \frac{1}{2} \left(\frac{1}{2} + v_j^n \right) \frac{h}{h_{j-1}^{n+1}}, \quad \beta_0^n = \frac{1}{2} \left[\left(\frac{1}{2} + v_j^n \right) \frac{h}{h_{j-1}^{n+1}} + \left(\frac{1}{2} - v_j^n \right) \frac{h}{h_j^{n+1}} \right], \quad \beta_1^n = \frac{1}{2} \left(\frac{1}{2} - v_j^n \right) \frac{h}{h_j^{n+1}},$$

here $v_j^n = \frac{f_j^n k^n}{h}$ and f_j^n is the slope of the straight line that approximates the integral curve $\sigma_j^n(t)$. Notice, the coefficients in (4.3.3) are non-negatives in the CFL interval $0 \leq v_j^n \leq \frac{1}{2}$. Indeed scheme (4.3.3) can be reduced to (4.3.2) by using $f_j^n = a$. From the above discussion we also see that the Lagrangian-Eulerian scheme (5.1.2), or (4.1.9)-(4.1.10), is also monotone for each time step and it converges to a weak entropic solution in the sense of Harten [75, 76]. Such reasoning is essentially the same as used in Harten's papers [75, 76] for the monotonicity property to the nonlinear case, but keeping in mind that actually we used f_j^n as an approximate value to be used in the CFL condition.

4.4 Equivalence between finite difference and finite volume Lagrangian-Eulerian formulations

In above sections, we construct, using the ideas of [57], the Lagrangian-Eulerian scheme to linear hyperbolic conservation laws (2.1.14) and the Lagrangian-Eulerian schemes to non-linear hyperbolic conservation laws (3.2.1) and (4.1.8). In [19, 57, 80, 154] the authors present distinct Lagrangian-Eulerian formulations to the case of linear [18, 17, 80] and non-linear [17, 19, 49, 51, 56, 57, 154] transport flow problems; to the purely linear transport problem the space-time integral curves coincide with characteristic equations [19, 80] (see also [27]). Note that the scheme (3.2.1) is reduced to scheme (2.1.14), with the substitution $H(u) = au$, and

also note that the scheme (4.1.8) is reduced to scheme (2.1.14) with the same substitution $H(u) = au$, we see that. With $H(u) = au$, we have $f_j^n = H(U_j^n)/U_j^n = (aU_j^n)/U_j^n = a$, then $\mathbb{W}(U_j^n, U_{j+1}^n) = \frac{a+a}{h+(a-a)k}(U_j^n + U_{j+1}^n) = \frac{2a}{h}(U_j^n + U_{j+1}^n)$, therefore,

$$\begin{aligned}
U_j^{n+1} &= \frac{1}{4}[U_{j-1}^n + 2U_j^n + U_{j+1}^n] - \frac{k}{4}(\mathbb{W}(U_j^n, U_{j+1}^n) - \mathbb{W}(U_{j-1}^n, U_j^n)) \\
&= \frac{1}{4}[U_{j-1}^n + 2U_j^n + U_{j+1}^n] - \frac{k}{4}\left(\frac{2a}{h}(U_j^n + U_{j+1}^n) - \frac{2a}{h}(U_{j-1}^n + U_j^n)\right) \\
&= \frac{1}{4}[U_{j-1}^n + 2U_j^n + U_{j+1}^n] - \frac{ak}{2h}(U_{j+1}^n - U_{j-1}^n) \\
&= \frac{1}{4}[U_{j-1}^n + 2U_j^n + U_{j+1}^n] - \frac{k}{2h}(H(U_{j+1}^n) - H(U_{j-1}^n))
\end{aligned} \tag{4.4.1}$$

with this, both schemes (3.2.1) and (4.1.8) are equivalents in the linear case.

4.5 Numerical experiments for hyperbolic problems with convex and non-convex fluxes

In order to give a somewhat concrete evidence we are computing “good approximations” to correct entropy solutions, we will illustrate the viability of the proposed Lagrangian-Eulerian scheme for the numerical simulation of initial value problems for convex and non-convex flux-type functions (we show such numerical experiments from Figure 3.1 to Figure 3.3, and Table 4.1, along with comment on the corresponding captions).

Example 4.5.1. Inviscid Burgers’ equation with smooth initial data.

As in the above section, we consider inviscid Burger’s equation. Numerical approximate solutions with scheme LEH1 (4.1.8) are shown to the Cauchy Problem (Initial Value Problem with convex flux function): $u_t + \left(\frac{u^2}{2}\right)_x = 0$, along with smooth initial data $u(x, 0) = 0.5 + \sin(x)$ (see, e.g., [99]). It is well-known the solution of this problem develops a shock discontinuity at the critical time $T_c = 1$, and then it exhibits pre-shock solution for $T_c < 1$ and post-shock solutions $T_c > 1$. In Figure 4.2 top pictures are shown the pre-shock solutions and in bottom pictures are shown post-shock solutions both computed with LEH1 scheme at time simulation $t = 2$ for 128 cells (left), 256 cells (middle) and 512 right.

Cells	LEH2 $\ u - U\ _{l_h^\infty}$	LEH2 $\ u - U\ _{l_h^1}$	LEH1 $\ u - U\ _{l_h^\infty}$	LEH1 $\ u - U\ _{l_h^1}$
32	3.264×10^{-1}	4.557×10^{-1}	2.783×10^{-1}	4.163×10^{-1}
64	1.581×10^{-1}	2.158×10^{-1}	1.242×10^{-1}	1.990×10^{-1}
128	7.466×10^{-2}	1.015×10^{-1}	5.673×10^{-2}	9.394×10^{-2}
256	3.615×10^{-2}	4.625×10^{-2}	2.645×10^{-2}	4.217×10^{-2}
528	1.892×10^{-2}	1.855×10^{-2}	1.428×10^{-2}	1.613×10^{-2}
LSF $E(h)$	$1.694 * h^{1.025}$	$3.00 * h^{1.136}$	$1.504 * h^{1.07}$	$2.83496 * h^{1.149}$

Table 4.1: Errors between the numerical approximations (U) and exact solutions (u) for problem $u_t + \left(\frac{u^2}{2}\right)_x = 0$ with continuous initial condition $u(x, 0) = 0.5 + \sin(x)$ at time frame $T = 0.5$ for pre-schok with LEH1 and LEH2 schemes.

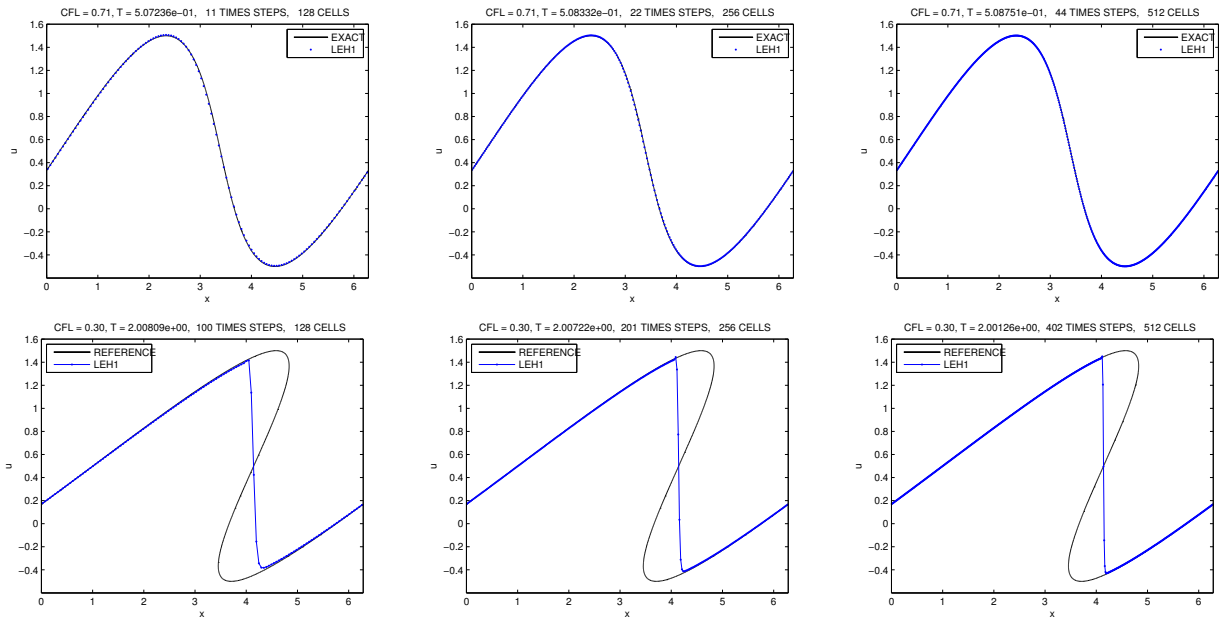


Figure 4.2: **Pre-shock** and **post-shock** solutions computed with LEH1

Example 4.5.2. Inviscid Burgers' equation with discontinuous initial data.

We have also conducted similar numerical experiments to that reported in Figure 4.2, but to problem $u_t + \left(\frac{u^2}{2}\right)_x = 0$ along with discontinuous initial data $u(x, 0) = \eta(x) = 1, x < 0$ and $u(x, 0) = \eta(x) = 0, x > 0$. In top of Figure 4.3 pictures are shown snapshot graphs at time $t = 2.4$ of simulation a shock wave moving from left to right. As above section we get a very nice looking numerical approximate solution with schemes LEH1 (4.1.8) and 128 cells (left), 256 cells (middle) and 512 right. Shock-wave waves are propagating at entirely entropy-correct Rankine-Hugoniot speed. We have also considered Burgers' problem $u_t + \left(\frac{u^2}{2}\right)_x = 0$ along with data $u(x, 0) = \eta(x) = 0, x < 0$ and $u(x, 0) = \eta(x) = 1, x > 0$. In bottom pictures of Figure 4.3 are shown snapshot graphs at time $t = 1$ of simulation for a moving rarefaction wave from left to right, where the rarefaction wave is spreading out correctly and matching with the exact solution there.

Example 4.5.3. Buckley-Leverett equation.

Buckley-Leverett equation. Numerical approximate solutions with scheme LEH1 (4.1.8) are shown to the Riemann Problem (Initial Value Problem with non-convex flux function): $u_t + f_x(u) = 0$, along with Riemann initial data $u(x, 0) \equiv \eta(x) = 1, x < 0$ and $u(x, 0) \equiv \eta(x) = 0, x > 0$. On physical ground, such initial data corresponds to waterflooding of an oil reservoir. The well known solution for this model comprises a leading shock wave (an oil bank) followed by an attached rarefaction wave. The smoothing of the saturation profile observed at the trailing edge of the rarefaction wave where $u = 0.8$, is solely the effect of numerical dissipation. The weak solution satisfying the Oleinik entropy condition is in very good agreement, along with the LEH1 and LEH2 schemes, propagating at entirely entropy-correct Rankine-Hugoniot speed and with the precisely post-shock value. In Figure are shown numerical approximation with scheme LEH1 (4.1.8) advanced at times $t = 0.3$ left, $t = 0.6$ and $t = 1$ with 128 cells (top) and 256 (bottom).

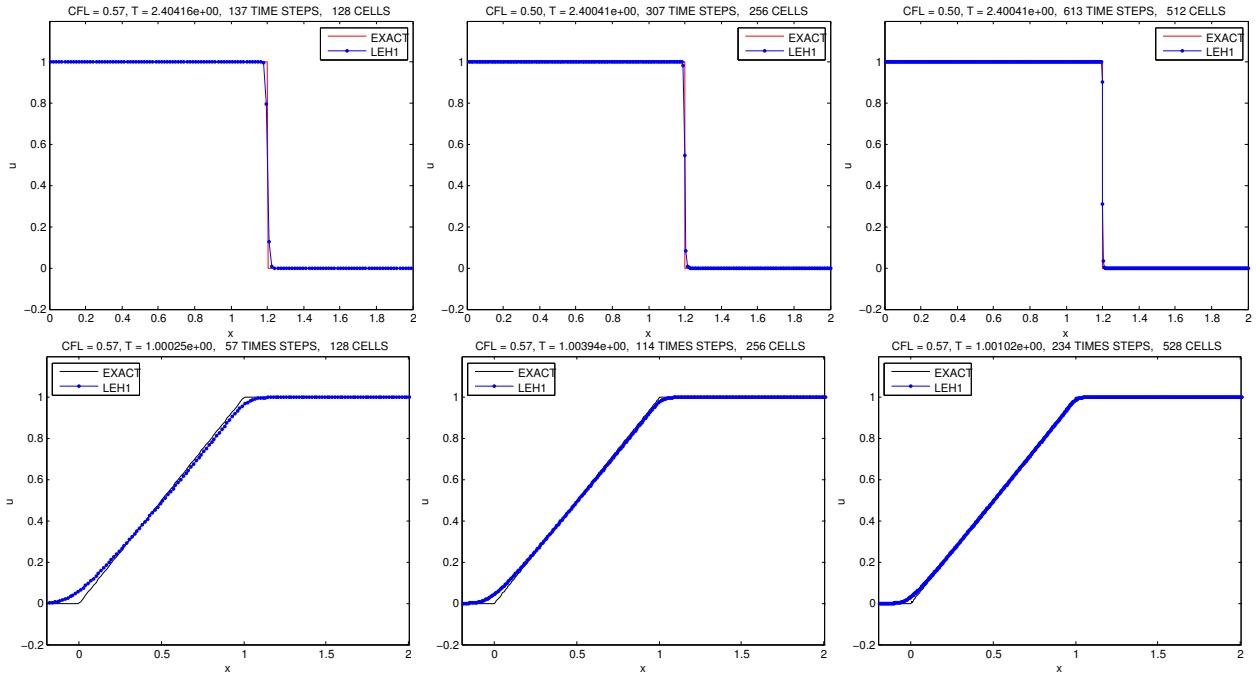


Figure 4.3: Numerical approximation with **discontinuous** initial data

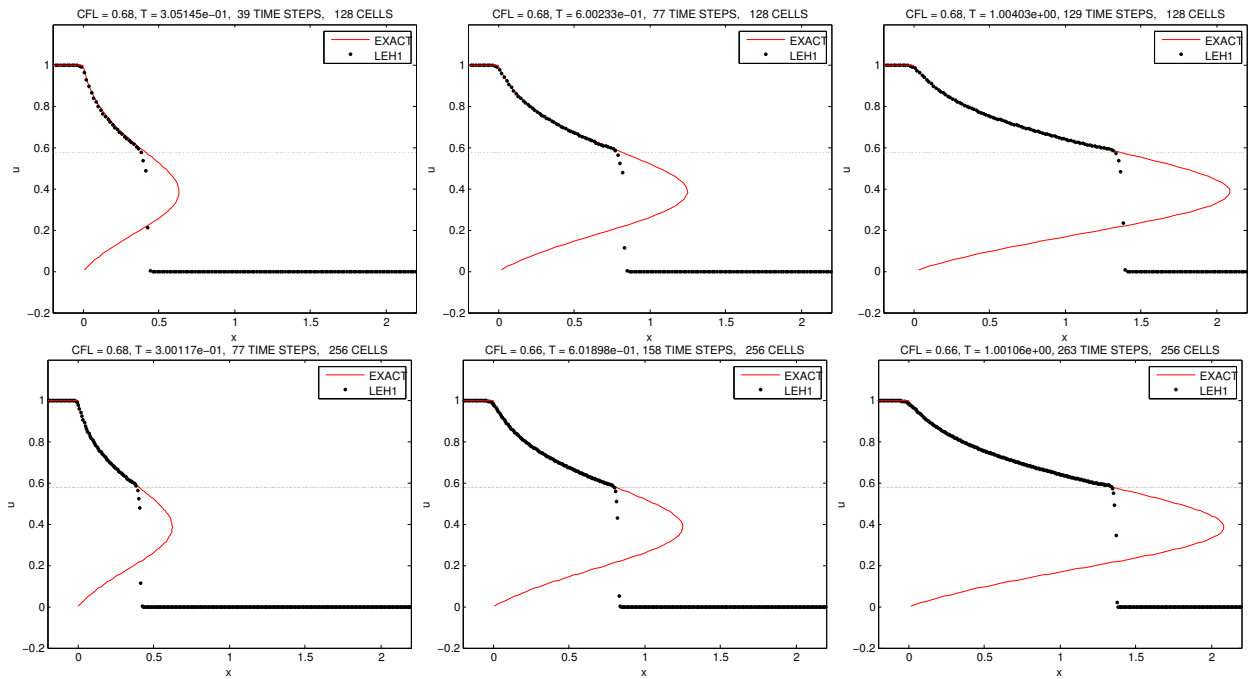


Figure 4.4: **Buckley-Leverett** with discontinuous initial data

Example 4.5.4. Other non-convex flux type.

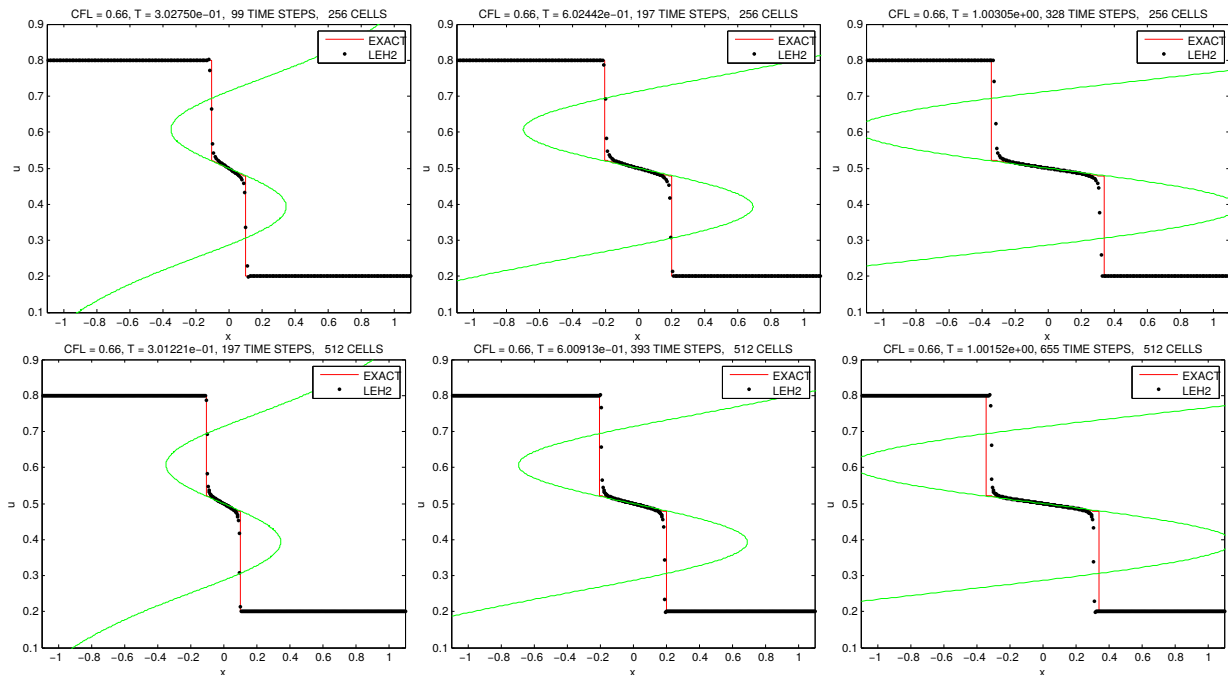


Figure 4.5: Numerical approximations with other **non-convex flux**

We have also considered another non-convex flux function, approximated with schemes LEH1, to the scalar conservation law $u_t + f_x(u) = 0$, namely $f(u) = 0.5(e^{-25(u-0.5)^2} + 8(u-0.5)^2)$, and with same Riemann data (see Figure 4.5). Again, the numerical solutions is in agreement with Oleinik entropy condition, whose approximate left and right shock waves are propagating with correct Rankine-Hugoniot speed and entropy-correct post-shock values. At the two rows of pictures are shown snapshot graphs at simulation times $t = 0.3$ (left), $t = 0.6$ (middle) and $t = 1$ (right) with 256 cells (top) and 512 cells (bottom). In the table 4.1 are shown the errors in the l_h^∞ and l_h^1 norms as also to the LEH1 and LEH2 methods and the accuracy order in the approximation, the table 4.1 reveals that the convergence rate is approximately 1. The theory described in above sections shows that both the methods LEH1 and LEH2 are accurate of order 1.

Chapter 5

The Lagrangian-Eulerian scheme for hyperbolic balance laws

So far, we have shown some representative numerical experiments for scalar nonlinear problems for which we were able to verify the correct (entropy) behavior of the approximations computed by the new Lagrangian-Eulerian scheme. Nonetheless, as the computational grid is refined the approximate solution looks reasonable and has well-resolved discontinuities. This give us some confidence to speculate that the method is somewhat stable, avoiding the impractical requirement of extremely very fine meshes, to satisfy the task of computing qualitatively entropy-correct approximations. Thus, we have some hope to use a version of the *Lax-Wendroff theorem* in the sense of that discussed in [34, 123] (see also [67] for more details) on the choice of a family of path-conservative numerical schemes for hyperbolic systems of balance laws, but in a conservative form of the conservation law; in [34, 123], the authors considered hyperbolic system in nonconservative form.

We are interested in designing well-balanced conceptually simple schemes, which have a well balanced property for static and moving equilibrium, applicable to a wide class of systems with source. One may find, in a variety of physical problems, source terms that are balanced by internal forces and this balance supports multiple steady-state solutions that are stable. The well-balance property can be formally enunciated as follows. Consider the system of balance laws as such,

$$\frac{\partial u}{\partial t} + \frac{\partial(H(u))}{\partial x} = G(u), \quad (5.0.1)$$

we denote u^e the stationary solution, which satisfies the equation,

$$\frac{\partial(H(u^e))}{\partial x} = G(u^e), \quad (5.0.2)$$

we say that a numerical scheme is **well-balanced**, if it fully satisfies a discrete version of the equilibrium equation (5.0.2). If a method is not well-balanced, the truncation error of solutions near of equilibrium state may be larger than $u(x, t) - u^e(x)$. Our numerical experiments for solving balance laws have shown strong numerical evidence that such **well-balanced** property is satisfied when we applied our novel Lagrangian-Eulerian scheme for several models of balance laws.

Consider the scalar balance law problem,

$$\frac{\partial u}{\partial t} + \frac{\partial H(u)}{\partial x} = G(u), \quad t > 0, \quad -\infty < x < \infty, \quad u(x, 0) = \eta(x) \quad -\infty < x < \infty, \quad (5.0.3)$$

under the assumption $\iint_{D_j^n} G(u) dx dt < \infty$. Now, write (5.0.3) as follows,

$$\nabla_{t,x} \cdot \begin{bmatrix} u \\ H(u) \end{bmatrix} = G(u) \quad t > 0, \quad -\infty < x < \infty, \quad u(x, 0) = \eta(x) \quad -\infty < x < \infty. \quad (5.0.4)$$

Now, lets us write (5.0.4) over the local space-time ‘‘Integral tube’’ D_j^n (see equation (2.1.6) and the left picture in Figure 2.1),

$$\iint_{D_j^n} \nabla_{t,x} \cdot \begin{bmatrix} u \\ H(u) \end{bmatrix} dx dt = \iint_{D_j^n} G(u) dx dt. \quad (5.0.5)$$

Following the same arguments in Section 2, we apply first the divergence theorem in (5.0.5) and, by means of the impervious boundaries given by $\sigma_j^n(t)$, reads:

$$\int_{\bar{x}_{j-\frac{1}{2}}^{n+1}}^{\bar{x}_{j+\frac{1}{2}}^{n+1}} u(x, t^{n+1}) dx = \int_{x_j^n}^{x_{j+1}^n} u(x, t^n) dx + \iint_{D_j^n} G(u) dx dt. \quad (5.0.6)$$

This equation can be viewed as *the local space-time Lagrangian-Eulerian conservation relation* for the balance law (5.0.6). Finally, we use (5.0.6) then to define,

$$\bar{U}_j^{n+1} = \frac{1}{h_j^{n+1}} \int_{\bar{x}_{j-\frac{1}{2}}^{n+1}}^{\bar{x}_{j+\frac{1}{2}}^{n+1}} u(x, t^{n+1}) dx = \frac{1}{h_j^{n+1}} \left[\int_{x_j^n}^{x_{j+1}^n} u(x, t^n) dx + \iint_{D_j^n} G(u) dx dt \right], \quad (5.0.7)$$

and its associated projection step over the original mesh grid,

$$U_j^{n+1} = \frac{1}{h} \left[\left(\frac{h}{2} + f_j^n k \right) \bar{U}_{j-1}^{n+1} + \left(\frac{h}{2} - f_j^n k \right) \bar{U}_j^{n+1} \right]. \quad (5.0.8)$$

The Lagrangian-Eulerian scheme for balance law (LEB1) is fully defined by combining equations (5.0.7) and (5.0.8). Clearly, the key point here is how to design a discretization in a manner that an accurate balance between the gradients of the flux function and the source term is retained. Thus, let us now first extend the designed proposed scheme for linear hyperbolic conservation laws to the case of balance laws in order to describe the features of the Lagrangian-Eulerian procedure.

5.1 Linear case for balance laws

For the sake of simplicity, let us start with the following balance law,

$$\begin{cases} \frac{\partial u}{\partial t} + \frac{\partial(au)}{\partial x} = G(x, t), & t > 0, \quad -\infty < x < \infty, \\ u(x, 0) = \eta(x), & -\infty < x < \infty. \end{cases} \quad (5.1.1)$$

As in Section 2, the combination of (5.0.7) and (5.0.8) give us,

$$\frac{U_j^{n+1} - \frac{1}{4} (U_{j-1}^n + 2U_j^n + U_{j+1}^n)}{k} - a \frac{U_{j+1}^n - U_{j-1}^n}{2h} = \frac{1}{kh} \left[\begin{aligned} & \frac{1}{h} \left(\frac{h}{2} + ak \right) \iint_{D_{j-1}^n} G(x, t) dx dt \\ & + \frac{1}{h} \left(\frac{h}{2} - ak \right) \iint_{D_j^n} G(x, t) dx dt \end{aligned} \right]. \quad (5.1.2)$$

At this point, let us point-out a distinctive aspect of the new Lagrangian-Eulerian approach. First, let us consider the “hyperbolic counterpart” of the balance law (5.1.1), i.e., $G(u) \equiv 0$ and $u_t + au_x = 0$, $u(x, 0) = \eta(x)$, along with the well known exact solution $u(x, t) = \eta(x - at)$. If we think mesh grid parameters in space h and time k obey a CFL condition constraint such as (2.1.28), then we have the following mesh grid *representation* of the local approximate solution given by $u(x_j, t^{n+1}) = u(x_j - ak, t^n) \equiv \eta_j(h - ak)$. By construction of the Lagrangian-Eulerian scheme, points (x_j, t^n) and (x_j, t^{n+1}) are inside the space-time local control finite volume D_j^n , and away from the parameterized curves $\sigma_j^n(t)$ and $u(x_j, t^{n+1}) = \eta(h - ak)$ is a smooth function in each D_j^n . Furthermore, it is worth pointing out that in the linear hyperbolic case the integral curves (integral tubes) coincide with the *characteristic curves*. Thus, the source term can be solved by forward tracking the boundary of grid cells from the parameterized curves $\sigma_j^n(t)$ along the so-called integral tubes. Thus, we can recast (5.1.2) as follows:

$$\frac{U_j^{n+1} - \frac{1}{4}(U_{j-1}^n + 2U_j^n + U_{j+1}^n)}{k} - a \frac{U_{j+1}^n - U_{j-1}^n}{2h} = \frac{1}{kh} \left[\begin{array}{l} \frac{1}{h} [\eta_{j-1}^{-1}(h/2 + ak)] \iint_{D_{j-1}^n} G(x, t) dx dt \\ + \frac{1}{h} [\eta_j^{-1}(h/2 - ak)] \iint_{D_j^n} G(x, t) dx dt \end{array} \right]. \quad (5.1.3)$$

It is worth mentioning that a characteristic feature of the hyperbolic balance law is the inherent existence of non-trivial equilibrium solutions. Then, in order to design a scheme for inhomogeneous conservation laws a key point is how to discretize the flux function and the source term keeping the proper balance a discrete analogue of this balance linked to equilibrium steady state solutions. The basic idea here is to decompose the integral on the right hand side of (5.1.2) into suitable parts. Equation (5.1.3) means that the dynamic of the impervious boundaries given by the parameterized curves $\sigma_j^n(t)$ D_j^n to the “Integral tube” D_j^n (see (2.1.6) and left picture in Figure 2.1) naturally provide an *unbiased* upwinding in a robust fashion since within this decomposition leads to a quadrature rule for the integral of the source term $G(x, t)$ in which is Riemann-solver-free. This is the new view point of the Lagrangian-Eulerian scheme (5.1.3) to a well-balancing discretization between source term and the hyperbolic flux term. Further, a set of representative numerical experiments based on well known mathematical models available in the literature to compare and to demonstrate the application of the Lagrangian-Eulerian method with reasonable accuracy. The idea of the analogue nonlinear scheme is quite straightforward.

On the other hand, (5.1.3) is the discrete model of equation (5.1.1). Thus, we can write equation (5.1.2) as,

$$R_{h,k}G = P_{h,k}U + O(h) + O(k), \quad (5.1.4)$$

with the operator $P_{h,k}$ as such in (2.1.16):

$$R_{h,k}G = \frac{1}{kh} \left[\frac{1}{h} \left(\frac{h}{2} + ak \right) \iint_{D_{j-1}^n} G(x, t) dx dt + \frac{1}{h} \left(\frac{h}{2} - ak \right) \iint_{D_j^n} G(x, t) dx dt \right]. \quad (5.1.5)$$

In this linear case, suppose we can perform a exact quadrature rule to the integrals that

appears in (5.1.5). Thus, if $G = \frac{\partial \phi}{\partial t} + a \frac{\partial \phi}{\partial x} = P\phi$ then (see [142]),

$$\begin{aligned}
R_{h,k}P\phi &= \frac{1}{kh} \left[\frac{1}{h} \left(\frac{h}{2} + ak \right) \iint_{D_{j-1}} P\phi(x,t) \, dx \, dt + \frac{1}{h} \left(\frac{h}{2} - ak \right) \iint_{D_j} P\phi(x,t) \, dx \, dt \right] \\
&= \frac{1}{kh} \left[\frac{1}{h} \left(\frac{h}{2} + ak \right) \iint_{D_{j-1}} \left(\frac{\partial \phi}{\partial t} + a \frac{\partial \phi}{\partial x} \right) \, dx \, dt + \frac{1}{h} \left(\frac{h}{2} - ak \right) \iint_{D_j} \left(\frac{\partial \phi}{\partial t} + a \frac{\partial \phi}{\partial x} \right) \, dx \, dt \right] \\
&= \frac{1}{kh} \left[\frac{1}{h} \left(\frac{h}{2} + ak \right) \iint_{D_{j-1}} \nabla_{t,x} \left[\begin{array}{c} \phi \\ a\phi \end{array} \right] \, dx \, dt + \frac{1}{h} \left(\frac{h}{2} - ak \right) \iint_{D_j} \nabla_{t,x} \left[\begin{array}{c} \phi \\ a\phi \end{array} \right] \, dx \, dt \right], \tag{5.1.6}
\end{aligned}$$

and by the application of the divergence theorem reads,

$$R_{h,k}P\phi = \frac{1}{kh} \left[\frac{1}{h} \left(\frac{h}{2} + ak \right) \oint_{\partial D_{j-1}} \left[\begin{array}{c} \phi \\ a\phi \end{array} \right] \cdot n \, dx \, dt + \frac{1}{h} \left(\frac{h}{2} - ak \right) \oint_{\partial D_j} \left[\begin{array}{c} \phi \\ a\phi \end{array} \right] \cdot n \, dx \, dt \right]. \tag{5.1.7}$$

By construction of integral tubes, we use the fact of curves σ_j^n be impervious over regions D_j^n to get,

$$R_{h,k}P\phi = \frac{1}{kh} \left[\frac{1}{h} \left(\frac{h}{2} + ak \right) \left(\bar{I}_{j-1}^{n+1} - I_{j-\frac{1}{2}}^n \right) + \frac{1}{h} \left(\frac{h}{2} - ak \right) \left(\bar{I}_j^{n+1} - I_{j+\frac{1}{2}}^n \right) \right], \tag{5.1.8}$$

where

$$\bar{I}_j^{n+1} = \int_{\bar{x}_{j-\frac{1}{2}}^{n+1}}^{\bar{x}_{j+\frac{1}{2}}^{n+1}} \phi(x, t^{n+1}) \, dx \quad \text{and} \quad I_{j+\frac{1}{2}}^n = \int_{x_j^n}^{x_{j+1}^n} \phi(x, t^n) \, dx. \tag{5.1.9}$$

Notice that all specialized machinery developed like numerical quadrature rule for integrals as well as nonlinear reconstructions (see, e.g., [20, 21, 22, 32, 58, 80]) can be employed on the RHS of (5.1.9). But, in order to better account the contribution of new Lagrangian-Eulerian procedure, namely the balancing between the computation of the numerical flux function and the source term by means of the naturally *unbiased* upwinding Riemann-solver-free, we use standard quadrature rules. Indeed, we approximate integrals \bar{I}_j^{n+1} and $I_{j+\frac{1}{2}}^n$ that appears in (5.1.9) with *the midpoint rule* and *the trapezoidal rule*, respectively, given by

$$\begin{aligned}
\bar{I}_j^{n+1} &= \int_{\bar{x}_{j-\frac{1}{2}}^{n+1}}^{\bar{x}_{j+\frac{1}{2}}^{n+1}} \phi(x, t^{n+1}) \, dx \approx h \phi(\bar{x}_j^{n+1}, t^{n+1}) + \frac{\phi_{xx}(\bar{\xi}_j^n) h^3}{24} \\
&= h \bar{\phi}_j^{n+1} + \frac{\phi_{xx}(\bar{\xi}_j^n) h^3}{24}, \tag{5.1.10}
\end{aligned}$$

$$\begin{aligned}
I_{j+\frac{1}{2}}^n &= \int_{x_j^n}^{x_{j+1}^n} \phi(x, t^n) \, dx \approx \frac{h}{2} \left[\phi(x_j^n, t^n) + \phi(x_{j+1}^n, t^n) \right] - \frac{\phi_{xx}(\xi_{j+\frac{1}{2}}^n) h^3}{12} \\
&= \frac{h}{2} \left(\phi_j^n + \phi_{j+1}^n \right) - \frac{\phi_{xx}(\xi_{j+\frac{1}{2}}^n) h^3}{12}, \tag{5.1.11}
\end{aligned}$$

where $\bar{\xi}_j^n \in \left(\bar{x}_{j-\frac{1}{2}}^{n+1}, \bar{x}_{j+\frac{1}{2}}^{n+1} \right)$ and $\xi_{j+\frac{1}{2}}^n \in \left(x_j^n, x_{j+1}^n \right)$. Now, plugging (5.1.10) and (5.1.11) into

(5.1.8) and performing the projection step over the original grid (5.0.8), give us,

$$\begin{aligned}
R_{h,k}P\phi &= \frac{1}{kh} \left[\left(\frac{h}{2} + ak \right) \left(\bar{\phi}_{j-1}^{n+1} - \frac{1}{2} (\phi_{j-1}^n + \phi_j^n) \right) + \left(\frac{h}{2} - ak \right) \left(\bar{\phi}_j^{n+1} - \frac{1}{2} (\phi_j^n + \phi_{j+1}^n) \right) \right] \\
&+ \frac{1}{kh} \left[\left(\frac{h}{2} + ak \right) \left(\frac{\phi_{xx}(\bar{\xi}_{j-1}^n)h^2}{24} + \frac{\phi_{xx}(\xi_{j-\frac{1}{2}}^n)h^2}{12} \right) + \left(\frac{h}{2} - ak \right) \left(\frac{\phi_{xx}(\bar{\xi}_j^n)h^2}{24} + \frac{\phi_{xx}(\xi_{j+\frac{1}{2}}^n)h^2}{12} \right) \right] \\
&= \frac{1}{k} \left[\phi_j^{n+1} - \frac{1}{2h} \left(\frac{h}{2} + ak \right) (\phi_{j-1}^n + \phi_j^n) - \frac{1}{2h} \left(\frac{h}{2} - ak \right) (\phi_j^n + \phi_{j+1}^n) \right] + O(h) + O(k).
\end{aligned} \tag{5.1.12}$$

Under assumption of exact integration of the linear source term we can recast (5.1.12) as,

$$\begin{aligned}
R_{h,k}P\phi &= \frac{\phi_j^n - \frac{1}{4} ([\phi_{j-1}^n + \phi_j^n] + [\phi_j^n + \phi_{j+1}^n])}{k} + a \frac{\phi_{j+1}^n - \phi_{j-1}^n}{2h} + O(h) + O(k) \\
&= P_{h,k}\phi + O(h) + O(k),
\end{aligned} \tag{5.1.13}$$

and the truncation error (see [142]) of the Lagrangian-Eulerian scheme is $O(h) + O(k)$ and accurate of order (1, 1). As announced, all specialized machinery developed numerical quadrature rule for integrals as well as nonlinear reconstructions (see, e.g., [32, 21, 22, 58, 80, 20]) can be employed on the RHS of (5.1.9). But, in order to better account the contribution of new Lagrangian-Eulerian procedure, namely the appropriate balancing between the computation of the numerical flux function (i.e., the discrete space-time divergence operator) and the source term by means of the naturally *unbiased* upwinding Riemann-solver-free, we use standard quadrature rules. This will be discussed in what follows.

5.1.1 Midpoint rule

We will start from the Lagrangian-Eulerian scheme (5.1.2)-(5.1.3), which in turn is related to (5.1.4)-(5.1.5). In addition, for the quadrature rule to make sense, we point out we performing the pertinent computations under the CFL constrain (2.1.28), from time level t^{n+1} to t^n such that $t^{n+1} = t^n + k$ and that

$$\sigma_{j+1}^n(t) - \sigma_j^n(t) = a(t - t^n) + x_{j+1}^n - a(t - t^n) + x_j^n = x_{j+1}^n - x_j^n = h$$

It is sufficient to consider the integration just over one ‘‘Integral tube’’ D_j^n ; the other case

D_{j-1}^n is similar. Thus,

$$\begin{aligned}
\iint_{D_j^n} G(x, t) \, dx \, dt &\approx \int_{t^n}^{t^{n+1}} \int_{\sigma_j^n(t)}^{\sigma_{j+1}^n(t)} G(x, t) \, dx \, dt \\
&= \int_{t^n}^{t^{n+1}} [\sigma_{j+1}^n(t) - \sigma_j^n(t)] G\left(\frac{\sigma_{j+1}^n(t) + \sigma_j^n(t)}{2}, t\right) \, dt \\
&= \int_{t^n}^{t^{n+1}} h G\left(\frac{\sigma_{j+1}^n(t) + \sigma_j^n(t)}{2}, t\right) \, dt \\
&= h k G\left(\frac{\sigma_{j+1}^n\left(\frac{t^{n+1}+t^n}{2}\right) + \sigma_j^n\left(\frac{t^{n+1}+t^n}{2}\right)}{2}, \frac{t^{n+1} + t^n}{2}\right) \\
&= h k G\left(\frac{\sigma_{j+1}^n\left(\frac{2t^n+k}{2}\right) + \sigma_j^n\left(\frac{2t^n+k}{2}\right)}{2}, \frac{t^n + 2k}{2}\right) \\
&= h k G\left(\frac{\sigma_{j+1}^n\left(t^n + \frac{k}{2}\right) + \sigma_j^n\left(t^n + \frac{k}{2}\right)}{2}, t^n + \frac{k}{2}\right) \\
&= h k G\left(\frac{(t^n + \frac{k}{2} - t^n)a + x_{j+1}^n + (t^n + \frac{k}{2} - t^n)a + x_j^n}{2}, t^n + \frac{k}{2}\right).
\end{aligned} \tag{5.1.14}$$

Equation (5.1.14) can be recast as follows,

$$\iint_{D_j^n} G(x, t) \, dx \, dt \approx k h G\left(x_j^n + \frac{1}{2}(ak + h)t^n + \frac{k}{2}\right). \tag{5.1.15}$$

Now, plugging (5.1.15) into the operator (5.1.5) gives,

$$R_{h,k}G = \frac{1}{h}\left(\frac{h}{2} + ak\right) G\left(x_{j-1}^n + \frac{1}{2}(ak + h)t^n + \frac{k}{2}\right) + \frac{1}{h}\left(\frac{h}{2} - ak\right) G\left(x_j^n + \frac{1}{2}(ak + h)t^n + \frac{k}{2}\right). \tag{5.1.16}$$

For a smooth function $G(x, t)$, we might write from (5.1.16),

$$R_{h,k}G = G - \frac{ak}{2}g_x + \frac{k}{2}G_t + O(k^2) + O(h^2), \tag{5.1.17}$$

and then,

$$\begin{aligned}
R_{h,k}P\phi &= \phi_t + a\phi_x - \frac{ak}{2}(\phi_t + a\phi_x)_x + \frac{k}{2}(\phi_t + a\phi_x)_t + O(k^2) + O(h^2) \\
&= \phi_t + a\phi_x - \frac{ak}{2}\phi_{tx} - \frac{a^2k}{2}\phi_{xx} + \frac{k}{2}\phi_{tt} + \frac{ak}{2}\phi_{xt} + O(k^2) + O(h^2).
\end{aligned} \tag{5.1.18}$$

For a sufficiently smooth ϕ we have $\phi_{tx} = \phi_{xt}$, and write,

$$R_{h,k}P\phi = \phi_t + a\phi_x + \frac{k}{2}\phi_{tt} - \frac{a^2k}{2}\phi_{xx} + O(k^2) + O(h^2), \tag{5.1.19}$$

or more conveniently in the form,

$$P_{h,k}\phi - R_{h,k}P\phi = -\frac{h^2}{2k} \left[\frac{1}{2} - v^2 \right] \phi_{xx} + O(k^2) + O(h^2). \quad (5.1.20)$$

According to [142], we can say the Lagrangian-Eulerian scheme for balance law (5.0.7)-(5.0.8) is accurate of order (1, 1) when we use the midpoint rule to approximate the space-time local integral tube D_j^n . Yet, in the sense of [142], with the ratio h/k fixed, this imply $P_{h,k}\phi - R_{h,k}P\phi = O(h)$.

5.1.2 The trapezoidal rule

The trapezoidal rule is quite similar to the previous Section 5.1.1. Thus, integral over D_j^n reads,

$$\iint_{D_j^n} G(x, t) dx dt \approx \frac{kh}{4} [G(x_j^n + h + ak, t^n + k) + G(x_j^n + ak, t^n + k) + G(x_j^n + h, t^n) + G(x_j^n, t^n)] \quad (5.1.21)$$

replacing this equation for D_{j-1} and D_j in the operator $R_{h,k}G$, we get

$$R_{h,k}G = G - \frac{ak}{2}G_x + \frac{k}{2}G_t + O(h^2) + O(k^2). \quad (5.1.22)$$

As $P\phi = \phi_t + a\phi_x = G$ we might write,

$$R_{h,k}P\phi = (\phi_t + a\phi_x) - \frac{ak}{2}(\phi_t + a\phi_x)_x + \frac{k}{2}(\phi_t + a\phi_x)_t + O(h^2) + O(k^2). \quad (5.1.23)$$

Notice, the accuracy $O(1)$ is equal to the Midpoint rule,

$$P_{h,k}\phi - R_{h,k}P\phi = -\frac{h^2}{2k} \left[\frac{1}{2} - v^2 \right] \phi_{xx} + O(k^2) + O(h^2). \quad (5.1.24)$$

By the above calculations we have consistency with $O(1)$ for the Lagrangian-Eulerian scheme (5.0.7)-(5.0.8), with respect to the linear balance law (5.1.1), for both quadratures: *mid point rule* and *trapezoidal rule*. In the light of the modified equation analysis to the purely linear hyperbolic case, notice the diffusive term in ϕ_{xx} suggests that a CFL condition to the Lagrangian-Eulerian scheme based on (5.1.20) and (5.1.24) is $|v| \leq \frac{1}{\sqrt{2}}$; $v = ak/h$. If this is the case, we would expect to achieve high resolution if we set $v = \sqrt{2}/2$. Next, we turn to the stability analysis.

5.1.3 Stability and convergence for Lagrangian-Eulerian scheme for linear balance laws

To prove the stability of the Lagrangian-Eulerian scheme (5.0.7)-(5.0.8) for balance law (5.1.1) we must search the amplification factor as in the linear hyperbolic linear case. Thus, set just $U_j^n = \bar{g}^n e^{i\xi jh}$ and plug it into (5.1.2) along with $R_{h,k}G = 0$ to get,

$$\begin{aligned} \bar{g}(\xi)^{n+1} e^{i\xi jh} &= \frac{1}{4} \left[\bar{g}(\xi)^n e^{i\xi(j-1)h} + 2\bar{g}(\xi)^n e^{i\xi jh} + \bar{g}(\xi)^n e^{i\xi(j+1)h} \right] - \frac{ak}{2h} \left[\bar{g}(\xi)^n e^{i\xi(j+1)h} - \bar{g}(\xi)^n e^{i\xi(j-1)h} \right] \\ &= \frac{1}{4} e^{i\xi jh} \bar{g}(\xi)^n \left[e^{-i\xi h} + 2 + e^{i\xi h} \right] - \frac{ak}{2h} e^{i\xi jh} \bar{g}(\xi)^n \left[e^{i\xi h} - e^{-i\xi h} \right]. \end{aligned} \quad (5.1.25)$$

From (5.1.25), the amplification factor now reads,

$$\bar{g}(\xi) = \frac{1}{4} (2 + 2 \cos(\xi h)) - \frac{1}{2} v (2i \sin(\xi h)) = \frac{1}{2} (1 + \cos(\xi h)) - vi \sin(\xi h). \quad (5.1.26)$$

If $|v| \leq \sqrt{2}/2$ we have $|g(\xi)| < 1$ and then stability for the Lagrangian-Eulerian scheme (5.0.7)-(5.0.8) for balance law (5.1.1). Moreover, consistency plus stability means convergence in the scope of the Lax Equivalence theorem, just in the purely hyperbolic case.

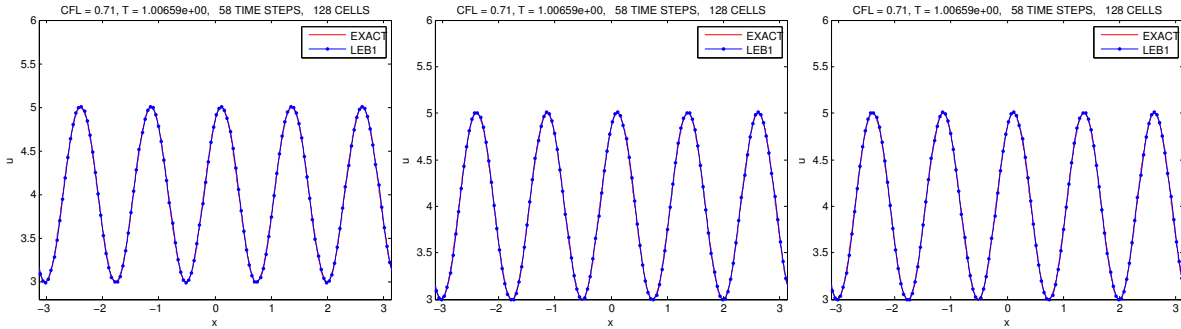


Figure 5.1: Numerical approximations with the Lagrangian-Eulerian scheme LEB1 (5.0.7)-(5.0.8) for balance law problem $u_t + 2u_x = 11\cos(5x+t)$ subject to the initial condition $u(x, 0) = 4 + \sin(5x)$ at time $T = 1$ of simulation with the limiting Courant number $v = \sqrt{2}/2$.

Cells	Exact $\ u - U\ _{l_h^\infty} (\ u - U\ _{l_h^1})$	Midpoint $\ u - U\ _{l_h^\infty} (\ u - U\ _{l_h^1})$	Trap $\ u - U\ _{l_h^\infty} (\ u - U\ _{l_h^1})$
32	$3.153 \times 10^{-1} (2.526 \times 10^0)$	$5.590 \times 10^{-1} (4.232 \times 10^0)$	$2.3151 \times 10^{-1} (1.997 \times 10^0)$
64	$7.232 \times 10^{-2} (6.634 \times 10^{-1})$	$1.382 \times 10^{-1} (1.231 \times 10^0)$	$8.484 \times 10^{-2} (7.478 \times 10^{-1})$
128	$1.705 \times 10^{-2} (1.574 \times 10^{-1})$	$4.526 \times 10^{-2} (3.898 \times 10^{-1})$	$3.624 \times 10^{-2} (3.106 \times 10^{-1})$
256	$4.056 \times 10^{-3} (3.857 \times 10^{-2})$	$1.881 \times 10^{-2} (1.585 \times 10^{-1})$	$1.747 \times 10^{-3} (1.467 \times 10^{-1})$
LSF $E(h)$	$9.415 * h^{2.093} (69.067 * h^{2.018})$	$6.949 * h^{1.629} (51.968 * h^{1.587})$	$1.663 * h^{1.248} (14.588 * h^{1.257})$

Table 5.1: Errors between the approximate solution U and the exact solution u .

Next, Figure 5.1 show numerical experiments to a linear balance problem in order to verify properties discussed just above. Numerical approximations with the Lagrangian-Eulerian scheme LEB1 (5.0.7)-(5.0.8) for balance law problem $u_t + 2u_x = 11\cos(5x+t)$ subject to the initial condition $u(x, 0) = 4 + \sin(5x)$ at time $T = 1$ of simulation with the limiting Courant number $v = \sqrt{2}/2$. On the top frames are shown the computed solutions: exact (left), midpoint (middle) and trapezoidal (right) for the computation of the source term over the local space-time integral tube D_j^n .

In Table 5.1 are shown the corresponding errors between the numerical approximations (U) and exact solutions (u) for the linear balance problem under consideration. It is expected $O(2)$ with Courant number $v = \sqrt{2}/2$, but it is not observed in the top pictures (see the numbers at the table) despite of the very good resemblance between the approximate midpoint and trapezoidal and exact solutions.

In figure 5.2 is shown Cauchy problem for linear scalar balance law: On the top row is shown accurate numerical approximations at times $t = 0$ (left), $t = 0.5$ (middle) and $t = 2$ (right), whose computed solutions are in very good agreement in the exact behavior of the analytical solution, which in turn leads to formation of high gradients as time evolves along with the correct

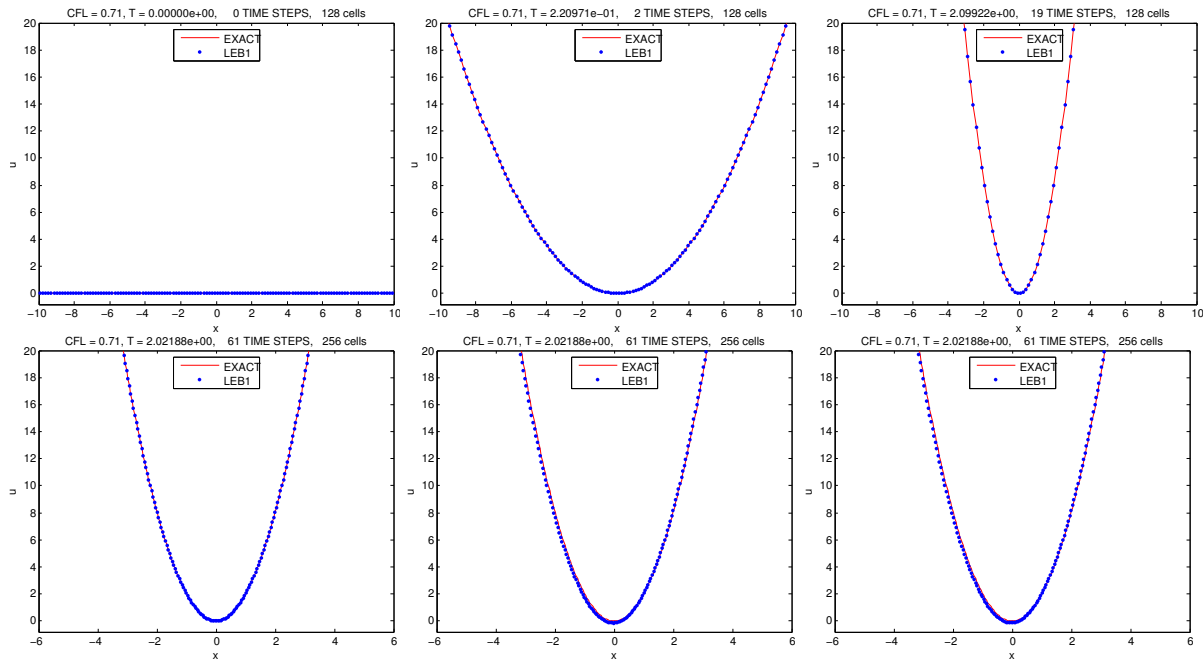


Figure 5.2: Cauchy problem for linear scalar balance law: We consider the differential equation $u_t + u_x = 2xt + x^2$, $-\infty < x < \infty$, $t > 0$, along with smooth initial data (top left) $u(x, 0) = 0$, $-\infty < x < \infty$, whose the well know exact solution is $u(x, t) = x^2t$.

Cells	Exact $\ u - U\ _{l_h^\infty} (\ u - U\ _{l_h^1})$	Midpoint $\ u - U\ _{l_h^\infty} (\ u - U\ _{l_h^1})$	Trap $\ u - U\ _{l_h^\infty} (\ u - U\ _{l_h^1})$
32	$4.972 \times 10^{-2} (5.966 \times 10^{-1})$	$7.844 \times 10^0 (4.201 \times 10^1)$	$7.658 \times 10^0 (4.159 \times 10^1)$
64	$1.243 \times 10^{-2} (1.491 \times 10^{-1})$	$3.947 \times 10^0 (2.094 \times 10^1)$	$3.902 \times 10^0 (2.084 \times 10^1)$
128	$3.010 \times 10^{-3} (3.612 \times 10^{-2})$	$1.910 \times 10^0 (1.011 \times 10^1)$	$1.897 \times 10^0 (1.009 \times 10^1)$
256	$7.040 \times 10^{-4} (8.885 \times 10^{-3})$	$9.382 \times 10^{-1} (4.966 \times 10^0)$	$9.354 \times 10^{-1} (4.96 \times 10^0)$
LSF $E(h)$	$0.37 * h^{2.025} (4.37754 * h^{2.03})$	$21.6 * h^{1.02} (116.017 * h^{1.029})$	$20.9 * h^{1.01} (114.498 * h^{1.02})$

Table 5.2: Errors between numerical solution U and the exact solution u .

representation of a equilibrium point type, but dissociated from a behavior of stagnation point at zero position. Only 128 mesh grid was used in this simulations. The *unbiased* upwinding Riemann-solver-free Lagrangian-Eulerian framework (5.0.7)-(5.0.8) seems to perform a well-balancing between the computation of the numerical flux function and the source term in order to capture the correct structure of the solution, which it turn is clearly time dependent of the source term. On the bottom row is shown superimposed pictures with the analytical solution (solid line) for the above Cauchy problem and the numerical approximations (with 256 mesh grids) given by the Lagrangian-Eulerian scheme (5.0.7)-(5.0.8) with discretization rules for the source term: exact (left), midpoint (middle) and trapezoidal (right). The expected order of accuracy (see Section 5.1.3) is $O(1)$ as we can see from the error shown in the Table in l_h^∞ and l_1^∞ norms.

5.2 Nonlinear balance law

Let us now turn our attention to the Lagrangian-Eulerian procedure developed for linear hyperbolic conservation laws to the case of nonlinear scalar and systems of balance

laws. Again, the key point here is to design well-balanced discretization of the flux function and the source term. From the very beginning of Section 5, we design the Lagrangian-Eulerian numerical procedure (5.0.7)-(5.0.8), for balance law of type in (5.0.3) given by,

$$\begin{aligned}\bar{U}_j^{n+1} &= \frac{1}{h_j^{n+1}} \int_{\bar{x}_{j-\frac{1}{2}}^{n+1}}^{\bar{x}_{j+\frac{1}{2}}^{n+1}} u(x, t^{n+1}) dx = \frac{1}{h_j^{n+1}} \left[\int_{x_j^n}^{x_{j+1}^n} u(x, t^n) dx + \iint_{D_j^n} G(u) dx dt \right], \\ U_j^{n+1} &= \frac{1}{h} \left[\left(\frac{h}{2} + f_j^n k \right) \bar{U}_{j-1}^{n+1} + \left(\frac{h}{2} - f_j^n k \right) \bar{U}_j^{n+1} \right].\end{aligned}$$

The combination of the above equations (see (5.0.7)-(5.0.8)) gives the *Lagrangian-Eulerian scheme 1 (LEB1)*:

$$\begin{aligned}U_j^{n+1} &= \frac{1}{4} (U_{j-1}^n + 2U_j^n + U_j^n) - \frac{k}{4} (\mathbb{W}(U_{j+1}^n, U_j^n) - \mathbb{W}(U_{j-1}^n, U_j^n)) \\ &\quad + \frac{1}{h} \left[\frac{1}{h} \left(\frac{h}{2} + f_j^n k \right) \iint_{D_{j-1}^n} G(u(x, t)) dx dt + \frac{1}{h} \left(\frac{h}{2} - f_j^n k \right) \iint_{D_j^n} G(u(x, t)) dx dt \right],\end{aligned}\tag{5.2.1}$$

along with CFL condition 4.1.2. where $f_j^n = H(U_j^n)/U_j^n \approx H(U)/U$; see (5.0.3).

On the other hand, from scheme (3.2.1), it is also possible design a *difference finite Lagrangian-Eulerian scheme 2 (LEB2)*:

$$\begin{aligned}U_j^{n+1} &= \frac{1}{4} (U_{j-1}^n + 2U_j^n + U_{j+1}^n) - \frac{k}{2h} (H(U_{j+1}^n) - H(U_{j-1}^n)) \\ &\quad + \frac{1}{h} \left[\frac{1}{h} \left(\frac{h}{2} + f_j^n k \right) \iint_{D_{j-1}^n} G(u(x, t)) dx dt + \frac{1}{h} \left(\frac{h}{2} - f_j^n k \right) \iint_{D_j^n} G(u(x, t)) dx dt \right].\end{aligned}\tag{5.2.2}$$

along the CFL condition

$$\frac{\max\{\max_j\{H'(U_j)\}, \max_j\{f_j^n\}\} k}{h} \leq \frac{\sqrt{2}}{2}.\tag{5.2.3}$$

The keystone in both methods LEB1 (5.2.1) and LEB2 (5.2.2) is to perform a well-balancing between the computation of the numerical flux function and the source term by means of the naturally *unbiased* upwinding Riemann-solver-free for nonlinear problems dictates by the parameterized curves $\sigma_j^n(t)$ to model the ‘‘Integral tube’’ D_j^n (see (2.1.6) and (2.1.12), and pictures in Figure 2.1). The schemes LEB1 (5.2.1) and LEB2 (5.2.2), they admit a conservative numerical flux function (4.1.9)-(4.1.10) and (3.2.3)-(3.2.4). Indeed, notice the resemblance between (5.1.2) for the linear balance law and equation (5.2.1). Quantities $\left(\frac{h}{2} + f_j^n k\right)$ and $\left(\frac{h}{2} - f_j^n k\right)$ are not the characteristic curves associated with the quasilinear form of the homogeneous counterpart of the balance law, i.e., $u_t + H_x(u) = 0$, but rather they are precisely an approximation of the conservative integral tubes that are naturally extracted from the conservative integral form of the nonlinear balance law given by (5.0.3), which in turn dictates the dynamics of the local space-time control volume D_j^n and the position $\sigma_j^n(t)$ to any quadrature rule of the source term $G(u)$ of the RHS of (5.0.3). In addition, the balance problem is then solved by forward tracking the boundary of grid cells along the so-called integral tubes. This is a distinct feature

of the proposed Lagrangian-Eulerian approach. For instance, the similar Eulerian-Lagrangian schemes in [22, 21, 20, 80] are designed to handle trace-back integration related to purely hyperbolic problems rather than balance laws. Next, let us discuss three quadrature rules, based on the above framework.

For simplicity of notation in what follows, consider $\Phi = \Phi(x, t) \in C^\infty(\mathbb{R})$ (i.e., under a CFL constraint) such that $\Phi_t + f_x(\Phi) = G(\Phi)$ in order to seek the appropriate approximations for grid functions for $\Phi(x, t)$ in the flux and source term for schemes (5.2.1) and (5.2.2).

5.2.1 Predictor-corrector method

First, suppose $U_j^{n+\frac{1}{2}}$ as a known predictor value for $\Phi(x, t)$ at space-time point (x_j, t^n) . Thus, write the source term approximation as,

$$\iint_{D_j^n} G(\Phi(x, t)) dx dt \approx \iint_{D_j^n} G(U_j^{n+\frac{1}{2}}) dx dt = G(U_j^{n+\frac{1}{2}}) \iint_{D_j^n} dx dt = G(U_j^{n+\frac{1}{2}}) \mathcal{A}(D_j^n),$$

where

$$\mathcal{A}(D_j^n) = \int_{t^n}^{t^{n+1}} \int_{\sigma_j^n(t)}^{\sigma_{j+1}^n(t)} dx dt = \int_{t^n}^{t^{n+1}} (\sigma_{j+1}^n(t) - \sigma_j^n(t)) dt.$$

Since $\sigma_{j+1}^n(t) - \sigma_j^n(t) = (t - t^n)f_{j+1}^n + x_{j+1}^n - (t - t^n)f_j^n - x_j^n = (t - t^n)(f_{j+1}^n - f_j^n) + h$, we recast (5.2.1) as,

$$\mathcal{A}(D_j^n) = k \left[\frac{k}{2}(f_{j+1}^n - f_j^n) + h \right].$$

Now, in view of the balance law $\Phi_t + f_x(\Phi) = G(\Phi)$ we might write $\Phi_t = G(\Phi) - f_x(\Phi)$ and thus reads,

$$G(\Phi_j^{n+\frac{1}{2}}) \approx G(\Phi(x_j^n, t^n) + \frac{k}{2}\Phi_t(x_j^n, t^n)) = G \left[\Phi_j^n + \frac{k}{2}(G(\Phi_j^n) - (f(\Phi))_x)_j^n \right].$$

We point out that quantity $f_x(\Phi(x, t))_j^n$ denotes the numerical derivative of function $f(\Phi)$ with respect to space variable x evaluated at point (x_j, t^n) . Indeed, a family of slope limiters can be used here, as such the *Mimmod limiter*: $((f(\Phi))_x)_j^n = MM\{\Delta f_{j+\frac{1}{2}}, \Delta f_{j-\frac{1}{2}}\}$ where $MM\{x, y\} \equiv MinMod\{x, y\} = \frac{1}{2}[sgn(x) + sgn(y)] \cdot Min(|x|, |y|)$ (see elsewhere, e.g., [2, 39, 99, 109, 115, 124]). Finally, from equations (5.2.1) and (5.2.1), we might write,

$$\iint_{D_j^n} G(\Phi(x, t)) dx dt \approx k G \left[U_j^n + \frac{k}{2}(G(U_j^n) - f_x(\Phi)_j^n) \right] \left[\frac{k}{2}(f_{j+1}^n - f_j^n) + h \right]. \quad (5.2.4)$$

Next, we turn to more simple quadrature, which in turn requires much less regularity of the source term.

5.2.2 Midpoint method

Considering the approximations for the parameterized curves $\sigma_r^n(t)$ at $t = t^{n+\frac{1}{2}}$ associated to the integral tubes D_r^n , $r = j, j + 1$ one might write,

$$\begin{aligned} \iint_{D_j^n} G(\Phi(x, t)) dx dt &\approx \int_{t^n}^{t^{n+1}} (\sigma_{j+1}^n(t) - \sigma_j^n(t)) G\left(\Phi\left(\frac{\sigma_{j+1}^n(t) + \sigma_j^n(t)}{2}, t\right)\right) dt \approx \\ &\approx kh G\left(\Phi\left(\frac{\sigma_{j+1}^n(t^{n+\frac{1}{2}}) + \sigma_j^n(t^{n+\frac{1}{2}})}{2}, t^{n+\frac{1}{2}}\right)\right) \approx kh G\left(\Phi\left(x_j^n + \frac{1}{2}(f_j^n k + h), t^n + \frac{k}{2}\right)\right) \approx \\ &\approx kh G\left(\Phi(x_j, t^n) + \frac{1}{2}(f_j^n k + h)(\Phi_x)_j^n + \frac{k}{2}(G(\Phi_j^n) - f_x(\Phi_j^n))\right). \end{aligned} \quad (5.2.5)$$

Finally, the approximation for the source term by means of the midpoint rule gives:

$$\iint_{D_j^n} G(u(x, t)) dx dt \approx kh G\left(U_j^n + \frac{1}{2}(f_j^n k + h)(u_x)_j^n + \frac{k}{2}(G(U_j^n) - f_x(\Phi_j^n))\right), \quad (5.2.6)$$

where $(u_x)_j^n = MM(\Delta u_{j+\frac{1}{2}}, \Delta u_{j-\frac{1}{2}})$ and $f_x(\Phi_j^n) = MM(\Delta f_{j+\frac{1}{2}}, \Delta f_{j-\frac{1}{2}})$, as before.

5.2.3 Trapezoidal method

Considering the approximations for the parameterized curves $\sigma_r^n(t)$ at $t = t^{n+\frac{1}{2}}$ associated to the integral tubes D_r^n , $r = j, j + 1$ one might write,

$$\begin{aligned} \iint_{D_j^n} G(\Phi(x, t)) dx dt &\approx \int_{t^n}^{t^{n+1}} \frac{1}{2} (\sigma_{j+1}^n(t) - \sigma_j^n(t)) \left(G\left(\Phi(\sigma_{j+1}^n(t), t)\right) + G\left(\Phi(\sigma_j^n(t), t)\right)\right) dt \approx \\ &\approx \frac{k}{2} (\sigma_{j+1}^n(t^{n+\frac{1}{2}}) - \sigma_j^n(t^{n+\frac{1}{2}})) \left(G\left(\Phi(\sigma_{j+1}^n(t^{n+\frac{1}{2}}), t^{n+\frac{1}{2}})\right) + G\left(\Phi(\sigma_j^n(t^{n+\frac{1}{2}}), t^{n+\frac{1}{2}})\right)\right) = \\ &= \frac{k}{2} \frac{h_j^{n+1}}{2} \left(G\left(\Phi\left(x_{j+1} + \frac{k}{2} f_{j+1}^n, t^n + \frac{k}{2}\right)\right) + G\left(\Phi\left(x_j + \frac{k}{2} f_j^n, t^n + \frac{k}{2}\right)\right)\right) \frac{k h_j^{n+1}}{4} \end{aligned} \quad (5.2.7)$$

Finally, the approximation for the source term by means of the trapezoidal rule gives:

$$\iint_{D_j^n} G(u(x, t)) dx dt \approx \frac{k h_j^{n+1}}{4} \left(\begin{aligned} &G\left(U_{j+1}^n + \frac{k}{2}(f_{j+1}^n)(u_x)_{j+1}^n + \frac{k}{2}(G(U_{j+1}^n) - f_x(u)_{j+1}^n)\right) \\ &+ G\left(U_j^{n+1} + \frac{k}{2}(f_j^n)(u_x)_j^n + \frac{k}{2}(G(U_j^n) - f_x(u)_j^n)\right) \end{aligned} \right). \quad (5.2.8)$$

Other type of approximations for the source term can be performed when the source term has the form $G(x, u) = \frac{da(x)}{dx}$ or $G(x, u) = u \frac{da(x)}{dx}$. In these cases the approximations to the integral tubes D_r^n , $r = j, j + 1$ are as follows,

$$\begin{aligned} \iint_{D_j^n} G(x, u) dA &= \int_{t^n}^{t^{n+1}} \int_{\sigma_j^n(t)}^{\sigma_{j+1}^n(t)} \frac{da(x)}{dx} dx dt = \int_{t^n}^{t^{n+1}} (a(\sigma_{j+1}^n(t)) - a(\sigma_j^n(t))) dt \\ &\approx k (a(\sigma_{j+1}^n(t^{n+\frac{1}{2}})) - a(\sigma_j^n(t^{n+\frac{1}{2}}))) \\ &= k \left(a\left(x_{j+1} + \frac{k}{2} f_{j+1}^n\right) - a\left(x_j + \frac{k}{2} f_j^n\right)\right), \end{aligned} \quad (5.2.9)$$

by the source term $G(x, u) = u \frac{da(x)}{dx}$, supported in balance law, we use the predictor $\bar{U}_j^{n+1} \approx \frac{h}{h_j^{n+1}}(U_j^n + U_{j+1}^n)$

$$\begin{aligned}
\iint_{D_j^n} G(x, u) dA &= \int_{t^n}^{t^{n+1}} \int_{\sigma_j^n(t)}^{\sigma_{j+1}^n(t)} u \frac{da(x)}{dx} dx dt \approx \int_{t^n}^{t^{n+1}} \int_{\sigma_j^n(t)}^{\sigma_{j+1}^n(t)} \bar{U}_j^{n+1} \frac{da(x)}{dx} dx dt \\
&= \frac{h}{h_j^{n+1}} (U_j^n + U_{j+1}^n) \int_{t^n}^{t^{n+1}} (a(\sigma_{j+1}^n(t)) - a(\sigma_j^n(t))) dt \\
&\approx \frac{kh}{h_j^{n+1}} (U_j^n + U_{j+1}^n) (a(\sigma_{j+1}^n(t^{n+\frac{1}{2}})) - a(\sigma_j^n(t^{n+\frac{1}{2}}))) \\
&= \frac{kh}{h_j^{n+1}} (U_j^n + U_{j+1}^n) \left(a(x_{j+1} + \frac{k}{2} f_{j+1}^n) - a(x_j + \frac{k}{2} f_j^n) \right).
\end{aligned} \tag{5.2.10}$$

5.3 Stability of the Lagrangian Eulerian scheme to non-linear balance law

In order to prove stability of the numerical method, we will make use of results established in [142]. We start with the following theorem

Theorem 5.3.1. A one-step finite difference scheme (with constant coefficient) is stable in a stability region Λ if and only if there is a constant K (independent of θ , k and h) such that

$$|g(\theta, k, h)| \leq 1 + Kk, \quad \text{with } (k, h) \in \Lambda. \tag{5.3.1}$$

If $g(\theta, k, h)$ is independent of h and k , the stability condition can be replaced with restricted stability condition $|g(\theta)| \leq 1$.

To show stability properties of the Lagrangian-Eulerian scheme (5.2.1) for balance laws (5.0.3), we make use of a slightly modification of the linear Lagrangian-Eulerian scheme (2.1.15). Indeed, we will also use the next result also stated in [142].

Corollary 5.3.1. If a scheme as in Theorem 5.3.1 is modified so that the modifications result only in the addition to the amplification factor of terms that are $O(k)$ uniformly in ξ , then the modified scheme is stable if and only if the original scheme is stable.

Thus, we might write the nonlinear balance law (5.0.3) in the quasilinear form (e.g., under a stability condition (4.1.2)),

$$\frac{\partial u}{\partial t} + f'(u) \frac{\partial u}{\partial x} = G(u). \tag{5.3.2}$$

Therefore, in view of the local volume D_j^n equation (5.3.2) can be recast as in the form of the linear balance law,

$$\frac{\partial u}{\partial t} + a \frac{\partial u}{\partial x} = G(u), \tag{5.3.3}$$

where we take $G(u) = u$ and $a = \max |f'(u)|$ over D_j^n . Thus, the Lagrangian-Eulerian scheme (5.2.1) to the nonlinear balance law (5.3.2) will be approximate locally in D_j^n by,

$$\begin{aligned} U_j^{n+1} &= \frac{1}{4} (U_{j-1}^n + 2U_j^n + U_{j+1}^n) - \frac{ak}{2h} (U_{j+1}^n - U_{j-1}^n) \\ &+ \frac{1}{h} \left[\frac{1}{h} \left(\frac{h}{2} + ak \right) \iint_{D_{j-1}^n} u(x, t) dx dt + \frac{1}{h} \left(\frac{h}{2} - ak \right) \iint_{D_j^n} u(x, t) dx dt \right]. \end{aligned} \quad (5.3.4)$$

In what follows we will now show the stability property to the ‘‘predictor corrector’’. Indeed, we will also show in the subsequent section that the same analysis holds to other discretization as such the ‘‘midpoint rule’’ as well as ‘‘the trapezoidal rule’’.

5.3.1 Predictor corrector approximation

Thus, from equation (5.2.4) we have that,

$$\iint_{D_j^n} u(x, t) dx dt \approx k h \left(U_j^n + \frac{k}{2} (U_j^n - a(u_x)_j^n) \right) \approx k h \left[\left(1 + \frac{k}{2} \right) U_j^n + O(k) \right]. \quad (5.3.5)$$

Plugging equation (5.3.5) in the integral source term in the equation (5.3.4) reads,

$$S_j^n = k \left(\frac{1}{2} + v \right) \left(1 + \frac{k}{2} \right) U_{j-1}^n + k \left(\frac{1}{2} - v \right) \left(1 + \frac{k}{2} \right) U_j^n + O(k^2). \quad (5.3.6)$$

Replacing (5.3.6) into the Lagrangian-Eulerian scheme (5.3.4) and setting $U_j^n = \bar{g}(\xi)^n e^{i\xi j h}$, it is an exercise get the the amplification factor $\bar{g}(\xi)$ associated to the Lagrangian-Eulerian scheme (5.2.1) given by,

$$\bar{g}(\xi) = \frac{1}{2} (1 + \cos(\xi h)) + v i \sin(\xi h) + k \left(\frac{1}{2} + v \right) \left(1 + \frac{k}{2} \right) e^{-i\xi h} + k \left(\frac{1}{2} - v \right) \left(1 + \frac{k}{2} \right) + O(k^2). \quad (5.3.7)$$

First, remember that $g(\xi) = \frac{1}{2} (1 + \cos(\xi h)) + v i \sin(\xi h)$ is the amplification factor of the Lagrangian Eulerian scheme to the linear case, which in turn we proved to be stable. Therefore, we might write $\bar{g}(\xi)$ in terms as the amplification factor Lagrangian Eulerian scheme to the linear case as follows,

$$\bar{g}(\xi) = g(\xi) + k \left(\frac{1}{2} + v \right) \left(1 + \frac{k}{2} \right) e^{-i\xi h} + k \left(\frac{1}{2} - v \right) \left(1 + \frac{k}{2} \right) + O(k^2). \quad (5.3.8)$$

One can easily see that $|e^{-i\xi h}| = 1$ and then,

$$|\bar{g}(\xi)| \leq |g(\xi)| + O(k) \leq 1 + O(k). \quad (5.3.9)$$

Thus, by (5.3.9) and Corollary 5.3.1 we conclude that the Lagrangian Eulerian scheme (5.2.1) is ℓ^2 -stable.

5.3.2 An approximation of the source term by the Midpoint quadrature rule

Now, consider an approximation of the source term (5.2.6) by the Midpoint quadrature rule,

$$\iint_{D_j^n} u(x, t) dx dt \approx kh \left(U_j^n + \frac{1}{2}(ak + h)(u_x)_j^n + \frac{k}{2}(U_j^n - a(u_x)_j^n) \right), \quad (5.3.10)$$

then

$$\iint_{D_j^n} u(x, t) dx dt \approx kh \left(\left(1 + \frac{k}{2}\right)U_j^n + \frac{h}{2}(u_x)_j^n \right). \quad (5.3.11)$$

Now, from the above, we notice that $h = O(k)$. Therefore,

$$\iint_{D_j^n} u(x, t) dx dt \approx kh \left(\left(1 + \frac{k}{2}\right)U_j^n + O(k) \right). \quad (5.3.12)$$

Finally, by plugging the above equation (5.3.12) into the modified linear scheme (5.3.4) reads,

$$|\bar{g}(\xi)| \leq |g(\xi)| + O(k) \leq 1 + O(k). \quad (5.3.13)$$

Therefore, again by the Corollary 5.3.1 we are able to conclude that the Lagrangian Eulerian scheme (5.2.1) is ℓ^2 -stable by means of the approximation of the source term by the Midpoint quadrature rule.

5.3.3 An approximation of the source term by the Trapezoidal quadrature rule

Now, consider an approximation of the source term (5.2.6) by the Trapezoidal quadrature rule,

$$\begin{aligned} \iint_{D_j^n} u(x, t) dx dt &\approx \frac{kh}{4} \left(\begin{aligned} &\left(U_{j+1}^n + \frac{k}{2}a(u_x)_{j+1}^n + \frac{k}{2}(U_{j+1}^n - a(u_x)_{j+1}^n) \right) \\ &+ \left(U_j^{n+1} + \frac{k}{2}a(u_x)_j^n + \frac{k}{2}(U_j^n - a(u_x)_j^n) \right) \end{aligned} \right) \\ &= \frac{kh}{4} \left(\left(1 + \frac{k}{2}\right)U_{j+1}^n + \left(1 + \frac{k}{2}\right)U_j^n \right) = \frac{kh}{4} \left(1 + \frac{k}{2}\right) (U_{j+1}^n + U_j^n), \end{aligned} \quad (5.3.14)$$

By replacing equation (5.3.14) into the source term in the equation (5.3.4) reads,

$$\begin{aligned} S_j^n &= \frac{1}{h} \left[\frac{1}{h} \left(\frac{h}{2} + ak \right) \iint_{D_{j-1}^n} u(x, t) dx dt + \frac{1}{h} \left(\frac{h}{2} - ak \right) \iint_{D_j^n} u(x, t) dx dt \right] \\ &\approx \frac{1}{h} \left[\frac{1}{h} \left(\frac{h}{2} + ak \right) \frac{kh}{4} \left(1 + \frac{k}{2}\right) (U_{j-1}^n + U_j^n) + \frac{1}{h} \left(\frac{h}{2} - ak \right) \frac{kh}{4} \left(1 + \frac{k}{2}\right) (U_{j+1}^n + U_j^n) \right] \\ &= \frac{k}{4} \left(\frac{1}{2} + v \right) \left(1 + \frac{k}{2}\right) (U_{j-1}^n + U_j^n) \frac{k}{4} \left(\frac{1}{2} - v \right) \left(1 + \frac{k}{2}\right) (U_{j+1}^n + U_j^n). \end{aligned} \quad (5.3.15)$$

Plugging equation (5.3.15), along with $U_j^n = \bar{g}(\xi)^n e^{i\xi j h}$, into the Lagrangian-Eulerian scheme (5.3.4) we can establish that the amplification factor $\bar{g}(\xi)$ of the Lagrangian-Lagrangian scheme to nonlinear balance law is given by,

$$\begin{aligned} \bar{g}(\xi) &= \frac{1}{2}(1 + \cos(\xi h)) + v i \sin(\xi h) + \frac{k}{4} \left(\frac{1}{2} + v \right) \left(1 + \frac{k}{2} \right) (e^{-i\xi h} + 1) \\ &+ \frac{k}{4} \left(\frac{1}{2} - v \right) \left(1 + \frac{k}{2} \right) (1 + e^{i\xi h}) + O(k^2). \end{aligned} \quad (5.3.16)$$

From (5.3.16) one can get,

$$|\bar{g}(\xi)| \leq |g(\xi)| + O(k) \leq 1 + O(k). \quad (5.3.17)$$

Therefore, by Corollary 5.3.1 we conclude that the Lagrangian-Eulerian scheme (5.2.1) is ℓ^2 -stable.

5.4 Numerical experiments for nonlinear scalar balance laws

Model Problem 5.4.1. Greenberg and LeRoux (SINUM, 1996) [71].

In [71], they concentrated on the approximation of a Cauchy prototype problem for an inhomogeneous and genuinely nonlinear balance law endowed with a linear term. There were an interest in the computation of balance laws with multiple nonnegative equilibria or stable steady solutions. On physical grounds, this can be motivate for instance by gravity-driven flows such as those described by the shallow water equations over a nonuniform ocean bottom. For concreteness, Greenberg and LeRoux considered a balance law (5.0.3) with flux function $f(u) = u^2/2$ and source term of the RHS of (5.0.3) as $G(u) = u a_x(x)$ with $a(x) = 0.9(\cos(\pi \frac{x-1}{2}))^{30}$, $0 \leq x \leq 2$ and 0 otherwise. The first numerical experiment pictures in Figure 5.3 involves a smooth steady flow that correspond to steady solutions for which $u + a = 1$ which is shown in solid line at these picture computed with Lagrangian-Eulerian scheme LEB1 (top) and LEB2 (bottom) at time $t = 1$ with: 256 cells (left), 512 cells (middle) and 1024 cells (right).

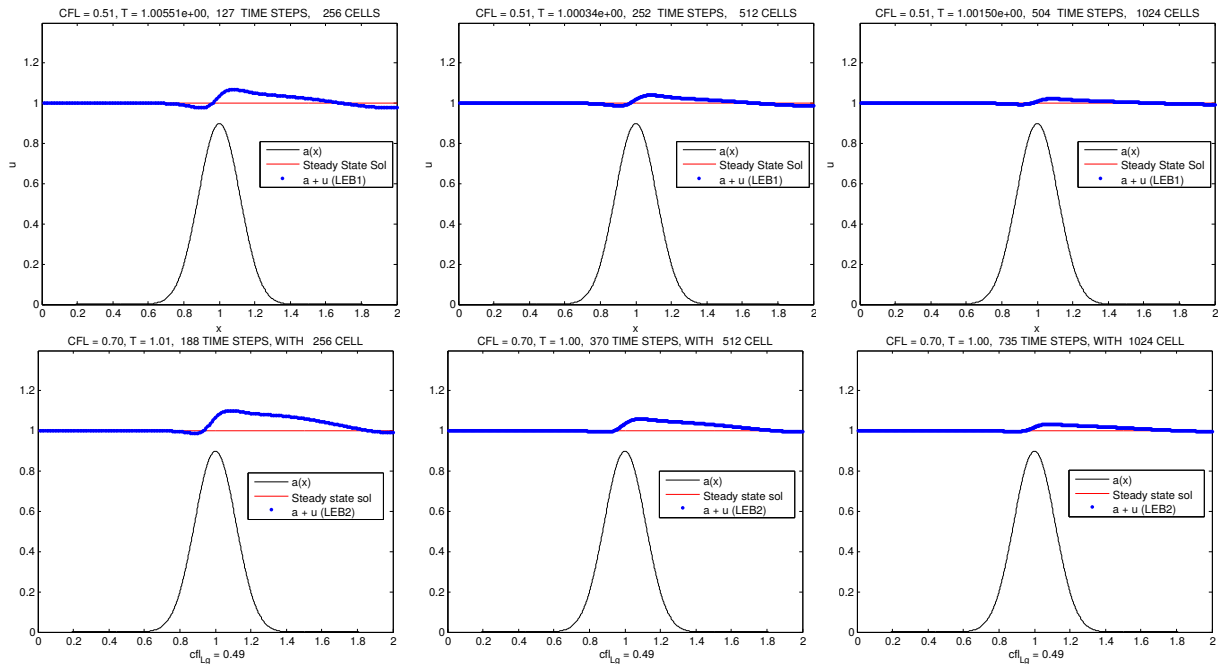


Figure 5.3: **Steady solutions** for which $u + a = 1$ at time $t = 1$

In this numerical experiment are shown on the top picture to LEB1 scheme (5.2.1) and bottom to LEB2 scheme (5.2.2), where $a(x)$ is as defined above for the Greenberg and LeRoux problem such that the initial data is the steady state solution $u(x, 0) = -a(x)$, $x \in \mathbb{R}$, which in turn should be maintained for all times of simulation. The mild spurious fluctuations generated by the LEB1 and LEB2 are not physically correct although it is worth remarking the reduction of the error as the mesh grid is refined leading to a qualitatively correct approximation of the Cauchy problem keeping the horizontal line is the equilibrium solution $u + a = 1$. While the second numerical pictures in Figure 5.4 involves a non-stationary shock wave connecting two states that correspond to steady solutions for which $u + a = 1.3$ left and $u + a = 1$ right. In this numerical experiment is shown on the top picture with LEB1 scheme and bottom with LEB2 scheme, in the numerical test, the initial data is $u(x, 0) = 1 - a(x)$, $x > 0.2$ and $u(x, 0) = 1.3 - a(x)$, $x < 0.2$. Again, both schemes LEB1 and LEB2 give a clearly qualitatively correct monotone decreasing curve as the mesh grid is refined keeping the total height $u + a$ at $t = 1.5$. 256 cells (left), 512 cells (middle) and 1024 cells (right). So far no high-order upwind techniques were considered nor nonlinear reconstruction were used. We only use these schemes in a very simple form. Then, we expect to improve such balance between source term and flux to reduce the error in coarse grids. These “simple schemes” however provides even better satisfactory results when computing some specific well known unsteady and steady cases as will be discussed in what follows

Model Problem 5.4.2. Greenberg, LeRoux, Baraille and Noussair (SINUM, 1997) [70].

In [70], Greenberg et al. continued the study initiated in [71] on the design of robust and efficient numerical procedures for scalar balance laws of type (5.0.3). In [70], it was proposed a series of numerical experiments order to observe the transient behavior towards steady-state equilibrium solutions. Precisely, they confined their attention to scalar Cauchy problems of type $u_x + f_x(u) = a_x(x)$, $-\infty < x < \infty$, where $f(u)$ is smooth, even, convex function satisfying

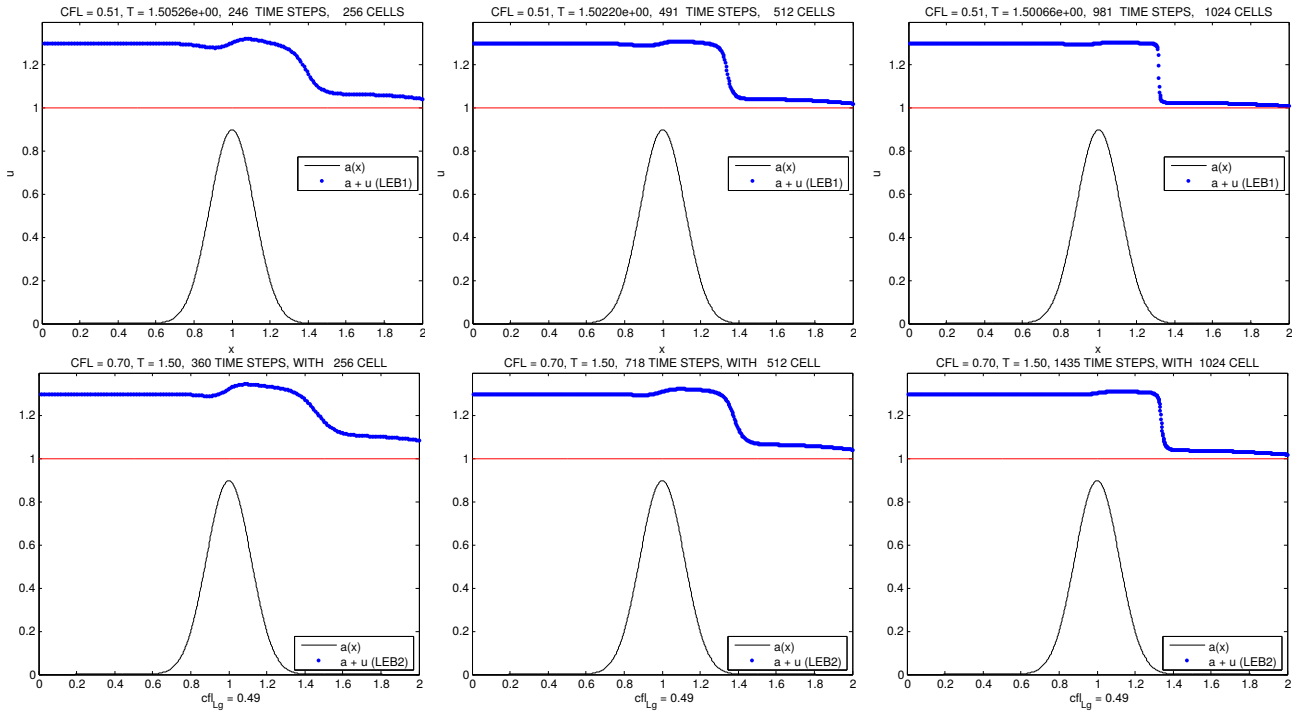


Figure 5.4: **Non-stationary shock wave** connecting two states that correspond to steady solutions for which $u + a = 1.3$ left and $u + a = 1$ right.

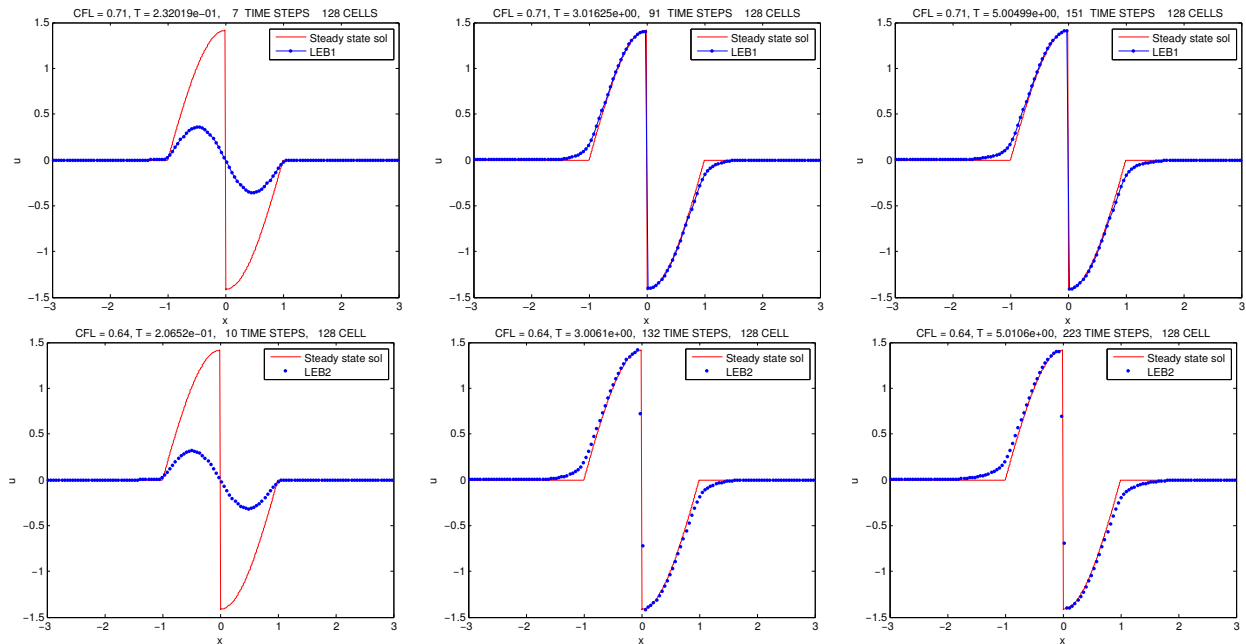
Cells	LEB1 $\ u - U\ _{l_h^1}$	LEB1 $\ u - U\ _{l_h^2}$	LEB2 $\ u - U\ _{l_h^1}$	LEB2 $\ u - U\ _{l_h^2}$
32	5.62×10^{-1}	3.17×10^{-1}	3.23×10^{-1}	3.58×10^{-1}
64	2.97×10^{-1}	1.82×10^{-1}	1.82×10^{-1}	1.61×10^{-1}
128	1.59×10^{-1}	1.09×10^{-1}	1.01×10^{-1}	9.92×10^{-2}
256	8.45×10^{-2}	6.59×10^{-2}	5.47×10^{-2}	6.05×10^{-2}

Table 5.3: Errors between the approximate solution U and exact solution u , schemes LEB1 and LEB2 (test 1).

$f(0) = 0$ and $f(u) > 0$, $-\infty < u < \infty$ and $a(x)$ is a bounded, piecewise smooth function. The interested reader is referred to [70] (see also [71]) for a detailed description of analytical solutions to all design prototype Cauchy problems.

Here we will discuss two case introduced in Greenberg et al. [70] for a balance law of type (5.0.3) as announced above with flux function $f(u) = u^2/2$ and two kinds of source term for the RHS of (5.0.3).

The first test problem, see pictures in Figures 5.5, is given by $G(u) = a_x(x)$ with $a(x) = 0$, $x < -1$, $a(x) = \cos^2(x\pi/2)$, $-1 \leq x \leq 1$, and $a(x) = 0$, $1 < x$. In this example (top and bottom pictures) includes snapshot plots taken at different times of simulation for transient solutions. On the top are shown numerical approximations with LEB1 scheme, and on the bottom are shown numerical approximations with LEB2 scheme. We get a centered expansive rarefaction waves emerging from positions $x = -1$ and $x = 1$ located at the computational domain. The schemes LEB1 and LEB2 accurately resolve the rarefaction-shock interactions at the trailing edges of the support as expected from the analytical analysis reported in [70] (see

Figure 5.5: A steady state **shock** solution

Cells	LEB1 $\ u - U\ _{l_h}$	LEB1 $\ u - U\ _{l_h^2}$	LEB2 $\ u - U\ _{l_h}$	LEB2 $\ u - U\ _{l_h^2}$
32	3.16×10^{-1}	1.94×10^{-1}	6.64×10^{-1}	3.12×10^{-1}
64	1.67×10^{-1}	1.02×10^{-1}	3.05×10^{-1}	1.44×10^{-1}
128	8.59×10^{-2}	5.25×10^{-2}	1.48×10^{-1}	6.97×10^{-2}
256	4.37×10^{-2}	2.67×10^{-2}	7.30×10^{-2}	3.42×10^{-2}

Table 5.4: Errors between the approximate solution U and exact solution u , LEB1 and LEB2 schemes (test 2).

also [67]). It also shown a grid refinement in which is observed $O(1)$ for each scheme (see Table 5.3).

The second test problem, see pictures in Figures 5.6, is somewhat similar, but the solution exhibits a distinct character, and it is given by $G(u) = a_x(x)$ with $a(x) = 0, x < -1, a(x) = -\cos^2(x\pi/2), -1 \leq x \leq 1, a(x) = 0, 1 < x$. All numerical solutions reported in Figures 5.5 and 5.6 top were computed with the Lagrangian-Eulerian scheme LEB1 (5.2.1), along with a uniform mesh grid under CFL stability criterion (2.1.28), the numerical solutions in Figures 5.5 and 5.6 bottom were computed with the Lagrangian-Eulerian scheme LEB2 (5.2.2). A numerical refinement study for such test problem are also reported in Figure 5.5, for the discrete counterparts L_1 and L_2 norms with observed $O(1)$ (see Table 5.4).

In the approximations of figure 5.6, both LEB1 and LEB2 schemes, shown front-type solutions are formed at position located at $x = -1$ and $x = 1$, which in turn move towards to the left and to the right of the computational domain, at entirely entropy-correct speed and showing that the steady state is perfectly maintained with no spurious fluctuations at the equilibrium solution as time evolves. Again, so far no high-order upwind techniques were considered nor nonlinear reconstruction were used. We point out the our Lagrangian-Eulerian scheme LEB2 was used in a very simple form. Indeed, it is well known that numerical schemes for balance

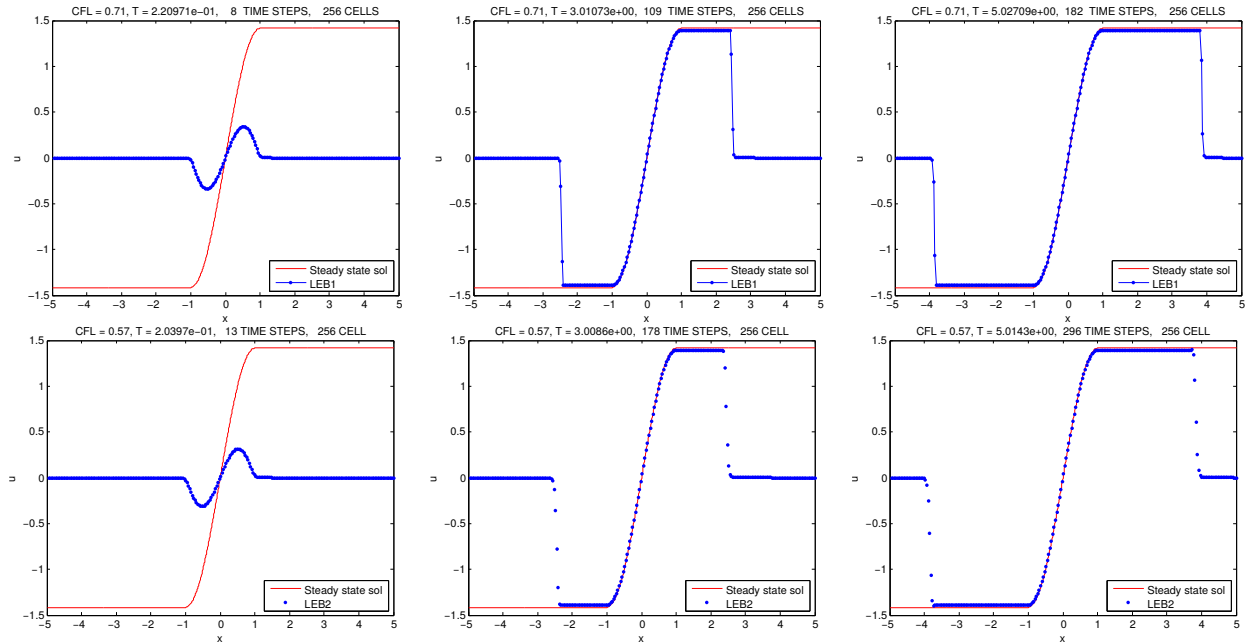


Figure 5.6: **Front-type solutions** are formed at position located at $x = -1$ and $x = 1$

laws need to be able to compute accurately steady state, or nearly steady state, i.e., it means solutions for which the flux gradients are non-zero but are exactly or approximately, balanced by the source terms. Numerical schemes with respect such balance that occurs on the steady flow are called “Well Balanced”. Thus, based on the computed solution we can say that our Lagrangian-Eulerian show some numerical evidence to preserve such nice property [70, 71] (see also [67]).

Model Problem 5.4.3. Greenberg and LeRoux (SINUM, 1997) [45, 70].

Greenberg and LeRoux also propose an physical grounds, this can be motivated for instance by gravity-driven flows such as those described by the shallow water equations over a nonuniform ocean bottom.

Greenberg and LeRoux considered a balance law (5.0.3), with flux function $f(u) = u^2/2$ and source term of the RHS of (5.0.3) as $G(u) = a_x(x)$ with $a(x) = \cos^2(\frac{\pi x}{2})$, $-1 \leq x \leq 1$ and 0 otherwise, with initial data $u_0(x) = 1$, $-1 \leq x \leq 1$ and 0 otherwise, these numerical experiments, which are calculated with LEB1 scheme, are shown in Figure 5.7). In the numerical experiment top row of pictures, a shock emerges from $x = 1$, which is correctly captured by our Lagrangian Eulerian scheme LEB1 without spurious oscillatory behavior, as the transient solution evolves towards the steady state flow, while in bottom row of pictures is shown a grid refinement in three different times $T = 5, 15, 25$ with the aim to show the convergence. Notice, a “N-type” wave solution emerge from $x = 1$, which move slowly to the right and tend to the steady state solution, as is claimed in [70].

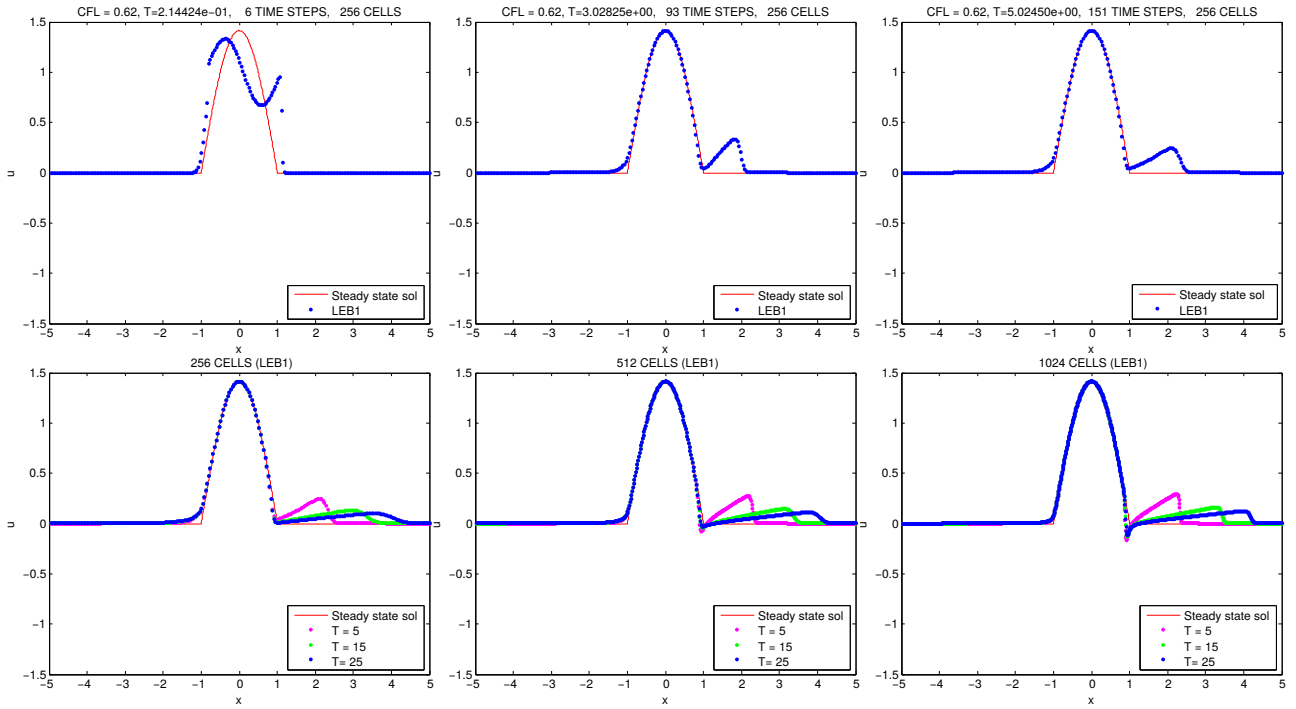


Figure 5.7: Steady state solution with N-wave

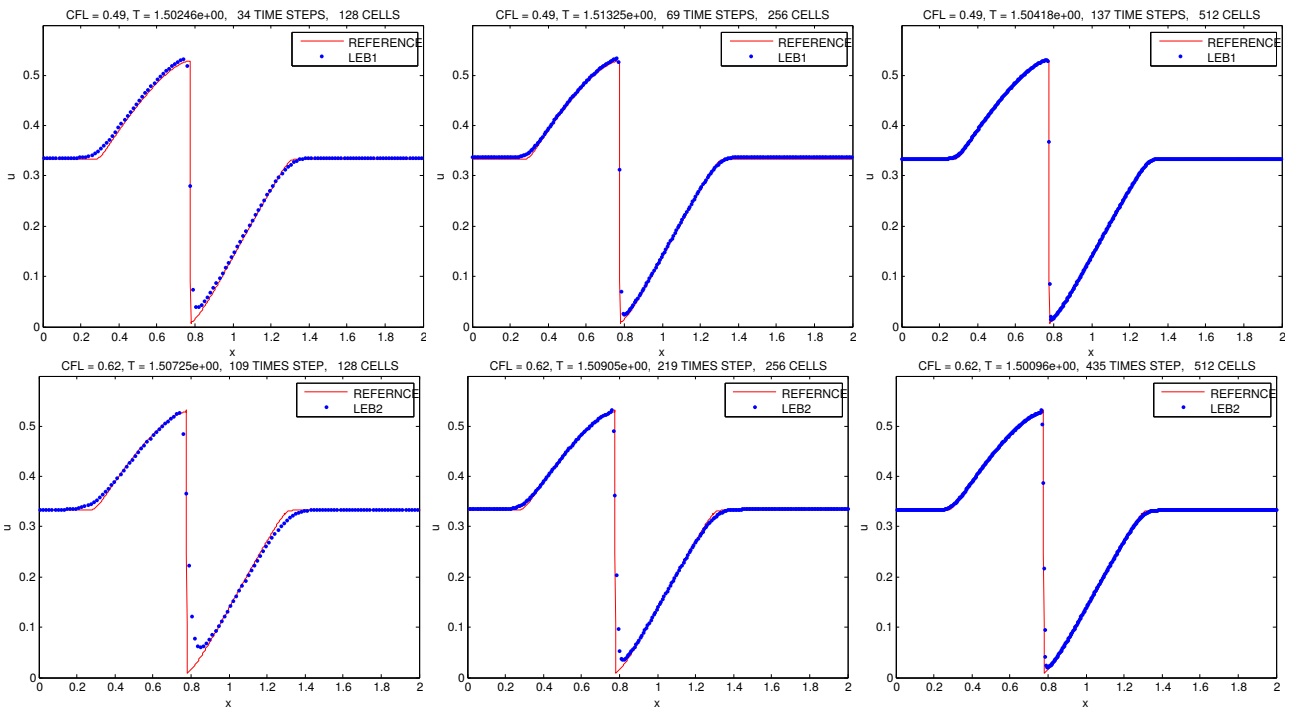


Figure 5.8: Approximated solution with a smooth source function with multiple equilibria.

Model Problem 5.4.4. Langseth, Tveito, and Winther (SINUM) [104].

In [104], Langseth et al. confined their attention to scalar Cauchy problems of type $u_x + f_x(u) = G(u)$, $-\infty < x < \infty$, where $f(u)$ is smooth, even, convex function satisfying $f(0) = 0$ and $f(u) > 0$, $-\infty < u < \infty$ and $G(u) = u(1 - u)$, a smooth source function with multiple equilibria in the domain of interest, hence it is not a decreasing function. For concreteness, Langseth et al. considered the Burgers flux function $f(u) = u^2/2$ along with initial condition $u(x, 0) = 0.1 + 0.1 \sin(2\pi x)$, $0 \leq x \leq 1$ and $u(x, 0) = 0.1$, elsewhere. In Figure 5.8 it is shown the numerical approximations by means of the LEB2 scheme 5.2.1 along with the midpoint rule quadrature rule to the source term that appears in (5.2.6). In the case of no availability of an analytic solution (see [104]), an approximation to the expected “exact solution” is computed using a very fine mesh (2048 cells) numerical solution as the reference solution (solid line in Figure 5.8), for comparison purpose with numerical approximations with 128 cells (left), 256 cells (Middle) and 512 cells (right). Such solutions are in a very good agreement with that reported in [104], where the initial data give rise into a shock. But due to the balance between flux function and source term, the left and right state of the shock will increase and asymptotically reach the steady-state equilibrium $u = 1$. Comparing the computed solution with LEB2 scheme 5.2.1 and that one reported in [104], it is found that the our solution is quite accurate and capturing all qualitative details, even in a coarse grid (left picture in Figure 5.8). Again, our Lagrangian-Eulerian scheme seems to be well-balanced in the sense that the method captured the correct steady states entropy-solution as reported in [104].

Model Problem 5.4.5. Leveque and Yee (JCP), [112].

The model problem proposed by LeVeque and Yee is a scalar linear advection problem with a nonlinear reaction source term, which can be stiff. The governing PDE reads as,

$$\frac{\partial u}{\partial t} + \frac{\partial u}{\partial x} = -\beta u(u - 1)(u - \mu), \quad 0 < \mu < 1, \quad \beta > 0, \quad (5.4.1)$$

As in [112] (see also [45, 58]) we choose $\mu = 0.5$ Indeed, the model problem (5.4.1) with $f(u) = u$ and $\mu = 0.5$ was used in [112] to illustrate a current well-known deficiency of most numerical schemes for hyperbolic conservation laws with stiff source terms: the occurrence of numerical fronts that propagate at non-physical speeds. Notice, the source term in (5.4.1) has multiple equilibrium points, hence it does not fit in the general framework established in [36]. In general, we cannot expect monotonicity for the L_∞ norm, or the TV semi-norm (see [36, 45]) of solutions to (5.4.1), and these properties cannot be expected to hold either in the numerical solutions obtained with the first or second order schemes considered in [36], which in turn are based on semi-implicit and fully implicit Runge-Kutta discretization. Remember, here we are primarily interested in the design the Lagrangian-Framework in the most explicit setting. In (5.4.1), the parameter β controls the stiffness character of the model. For $\beta > 0$, the associated ODE $u = \beta u(u - 1)(u - \mu)$ has stable equilibria at $u = 0$ and $u = 1$, and an unstable equilibrium precisely at $u = \mu$ (see, e.g., [36, 45, 109] for more general details). For $f(u) = u$ as above, and under Riemann type data $u^l = 1$ (left) and $u^r = 0$ (right), the solution is a single discontinuous profile joining the left and right states, that moves with the speed determined by the homogeneous conservation law equal to 1, as is the case of the linear model under consideration (5.4.1). Indeed, solutions to the model problem (5.4.1) exhibits the following property (see, e.g., [36, 45]), *If $u_0(x) \leq w_0(x)$, then the corresponding entropy solutions satisfy*

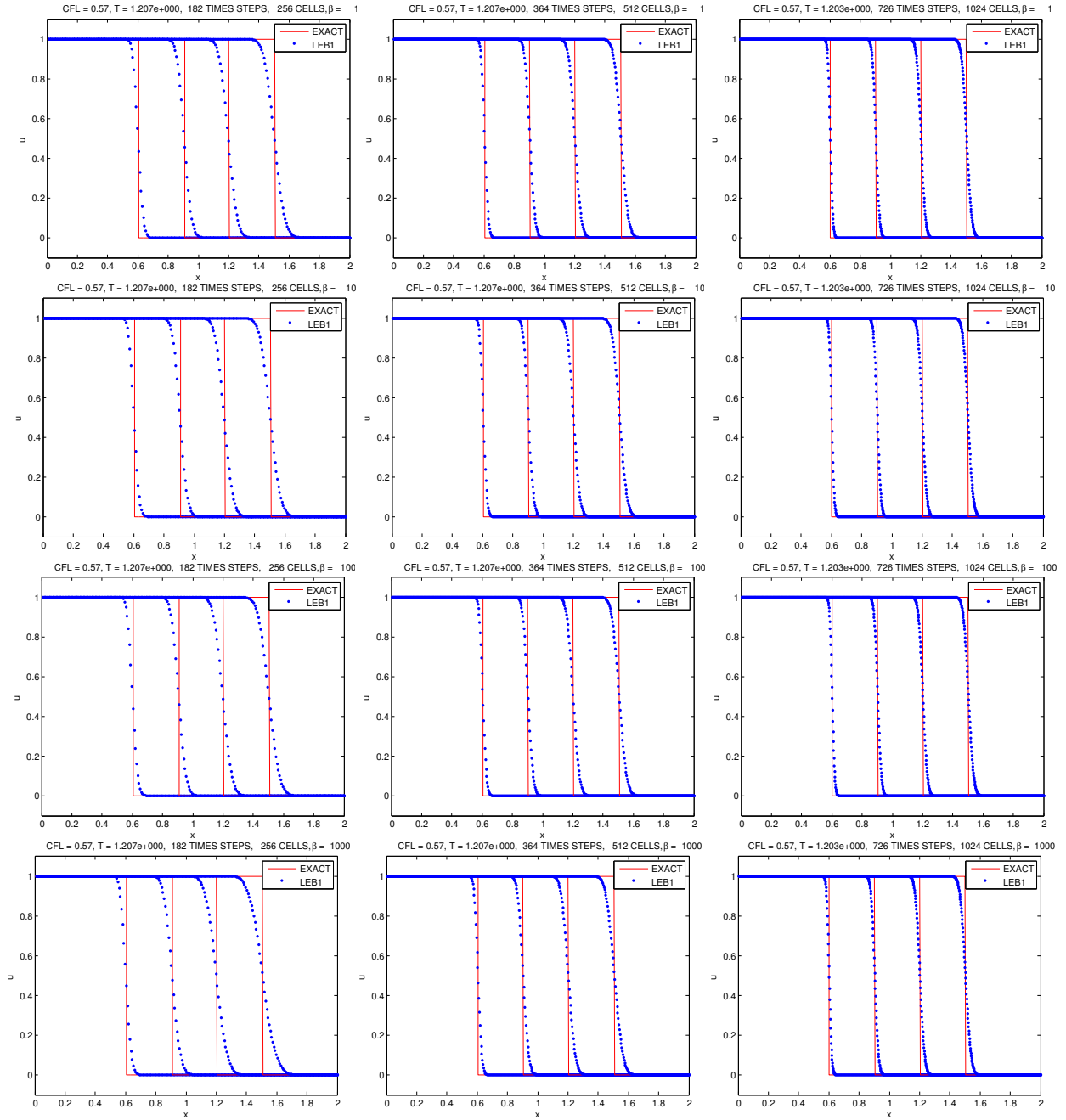


Figure 5.9: approximated solutions for linear advection problem with a nonlinear reaction source term stiff

$u(x, t) \leq w(x, t)$. In light of the *invariant region* (see [45]) linked to a *weak stability concept for explicit, implicit and semi-implicit first order schemes and D-IMEX schemes*, this property means that for model problem (5.4.1), if $0 \leq u(x, 0) \leq 1$ then $0 \leq u(x, t) \leq 1, \forall t > 0$. In the sense of [45], this simply states that $[0, 1]$ is an invariant domain for the balance law (5.4.1). Thus, it seems reasonable to require similar inequalities ($0 \leq U_j^n \leq 1$ for $1 \leq n$ and $\forall j = 1, \dots, T$ (final time index). to hold for the discrete counterpart solution of (5.4.1). Furthermore, such “weak monotonicity” is not ensured (see [109, 112]) by the use of classical flux-limiters in the discretization of the flux function counterpart of the balance law (5.4.1).

Hence, we cannot expect this property to hold for higher order classical IMEX schemes (see [58]). As in [58, 109, 112] no oscillations nor overshoots were observed in our numerical approximations computed by LEB1 5.2.1 (see Figure 5.9), we recall that LEB1 and LEB2 schemes are equivalent in this problem, but with the good distinct feature that we do not use any *flux function limiter* for all cases for $\beta = 1, 10, 100$ and 1000 . Indeed, the numerical solution remains within interval $[0, 1]$ (or the *invariant region property is preserved in the sense of [45]*). Moreover, the LEB1 scheme provide the correct entropy-speed of the jump discontinuity for all cases considered for β . In Figure 5.9, from top to bottom is shown numerical approximations computed by LEB1 scheme 5.2.1 to the above discussed problem at time $t = 0.5$, 256 cells (left), 512 cells (middle) and 1024 cells (right).

Model Problem 5.4.6. A Puzzling Numerical Example, SIMAI Springer Series 2, L. Gosse Springer-Verlag Italia 2013 [67].

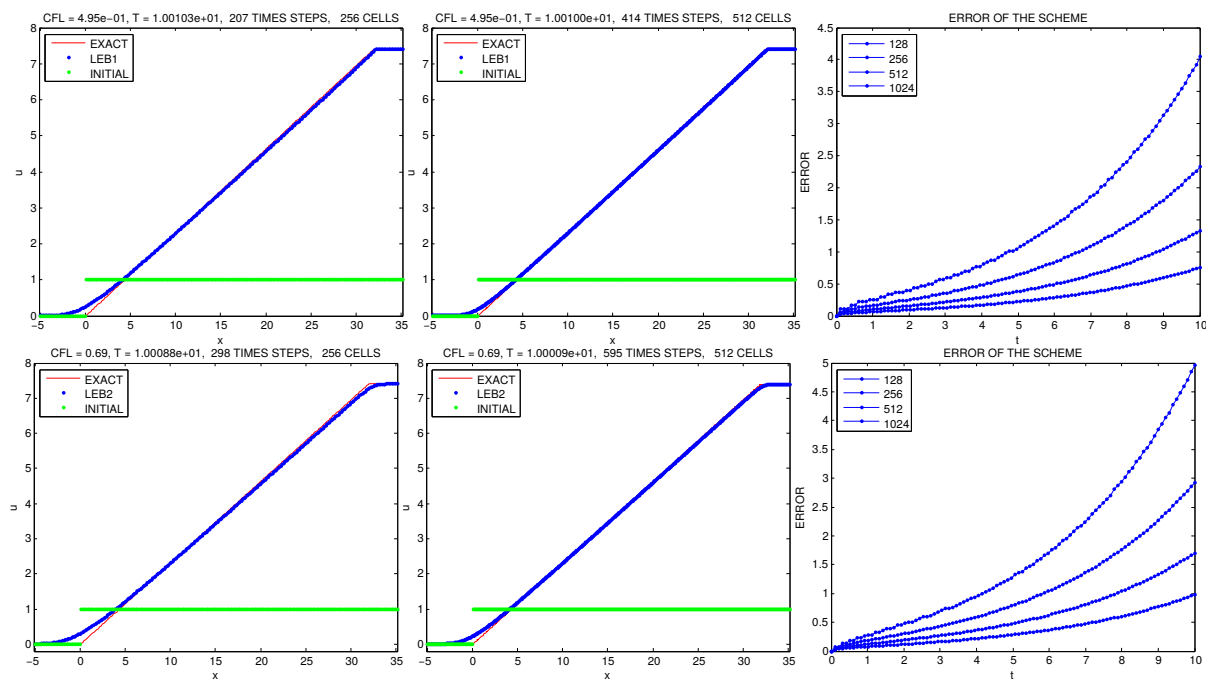


Figure 5.10: Numerical approximations with L^1 -error.

The main goal of the present example is, as in [67], to emphasize the qualitative difference between time-splitting, (or fractional step methods) and well-balanced numerical schemes when it comes to computing the entropy solution [96] of a simple scalar, yet non-resonant, balance law $\partial_t u + \partial_x(f(u)) = k(x)g(u)$, $0 < k \in L^1 \cap C^0(\mathbb{R})$, f is genuinely non-linear and $g \in C^1(\mathbb{R})$,

see [67] for more details. In this particular problem it is considered $f(u) = u^2/2$, $k(x) = 0.2$ and $g(u) = u$ with initial data $u_0(x) = Y(x)$, Y the Heaviside function. This results in the classical “one-half” order of convergence in L^1 , which is known to be optimal for Godunov type [135, 145], denoting the entropy solution u and its numerical approximation by $u^{\Delta t}$; see [145] that states: $\forall t \in [0, T]$, $\|u^{\Delta t}(t, \cdot) - u(t, \cdot)\|_{L^1(\mathbb{R})} \leq C\sqrt{\Delta t}$. The analysis discussed in [144] reveals that the “constant C” is actually an exponential in time, which results in the more rigorous statement: $\forall t \in [0, T]$, $\|u^{\Delta t}(t, \cdot) - u(t, \cdot)\|_{L^1(\mathbb{R})} \leq C \exp(\max[g'(u)]t)\sqrt{\Delta t}$. This estimate is disastrous from a computational standpoint, because in order to keep the absolute error below a given tolerance, the computational grid’s parameters are meant to decrease exponentially with time (except if $g' \leq 0$, for which $TV(u)(t, \cdot)$ decays exponentially too). In Figure 5.10 are shown numerical approximation with our Lagrangian Eulerian schemes to balance law LEB1 (5.2.1) top and LEB2 (5.2.2) bottom; grid refinement with L^1 -error (right) seems to show that the approximation with our scheme converges to the steady solution. Approximations with 256 cells (left) and 512 cells (middle) are shown in Figure 5.10 as expected from [67].

Model Problem 5.4.7. An Inhomogeneous N-Wave, Youngsoo Ha and Yong Jung Kim (JCP, 2006) & L. Gosse (Numer. Math, 2004) [68, 74].

In [74], it was developed a theoretical tool to examine properties of numerical schemes designed for advection problems. Based on this framework, [68] proposed further analysis for balance law problems to account transient regime, which in turn give rise to a similarity-solution analysis of the balance law model

$$\frac{\partial u}{\partial t} + \frac{\partial f(u)}{\partial x} = u, \quad f(u) = \frac{u^4}{4}, \quad u_0(x) = \operatorname{sgn}(x)(3|x|)^{\frac{1}{3}}\chi_{|x| < \frac{1}{2}}, \quad (5.4.2)$$

where χ_A is the characteristic function of a set A . And the solution, according with [74], is

$$u(x, t) = \operatorname{sgn}(x)(3|x|)^{\frac{1}{3}}\chi_{|x| < \frac{1}{2} \exp(\frac{3t}{4})}, \quad t > 0 \quad (5.4.3)$$

The numerical scheme (5.2.1) was applied on the above problem, with different mesh sizes to reproduce the numerical results that are displayed in Figure 5.11, where the mesh grid was refined from 256 cells to 4096 cells into the interval $[-4, 4]$ and the simulation time evolves from time $t = 0$ to $T = 2.65$. In Figure 5.11 (bottom right frame) is displayed an amplification with exponential behavior of the absolute L^1 as the grid is refined. Notice the resemblance between the numerical approximation and the exact solution, as well as the decreasing of the error, as computational grid is refined. The overall computational time was less than one minute in a non-compiled programming language in the finest computational mesh grid. Numerical computed solutions with Lagrangian-Eulerian scheme LEB1 (5.2.1) and LEB2 (5.2.2), and predictor corrector by the source term integral, to the model problem announced above and proposed as one tool to examine the properties of numerical schemes for advection equation in [74].

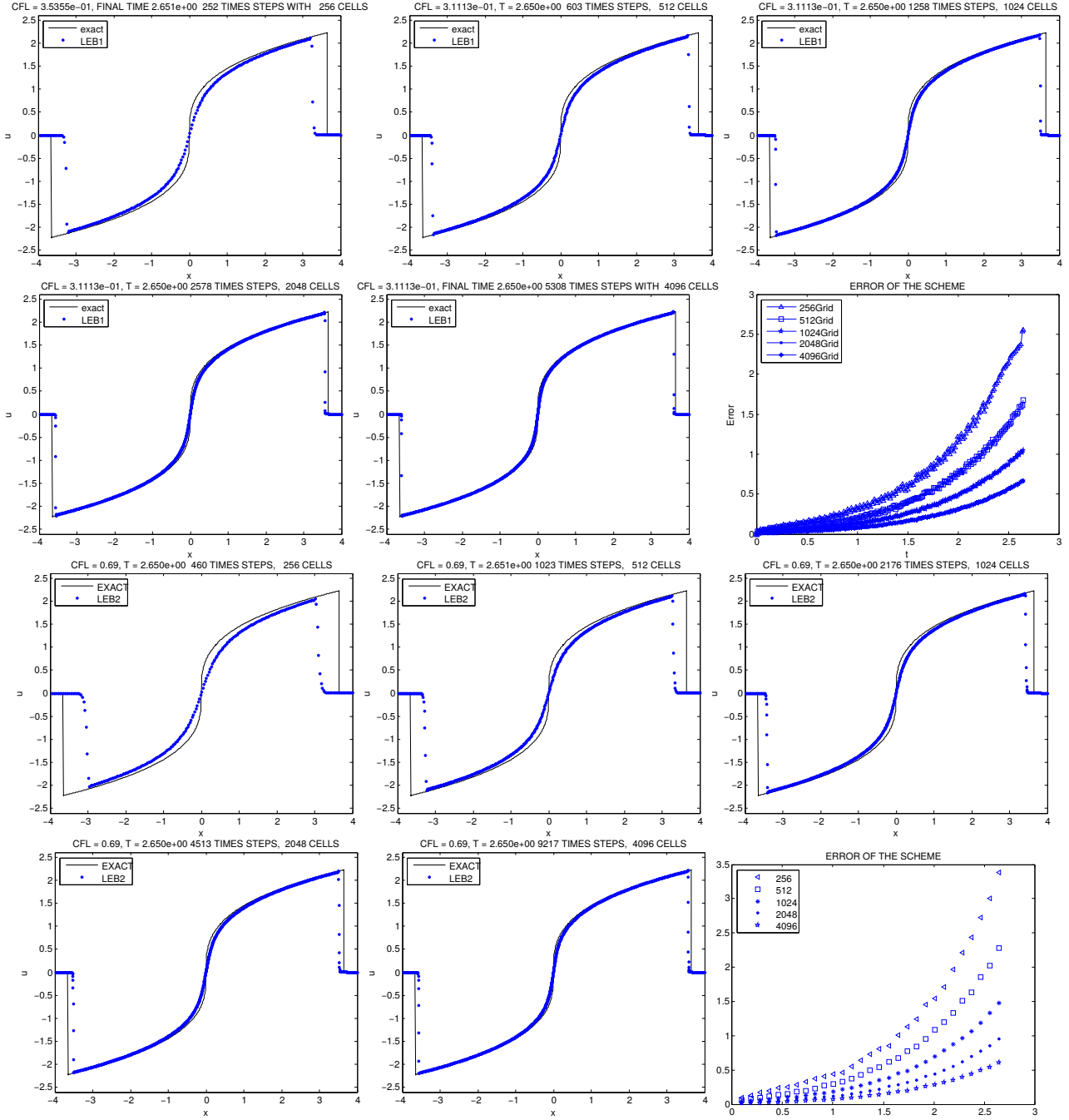


Figure 5.11: Approximated solutions for an Inhomogeneous N-Wave

Model Problem 5.4.8. Effect for Riccati Source Term in LeVeque-Yee (JCP, 1990) & L. Gosse (Numer. Math, 2004) problems type [68, 112].

This problem is inspired in [112], where an study for Hyperbolic conservation laws method was made in the case which the source term is a stiff term. In [68] was taken up again this problem, but in this time with a Riccati source term, the problem is the following hyperbolic balance law.

$$\frac{\partial u}{\partial t} + \frac{\partial f(u)}{\partial x} = \pm k(x) (1 + u)(2 - u), \quad k(x) = 2 \left(1 + \sin \left(\frac{\pi x}{10} \right) \right), \quad x \in [-0.1, 49.9]. \quad (5.4.4)$$

with initial data $u(x, 0) = 2$, $x \leq 0$ and $u(x, 0) = -1$, $x > 0$. The solution is an entropic shock at constant speed $\sigma = \frac{1}{2}$, but as a consequence of the viscosity this solution is very difficult to reproduce numerically in a correct way like is explained in [68]. Agreeing with the sign before k , there will be stabilities or instabilities on the points $u = -1$ and $u = 2$. For example, 2 is stable point and -1 is unstable point when the sign is a positive sign, the values created by numerical viscosity are increased by the source term thus speeding up the shock. By other hand, -1 is stable point and 2 is a unstable point in otherwise, the values created by numerical viscosity are decreased by the source term thus slowing down the shock. In Figure 5.12 are shown numerical computed solutions with Lagrangian-Eulerian scheme LEB1 (5.2.1) and scheme LEB2 (5.2.2), using trapezoidal rule by the source term integral, to the model problem announced above in 5.4.4. The exact solution is shown in solid line for comparison purpose with numerical approximations to positive sign before k with 512 cells (left top) and 1024 cells (Middle top) and one study of mesh refinement to error in L^1 norm in relation to time (right top) with time advanced at $T = 70$, it can be noted in this example as the approximation is speeding up the shock in according to [68] in its analyses of stability points and instability points. To negative sign before k we shown approximations with 512 cells (left bottom) and 1024 cells (Middle bottom) and again one study of mesh refinement to error in L^1 norm in relation to time (right bottom), the velocity of the approximation is now slower than the shock. In those approximations can be noted as the numerical scheme is convergent to exact solution, and how the errors are rapidly to zero as the grid is refined and very efficient computationally and without spurious oscillations in regions with sharp fronts and low numerical diffusion.

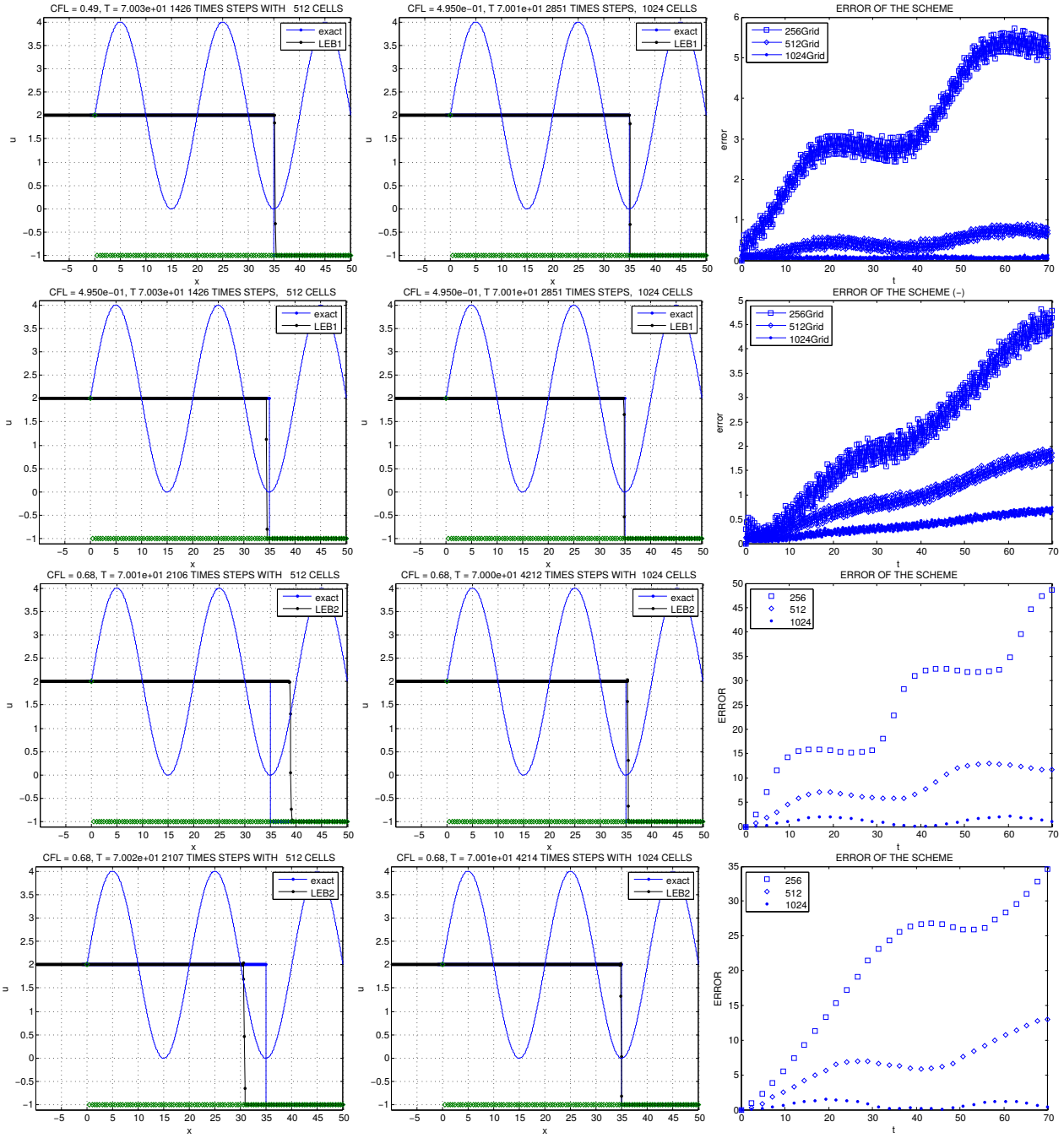


Figure 5.12: Approximate solution to effect for Riccati source term

Chapter 6

The Lagrangian-Eulerian scheme for systems of hyperbolic conservation laws and balance laws

We will focus our attention to describe how to extend the scalar Lagrangian-Eulerian procedure to the one-dimensional system of balance laws $u_t + f_x(u) = G(u)$, where now $u(x, t)$ can be viewed as the unknown n -vector of the form $u = (u_1(x, t), u_2(x, t), \dots, u_n(x, t))^T$, and $f(u)$ is the flux vector function such that $f(u) = (f_1(u), f_2(u), \dots, f_n(u))^T$. Essentially, the analogue Lagrangian-Eulerian scheme for system of balance laws retain all the simplicities of the one single equation case, which in turn is carried out by a straightforward component-wise application of the scalar framework. Thus, for simplicity of presentation, let us consider the following prototype 3×3 system of balance laws.

6.1 Extension to systems of hyperbolic conservation laws and balance laws

We consider the system of balance laws

$$Q_t + [F(Q)]_x = G(Q), \quad (6.1.1)$$

where $F(Q) = [f_1(Q), f_2(Q), f_3(Q)]$, $Q = [u, v, w]$, $u = u(x, t)$, $v = v(x, t)$ and $w = w(x, t)$, along with $G(Q) = [g_1(Q), g_2(Q), g_3(Q)]$. System (6.1.1) can be written in open form as,

$$u_t + [f_1(u, v, w)]_x = g_1(u, v, w), \quad v_t + [f_2(u, v, w)]_x = g_2(u, v, w), \quad w_t + [f_3(u, v, w)]_x = g_3(u, v, w). \quad (6.1.2)$$

As before, we consider the space-time control finite volumes for each variable u, v, w as follows,

$$D_{s,j}^n = \{(t, x) / t^n \leq t \leq t^{n+1}, \quad \sigma_{s,j}^n(t) \leq x \leq \sigma_{s,j+1}^n(t)\}, \quad s = u, v, w, \quad (6.1.3)$$

where $\sigma_{u,j}^n(t)$, $\sigma_{v,j}^n(t)$ and $\sigma_{w,j}^n(t)$ are parametrized curves such that $\sigma_{u,j}^n(t^n) = x_j^n$, $\sigma_{v,j}^n(t^n) = x_j^n$ and $\sigma_{w,j}^n(t^n) = x_j^n$. These curves $\sigma_{s,j}^n(t)$, $s = u, v, w$ define the ‘‘lateral boundaries’’ of integral tubes for each primitive variable u, v, w , which in turn will be used to design a balancing *unbiased* upwinding Riemann-solver-free discretization between the numerical flux functions and the source terms by forward tracking the boundaries along the so-called integral tubes (see

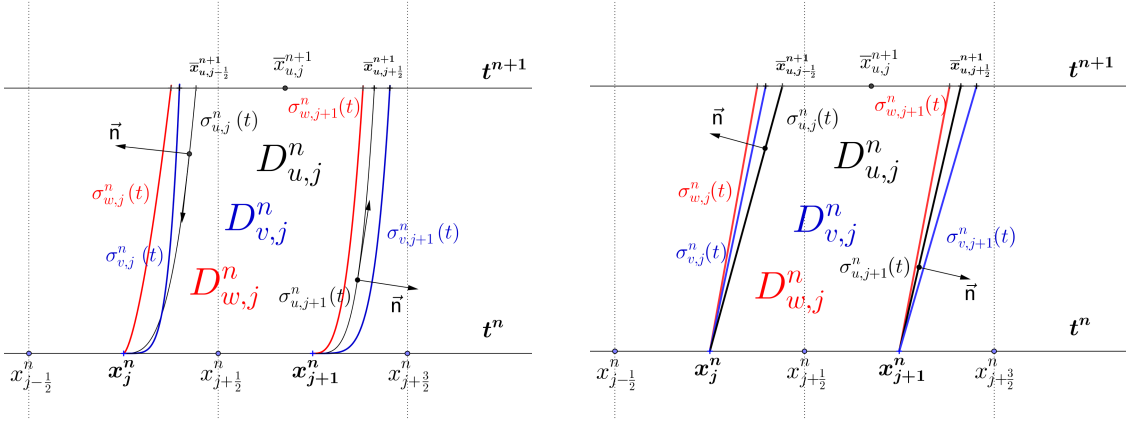


Figure 6.1: On the left (resp. right) is shown an illustration of the continuous (resp. discrete) local space-time domain $D_{s,j}^n$, for each $s = u, v, w$.

left picture in the Figure 6.1). Formally, the divergence theorem can be used in the (6.1.3), the space-time finite volumes $D_{u,j}^n$, $D_{v,j}^n$ and $D_{w,j}^n$. By construction of the algorithm, as before, this implies that curves $\sigma_{s,j}^n(t)$ and $\sigma_{s,j+1}^n(t)$, for $s = u, v, w$ are naturally zero-flux boundaries. Similarly, from this fact the space-time $D_{s,j}^n$, $s = u, v, w$ are then called as “Integral tubes” for $t^n \leq t \leq t^{n+1}$. As a consequence we get $\left[1, \frac{d\sigma_{s,j}^n(t)}{dt}\right] \perp n_s$ and $\left[1, \frac{d\sigma_{s,j+1}^n(t)}{dt}\right] \perp n_s$ since the slopes $\frac{d\sigma_{s,j}^n(t)}{dt}$ are one-to-one equal to the slope of the vector $[s, f_k(Q)]$, $s = u, v, w$; $k = 1, 2, 3$, respectively, over the parametrized curves $\sigma_{s,j}^n(t)$ and $\sigma_{s,j+1}^n(t)$, $s = u, v, w$, $j \in \mathbb{Z}$. Therefore $\sigma_{s,j}^n(t)$, $s = u, v, w$ are solutions of the set of ODEs,

$$\frac{d\sigma_{s,j}^n(t)}{dt} = \frac{f_k(u, v, w)}{s}, \quad \sigma_{s,j}^n(t^n) = x_j^n, \quad t^n \leq t \leq t^{n+1}, \quad \text{for each } s = u, v, w; k = 1, 2, 3, \quad (6.1.4)$$

where $u, v, w \neq 0$. As a consequence of the divergence theorem and the above equations (6.1.3)-(6.1.4), the integrals over curves $\sigma_{s,j}^n(t)$, $s = u, v, w$ vanish and the line integral over the boundary of the region $\partial D_{s,j}^n$ leads to,

$$\int_{\bar{x}_{j-1/2}^{n+1}}^{\bar{x}_{j+1/2}^{n+1}} s(x, t^{n+1}) dx = \int_{x_j^n}^{x_{j+1}^n} s(x, t^n) dx + \iint_{D_{s,j}^n} g_k(u, v, w) dx dt, \quad (6.1.5)$$

where $s = u, v, w$; $k = 1, 2, 3$, respectively, and we can define as before $\bar{x}_{s,j-1/2}^{n+1} = \sigma_{s,j}^n(t^{n+1})$ and $\bar{x}_{s,j+1/2}^{n+1} = \sigma_{s,j+1}^n(t^{n+1})$. Equation (6.1.5) is called “locally conservative relation” to the system of balance laws (6.1.2). Thus, the approximations of the variables u, v, w for system are a rather component-wise extension of the scalar framework given by,

$$\begin{aligned} U_j^n &= \frac{1}{h} \int_{x_{j-1/2}^n}^{x_{j+1/2}^n} u(x, t^n) dx, & \text{and} & \quad \bar{U}_j^{n+1} = \frac{1}{h_{u,j}^{n+1}} \int_{\bar{x}_{j-1/2}^{n+1}}^{\bar{x}_{j+1/2}^{n+1}} u(x, t^{n+1}) dx \quad j \in \mathbb{Z}, \\ V_j^n &= \frac{1}{h} \int_{x_{j-1/2}^n}^{x_{j+1/2}^n} v(x, t^n) dx, & \text{and} & \quad \bar{V}_j^{n+1} = \frac{1}{h_{v,j}^{n+1}} \int_{\bar{x}_{j-1/2}^{n+1}}^{\bar{x}_{j+1/2}^{n+1}} v(x, t^{n+1}) dx \quad j \in \mathbb{Z}, \\ W_j^n &= \frac{1}{h} \int_{x_{j-1/2}^n}^{x_{j+1/2}^n} w(x, t^n) dx, & \text{and} & \quad \bar{W}_j^{n+1} = \frac{1}{h_{w,j}^{n+1}} \int_{\bar{x}_{j-1/2}^{n+1}}^{\bar{x}_{j+1/2}^{n+1}} w(x, t^{n+1}) dx \quad j \in \mathbb{Z}, \end{aligned} \quad (6.1.6)$$

respectively, and the initial condition is $U(x_j^0, t^0) = U_j^0$, $V(x_j^0, t^0) = V_j^0$ and $W(x_j^0, t^0) = W_j^0$ over the local space-time cells $[x_{j-\frac{1}{2}}^0, x_{j+\frac{1}{2}}^0]$, $j \in \mathbb{Z}$. Next, we use (6.1.6) into to ‘‘locally conservative relation’’ to get,

$$\bar{S}_j^{n+1} = \frac{1}{h_{s,j}^{n+1}} \int_{\bar{x}_{j-\frac{1}{2}}^{n+1}}^{\bar{x}_{j+\frac{1}{2}}^{n+1}} s(x, t^{n+1}) dx = \frac{1}{h_{s,j}^{n+1}} \left[\int_{x_j^n}^{x_{j+1}^n} s(x, t^n) dx + \iint_{D_{s,j}^n} g_k(u, v, w) dx dt \right]. \quad (6.1.7)$$

In (6.1.7) $S = (U, V, W)$ and $s = (u, v, w)$ denotes a representation of a component-wise extension of the scalar case to systems of balance law in compact form (6.1.1). Next, the local approximations \bar{S}_j^{n+1} , $j \in \mathbb{Z}$ are projected over the original grid and reads,

$$S_j^{n+1} = \frac{1}{h} \left[c_{s,0j} \bar{S}_{j-1}^{n+1} + c_{s,1j} \bar{S}_j^{n+1} \right]. \quad (6.1.8)$$

Here $c_{s,0j} = (\frac{h}{2} + f_{s,j}^n k^n)$, $c_{s,1j} = h - c_{s,0j} = (\frac{h}{2} - f_{s,j}^n k^n)$ and we use the approximation $f_{s,j}^n = \frac{f_k(U_j^n, V_j^n, W_j^n)}{S_j^n} \approx \frac{f_k(u, v, w)}{s}$, $S = U, V, W$, $s = u, v, w$ and $k = 1, 2, 3$, respectively. Notice that now the curve $\sigma_{s,j}^n(t)$ is a simple straight line for $f_{s,j}^n$ (see right picture in Figure 6.1), along with $k^n = \Delta t^n = t^{n+1} - t^n$. Finally, combination of equations (6.1.7) and (6.1.8) form the building-block for the new Lagrangian-Eulerian scheme. Thus, for each discrete variable $S = U, V, W$, we define $\mathbb{W}_s(S_j^n, S_{j+1}^n) \equiv \frac{f_{s,j}^n + f_{s,j+1}^n}{h_{s,j}^{n+1}} (S_j^n + S_{j+1}^n)$, $s = u, v, w$, we get,

$$\begin{aligned} U_j^{n+1} &= \frac{1}{4} (U_{j-1}^n + 2U_j^n + U_{j+1}^n) - \frac{k^n}{4} \left(\mathbb{W}_u(U_j^n, U_{j+1}^n) - \mathbb{W}_u(U_{j-1}^n, U_j^n) \right) \\ &\quad + \frac{1}{h} \left[\frac{1}{h} \left(\frac{h}{2} + f_{u,j}^n k \right) \iint_{D_{u,j-1}^n} g_1(u, v, w) dx dt + \frac{1}{h} \left(\frac{h}{2} - f_{u,j}^n k \right) \iint_{D_{u,j}^n} g_1(u, v, w) dx dt \right], \end{aligned} \quad (6.1.9)$$

$$\begin{aligned} V_j^{n+1} &= \frac{1}{4} (V_{j-1}^n + 2V_j^n + V_{j+1}^n) - \frac{k^n}{4} \left(\mathbb{W}_v(V_j^n, V_{j+1}^n) - \mathbb{W}_v(V_{j-1}^n, V_j^n) \right) \\ &\quad + \frac{1}{h} \left[\frac{1}{h} \left(\frac{h}{2} + f_{v,j}^n k \right) \iint_{D_{v,j-1}^n} g_2(u, v, w) dx dt + \frac{1}{h} \left(\frac{h}{2} - f_{v,j}^n k \right) \iint_{D_{v,j}^n} g_2(u, v, w) dx dt \right], \end{aligned} \quad (6.1.10)$$

$$\begin{aligned} W_j^{n+1} &= \frac{1}{4} (W_{j-1}^n + 2W_j^n + W_{j+1}^n) - \frac{k^n}{4} \left(\mathbb{W}_w(W_j^n, W_{j+1}^n) - \mathbb{W}_w(W_{j-1}^n, W_j^n) \right) \\ &\quad + \frac{1}{h} \left[\frac{1}{h} \left(\frac{h}{2} + f_{w,j}^n k \right) \iint_{D_{w,j-1}^n} g_3(u, v, w) dx dt + \frac{1}{h} \left(\frac{h}{2} - f_{w,j}^n k \right) \iint_{D_{w,j}^n} g_3(u, v, w) dx dt \right], \end{aligned} \quad (6.1.11)$$

along with the CFL condition $\max_j \{f_{u,j}^n, f_{v,j}^n, f_{w,j}^n\} (k/h) \leq \sqrt{(2)}/2$ and with initials conditions $U_j^0 = u(x_j^0, 0)$, $V_j^0 = v(x_j^0, 0)$ and $W_j^0 = w(x_j^0, 0)$.

The extension of the Lagrangian-Eulerian scheme finite difference (5.2.2) to system of hyperbolic balance law can be write as

$$\begin{aligned}
U_j^{n+1} &= \frac{1}{4}(U_{j-1}^n + 2U_j^n + U_{j+1}^n) - \frac{k}{2h} [f_1(U_{j+1}^n, V_{j+1}^n, W_{j+1}^n) - f_1(U_{j-1}^n, V_{j-1}^n, W_{j-1}^n)] \\
&\quad + \frac{1}{h} \left[\frac{1}{h} \left(\frac{h}{2} + f_{u,j}^n k \right) \iint_{D_{u,j-1}^n} g_1(u, v, w) \, dx \, dt + \frac{1}{h} \left(\frac{h}{2} - f_{u,j}^n k \right) \iint_{D_{u,j}^n} g_1(u, v, w) \, dx \, dt \right],
\end{aligned} \tag{6.1.12}$$

$$\begin{aligned}
V_j^{n+1} &= \frac{1}{4}(V_{j-1}^n + 2V_j^n + V_{j+1}^n) - \frac{k}{2h} [f_2(U_{j+1}^n, V_{j+1}^n, W_{j+1}^n) - f_2(U_{j-1}^n, V_{j-1}^n, W_{j-1}^n)] \\
&\quad + \frac{1}{h} \left[\frac{1}{h} \left(\frac{h}{2} + f_{v,j}^n k \right) \iint_{D_{v,j-1}^n} g_2(u, v, w) \, dx \, dt + \frac{1}{h} \left(\frac{h}{2} - f_{v,j}^n k \right) \iint_{D_{v,j}^n} g_2(u, v, w) \, dx \, dt \right],
\end{aligned} \tag{6.1.13}$$

$$\begin{aligned}
W_j^{n+1} &= \frac{1}{4}(W_{j-1}^n + 2W_j^n + W_{j+1}^n) - \frac{k}{2h} [f_3(U_{j+1}^n, V_{j+1}^n, W_{j+1}^n) - f_3(U_{j-1}^n, V_{j-1}^n, W_{j-1}^n)] \\
&\quad + \frac{1}{h} \left[\frac{1}{h} \left(\frac{h}{2} + f_{w,j}^n k \right) \iint_{D_{w,j-1}^n} g_3(u, v, w) \, dx \, dt + \frac{1}{h} \left(\frac{h}{2} - f_{w,j}^n k \right) \iint_{D_{w,j}^n} g_3(u, v, w) \, dx \, dt \right],
\end{aligned} \tag{6.1.14}$$

along with the CFL condition $\max_j \{ \|F'(U_j^n, V_j^n, W_j^n)\|_2, f_{u,j}^n, f_{v,j}^n, f_{w,j}^n \} (k/h) \leq \sqrt{2}/2$, where F is the vector function $F = [f_1, f_2, f_3]$. Note that the CFL condition to the Lagrangian-Eulerian scheme (6.1.12), (6.1.13) and (6.1.14) is a extension of the scalar case (5.2.2), in which is considered the eigenvalues of Jacobian matrix of F .

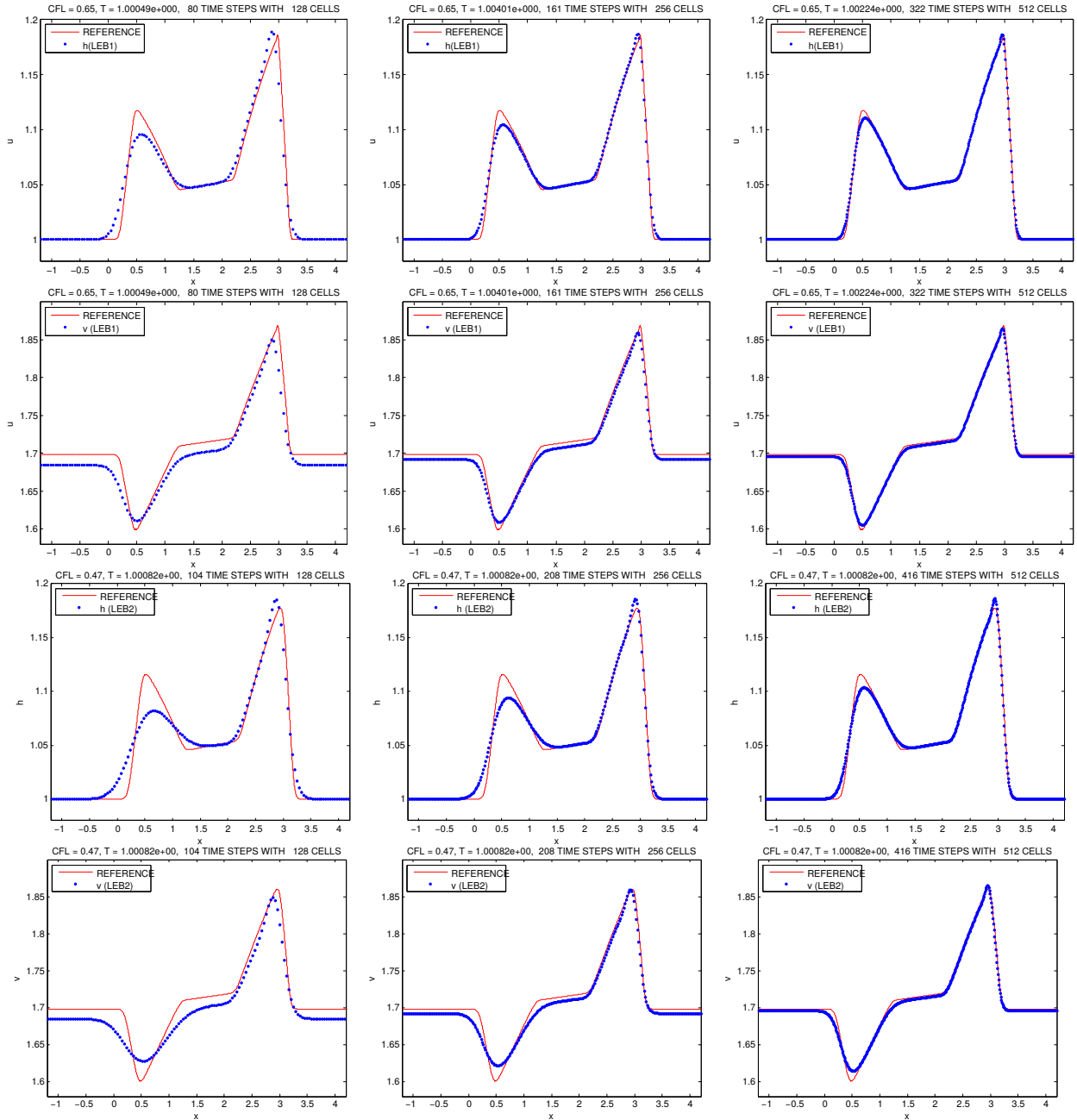
6.2 Numerical experiments for systems of nonlinear balance laws

Model Problem 6.2.1. Langseth, Tveito, and Winther (SINUM) [104].

In [104], it was considered a 2×2 nonlinear system of balance laws in the form of (6.1.1) modeling the flow of water downing in a channel having a rectangular cross section and inclined at a constant angle θ to the horizontal. This is a prototype model for shallow-water flow (see also [71, 109] and reference therein for more details) in an inclined channel with friction the system may be written as (in dimensionless and scaled variables)

$$\begin{bmatrix} h \\ hv \end{bmatrix}_t + \begin{bmatrix} hv \\ v^2 h + \frac{1}{2} h^2 \end{bmatrix}_x = \begin{bmatrix} 0 \\ h - C \frac{1+h}{\tan(\theta)} v^2 \end{bmatrix}, \tag{6.2.1}$$

where h is the height of the free surface and v is the averaged horizontal velocity. Precisely, as in [104], the friction coefficient C is taken to be 0.1, while the inclination angle $\theta = \pi/6$.

Figure 6.2: Numerical approximation for **shallow water system**

On physical grounds, in model problem it was assumed the hydrostatic balance in the vertical direction and ignored surface tension. Further, the viscous effects is approximately through the introduction of a friction force exerted of the fluid by the solid boundaries of the channel (account as a source term that appears on the RHS of (6.2.1)). Indeed, model (6.2.1) correspond to uniform flow ($v_0=\text{constant}$ and $h_0=\text{constant}$) with the frictional and gravitational forces in perfect balance. In order to study the balance between convective/source in the model (6.2.1), it is considered as initial conditions a *perturbation of a uniform flow*, in which the gravitational and frictional forces balance as expected from the model problem. As in [104], the initial velocity is taken to be $v_0 = 1.699$, while the initial height of the free surface consists of a *triangular perturbation* of the uniform flow level, $h_0(x) = x + 1.5$, $-0.5 \leq x \leq 0$, $h_0(x) = -x + 1.5$, $0 \leq x \leq 0.5$, and 1 elsewhere. In Figure 6.2 it is shown the numerical approximations by means of the LEB2 scheme 5.2.1 to the initial value problem described just above. As in [104], with no friction ($C = 0$), two symmetrical waves will arise from the announced initial data. On the other hand, the introduction of friction not only down the velocity of these waves, but also changes the shape. For instance, if $C = 0.1$ is considered, one can still observe two waves, but the symmetry is now lost. Here is shown computed solutions for h (height of the free surface on the top frames (resp. third row)) and for v (averaged horizontal velocity in frames on the second row (resp. bottom frames)) with scheme (6.1.9)-(6.1.11) and scheme (6.1.12)-(6.1.14) respectively, both extended to system of hyperbolic law and balance law from the scalar cases LEB1 and LEB2 respectively, as were discussed in above section for each case. The initial value problem described just above at simulation time $t = 1$, for four computations, one using 2048 cells, namely the reference “exact” solution and another three: 128 cells (left), 256 cells (middle), 512 cells (right). The numerical solutions are in a very good agreement to that reported in [104], corresponding to the balance between the frictional and and gravitational forces at time evolves. The approximation of the source terms in this example of system of balance laws was performed by means of the predictor formula (5.2.1).

Model Problem 6.2.2. Pareschi, (SINUM) [130].

In Pareschi [130] (see also [30]), it was considered the Broadwell model of rarefied gas dynamics. The kinetic model is characterized by a 2×2 balance laws system with relaxation source term of the form,

$$\frac{\partial U}{\partial t} + \frac{\partial f(U)}{\partial x} = \frac{1}{\epsilon} S_t(U), \quad (6.2.2)$$

where, $U = [\rho \ m \ z]^\top$, $f(U) = [m \ z \ m]^\top$ and $S_t(U) = [0 \ 0 \ R(U)]^\top$, and $R(U) = \frac{1}{2}(\rho^2 + m^2 - 2\rho z)$. Following the classical fluid dynamics formulation, the primitive variables are the density ρ , the momentum m , and the velocity u , defined by $\rho = f + 2h + g$, $m = f - g$, and $u = m/\rho$. The only conserved quantities are the density ρ and the momentum m . With respect to balance law Broadwell equations (6.2.2), ϵ is the mean free path, and f , h , and g denote the mass densities of gas particles with characteristic speed 1, 0, and -1 , respectively, in the space x and time t coordinate system. In addition, it is well known the if one defines $z = f + g$ then the we get precisely the the balance law (6.2.2).

Note that if the fluid variables ρ , m , and z are known then the mass densities of gas particles f , g , and h can be recovered from the above definitions and reads: $f = 0.5(z+m)$, $g = 0.5(z-m)$ and $h = 0.5(\rho - z)$. First, we compute the Broadwell equation with the Lagrangian-Eulerian scheme (6.1.7)-(6.1.8), or (6.1.9)-(6.1.11), along with the Riemann data: $\rho_l = 3$, $m_l = 2$ and $z_l = 2$, if $x < 0.2$ and $\rho_r = 2$, $m_r = 1.13962$, and $z_r = 2$ if $0.2 < x$. It is well known (see, e.g.,

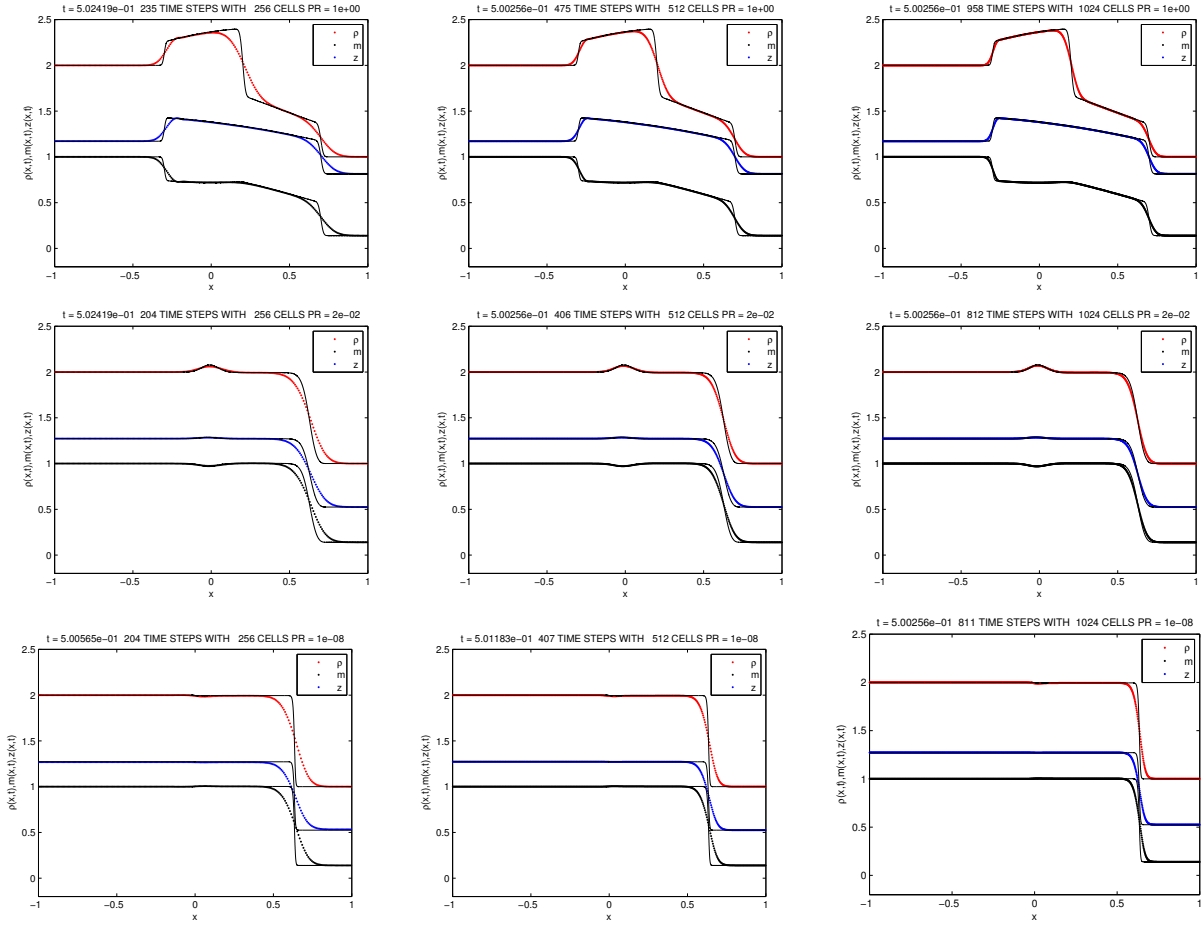


Figure 6.3: Numerical solutions of the **Broadwell balance law problem**.

[30, 130]), the solution for Broadwell model with such initial data for the relaxation parameter (the mean free path) for $\epsilon = 10^0$ (top), – with the “exact” reference solution being calculated with 2048 cells –, for $\epsilon = 2 \times 10^{-2}$ (middle), – with the “exact” reference solution calculated with 2048 cells –, and for $\epsilon = 10^{-8}$ (bottom), with the “exact” reference calculated with 4096 cells; all such numerical solutions are shown in Figure 6.3. We will first recast the system problem of balance laws (6.2.2) by writing $\tilde{\rho} = \rho + 1$, $\tilde{m} = m + 1$ and $\tilde{z} = z + 1$, in open form as,

$$\frac{\partial \tilde{\rho}}{\partial t} + \frac{\partial \tilde{m}}{\partial x} = 0, \quad \frac{\partial \tilde{m}}{\partial t} + \frac{\partial \tilde{z}}{\partial x} = 0, \quad \frac{\partial \tilde{z}}{\partial t} + \frac{\partial \tilde{m}}{\partial x} = \frac{1}{2\epsilon} \left((\tilde{\rho} - 1)^2 + (\tilde{m} - 1)^2 - 2(\tilde{\rho} - 1)(\tilde{z} - 1) \right) \quad (6.2.3)$$

and the initial data $\tilde{U}_l = [3, 2, 2]^T$, $x < 0.2$ and $\tilde{U}_r = [2, 1.13962, 2]^T$, $x > 0.2$. The finite volumes in this case are,

$$D_{s,j}^n = \{(x, t) : t^n \leq t \leq t^{n+1}, \sigma_{s,j}^n(t) \leq x \leq \sigma_{s,j+1}^n(t)\}, \quad s = \tilde{\rho}, \tilde{m}, \tilde{z}, \quad (6.2.4)$$

where, $\sigma_{\tilde{\rho},j}^n(t)$, $\sigma_{\tilde{m},j}^n(t)$ and $\sigma_{\tilde{z},j}^n(t)$ are solution at $t^n < t < t^{n+1}$ of the follows systems equation,

$$\left\{ \begin{array}{l} \frac{d\sigma_{\tilde{\rho},j}(t)}{dt} = \frac{\tilde{m}}{\tilde{\rho}} \\ \sigma_{\tilde{\rho},j}(t^n) = x_j^n \end{array} \right\}, \quad \left\{ \begin{array}{l} \frac{d\sigma_{\tilde{m},j}(t)}{dt} = \frac{\tilde{z}}{\tilde{m}} \\ \sigma_{\tilde{m},j}(t^n) = x_j^n \end{array} \right\}, \quad \left\{ \begin{array}{l} \frac{d\sigma_{\tilde{z},j}(t)}{dt} = \frac{\tilde{m}}{\tilde{z}} \\ \sigma_{\tilde{z},j}(t^n) = x_j^n \end{array} \right\}. \quad (6.2.5)$$

The approximated solution to each problem above is $\sigma_{s,j}(t) = (t - t^n)f_{s,j}^n + x_j^n$, where $f_{\rho,j}^n = M_j^n/R_j^n$, $f_{\tilde{m},j}^n = Z_j^n/M_j^n$ and $f_{\tilde{z},j}^n = M_j^n/Z_j^n$ respectively. The approximations \bar{R}_j^{n+1} , \bar{M}_j^{n+1} and \bar{Z}_j^{n+1} in the t^{n+1} time are,

$$\begin{aligned}\bar{R}_j^{n+1} &= \frac{1}{2h_j^{n+1}} \left[h \left(R_j^n + R_{j+1}^n \right) \right], & \bar{M}_j^{n+1} &= \frac{1}{2h_j^{n+1}} \left[h \left(M_j^n + M_{j+1}^n \right) \right], \\ \bar{Z}_j^{n+1} &= \frac{1}{2h_j^{n+1}} \left[h \left(Z_j^n + Z_{j+1}^n \right) + \iint_{D_j^n} G(\tilde{\rho}, \tilde{m}, \tilde{z}) dA \right],\end{aligned}\quad (6.2.6)$$

where,

$$\iint_{D_j^n} G(\tilde{\rho}, \tilde{m}, \tilde{z}) dA = \iint_{D_j^n} \frac{1}{2\epsilon} \left((\tilde{\rho} - 1)^2 + (\tilde{m} - 1)^2 - 2(\tilde{\rho} - 1)(\tilde{z} - 1) \right) dA. \quad (6.2.7)$$

Next, we perform the following projections for quantities R_j^{n+1} , M_j^{n+1} and Z_j^{n+1} , as follows:

$$\begin{aligned}R_j^{n+1} &= \frac{1}{h} \left[\left(\frac{1}{2}h + f_{\rho,j}^n \right) \bar{R}_{j-1}^{n+1} + \left(\frac{1}{2}h - f_{\rho,j}^n \right) \bar{R}_j^{n+1} \right], \\ M_j^{n+1} &= \frac{1}{h} \left[\left(\frac{1}{2}h + f_{\tilde{m},j}^n \right) \bar{M}_{j-1}^{n+1} + \left(\frac{1}{2}h - f_{\tilde{m},j}^n \right) \bar{M}_j^{n+1} \right], \\ Z_j^{n+1} &= \frac{1}{h} \left[\left(\frac{1}{2}h + f_{\tilde{z},j}^n \right) \bar{Z}_{j-1}^{n+1} + \left(\frac{1}{2}h - f_{\tilde{z},j}^n \right) \bar{Z}_j^{n+1} \right].\end{aligned}\quad (6.2.8)$$

Furthermore, the solution of problem in the time $t = 0.5$ are given by “ $R_j^{n+1} - 1$ ”, “ $M_j^{n+1} - 1$ ” and “ $Z_j^{n+1} - 1$ ”. To approximate the integral (6.2.7) in time $t = t^{n+1}$, we consider the approximation R_j^n , M_j^n and Z_j^n constants, then,

$$\begin{aligned}\iint_{D_j^n} G(\tilde{\rho}, \tilde{m}, \tilde{z}) dA &\approx \iint_{D_j^n} \frac{1}{2\epsilon} \left((R_j^n - 1)^2 + (M_j^n - 1)^2 - 2(R_j^n - 1)(\tilde{z} - 1) \right) dA \\ &= \frac{1}{2\epsilon} \left((R_j^n - 1)^2 + (M_j^n - 1)^2 \right) \iint_{D_j^n} dA - \frac{1}{\epsilon} (R_j^n - 1) \iint_{D_j^n} (\tilde{z} - 1) dA.\end{aligned}\quad (6.2.9)$$

Notice we have to perform a quadrature rule to compute the quantity,

$$\iint_{D_j^n} \tilde{z}(x, t) dA, \quad (6.2.10)$$

whose integrand Z_j^n is discontinuous in the end points $[x_{j-\frac{1}{2}}^n, x_{j+\frac{1}{2}}^n]$ of the over control volume D_j^n as well as \bar{Z}_j^{n+1} is discontinuous in the cell $[\bar{x}_{j-\frac{1}{2}}^{n+1}, \bar{x}_{j+\frac{1}{2}}^{n+1}]$. This quadrature requires additional attention with respect to the relaxation scale factor $\frac{1}{\epsilon}$. To encompass this difficulty into the approximation of the source term, we make use of the semi-open Newton-Cotes Formulas to account the integral (6.2.10). In this case, we use the Newton-Cotes formula along with four discrete points $a = x_j^n = x_0$, x_1 , x_2 , $x_3 = b = x_{j+\frac{1}{2}}^n$ away from the left side endpoint of discontinuity. In a similar way, we use the discrete points $a = x_{j+\frac{1}{2}}^n = x_0$, x_1 , x_2 , $x_3 = b = x_{j+1}^n$ and we might write,

$$\int_a^b f(x) dx \approx \frac{3h}{4} (y_1 + 3y_3) \quad (6.2.11)$$

where $h = \frac{b-a}{3}$. Notice that the endpoint $x_{j+\frac{1}{2}}$ is not included in the Newton-Cotes formula. Thus, in order to perform the approximation of the source term we write (6.2.7) as,

$$\iint_{D_j^n} \tilde{z}(x, t) dA = \int_{t^n}^{t^{n+1}} \int_{\sigma_j^n(t)}^{\sigma_{j+1}^n(t)} \tilde{z}(x, t) dx dt \approx \int_{t^n}^{t^{n+1}} \int_{\sigma_j^n(t)}^{\gamma_j^n(t)} \tilde{z}(x, t) dx dt + \int_{t^n}^{t^{n+1}} \int_{\gamma_j^n(t)}^{\sigma_{j+1}^n(t)} \tilde{z}(x, t) dx dt, \quad (6.2.12)$$

where γ_j^n is the characteristic curve in the control volume D_j^n . Notice that $\gamma_j^n(x_{j+\frac{1}{2}}^n)$ is the point of discontinuity, therefore we consider the approximate points $(\gamma_j^n)^-$ and $(\gamma_j^n)^+$. Thus, we approximate γ_j^n , to the left and to the right, by the straight lines $(\gamma_j^n)^-$ and $(\gamma_j^n)^+$ from such ‘‘initial points’’ to the same endpoint $\bar{x}_{j+\frac{1}{2}}^{n+1}$. Thus, we are able to compute the integral by,

$$\iint_{D_j^n} \tilde{z}(x, t) dA \approx \int_{t^n}^{t^{n+1}} \int_{\sigma_j^n(t)}^{\gamma_j^n(t)^-} \tilde{z}(x, t) dx dt + \int_{t^n}^{t^{n+1}} \int_{\gamma_j^n(t)^+}^{\sigma_{j+1}^n(t)} \tilde{z}(x, t) dx dt. \quad (6.2.13)$$

Then, let $A_j^n(t) = \gamma_j^n(t)^- - \sigma_j^n(t)$, $B_j^n(t) = \sigma_{j+1}^n(t) - \gamma_j^n(t)^+$ and using the Newton Cotes formula (6.2.11) to approximate the x -integrals, we get:

$$\begin{aligned} \iint_{D_j^n} \tilde{z}(x, t) dA &\approx \int_{t^n}^{t^{n+1}} \frac{3A_j^n(t)}{4} \left(\tilde{z}(\sigma_j^n(t), t) + 3\tilde{z}(\gamma_j^n(t)^-, t) \right) dt \\ &\quad + \int_{t^n}^{t^{n+1}} \frac{3B_j^n(t)}{4} \left(\tilde{z}(\sigma_{j+1}^n(t), t) + 3\tilde{z}(\gamma_j^n(t)^+, t) \right) dt \\ &= \left[\begin{array}{l} 0.5\Delta t^n \frac{3}{4} \left(0.5h_j^{n+1} \left(\tilde{z}(\sigma_j^n(t^{n+1}), t^{n+1}) + 3\tilde{z}(\gamma_j^n(t^{n+1})^-, t^{n+1}) \right) \right. \\ \quad \left. + 0.5h \left(\tilde{z}(\sigma_j^n(t^n), t^n) + 3\tilde{z}(\gamma_j^n(t^n)^-, t^n) \right) \right) \\ 0.5\Delta t^n \frac{3}{4} \left(0.5h_j^{n+1} \left(\tilde{z}(\sigma_{j+1}^n(t^{n+1}), t^{n+1}) + 3\tilde{z}(\gamma_j^n(t^{n+1})^+, t^{n+1}) \right) \right. \\ \quad \left. + 0.5h \left(\tilde{z}(\sigma_{j+1}^n(t^n), t^n) + 3\tilde{z}(\gamma_j^n(t^n)^+, t^n) \right) \right) \end{array} \right] \\ &= \left[\begin{array}{l} 0.5\Delta t^n \frac{3}{4} \left(0.5h_j^{n+1} \left(\bar{Z}_j^{n+1} + 3\bar{Z}_j^{n+1} \right) + 0.5h \left(Z_j^{n+1} + 3Z_j^{n+1} \right) \right) \\ 0.5\Delta t^n \frac{3}{4} \left(0.5h_j^{n+1} \left(\bar{Z}_j^{n+1} + 3\bar{Z}_j^{n+1} \right) + 0.5h \left(Z_{j+1}^n + 3Z_{j+1}^n \right) \right) \end{array} \right]. \end{aligned} \quad (6.2.14)$$

Thus, we might right,

$$\iint_{D_j^n} \tilde{z}(x, t) dA \approx \frac{3\Delta t^n}{2} \left[h_j^{n+1} \bar{Z}_j^{n+1} + 0.5h(Z_j^n + Z_{j+1}^n) \right], \quad (6.2.15)$$

and replacing this approximation into the integral (6.2.7) reads,

$$\begin{aligned}
\iint_{D_j^n} G(\tilde{\rho}, \tilde{m}, \tilde{z}) dA &\approx \iint_{D_j^n} \frac{1}{2\epsilon} \left((R_j^n - 1)^2 + (M_j^n - 1)^2 - 2(R_j^n - 1)(\tilde{z} - 1) \right) dA \\
&= \frac{1}{2\epsilon} \left((R_j^n - 1)^2 + (M_j^n - 1)^2 \right) A(D_j^n) \\
&\quad - \frac{3}{2} \frac{\Delta t^n}{\epsilon} (R_j^n - 1) \left(h_j^{n+1} \bar{Z}_j^{n+1} + 0.5h(Z_j^n + Z_{j+1}^n) \right) \\
&\quad + \frac{1}{\epsilon} (R_j^n - 1) A(D_j^n).
\end{aligned} \tag{6.2.16}$$

Plugging approximation (6.2.16) into the system (6.2.8) to write quantity \bar{Z}_j^{n+1} as a function of \bar{Z}^{n+1} gives,

$$\bar{Z}^{n+1} = \frac{1}{2h_j^{n+1} \left(1 + \frac{3\Delta t^n}{4\epsilon} \right) (R_j^n - 1)} \begin{bmatrix} \left(\frac{3h\Delta t^n (R_j^n - 1)}{4\epsilon} + h \right) (Z_j^n + Z_{j+1}^n) \\ + \frac{1}{2\epsilon} \left((R_j^n - 1)^2 + (M_j^n - 1)^2 \right) A(D_j^n) \\ + \frac{1}{\epsilon} (R_j^n - 1) A(D_j^n) \end{bmatrix} \tag{6.2.17}$$

We expect the Lagrangian-Eulerian scheme to be first order accurate based on the analysis to the scalar case. Although the first order approximations are not so good in coarse grids (i.e., a mesh grid with 256 cells) we point out numerical dissipation is reduced as the mesh grid is refined leading to a qualitatively correct solution of the Broadwell model. For the approximations in figure 6.3 we are using an explicit-unsplit algorithm for the numerical integration of hard balance problems in the most simple setting of discretization, we have some hope to extend such scheme in a cheap high order scheme with less numerical dissipation following some interest ideas as such those described in [30, 45, 58, 67, 70, 71, 104, 130], but keeping the same Lagrangian-Eulerian framework.

6.3 Numerical experiments for systems of nonlinear hyperbolic conservation laws

Notice, if we set the RHS of (6.1.1) equal to zero ($G(Q) \equiv 0$), we will get the prototype hyperbolic conservation law in the form $Q_t + [F(Q)]_x = 0$, keeping in mind that the meaning of the variable must be understood in the new framework. From (6.1.7)-(6.1.8), or (6.1.9)-(6.1.11), one easily sees that the Lagrangian-Eulerian scheme can be used for systems of conservation laws in a straightforward manner as follows (for comparison purposes, see the numerical solutions displayed in Figure 6.4 with respect to the classical initial value problem, whose full solution is well known in the vast literature of the subject).

Model Problem 6.3.1. Sod, (JCP) [140].

In this case, we solve the one-dimensional equations system of gas dynamics may be written in the vector (conservation) form:

$$\frac{\partial}{\partial t} \begin{bmatrix} \rho \\ m \\ E \end{bmatrix} + \frac{\partial}{\partial x} \begin{bmatrix} m \\ \rho u^2 + p \\ u(E + p) \end{bmatrix} = 0, \quad p = (\gamma - 1) \left(E - \frac{\rho}{2} u^2 \right), \quad (6.3.1)$$

where ρ , u , $m = \rho u$, p and E are, respectively, the density, the velocity, the momentum, the pressure, and the total energy. Here, the conserved quantities are $Q = (\rho, m, E)^T$ along with the flux function $F(Q) = (m, \rho u^2 + p, u(E + p))^T$. We solve this system subject to the Riemann initial data, $Q(x, 0) = Q_L$, $x \leq 0.5$ and $Q(x, 0) = Q_R$, $x > 0.5$. The Riemann problem was proposed by Sod [140]. The initial data are given by $Q_L = (1, 0, 2.5)$ and $Q_R = (0.125, 0, 0.25)$. To apply our Lagrangian-Eulerian scheme we consider the system (6.3.1) in the open form as:

$$\frac{\partial \rho}{\partial t} + \frac{\partial m}{\partial x} = 0, \quad \frac{\partial m}{\partial t} + \frac{\partial(\rho u^2 + p)}{\partial x} = 0, \quad \frac{\partial E}{\partial t} + \frac{\partial(uE + up)}{\partial x} = 0, \quad (6.3.2)$$

and still, the system above we can be written in the follow system balance laws,

$$\frac{\partial \rho}{\partial t} + \frac{\partial m}{\partial x} = 0, \quad \frac{\partial m}{\partial t} + \frac{\partial(\rho u^2)}{\partial x} = -\frac{\partial p}{\partial x}, \quad \frac{\partial E}{\partial t} + \frac{\partial(uE)}{\partial x} = -\frac{\partial(up)}{\partial x}, \quad (6.3.3)$$

The assumption of not flow through the integrals curves $\sigma_{s,j}^n(t)$, $s = \rho, m, E$, implies that,

$$\begin{cases} \frac{d\sigma_{s,j}(t)}{dt} = u & t^n < t < t^{n+1}, \\ \sigma_{s,j}(t^n) = x_j^n \end{cases} \quad (6.3.4)$$

then, the approximation of the $f_{s,j}^n = U_j^n$, where U_j^n is the velocity approximation. With this, the one integral tube is determined by,

$$D_j^n = \{(x, t) : t^n \leq t \leq t^{n+1}, \sigma_j^n(t) \leq x \leq \sigma_{j+1}^n(t)\} \quad (6.3.5)$$

where the solutions of the system of ordinary differential equation (6.3.4) are approximate by $\sigma_j^n(t) = (t - t^n)f_j^n + x_j^n$. Thus, thanks to the application on the divergence theorem over the finite volume $D_{s,j}^n$, give us the follow approximation at time t^{n+1} ,

$$\begin{aligned} \bar{R}_j^{n+1} &= \frac{1}{2h_j^{n+1}} \left[h \left(R_j^n + R_{j+1}^n \right) \right], \\ \bar{M}_j^{n+1} &= \frac{1}{2h_j^{n+1}} \left[h \left(M_j^n + M_{j+1}^n \right) + \iint_{D_j^n} p_x dA \right], \\ \bar{E}_j^{n+1} &= \frac{1}{2h_j^{n+1}} \left[h \left(E_j^n + E_{j+1}^n \right) + \iint_{D_j^n} (up)_x dA \right]. \end{aligned} \quad (6.3.6)$$

By applying the fundamental theorem of calculus on the source term into the balance law and the midpoint rule reads,

$$\begin{aligned} \iint_{D_j^n} (G(x, t))_x dA &= \int_{t^n}^{t^{n+1}} \left(G(\sigma_{j+1}^n(t), t) - G(\sigma_j^n(t), t) \right) dt \\ &\approx k^n \left[G(\sigma_{j+1}^n(t^{n+\frac{1}{2}}), t^{n+\frac{1}{2}}) - G(\sigma_j^n(t^{n+\frac{1}{2}}), t^{n+\frac{1}{2}}) \right], \end{aligned} \quad (6.3.7)$$

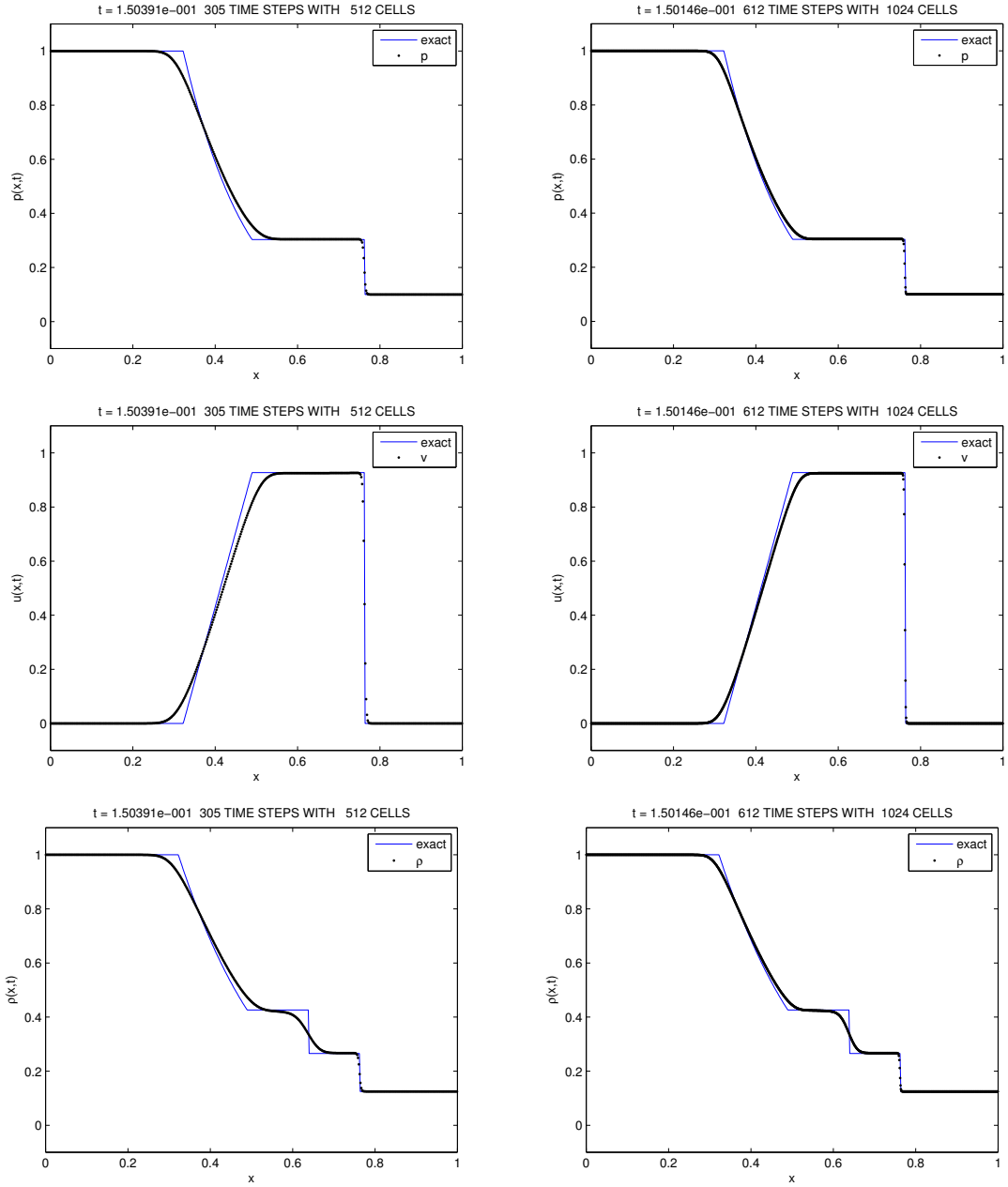


Figure 6.4: Numerical approximations of the **Sod problem** (6.3.1) computed with the Lagrangian-Eulerian scheme (6.1.9)-(6.1.11) (rewritten as (6.3.3))

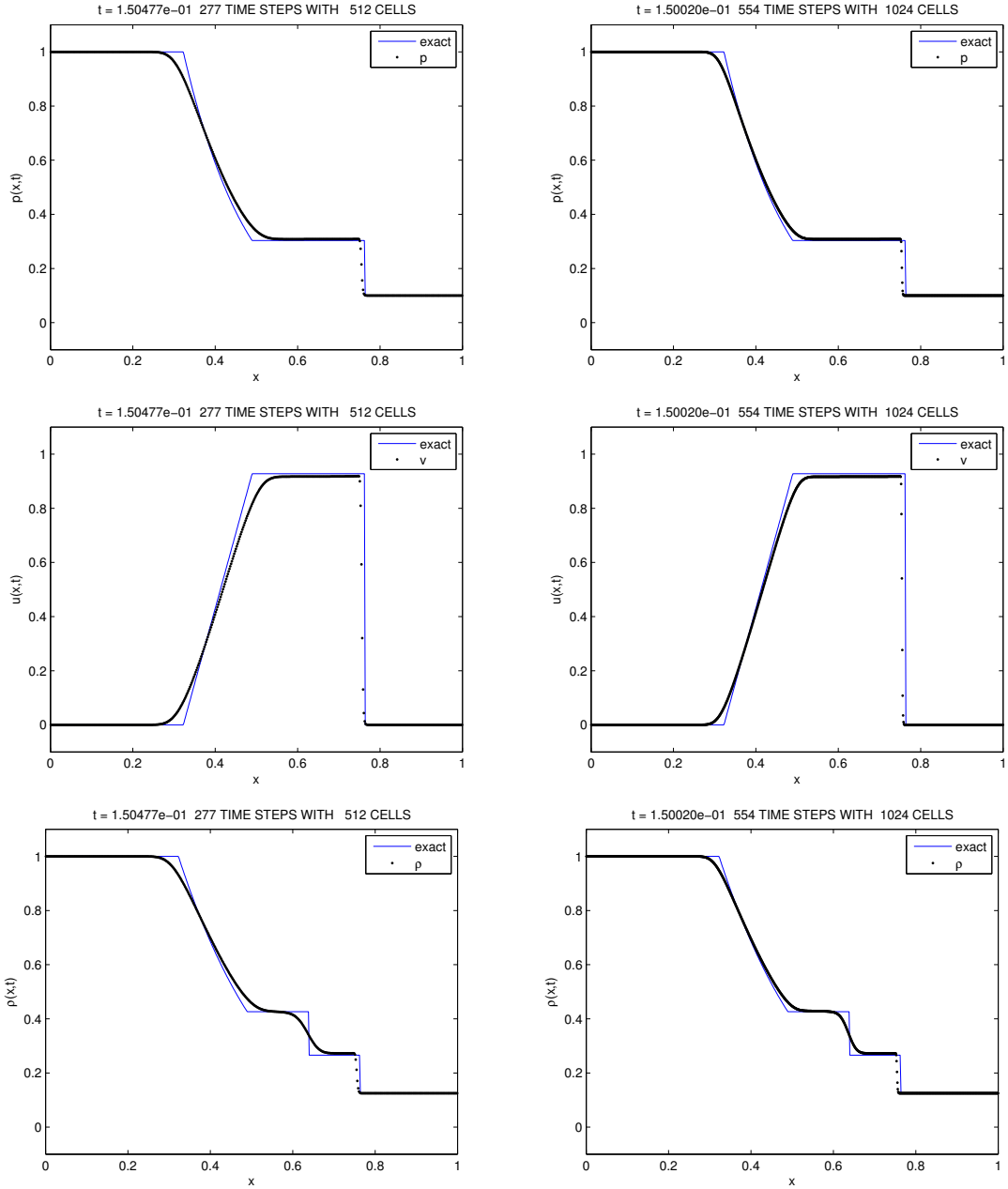


Figure 6.5: Numerical approximations of the **Sod problem** (6.3.1) computed with the Lagrangian-Eulerian scheme (6.1.12)-(6.1.14) (rewritten as (6.3.3)).

with $G(x, t) = p(x, t)$ and $G(x, t) = u(x, t)p(x, t)$ in each case. Next, the approximations in (6.3.6) are then projected on the original grid as follows,

$$S^{n+1} = \frac{1}{h} \left(\left(\frac{1}{2}h + f_j^n \right) \bar{S}_{j-1}^{n+1} + \left(\frac{1}{2}h - f_j^n \right) \bar{S}_j^{n+1} \right) \quad (6.3.8)$$

for $S = R, M, E$. The numerical approximations to the Sod problem [140] are shown in Figure 6.4 and in Figure 6.5 from left to right are shown the computed solutions for pressure, velocity and density – with 512 cells (top) and with 1024 cells (bottom) – at the simulation time $t = 0.15$. We point out that we were able to easily write the original Sod problem formed by a one-dimensional 3 by 3 system of hyperbolic conservation laws (6.3.1) as system of balance laws in order to use the Lagrangian-Eulerian framework (6.3.4)-(6.3.8), yielding an accurate numerical solutions without any extra computational cost and with simplicity, which in turn are in very good agreement with the correct qualitative behavior as in the original problem proposed by Sod [140].

Chapter 7

The extension of the Lagrangian-Eulerian scheme for hyperbolic conservation laws in two-space dimensions

We now turn our attention to introduce a new computational approach for the design of a new class of approximate solutions for multidimensional hyperbolic conservation laws. As natural, our first attempt will be a straightforward extension used in the one-dimensional case, which was defined in Chapter 2, but now applied to three dimensional variables (x , y and t) as $D_{i,j}^n \subset \mathbb{R}^3$, see Figure 7.1 (left), where i and j refer to (x_i, y_j) and n refers to time level t^n . The boundary of control volume $D_{i,j}^n$ will be denoted by $\partial D_{i,j}^n = R_{i,j}^n \cup S_{i,j}^n \cup \bar{R}_{i,j}^{n+1}$ where the control volume $R_{i,j}^n = [x_{i-\frac{1}{2}}^n, x_{i+\frac{1}{2}}^n] \times [y_{j-\frac{1}{2}}^n, y_{j+\frac{1}{2}}^n]$ in \mathbb{R}^2 is the “inflow” of the integral tube, $\bar{R}_{i,j}^{n+1}$ in \mathbb{R}^2 is the “outflow” of the integral tube, while $S_{i,j}^n$, in \mathbb{R}^3 , is the lateral (impervious) surface of the tube.

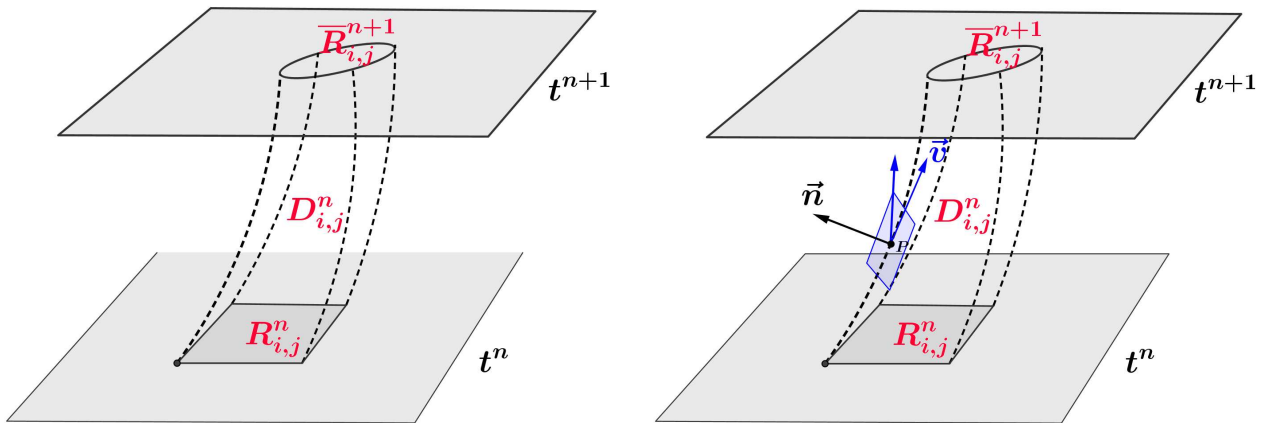


Figure 7.1: Integral tube in 3D

As before, we consider the hyperbolic conservation law in two dimensional variables in

divergence form,

$$\frac{\partial u}{\partial t} + \frac{\partial f(u)}{\partial x} + \frac{\partial g(u)}{\partial y} = 0 \quad \Longleftrightarrow \quad \nabla_{t,x,y} \begin{bmatrix} u \\ f(u) \\ g(u) \end{bmatrix} = 0. \quad (7.0.1)$$

Again, the integration over the control volume and the application of the divergence theorem gives,

$$\iiint_{D_{i,j}^n} \nabla_{t,x,y} \begin{bmatrix} u \\ f(u) \\ g(u) \end{bmatrix} dV = 0 \quad \Leftrightarrow \quad \int_{\partial D_{i,j}^n} \begin{bmatrix} u \\ f(u) \\ g(u) \end{bmatrix} \cdot \vec{n} d(\partial D_{i,j}^n) = 0. \quad (7.0.2)$$

The normal vector with respect to $R_{i,j}^n$ is, in usual convention, $[-1 \ 0 \ 0]^T$ and the vector normal in the outflow $\overline{R}_{i,j}^{n+1}$ is $[1 \ 0 \ 0]$. Then, the right side of (7.0.2) can be written as,

$$\int_{R_{i,j}^n} \begin{bmatrix} u \\ f(u) \\ g(u) \end{bmatrix} \cdot [-1 \ 0 \ 0]^T dA + \int_{S_{i,j}^n} \begin{bmatrix} u \\ f(u) \\ g(u) \end{bmatrix} \cdot \vec{n} dS + \int_{\overline{R}_{i,j}^{n+1}} \begin{bmatrix} u \\ f(u) \\ g(u) \end{bmatrix} \cdot [1 \ 0 \ 0]^T dA = 0. \quad (7.0.3)$$

We suppose there is not any flow through the surface $S_{i,j}^n$ ($S_{i,j}^n$ is impervious). So, the surface integral of $S_{i,j}^n$ is zero and therefore,

$$- \int_{R_{i,j}^n} u(x, y, t^n) dA + \int_{\overline{R}_{i,j}^{n+1}} u(x, y, t^{n+1}) dA = 0. \quad (7.0.4)$$

or

$$\int_{\overline{R}_{i,j}^{n+1}} u(x, y, t^{n+1}) dA = \int_{R_{i,j}^n} u(x, y, t^n) dA, \quad (7.0.5)$$

which we call **conservation identity**. The numerical approximations $U_{i,j}^n$ and $\overline{U}_{i,j}^{n+1}$ can be defined from equation (7.0.5). The difficulty with this approach is to define the normal vector along with the unique definition of tangent vector to the surface $S_{i,j}^n$ in the point (x_i, y_j, t^n) , see Figure 7.1 (right). Notice that in this point there is a tangent plane, then *integral surfaces* as well as *integral curves* coming from $[u \ f(u) \ g(u)]^T \cdot \vec{n} = 0$, as in the scalar case, are not easy to define (i.e., existence and uniqueness). In this work, we will use an alternative approach based on the novel Lagrangian-Eulerian framework to overcome this difficult task in order to solve numerically balance laws. This is achieved thanks to a convenient reformulation of the original conservation law by means of an equivalent system of balance laws.

In order to establish such connection between multidimensional hyperbolic conservation laws and system of balance laws, we will first introduce some notation to the subsequent application of the Lagrangian-Eulerian framework. For concreteness, and without loss of generality, we discuss a Lagrangian-Eulerian technique for approximation of the following two-dimensional initial value problem for hyperbolic of conservation laws,

$$\begin{cases} \frac{\partial u}{\partial t} + \frac{\partial f(u)}{\partial x} + \frac{\partial g(u)}{\partial y} = 0, & (x, y, t) \in \Omega \times (t^0, T], \\ u(x, y, t^0) = \eta(x, y), & (x, y) \in \Omega, \end{cases} \quad (7.0.6)$$

where Ω is a interior square domain in \mathbb{R}^2 , whose boundary we denoted by $\partial\Omega$ and $T > 0$. For the finite dimensional function spaces relying on solving the approximate problem associated to

(7.0.6), by the Lagrangian-Eulerian method for (7.0.6), we will introduce the following standard notation. The space region, $(\mathbb{R} \times \mathbb{R}) \times \overline{\mathbb{R}} = \{(x, y, t) : -\infty < x, y < \infty, t \geq 0\}$ will be replaced by the lattice $(\mathbb{Z} \times \mathbb{Z}) \times \mathbb{N} = \{(i, j, n) : i, j = 0, \pm 1, \pm 2, \dots; n = 0, 1, 2, \dots\}$ and we consider the sequence $U^n = (U^n)_{i,j}$, $i, j \in \mathbb{Z}$ for $n = 0, 1, 2, \dots$ for a given grid $\Delta x, \Delta y > 0$ and time level

$$t^n = \sum_{i=0}^n \Delta t^i, \quad (7.0.7)$$

with $t^0 = 0$, for non-constant time step Δt^i . In the time level t^n , we have $(x_i^n, y_j^n) = (ih, jh)$, $(x_{i+\frac{1}{2}}^n, x_{i-\frac{1}{2}}^n) = (i\Delta x + \frac{\Delta x}{2}, j\Delta y + \frac{\Delta y}{2})$ on the uniform local grid or original grid, here $h_{x,i}^n = \Delta x^n = x_{i+\frac{1}{2}}^n - x_{i-\frac{1}{2}}^n$, $i, j \in \mathbb{Z}$, and $h_{y,j}^n = \Delta y^n = y_{j+\frac{1}{2}}^n - y_{j-\frac{1}{2}}^n$, $i, j \in \mathbb{Z}$, where $(x_{i\pm\frac{1}{2}}^n, y_{i\pm\frac{1}{2}}^n)$ are the corner of the cell. For the non-uniform grid we have $h_{x,i}^{n+\frac{1}{2}} = \overline{\Delta x}^{n+\frac{1}{2}} = \overline{x}_{i+\frac{1}{2}}^{n+\frac{1}{2}} - \overline{x}_{i-\frac{1}{2}}^{n+\frac{1}{2}}$ in the time level $t^{n+\frac{1}{2}}$ and $h_{y,j}^{n+\frac{1}{2}+\frac{1}{2}} = \overline{\Delta y}^{n+\frac{1}{2}+\frac{1}{2}} = \overline{y}_{j+\frac{1}{2}}^{n+\frac{1}{2}+\frac{1}{2}} - \overline{y}_{j-\frac{1}{2}}^{n+\frac{1}{2}+\frac{1}{2}}$, in the time level t^{n+1} . Here, the pair of points (x_i^n, y_j^n) are the center of the cells $i, j \in \mathbb{Z}$, respectively. The approximate solution of u for (7.0.6), in each cell $[x_{i-\frac{1}{2}}^n, x_{i+\frac{1}{2}}^n] \times [y_{j-\frac{1}{2}}^n, y_{j+\frac{1}{2}}^n]$, is defined by, $i, j \in \mathbb{Z}$,

$$U(x_i, y_j, t^n) = U_{i,j}^n = \frac{1}{\Delta x \Delta y} \int_{x_{i-\frac{1}{2}}^n}^{x_{i+\frac{1}{2}}^n} \int_{y_{j-\frac{1}{2}}^n}^{y_{j+\frac{1}{2}}^n} u(x, y, t^n) dx dy, \quad (7.0.8)$$

and

$$\overline{U}_{i,j}^{n+\frac{1}{2}} = \frac{1}{h_{x,i}^{n+\frac{1}{2}} \Delta y} \int_{y_{j-\frac{1}{2}}^n}^{y_{j+\frac{1}{2}}^n} \int_{\overline{x}_{i-\frac{1}{2}}^{n+\frac{1}{2}}}^{\overline{x}_{i+\frac{1}{2}}^{n+\frac{1}{2}}} u(x, y, t^{n+\frac{1}{2}}) dx dy, \quad (7.0.9)$$

$$\overline{U}_{i,j}^{n+1} = \frac{1}{h_{y,j}^{n+1} \Delta x} \int_{x_{i-\frac{1}{2}}^{n+\frac{1}{2}}}^{x_{i+\frac{1}{2}}^{n+\frac{1}{2}}} \int_{\overline{y}_{j-\frac{1}{2}}^{n+1}}^{\overline{y}_{j+\frac{1}{2}}^{n+1}} u(x, y, t^{n+1}) dy dx,$$

respectively, along with the initial condition $U(x_j^0, y_j^0, t^0) = U_{i,j}^0$ in the cells $[x_{i-\frac{1}{2}}^0, x_{i+\frac{1}{2}}^0] \times [y_{j-\frac{1}{2}}^0, y_{j+\frac{1}{2}}^0]$, $i, j \in \mathbb{Z}$. Notice, in the equations (7.0.8) and (7.0.9), the quantity $u(x, y, t)$ is a solution of (7.0.6). The discrete counterpart of the space $L^p(\mathbb{R}^2)$ is $l_{\Delta x, \Delta y}^p$, the space of sequences $U = (U_{i,j})$, with $i, j \in \mathbb{Z}$, such that $\|U\|_{l_{\Delta x, \Delta y}^p} = \left(\Delta x \Delta y \sum_{i \in \mathbb{Z}} \sum_{j \in \mathbb{Z}} |U_{i,j}|^p \right)^{\frac{1}{p}}$, $1 \leq p < \infty$ where U is defined in the appropriate l_p -space (see, e.g., [110, 142]).

One monotone numerical scheme to (7.0.6) can be written, in sense of [42], as

$$\begin{aligned} U_{i,j}^{n+1} &= \mathcal{G}(U_{i-p,j-r}^n, \dots, U_{i+q+1,j+s+1}^n) \\ &= U_{i,j}^n - \lambda^x \Delta_+^x F_1(U_{i-p,i-r}^n, \dots, U_{i+q+1,j+s+1}^n) - \lambda^y \Delta_+^y F_2(U_{i-p,j-r}^n, \dots, U_{i+q+1,j+s+1}^n) \end{aligned} \quad (7.0.10)$$

In order that above equation be consistent with (7.0.6), it is must have

$$F_1(u, u, \dots, u) = f(u) \quad \text{and} \quad F_2(u, u, \dots, u) = g(u), \quad u \in \mathbb{R}, \quad (7.0.11)$$

Here, the functions F_1 and F_2 , are the numerical fluxes of the approximation. The difference approximation is monotone on the interval $[a, b]$ if \mathcal{G} a nondecreasing function of each argument $U_{i,j}^n$ so long as all arguments lie in $[a, b]$. Write $u(x, y, t) = (S(t)u_0)(x, y)$, where $S(t) : L^1(\mathbb{R}^2) \cap$

$L^\infty(\mathbb{R}^2) \rightarrow L^1(\mathbb{R}^2) \cap L^\infty(\mathbb{R}^2)$ for each $t \geq 0$ and $t \rightarrow S(t)u_0$ is continuous into $L^1(\mathbb{R}^2)$. To compute this solution numerically we set

$$u^{\Delta t} = \sum_{n=0}^{\infty} \sum_{k=-\infty}^{\infty} U_{j,k}^n \mathcal{X}_{j,k}^n \quad (7.0.12)$$

where $\mathcal{X}_{j,k}^n$ is the characteristic function in the respective cell.

7.1 The Lagrangian-Eulerian relation for hyperbolic conservation laws linked to balance laws

Although at very first glance our new Lagrangian-Eulerian computational strategy seems to be somewhat a variation, or rather a simple modification, of the classical dimensional splitting approach for multidimensional hyperbolic conservation laws [66, 77, 141] (see also [54, 111, 113, 158]), it is worth mentioning that **this is not the case**. In order to make such point very clear, we will briefly explain the key idea of the *classical dimensional splitting*, pointing out error mechanisms and computational aspects in such way to clarify this issue and mainly to avoid any misunderstanding with respect to our framework. Indeed, we precisely use the theory of balance laws in order to keep the dimensional coupling of the original multidimensional conservation law as well as design the construction of very good qualitative numerical approximations, which in turn seems to preserve all good mathematical properties of the good (entropy) solutions in all computed solutions, at least to the present moment in the current study, as we will discuss in details in Section 7.2.

Classical dimensional splitting, or fractional steps, has been widely used to extend one-dimensional numerical methods to multidimensional hyperbolic conservation law problems. The method was first introduced by Godunov [66] in connection with gas dynamics and later extended by Strang [141]. Indeed, Godunov's original scheme [66] is the forerunner of all upwind schemes. Its higher-order and multidimensional generalizations were constructed, analyzed, and implemented with great success during the 1970s and 1980s, see [32, 54, 66, 77, 109, 111, 113, 141, 150, 148, 158] and the references therein. In the context of the one-dimensional numerical methods, such schemes evaluate their cell-averages over the same spatial cells at all time steps. This in turn requires characteristic information along the discontinuous interfaces of these spatial cells. On this approach, it is necessary to trace the characteristic fans, using approximate Riemann solvers based on the dimensional splitting framework. The idea is quite simple.

Consider the two-dimensional nonlinear hyperbolic conservation law with initial data,

$$\begin{cases} \frac{\partial U}{\partial t} + \frac{\partial f(U)}{\partial x} + \frac{\partial g(U)}{\partial y} = 0, \\ U(x, y, t^n) = U^n. \end{cases} \quad (7.1.1)$$

The initial data at a time t^n is given by the set U^n of discrete cell average values $U_{i,j}^n$, where i denotes the x -direction and j denotes the y -direction. for $(x, t) \in \Omega \times (t^0, t^n]$, such that $\Delta t = t^n - t^{n-1}$, with $t^n = n\Delta t$. Let $\chi_x(t)$ and $\chi_y(t)$ denote approximate solutions operators

respectively of the initial value problems

$$\begin{aligned} \frac{\partial U}{\partial t} + \frac{\partial f(U)}{\partial x} &= 0, & U(x, y, t^n) &= U^n, \\ \frac{\partial U}{\partial t} + \frac{\partial g(U)}{\partial y} &= 0, & U(x, y, t^{n+1}) &= U^{n+\frac{1}{2}}, \end{aligned} \tag{7.1.2}$$

Then, for the first-order Godunov splitting method [66] the approximation is defined as,

$$U^{n+1} = \chi_y(\Delta t) U^{n+\frac{1}{2}} = \chi_y(\Delta t) \chi_x(\Delta t) U^n, \tag{7.1.3}$$

while for Strang's second-order splitting method [141] the approximation is defined as,

$$U^{n+2} = \chi_y(\Delta t/2) \chi_x(\Delta t) \chi_y(\Delta t/2) U^n, \tag{7.1.4}$$

the operators $\chi_x(t)$ and $\chi_y(t)$ are second order accuracy.

The two operator splittings (7.1.3) and (7.1.4) are examples of so-called multiplicative operator splittings. From the historical development point of view (just to mention and honor some pioneers of the subject), with no ambition of providing a complete survey, the idea of splitting formula of complicated operators into simpler operators that are treated separately, is both easy and fundamental, and as such has appeared under various names in different contexts. One of the first rigorous results is associated with the name of Trotter [149]. The fundamental question he asked was: Given two continuous semi-groups with corresponding generators, how can one define the semi-group corresponding to the sum of the two generators? The result, in the case of finite-dimensional matrices, goes back to Sophus Lie (1875) and important extensions were provided by Kato [95]. This result is often denoted as the **Lie-Trotter-Kato** formula or simply the **Trotter** formula. Applications by Trotter and Kato were to quantum mechanics. Several refinements of this method exist, for instance the Baker-Campbell-Hausdorff formula expresses the operator \mathcal{A} with the property that $e^{-tA_1} e^{-tA_2} = e^{-t\mathcal{A}}$

In a more concrete setting (e.g., applied to petroleum reservoir simulation) – and prior to Trotter and Kato – Douglas, Peaceman, and Rachford [48, 132] introduced a method called the alternating direction implicit (ADI) scheme, where multi-dimensional problems were successfully reduced to repeated one-dimensional problems. The ADI method was soon applied to petroleum reservoir simulation. During the period the ADI was being developed in the USA, a number of Soviet scientists were developing splitting methods (also known as fractional step or locally one-dimensional (LOD) methods) for solving time-dependent partial differential equations in two and three dimensions. Key advances were made by Yanenko, Samarskii, Marchuk and D'yakonov (see, e.g., english sources [59, 122, 136, 158]) to study a large variety of problems in mathematical and several applications.

Operator splitting techniques **may not always be the right answer**. The extent to which operator splitting will give an effective overall method **depends on the coupling of different elementary operators and the dynamics of the evolution problem**. It needs detailed knowledge of the behavior of the solutions to make a rather powerful method. Most of the refinements depend on further knowledge of properties of the underlying sub-problems.

Of course, for the equations (7.1.1), along with (7.1.2), the composition of the operators $\chi_x(t)$ and $\chi_y(t)$ can commute. For non-commuting operators an alternative splitting formula is obtained by reversing the order of the operators, but this will in general give a different

approximation. We remark that Crandall and Majda [41] proved that splitting methods (7.1.3) produce an approximation that converges to the unique entropy solution as temporal and spatial discretization tend to zero, when using monotone schemes [109]. Particular the theorem in [42]:

Theorem 7.1.1. Suppose $u_0 \in L^1(\mathbb{R}^2) \cap L^\infty(\mathbb{R}^2)$ and $a < u_0 < b$ a.e. Let (7.0.10) be a consistent conservation-form difference approximation to (7.1.1) which is monotone on $[a, b]$ and which has Lipschitz continuous numerical fluxes g_i , $i = 1, 2$. Let $U_{i,j}^n$ be given by (7.0.8), (7.0.12). Then as $\Delta t \rightarrow 0$ with $\Delta t/\Delta x$ and $\Delta t/\Delta y$ fixed, $U_{i,j}^n$ converges to $S(t)u_0$ in $L^1(\mathbb{R}^2)$ uniformly for bounded $t \geq 0$. More precisely,

$$\lim_{\Delta t \rightarrow 0} \sup_{0 \leq t \leq T} \iint_{\mathbb{R}^2} |u^{\Delta t}(x, y, t) - S(t)u_0(x, y)| dx dy = 0 \quad (7.1.5)$$

for each $T > 0$.

Thus, our Lagrangian-Eulerian scheme solves hyperbolic problems like a monotone scheme and converges to entropy solutions when a Godunov type splitting is used.

On the other hand, Teng [146] proved that in the general case (where the solution may contain discontinuities, i.e., shocks) the L^1 error bound of the splitting method (7.1.3) is of first-order $\mathcal{O}(\Delta t)^{1/2}$ (of course, this heavily depends on the underlying functional space). Furthermore, a similar error bound for the method (7.1.4) was derived in [114], when the one-dimensional solution operators are approximated by front-tracking; it was shown by means of a set of numerical examples that the accuracy is close to $\mathcal{O}(\Delta t)$. This unconditionally stable method was proposed by Holden and Risebro [79]; see also [77] for more recent developments. In our opinion, significant and relevant publications for this issue can be found in [150], which also describes a somewhat hybrid method between a front capturing method [39, 66, 91, 98, 109, 120, 129] and a front tracking method [63, 64, 150] as well as such articles, in turn, point out to a recent and good survey on the development of such techniques.

In the ‘‘classical’’ dimensional splitting approach, we point out that for each one of both splitting methods (7.1.4) and (7.1.3) – for each time step strategy – the numerical solution computed by means of the composition of the pertinent operator acts purely by one fixed dimension, namely in x -direction. Once we have that all information, the y -direction is then fixed and vice-versa with respect to the other case, when we have fixed the x -direction. In other works, for the computation of the operator $\chi_x(t)$, no explicit contribution of the operator $\chi_y(t)$ is accounted for. This means that for a selected time step for the approximate (or exact when possible) computation of the purely operator $\chi_x(t)$ (typically under a CFL condition), no characteristic information emanating from local interaction of the purely $\chi_y(t)$ operator is included in the solution.

Two sources of errors contribute to the total error in dimensional splitting; for more details we refer to the readers the references [32, 54, 66, 77, 109, 111, 113, 141, 148, 150, 158]. First, the temporal splitting errors arise since we split the multi-dimensional equation into a sequence of one-dimensional problems. Loosely speaking, we can say that the temporal error determines how well we are able to resolve the dynamics of the problem. Obviously, the temporal error decreases with decreasing splitting steps Δt (see, e.g. [77, 79, 114]). This is why it is expected to have a better results from the Strang’s splitting (7.1.3) (see [141]). Second, the other source of error comes from the discretization of each individual subequation (this is the issue we are pursuing by our new approach). For simplicity of notation, we will henceforth refer to this error

as the spatial error following the usual terminology used in the specialized literature. This comes from the observation that if the discretization method is sufficiently sophisticated to resolve the dynamics of the one-dimensional subequation, the associated discretization error will be reflected in the spatial resolution of the waves (local interaction) present in the approximate solution.

The basic idea of our new strategy is: for each time step we want to account into the spatial error related to each operator, for instance, \mathcal{S}_x – in the x -direction –, an appropriate contribution that comes from the other operator \mathcal{S}_y – namely in the y -direction, and vice-versa. We expect from this strategy to balance the local error mechanisms in order to reduce – or eliminate – the error that comes from the loss of local information induced by classical dimensional splitting.

It is well known that for the splitting method – in spirit of the approaches in (7.1.4) and (7.1.3) – using front tracking, the main spatial error contribution comes from the projection onto the regular grid after the evolution by a number of time steps. This error increases with decreasing Δt , since the number of times the projection is applied is inversely proportional to Δt . The accuracy of the one-dimensional front-tracking algorithm, on the other hand, grows linearly with $\Delta t \delta$ [77, 79, 91, 90, 92, 114]. Altogether this means that there are two error mechanisms that work in opposite directions: the temporal error decreases with decreasing Δt and the spatial error increases with decreasing Δt . To minimize the overall error we must therefore find the minimum where the temporal error balances the splitting error. Our aim is just to reduce the error that comes from the spatial error (discretization of the operator) since the time step is typically well controlled by a CFL-condition and by the underlying physics in order to not overestimate the shock layer. For instance, the width of the shock layer for a parabolic equation in the spirit of convection-diffusion transport problems of the form, $u = u(x, t)$, $u_t + f_x(u) = (\epsilon u_x)_x$, $\epsilon > 0$, is $O(\epsilon)$ (see [90, 92]). Using a splitting fractional time step Δt for such equations, the width of the numerical shock layer will be $O(\sqrt{\Delta t \epsilon})$ because the nonlinear self-sharpening mechanisms of the fractional flow function $f(u)$ is thrown away by the unphysical entropy loss due to Oleinik’s convexification [127, 128] introduced in the convective step by the hyperbolic scheme for $u_t + f_x(u) = 0$. Thus, to not overestimate the shock layer (the nonlinear balance between purely hyperbolic/parabolic terms), the splitting step should not be (significantly) larger than ϵ [90, 92]. Moreover, when dealing with approximations for balance laws (as we will discuss next) we will consider only unsplitting schemes in such way to properly balance the fluxes and the source at the discrete level. This means that the key issue is the “well-balancing” discretization in order to achieve the proper nonlinear balance between fluxes and source term linked to the original differential system as discussed in details in Section 1.1.

The main idea behind our approach is quite simple. First, consider the two-dimensional nonlinear hyperbolic conservation law with initial data (7.1.1). Consider now the cell-centered finite-volume cells,

$$D_{i,j}^n = \{(t, x, y) / t^n \leq t \leq t^{n+\frac{1}{2}}, y_{j-\frac{1}{2}}^n \leq y \leq y_{j+\frac{1}{2}}^n, \sigma_i^n(t) \leq x \leq \sigma_{i+1}^n(t)\},$$

$$D_{i,j}^{n+\frac{1}{2}} = \{(t, x, y) / t^{n+\frac{1}{2}} \leq t \leq t^{n+1}, x_{i-\frac{1}{2}}^{n+\frac{1}{2}} \leq x \leq x_{i+\frac{1}{2}}^{n+\frac{1}{2}}, \gamma_j^{n+\frac{1}{2}}(t) \leq y \leq \gamma_{j+1}^{n+\frac{1}{2}}(t)\},$$

where $\sigma_i^n(t)$ and $\gamma_j^n(t)$ are parametrized curves such that $\sigma_i^n(t^n) = x_i^n$ and $\gamma_j^{n+\frac{1}{2}}(t^{n+\frac{1}{2}}) = y_j^{n+\frac{1}{2}}$.

Our approach is based in writing (7.1.1) in the form of a coupled set of two balance laws along with initial and with numerical approximations $\left(\frac{\partial g(U)}{\partial y}\right)_j$ and $\left(\frac{\partial f(U)}{\partial x}\right)_i$ of the derivatives

$\frac{\partial f(U)}{\partial x}$ and $\frac{\partial g(U)}{\partial y}$ respectively,

$$\begin{cases} \frac{\partial U}{\partial t} + \frac{\partial f(U)}{\partial x} = - \left(\frac{\partial g(U)}{\partial y} \right)_j, & \text{in } D_{i,j}^n, \\ U(x, y, t^n) = U^n, \end{cases} \quad (7.1.6a)$$

$$\begin{cases} \frac{\partial U}{\partial t} + \frac{\partial g(U)}{\partial y} = - \left(\frac{\partial f(U)}{\partial x} \right)_i, & \text{in } D_{i,j}^{n+\frac{1}{2}}, \\ U(x, y, t^{n+\frac{1}{2}}) = U^{n+\frac{1}{2}}. \end{cases} \quad (7.1.6b)$$

Denote $S_x(t)$ and $S_y(t)$ as approximate solution operators for (7.1.6a) and (7.1.6b), respectively. Indeed, such approximate solution operators can be given by scheme (5.2.1) or (5.2.2) in both directions x or y . Thus, $U_{i,j}^{n+\frac{1}{2}} = S_x(\Delta t/2)U_{i,j}^n$ and $U_{i,j}^{n+1} = S_y(\Delta t/2)U_{i,j}^{n+\frac{1}{2}}$, so that the full scheme is given by,

$$U_{i,j}^{n+1} = S_y(\Delta t/2)S_x(\Delta t/2)U_{i,j}^n, \quad (7.1.7)$$

along with the CFL condition,

$$Mk/h \leq \sqrt{2}/2, \quad (7.1.8)$$

with $M = \max\{\max_j\{f'(U_{i,j}^n)\}, \max_j\{\frac{f(U_{i,j}^n)}{U_{i,j}^n}\}, \max_j\{g'(U_{i,j}^n)\}, \max_j\{\frac{g(U_{i,j}^n)}{U_{i,j}^n}\}\}$. The equations appearing in (7.1.6a) and (7.1.6b) can be viewed as a set of local balance laws in the time step $[t^n, t^{n+1}]$, but coupled via the source terms on the RHS of (7.1.6) and thus linked to the full problem (7.1.1). Then the procedure to solve (7.1.1) is quite simple as follows: in the time step from t^n to $t^{n+\frac{1}{2}}$ the information of the previous time, say in the y coordinate, is accounted through the source term for the balance law in the x coordinate. Similarly, in time step from $t^{n+\frac{1}{2}}$ to t^{n+1} , the information in the x coordinate is also accounted through of the source term for the balance law in the y coordinate.

Notice now that the one-dimensional system of balance laws operator, say $S_x(t)$, account simultaneously for contributions in both directions, namely, in the x -direction by the discretization of the flux function $f(v)$ in the purely hyperbolic operator $\frac{\partial f(v)}{\partial x}$ as well as in the y -direction by the discretization of the flux function $g(w)$ that appears in the source term $-\frac{\partial g(w)}{\partial y}$, and vice-versa with respect to the operator $S_y(t)$. Thus, the preceding discussion makes more clear why it was necessary to revisit the computational mathematics and theoretical mathematics of balance laws in a minimum extent, but with a solid oriented view to our new approach in order to establish a tightly-linked connection between multidimensional hyperbolic conservation laws and system of balance laws. Indeed, such discussion also support the need to revisit the Lagrangian-Eulerian framework in its original setting for linear hyperbolic conservation laws and its extension for scalar and system problems balance laws in one-space dimension, as discuss in details in Section 2 as well as in Section 5.

Of course, for the equations (7.1.1), along with (7.1.6), the composition of the operators $S_y(t)$ and $S_x(t)$ can commute. We performed preliminary and non exhaustive numerical experiments (Section 7.2) along with the composition approach in the Lagrangian-Eulerian framework with very good agreement with the well known solutions of the underlying test problems available in the vast literature to corroborate our findings.

Let us now turn our attention to the approximation of the two-dimensional hyperbolic solution operators (7.1.7) written in the form of one-dimensional balance law operators $S_x(t)$ and $S_y(t)$. Of course, such operators can either be constructed *directly* (i.e., exactly when

possible; see, e.g. [77]), or by using *dimensional splitting* [66, 141] or some kind of physics-based operator splitting [3, 4]. As announced, we will pursue the construction of unsplitting methods for the approximation of the equations (7.1.6) in order to preserve the delicate nonlinear balance between the nonlinear flux gradients, and the form of the source terms of the two-dimensional hyperbolic solution operators linked to the one-dimensional balance law operators $S_x(t)$ and $S_y(t)$ as in (7.1.7).

7.1.1 The locally conservative Lagrangian-Eulerian relation for scalar multidimensional hyperbolic conservation laws linked to one-dimensional system of balance laws

We first consider cell-centered finite-volume cell centers in the Lagrangian-framework as follows:

$$D_{i,j}^n = \{(t, x, y) / t^n \leq t \leq t^{n+\frac{1}{2}}, y_{j-\frac{1}{2}}^n \leq y \leq y_{j+\frac{1}{2}}^n, \sigma_i^n(t) \leq x \leq \sigma_{i+1}^n(t)\}, \quad (7.1.9)$$

and

$$D_{i,j}^{n+\frac{1}{2}} = \{(t, x, y) / t^{n+\frac{1}{2}} \leq t \leq t^{n+1}, x_{i-\frac{1}{2}}^{n+\frac{1}{2}} \leq x \leq x_{i+\frac{1}{2}}^{n+\frac{1}{2}}, \gamma_j^{n+\frac{1}{2}}(t) \leq y \leq \gamma_{j+1}^{n+\frac{1}{2}}(t)\}, \quad (7.1.10)$$

where $\sigma_i^n(t)$ and $\gamma_j^n(t)$ is a parametrized curve such that $\sigma_i^n(t^n) = x_i^n$ and $\gamma_j^{n+\frac{1}{2}}(t^{n+\frac{1}{2}}) = y_j^{n+\frac{1}{2}}$; i.e., define the space-time local control volumes $D_{i,j}^n$ and $D_{i,j}^{n+\frac{1}{2}}$. As previously announced, we now consider the reformulation of (7.1.1) in the space-time local control volumes $D_{i,j}^n$ and $D_{i,j}^{n+\frac{1}{2}}$ as two coupled systems of balance law equations which are to be solved simultaneously along with our locally conservative (by construction) Lagrangian-Eulerian framework as follows. Thus, write (7.1.1) as,

$$\begin{cases} \frac{\partial u}{\partial t} + \frac{\partial f(u)}{\partial x} = - \left(\frac{\partial g(u)}{\partial y} \right)_j, & (x, y, t) \in D_{i,j}^n, \\ \frac{\partial u}{\partial t} + \frac{\partial g(u)}{\partial y} = - \left(\frac{\partial f(u)}{\partial x} \right)_i, & (x, y, t) \in D_{i,j}^{n+\frac{1}{2}}, \end{cases} \quad (7.1.11)$$

and perform the pertinent Lagrangian-Eulerian integration over the finite volumes $D_{i,j}^n$ and $D_{i,j}^{n+\frac{1}{2}}$ for the coupled system of balance laws (7.1.11) to get:

$$\begin{cases} \iiint_{D_{i,j}^n} \left(\frac{\partial u}{\partial t} + \frac{\partial f(u)}{\partial x} \right) dV = - \iiint_{D_{i,j}^n} \left(\frac{\partial g(u)}{\partial y} \right)_j dV, \\ \iiint_{D_{i,j}^{n+\frac{1}{2}}} \left(\frac{\partial u}{\partial t} + \frac{\partial g(u)}{\partial y} \right) dV = - \iiint_{D_{i,j}^{n+\frac{1}{2}}} \left(\frac{\partial f(u)}{\partial x} \right)_i dV. \end{cases} \quad (7.1.12)$$

If we write the purely convection counterpart in the conservative divergence form (as introduced [57] for convection-diffusion problems) then,

$$\left\{ \begin{array}{l} \int_{y_{j-\frac{1}{2}}^n}^{y_{j+\frac{1}{2}}^n} \int_{t^n}^{t^{n+\frac{1}{2}}} \int_{\sigma_i^n(t)}^{\sigma_{i+1}^n(t)} \nabla_{t,x} \cdot \begin{pmatrix} u \\ f(u) \end{pmatrix} dx dt dy = - \int_{y_{j-\frac{1}{2}}^n}^{y_{j+\frac{1}{2}}^n} \int_{t^n}^{t^{n+\frac{1}{2}}} \int_{\sigma_i^n(t)}^{\sigma_{i+1}^n(t)} \left(\frac{\partial g(u)}{\partial y} \right)_j dx dt dy, \\ \int_{x_{i-\frac{1}{2}}^{n+\frac{1}{2}}}^{x_{i+\frac{1}{2}}^{n+\frac{1}{2}}} \int_{t^{n+\frac{1}{2}}}^{t^{n+1}} \int_{\gamma_j^{n+\frac{1}{2}}(t)}^{\gamma_{i+1}^{n+\frac{1}{2}}(t)} \nabla_{t,y} \cdot \begin{pmatrix} u \\ g(u) \end{pmatrix} dy dt dx = - \int_{x_{i-\frac{1}{2}}^{n+\frac{1}{2}}}^{x_{i+\frac{1}{2}}^{n+\frac{1}{2}}} \int_{t^{n+\frac{1}{2}}}^{t^{n+1}} \int_{\gamma_j^{n+\frac{1}{2}}(t)}^{\gamma_{i+1}^{n+\frac{1}{2}}(t)} \left(\frac{\partial f(u)}{\partial x} \right)_i dy dt dx. \end{array} \right. \quad (7.1.13)$$

Now, the application of the divergence theorem in the left-hand side of the coupled system of balance laws (7.1.13) reads,

$$\left\{ \begin{array}{l} \int_{y_{j-\frac{1}{2}}^n}^{y_{j+\frac{1}{2}}^n} \oint_{D_i^n} \vec{n}_x \cdot \begin{pmatrix} u \\ f(u) \end{pmatrix} d(\partial D_i^n) dy = - \int_{y_{j-\frac{1}{2}}^n}^{y_{j+\frac{1}{2}}^n} \int_{t^n}^{t^{n+\frac{1}{2}}} \int_{\sigma_i^n(t)}^{\sigma_{i+1}^n(t)} \left(\frac{\partial g(u)}{\partial y} \right)_j dx dt dy, \\ \int_{x_{i-\frac{1}{2}}^{n+\frac{1}{2}}}^{x_{i+\frac{1}{2}}^{n+\frac{1}{2}}} \oint_{D_j^n} \vec{n}_y \cdot \begin{pmatrix} u \\ g(u) \end{pmatrix} d(\partial D_j^n) dx = - \int_{x_{i-\frac{1}{2}}^{n+\frac{1}{2}}}^{x_{i+\frac{1}{2}}^{n+\frac{1}{2}}} \int_{t^{n+\frac{1}{2}}}^{t^{n+1}} \int_{\gamma_j^{n+\frac{1}{2}}(t)}^{\gamma_{i+1}^{n+\frac{1}{2}}(t)} \left(\frac{\partial f(u)}{\partial x} \right)_i dy dt dx. \end{array} \right. \quad (7.1.14)$$

Subjected to all considered preliminary intrinsic assumptions up to this moment, the fact (7.1.13) \Leftrightarrow (7.1.14), implies that the surface area of the parametric surface $\{(x, y, t) : x = \sigma_i^n(t), y_{j-\frac{1}{2}} \leq y \leq y_{j+\frac{1}{2}}\}$, $i \in \mathbb{Z}$ is naturally zero total flux normal to an impervious boundary of the finite volumes D_i^n and D_j^n as respectively depicted in equation (7.1.14). As discussed before in Chapters 2 and Chapter 5, the quantity $\sigma_i^n(t)$ is a solution of the associated system of ordinary differential equations related to the Lagrangian-Eulerian formulation of equations (7.1.14), as follows,

$$\frac{d\sigma_i^n(t)}{dx} = \frac{f(u)}{u}, \quad \sigma_i^n(t^n) = x_i^n, \quad t^n \leq t \leq t^{n+\frac{1}{2}}. \quad (7.1.15)$$

The same mathematical reasoning/argument can be used in $t^{n+\frac{1}{2}} \leq t \leq t^{n+1}$ to justify that the surface area of the parametric surface $\{(x, y, t) : x = \gamma_j^n(t), x_{i-\frac{1}{2}} \leq y \leq x_{i+\frac{1}{2}}\}$, $j \in \mathbb{Z}$ is naturally zero total flux normal to an impervious boundary of the pertinent finite volumes associated to D_i^n and D_j^n along with $\gamma_j^n(t)$, with in turn are solutions of the associated system of ordinary differential equations given by,

$$\frac{d\gamma_j^n(t)}{dx} = \frac{g(u)}{u}, \quad \gamma_j^n(t^n) = y_j^n, \quad t^{n+\frac{1}{2}} \leq t \leq t^{n+1}. \quad (7.1.16)$$

The equations (7.1.14) implies that,

$$\left\{ \begin{array}{l} \int_{y_{j-\frac{1}{2}}^n}^{y_{j+\frac{1}{2}}^n} \left[\int_{x_{i-\frac{1}{2}}^{n+\frac{1}{2}}}^{x_{i+\frac{1}{2}}^{n+\frac{1}{2}}} u(x, y, t^{n+\frac{1}{2}}) dx - \int_{x_i^n}^{x_{i+1}^n} u(x, y, t^n) dx \right] dy = - \int_{y_{j-\frac{1}{2}}^n}^{y_{j+\frac{1}{2}}^n} \int_{t^n}^{t^{n+\frac{1}{2}}} \int_{\sigma_i^n(t)}^{\sigma_{i+1}^n(t)} \left(\frac{\partial g(u)}{\partial y} \right)_j dx dt dy, \\ \int_{x_{i-\frac{1}{2}}^{n+\frac{1}{2}}}^{x_{i+\frac{1}{2}}^{n+\frac{1}{2}}} \left[\int_{y_{i-\frac{1}{2}}^{n+1}}^{y_{i+\frac{1}{2}}^{n+1}} u(x, y, t^{n+\frac{1}{2}}) dy - \int_{y_i^{n+\frac{1}{2}}}^{y_{i+1}^{n+\frac{1}{2}}} u(x, y, t^{n+\frac{1}{2}}) dy \right] dx = - \int_{x_{i-\frac{1}{2}}^{n+\frac{1}{2}}}^{x_{i+\frac{1}{2}}^{n+\frac{1}{2}}} \int_{t^{n+\frac{1}{2}}}^{t^{n+1}} \int_{\gamma_j^{n+\frac{1}{2}}(t)}^{\gamma_{i+1}^{n+\frac{1}{2}}(t)} \left(\frac{\partial f(u)}{\partial x} \right)_i dy dt dx, \end{array} \right. \quad (7.1.17)$$

or, (7.1.17) we can written as,

$$\left\{ \begin{array}{l} \int_{y_{j-\frac{1}{2}}^n}^{y_{j+\frac{1}{2}}^n} \int_{\bar{x}_{i-\frac{1}{2}}^{n+\frac{1}{2}}}^{\bar{x}_{i+\frac{1}{2}}^{n+\frac{1}{2}}} u(x, y, t^{n+\frac{1}{2}}) dx dy - \int_{y_{j-\frac{1}{2}}^n}^{y_{j+\frac{1}{2}}^n} \int_{x_i^n}^{x_{i+1}^n} u(x, y, t^n) dx dy = - \int_{y_{j-\frac{1}{2}}^n}^{y_{j+\frac{1}{2}}^n} \int_{t^n}^{t^{n+\frac{1}{2}}} \int_{\sigma_i^n(t)}^{\sigma_{i+1}^n(t)} \left(\frac{\partial g(u)}{\partial y} \right)_j dx dt dy, \\ \int_{x_{i-\frac{1}{2}}^{n+\frac{1}{2}}}^{x_{i+\frac{1}{2}}^{n+\frac{1}{2}}} \int_{\bar{y}_{i-\frac{1}{2}}^{n+1}}^{\bar{y}_{i+\frac{1}{2}}^{n+1}} u(x, y, t^{n+1}) dy dx - \int_{x_{i-\frac{1}{2}}^{n+\frac{1}{2}}}^{x_{i+\frac{1}{2}}^{n+\frac{1}{2}}} \int_{y_i^{n+\frac{1}{2}}}^{y_{i+1}^{n+\frac{1}{2}}} u(x, y, t^{n+\frac{1}{2}}) dy dx = - \int_{x_{i-\frac{1}{2}}^{n+\frac{1}{2}}}^{x_{i+\frac{1}{2}}^{n+\frac{1}{2}}} \int_{t^{n+\frac{1}{2}}}^{t^{n+1}} \int_{\gamma_j^{n+\frac{1}{2}}(t)}^{\gamma_{j+1}^{n+\frac{1}{2}}(t)} \left(\frac{\partial f(u)}{\partial x} \right)_i dy dt dx. \end{array} \right. \quad (7.1.18)$$

Now, to preserve consistent quantities in the cells of the computational domain, we firstly multiply the first equation in (7.1.18) by $1/(h_{x,j}^{n+\frac{1}{2}} \Delta y)$ as well as we multiply the second equation in (7.1.18) by the factor $1/(h_{y,i}^{n+\frac{1}{2}} \Delta x)$ and secondly we make use of (7.0.9) to obtain,

$$\left\{ \begin{array}{l} \bar{U}_{i,j}^{n+\frac{1}{2}} - \frac{\Delta x}{h_{x,j}^{n+\frac{1}{2}} \Delta y \Delta x} \int_{y_{j-\frac{1}{2}}^n}^{y_{j+\frac{1}{2}}^n} \int_{x_i^n}^{x_{i+1}^n} u(x, y, t^n) dx dy = - \frac{\Delta x}{h_{x,j}^{n+\frac{1}{2}} \Delta y \Delta x} \int_{y_{j-\frac{1}{2}}^n}^{y_{j+\frac{1}{2}}^n} \int_{t^n}^{t^{n+\frac{1}{2}}} \int_{\sigma_i^n(t)}^{\sigma_{i+1}^n(t)} \left(\frac{\partial g(u)}{\partial y} \right)_j dx dt dy, \\ \bar{U}_{i,j}^{n+1} - \frac{\Delta y}{h_{y,i}^{n+\frac{1}{2}} \Delta y \Delta x} \int_{x_{i-\frac{1}{2}}^{n+\frac{1}{2}}}^{x_{i+\frac{1}{2}}^{n+\frac{1}{2}}} \int_{y_i^{n+\frac{1}{2}}}^{y_{i+1}^{n+\frac{1}{2}}} u(x, y, t^{n+\frac{1}{2}}) dy dx = - \frac{\Delta y}{h_{y,i}^{n+\frac{1}{2}} \Delta y \Delta x} \int_{x_{i-\frac{1}{2}}^{n+\frac{1}{2}}}^{x_{i+\frac{1}{2}}^{n+\frac{1}{2}}} \int_{t^{n+\frac{1}{2}}}^{t^{n+1}} \int_{\gamma_j^{n+\frac{1}{2}}(t)}^{\gamma_{j+1}^{n+\frac{1}{2}}(t)} \left(\frac{\partial f(u)}{\partial x} \right)_i dy dt dx. \end{array} \right. \quad (7.1.19)$$

Now, from equation (7.1.19) and by means of relations (7.0.8)-(7.0.9), we finally get the Lagrangian-Eulerian scheme for the two-dimensional hyperbolic conservation law (7.1.1) is given by,

$$\left\{ \begin{array}{l} \bar{U}_{i,j}^{n+\frac{1}{2}} - \frac{\Delta x}{h_{x,j}^{n+\frac{1}{2}}} [U_{i,j}^n + U_{i,j+1}^n] = - \frac{\Delta x}{h_{x,j}^{n+\frac{1}{2}} \Delta y \Delta x} \int_{y_{j-\frac{1}{2}}^n}^{y_{j+\frac{1}{2}}^n} \int_{t^n}^{t^{n+\frac{1}{2}}} \int_{\sigma_i^n(t)}^{\sigma_{i+1}^n(t)} \left(\frac{\partial g(u)}{\partial y} \right)_j dx dt dy, \\ \bar{U}_{i,j}^{n+1} - \frac{\Delta y}{h_{y,i}^{n+\frac{1}{2}}} [U_{i,j}^{n+\frac{1}{2}} + U_{i,j+1}^{n+\frac{1}{2}}] = - \frac{\Delta y}{h_{y,i}^{n+\frac{1}{2}} \Delta y \Delta x} \int_{x_{i-\frac{1}{2}}^{n+\frac{1}{2}}}^{x_{i+\frac{1}{2}}^{n+\frac{1}{2}}} \int_{t^{n+\frac{1}{2}}}^{t^{n+1}} \int_{\gamma_j^{n+\frac{1}{2}}(t)}^{\gamma_{j+1}^{n+\frac{1}{2}}(t)} \left(\frac{\partial f(u)}{\partial x} \right)_i dy dt dx, \end{array} \right. \quad (7.1.20)$$

where

$$U_{i,j}^{n+\frac{1}{2}} = \frac{1}{\Delta x} \left[(0.5\Delta x + f_{x,i}^n) \bar{U}_{i-1,j}^{n+\frac{1}{2}} + (0.5\Delta x - f_{x,i}^n) \bar{U}_{i,j}^{n+\frac{1}{2}} \right], \quad (7.1.21)$$

along with $f_{x,j}^n \approx \frac{f(U_{i,j}^n)}{U_{i,j}^n}$. Finally, the approximate Lagrangian-Eulerian scheme for the two-dimensional hyperbolic problem (7.1.1) is given by,

$$U_{i,j}^{n+1} = \frac{1}{\Delta y} \left[(0.5\Delta y + g_{i,y}^{n+\frac{1}{2}}) \bar{U}_{i,j-1}^{n+1} + (0.5\Delta y - g_{i,y}^{n+\frac{1}{2}}) \bar{U}_{i,j}^{n+1} \right], \quad (7.1.22)$$

where $g_{i,y}^{n+\frac{1}{2}} \approx \frac{g(U_{i,j}^{n+\frac{1}{2}})}{U_{i,j}^{n+\frac{1}{2}}}$.

We use the following approximation proposed in [124] to approximate the derivatives $(\partial(f(u))/\partial x)_i$ and $(\partial(g(u))/\partial y)_j$

$$\left(\frac{\partial(f(u(x = x_i, y, t)))}{\partial x} \right)_i = \frac{1}{\Delta x} f'_i + O(\Delta x)$$

and

$$\left(\frac{\partial(g(u(x, y = y_j, t)))}{\partial y} \right)_j = \frac{1}{\Delta y} g'_j + O(\Delta y)$$

that are computed by means of a locally conservative non-oscillatory central differencing slope limiters. With this, we write

$$\begin{aligned} \int_{y_{j-\frac{1}{2}}^n}^{y_{j+\frac{1}{2}}^n} \int_{t^n}^{t^{n+\frac{1}{2}}} \int_{\sigma_i^n(t)}^{\sigma_{i+1}^n(t)} \frac{\partial g(u)}{\partial y} dx dt dy &\approx g'_j \int_{t^n}^{t^{n+\frac{1}{2}}} \int_{\sigma_i^n(t)}^{\sigma_{i+1}^n(t)} dx dt \\ &= g'_j \int_{t^n}^{t^{n+\frac{1}{2}}} \int_{\sigma_i^n(t)}^{\sigma_{i+1}^n(t)} dx dt, \end{aligned} \quad (7.1.23)$$

and

$$\begin{aligned} \int_{x_{i-\frac{1}{2}}^{n+\frac{1}{2}}}^{x_{i+\frac{1}{2}}^{n+\frac{1}{2}}} \int_{t^{n+\frac{1}{2}}}^{t^{n+1}} \int_{\gamma_j^{n+\frac{1}{2}}(t)}^{\gamma_{j+1}^{n+\frac{1}{2}}(t)} \frac{\partial f(u)}{\partial x} dy dt dx &\approx f'_i \int_{t^{n+\frac{1}{2}}}^{t^{n+1}} \int_{\gamma_j^{n+\frac{1}{2}}(t)}^{\gamma_{j+1}^{n+\frac{1}{2}}(t)} dy dt \\ &= f'_i \int_{t^{n+\frac{1}{2}}}^{t^{n+1}} \int_{\gamma_j^{n+\frac{1}{2}}(t)}^{\gamma_{j+1}^{n+\frac{1}{2}}(t)} dy dt, \end{aligned} \quad (7.1.24)$$

Thus, the Lagrangian-Eulerian scheme (7.1.21)-(7.1.22) for the two-dimensional hyperbolic problem (7.1.1), along with the pertinent approximation performed in (7.1.24), takes the form for implementation in a computer,

$$\left\{ \begin{aligned} \bar{U}_{i,j}^{n+\frac{1}{2}} - \frac{\Delta x}{h_{x,j}^{n+\frac{1}{2}}} [U_{i,j}^n + U_{i+1,j}^n] &= -\frac{g'_j}{h_{x,j}^{n+\frac{1}{2}}} \int_{t^n}^{t^{n+\frac{1}{2}}} \int_{\sigma_i^n(t)}^{\sigma_{i+1}^n(t)} dx dt, \\ U_{i,j}^{n+\frac{1}{2}} &= \frac{1}{\Delta x} \left[(0.5\Delta x + f_{x,j}^n) \bar{U}_{i-1,j}^{n+\frac{1}{2}} + (0.5\Delta x - f_{x,j}^n) \bar{U}_{i,j}^{n+\frac{1}{2}} \right], \\ \bar{U}_{i,j}^{n+1} - \frac{\Delta y}{h_{y,j}^{n+\frac{1}{2}}} [U_{i,j}^{n+\frac{1}{2}} + U_{i,j+1}^{n+\frac{1}{2}}] &= -\frac{f'_i}{h_{y,j}^{n+\frac{1}{2}}} \int_{t^{n+\frac{1}{2}}}^{t^{n+1}} \int_{\gamma_j^{n+\frac{1}{2}}(t)}^{\gamma_{j+1}^{n+\frac{1}{2}}(t)} dy dt \\ U_{i,j}^{n+1} &= \frac{1}{\Delta y} \left[(0.5\Delta y + g_{i,y}^{n+\frac{1}{2}}) \bar{U}_{i,j-1}^{n+1} + (0.5\Delta y - g_{i,y}^{n+\frac{1}{2}}) \bar{U}_{i,j}^{n+1} \right]. \end{aligned} \right. \quad (7.1.25)$$

which, we called in this work *Lagrangian-Eulerian to Hyperbolic laws in two Dimensional Variables* (LEH2D). We note that the two dimensional Lagrangian-Eulerian scheme is coupled by the source term in each time step, thus in the time step from t^n to $t^{n+\frac{1}{2}}$ the information of the previous times in the y coordinate is taken right through of the source term, and analogue in the time step from $t^{n+\frac{1}{2}}$ to t^{n+1} the information in the x coordinate is also taken of the source term. Actually, the two dimensional Lagrangian scheme solve one balance law in each time step, this is why that allows to the numerical scheme couples both directions x coordinate and y coordinate in each advance in the time. This important fact makes our two dimensional Lagrangian-Eulerian scheme to be seen as a numerical method of unsplit type. The scheme (7.1.25) is an extension of the Lagrangian-Eulerian scheme to the Balance law LEB1 (5.2.1) shown in previous chapters. Other possibility, to get a Lagrangian-Eulerian scheme for two Dimensional Variables, is to extend the scheme LEB2 (5.2.2). The extension for this scheme

gives the following numerical method,

$$\left\{ \begin{array}{l} U_{i,j}^{n+\frac{1}{2}} = \frac{1}{4}(U_{i-1,j}^n + 2U_{i,j}^n + U_{i+1,j}^n) - \frac{k/2}{2h} (f(U_{i+1,j}^n) - f(U_{i-1,j}^n)) \\ \quad + \frac{1}{h} \left[\frac{1}{h} \left(\frac{h}{2} + f_{x,j}^n k \right) \iint_{D_{i-1,j}^n} \frac{\partial g(u_j)}{\partial y} dx dt + \frac{1}{h} \left(\frac{h}{2} - f_{x,j}^n k \right) \iint_{D_{i,j}^n} \frac{\partial g(u_j)}{\partial y} dx dt \right], \\ U_{i,j}^{n+1} = \frac{1}{4}(U_{i,j-1}^{n+\frac{1}{2}} + 2U_{i,j}^{n+\frac{1}{2}} + U_{i,j+1}^{n+\frac{1}{2}}) - \frac{k/2}{2h} (g(U_{i,j+1}^{n+\frac{1}{2}}) - g(U_{i,j-1}^{n+\frac{1}{2}})) \\ \quad + \frac{1}{h} \left[\frac{1}{h} \left(\frac{h}{2} + g_{i,y}^{n+\frac{1}{2}} \right) \iint_{D_{i,j-1}^{n+\frac{1}{2}}} \frac{\partial f(u_i^n)}{\partial x} dy dt + \frac{1}{h} \left(\frac{h}{2} - g_{i,y}^{n+\frac{1}{2}} \right) \iint_{D_{i,j}^{n+\frac{1}{2}}} \frac{\partial f(u_i^n)}{\partial x} dy dt \right], \end{array} \right. \quad (7.1.26)$$

where $u_j^n = u(x, U_{i,j}^n, t)$ with j fixed, and $u_i^n = u(U_{i,j}^{n+\frac{1}{2}}, y, t)$ with i fixed. The two dimensional scheme (7.1.26) was called in this work *the finite difference two-dimensional Lagrangian-Eulerian scheme* and will denote by LEH2D2. Note that the two dimensional scheme (7.1.26) resolves numerically one balance law in $t^n < t < t^{n+\frac{1}{2}}$ using the scheme LEB2 in x -direction, and resolves one balance law in $t^{n+\frac{1}{2}} \leq t \leq t^{n+1}$ using the same scheme in y -direction.

Notice that the two dimensional Lagrangian-Eulerian schemes (7.1.25) and (7.1.26) retain the coupling between the systems of balance law equations (7.1.6) in order to preserve the delicate nonlinear balance between the nonlinear flux gradients and the form of the source terms of the two-dimensional hyperbolic solution operators, linked to the one-dimensional balance law operators \mathcal{S}_y and \mathcal{S}_x as in (7.1.3), or in (7.1.4). Such operators can either be constructed *directly* or by using *dimensional splitting* or some kind of physics-based operator splitting. Again, as announced, we performed a construction of an unsplitting directly approximation. In other words, the two dimensional Lagrangian-Eulerian scheme (7.1.25) retain the coupling between nonlinear flux gradients and the source term for each time step. Thus, in the time step from t^n to $t^{n+\frac{1}{2}}$ the information of the previous time step in the y -coordinate is used into the pertinent source term; the information is also used in a similar way from $t^{n+\frac{1}{2}}$ to t^{n+1} , associated to the x -coordinate. Therefore, our two dimensional Lagrangian-Eulerian scheme (7.1.25) takes the form of an unsplitting method.

Finally, we turn our attention to discuss performance of the extension of the Lagrangian-Eulerian scheme for systems of balance laws in one-space dimension for hyperbolic conservation laws in two-space dimensions, along with numerical experiments for nonlinear two-dimensional hyperbolic problems. The numerical results are compared with accurate approximate solutions or exact solutions whenever possible.

7.2 Numerical experiments for nonlinear hyperbolic law em 2D

Model Problem 7.2.1. Christov & Popov (JPC), Buckley-Leverett's problem with gravity [39].

In this example, we consider the flow model in two-phase immiscible incompressible fluid with gravity, for oil and water. This is the basic mathematical model for the reservoir water-flooding problem in oil recovery in engineering applications (see, e.g., [61]),

$$-\nabla \cdot [\mathbf{K}\lambda_{tot}(S_w)\nabla p] = q_{tot}, \quad (7.2.1)$$

$$\frac{\partial \phi S_w}{\partial t} + \frac{\partial(u_{tot}f(S_w))}{\partial x} + \frac{\partial(v_{tot}g(S_w))}{\partial y} = q_w, \quad (7.2.2)$$

where \mathbf{K} is the absolute permeability tensor, λ_{tot} is the total mobility, p is the thermodynamic pressure, ϕ is the porosity, $S_w \in [0, 1]$, S_w is the water saturation, and $\mathbf{u}_{tot} = (u_{tot}; v_{tot})$ is the total velocity (i.e., $\mathbf{u}_{tot} = u_w + u_o$). The pressure equation (7.2.1) as written is elliptic in the absence of compressibility. Because the total mobility depends of saturation, the pressure yields field changes as the displacement evolves, this is just a statement of Darcy's law combined with the conservation of mass. Once the pressure is computed from (7.2.1), the total velocity is given by Darcy's law: $u_{tot} = \mathbf{K}\lambda_{tot}(S_w)\nabla p$. The equation (7.2.2) is referred to as the saturation equation. Finally, in the absence of gravity and capillarity effects the x - and y -direction flux functions $f(S_w)$ and $g(S_w)$ are both just the fractional flow function of water, i.e., the non-convex Buckley-Leverett flux:

$$g(S_w) = f(S_w) = \frac{S_w^2}{S_w^2 + \frac{\mu_w}{\mu_o}(1 - C_g(1 - S_w)^2)}, \quad (7.2.3)$$

here μ_w and μ_o are the water and oil phase viscosities, respectively. For simplicity, in the simulations discussed here, we have chosen the following values of the parameters: \mathbf{K} is the 2 identity matrix, $\lambda_{tot}(S_w) = 1$, $\phi = 1$, $q_{tot} = q_w = 0$. Generally, the complete solution of the system (7.2.1) and (7.2.2) is obtained by the implicit method for the pressure equation (7.2.1) and the explicit method for the hyperbolic equation. Such approach is called an Implicit Pressure Explicit saturation (IMPES) sequential solver.

In this example, we consider the Buckley-Leverett problem with gravity proposed in [39, 124]. The equations are significantly more challenging when gravitational effects are included in the saturation equation, resulting in different (non-convex) flux functions in the x - and y -directions. In this case, the flux in the y -direction, $f(\cdot)$, is once again the Buckley-Leverett flux (flow). However, for the flux in the y -direction we have,

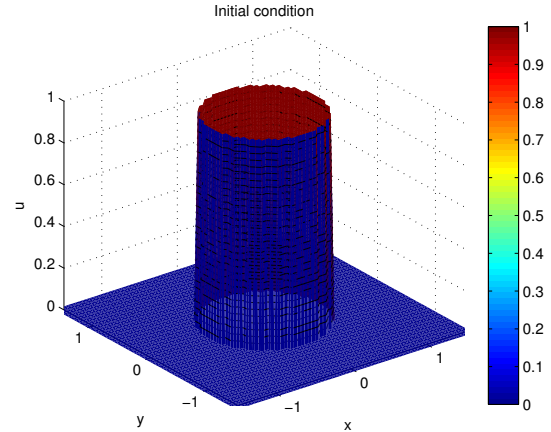
$$g(S_w) = f(S_w)(1 - C_g(1 - S_w)^2), \quad (7.2.4)$$

and we consider

$$\frac{\partial S_w}{\partial t} + \frac{\partial(f(S_w))}{\partial x} + \frac{\partial(g(S_w))}{\partial y} = 0, \quad (7.2.5)$$

with $(x, y, t) \in [-1.5, 1.5] \times [-1.5, 1.5] \times [0, 0.5]$, and initial condition,

$$u(x, y, 0) = \begin{cases} 1, & x^2 + y^2 < 0.5, \\ 0, & \text{otherwise.} \end{cases} \quad (7.2.6)$$



Finally, we notice that we impose the solid wall (slip) boundary condition $\mathbf{u}_{tot} \cdot \mathbf{n} = 0$ everywhere on the boundary $\partial\Omega$, where \mathbf{n} is the outward unit normal to $\partial\Omega$, upon the system (7.2.1) and (7.2.2). This means that there are no inflow boundaries and, hence, no boundary conditions on S_w . Here we have two situations we want to test our Eulerian-Lagrangian scheme: (1) a rudimentary test to address the issue of grid orientation effects (this anomalous phenomenon is observed when computational grid is rotated and substantially different numerical solutions are obtained for a similar problem) and (2) accommodation of no flow boundary condition, exact or approximate. Finally, we remark that we will compare our numerical solutions shown in Figure 7.2 and Figure 7.3 for the Buckley-Leverett's problem described above (7.2.1)-(7.2.6), along with accurate Buckley-Leverett's numerical solutions extracted from [39].

In Figure 7.2 and Figure 7.3 are shown the Buckley-Leverett's numerical solutions computed with the two-dimensional Lagrangian-Eulerian scheme LEH2D (7.1.25) with respect to the reservoir waterflooding problem with gravity described in (7.2.1)-(7.2.6). From top to bottom are shown of the left (resp. right) column a "3D-plot's view angle" (resp. contour curves) of numerical approximations of the water saturation. For comparison purposes, we are comparing our numerical solutions along with those extracted from [39]. Moreover, for a preliminary computational efficiency understanding, we also included the time elapsed into a mesh refinement study: 0.2990 secs (64×64 cells), 1.4259 secs (128×128 cells), 7.7959 secs (256×256 cells), 52.3522 secs (512×512 cells), 937.7651 secs (1024×1024 cells) and $3.6905e+03$ secs (2048×2048 cells).

Analogously, in Figures 7.4 and 7.5 are shown the Buckley-Leverett's numerical solutions computed with the two-dimensional Lagrangian-Eulerian scheme LEH2D2 (7.1.26). From top to bottom are shown of the left (resp. right) column a "3D-plot's view angle" (resp. contour curves) of numerical approximations of the water saturation and the simulation time along with 64×64 cells (top) and 2.4087 sec, 128×128 cells (middle) and 2.40 secs and 256×256 cells (bottom) 11.41 secs. Based in these experiments, we note that our both Lagrangian-Eulerian methods, LEH2D 7.1.25 and LEH2D2 7.1.26, to solve hyperbolic conservation laws in two dimensional variables are very efficient computationally and without spurious oscillations in regions with sharp fronts, no mesh orientation dependence and low numerical diffusion.

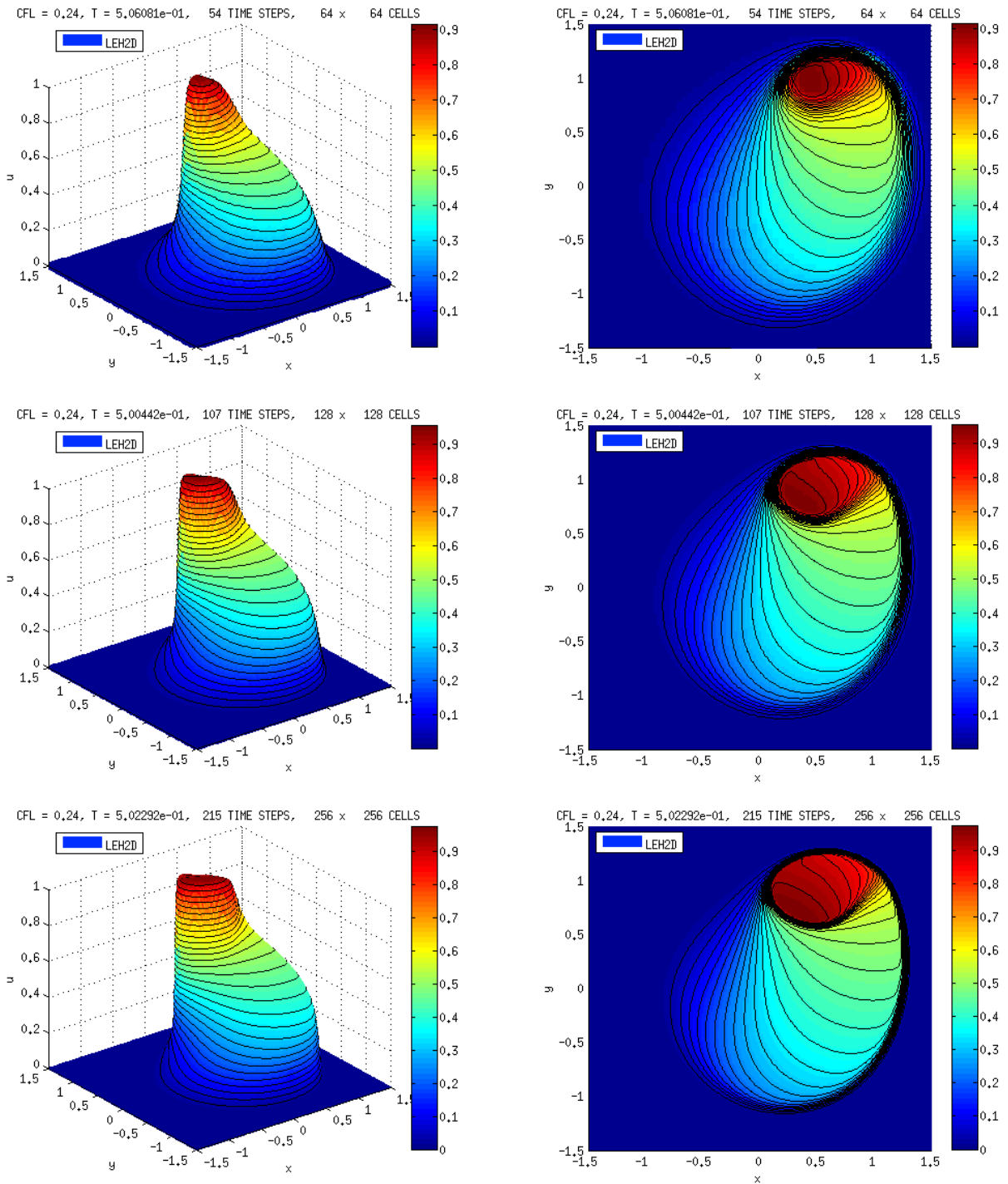


Figure 7.2: From top to bottom are shown the Buckley-Leverett's numerical solutions at $T = 0.5$ computed with the two-dimensional Lagrangian-Eulerian scheme LEH2D (7.1.25); "3D-plot's view angle" (left) and contour curves (right) with respect to the reservoir waterflooding problem with gravity described in (7.2.1)-(7.2.6).

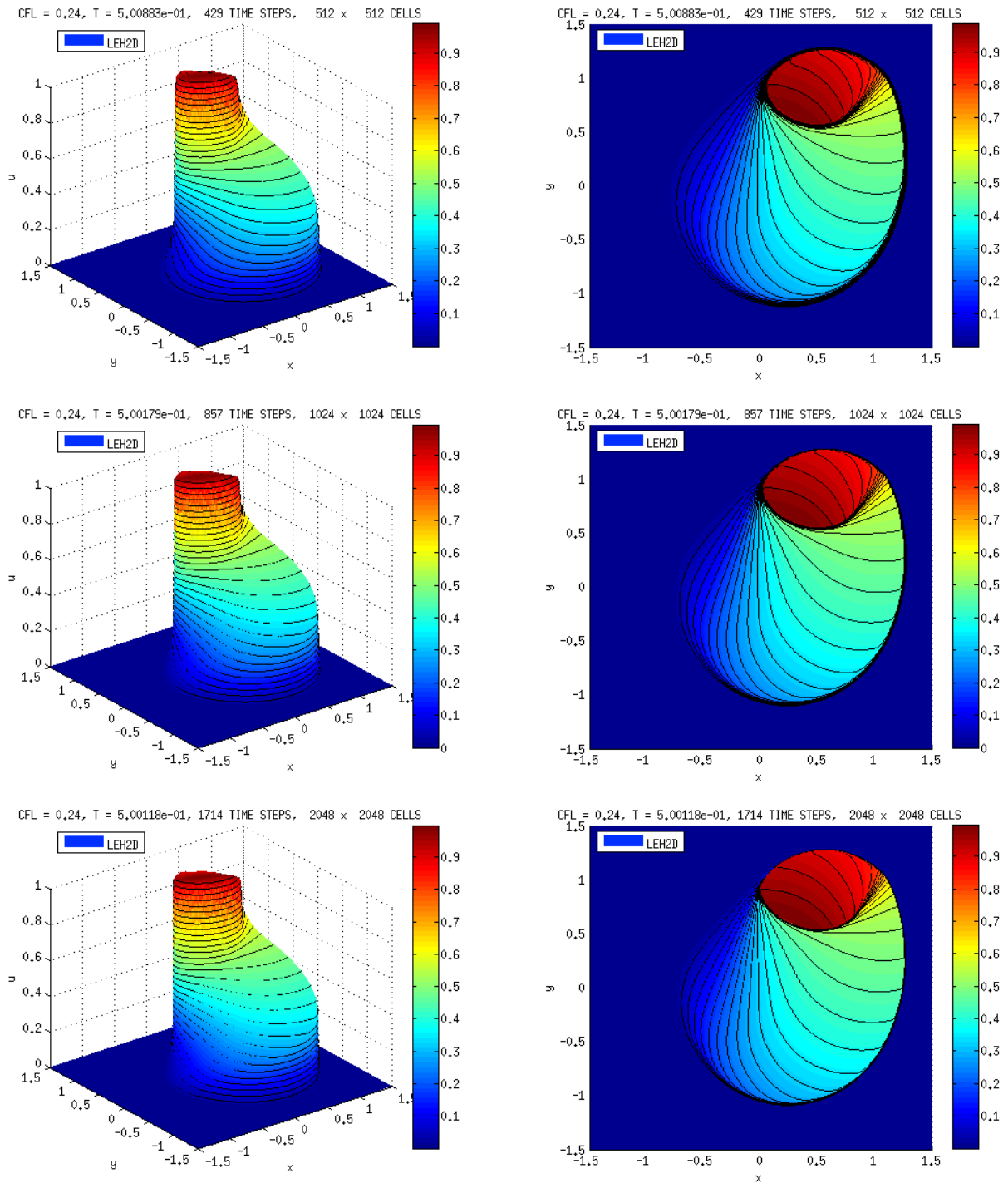


Figure 7.3: From top to bottom are shown the Buckley-Leverett's numerical solutions at $T = 0.5$ computed with the two-dimensional Lagrangian-Eulerian scheme LEH2D (7.1.25); "3D-plot's view angle" (left) and contour curves (right) with respect to the reservoir waterflooding problem with gravity described in (7.2.1)-(7.2.6).

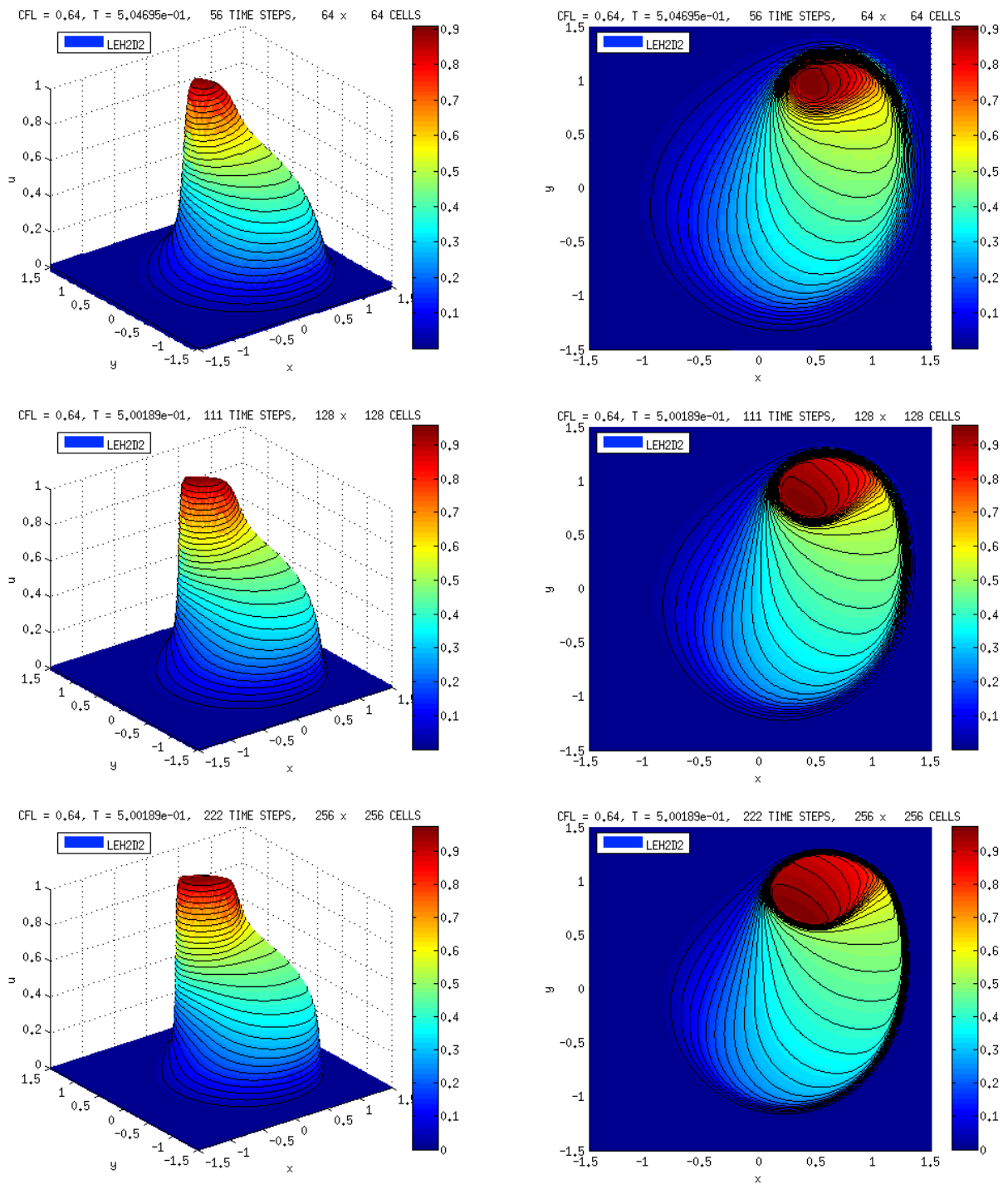


Figure 7.4: From top to bottom are shown the Buckley-Leverett's numerical solutions at $T = 0.5$ computed with the two-dimensional Lagrangian-Eulerian scheme LEH2D2 (7.1.26); “3D-plot's view angle” (left) and contour curves (right) with respect to the reservoir waterflooding problem with gravity described in (7.2.1)-(7.2.6).

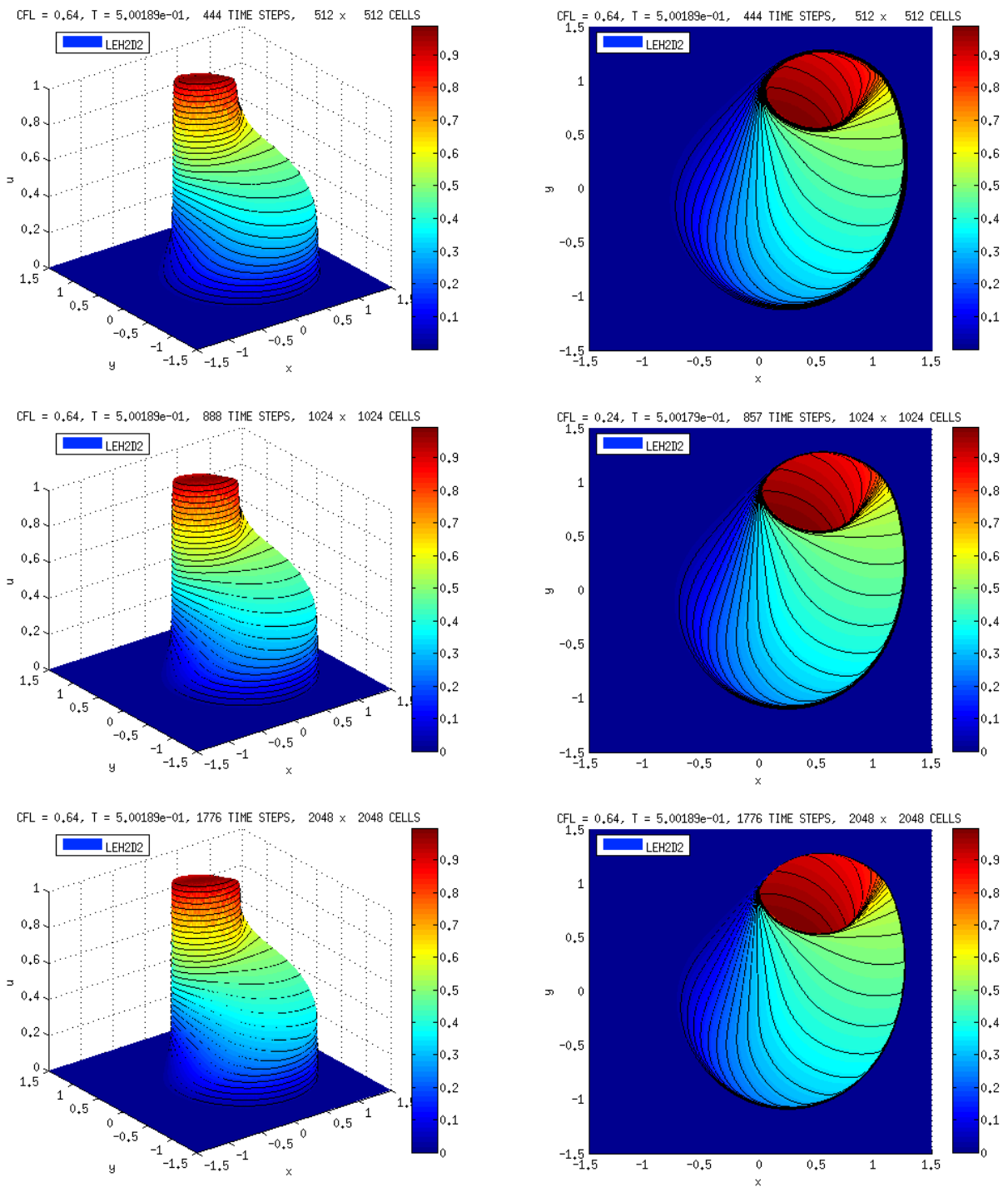


Figure 7.5: From top to bottom are shown the Buckley-Leverett's numerical solutions at $T = 0.5$ computed with the two-dimensional Lagrangian-Eulerian scheme LEH2D2 (7.1.26); “3D-plot's view angle” (left) and contour curves (right) with respect to the reservoir waterflooding problem with gravity described in (7.2.1)-(7.2.6).

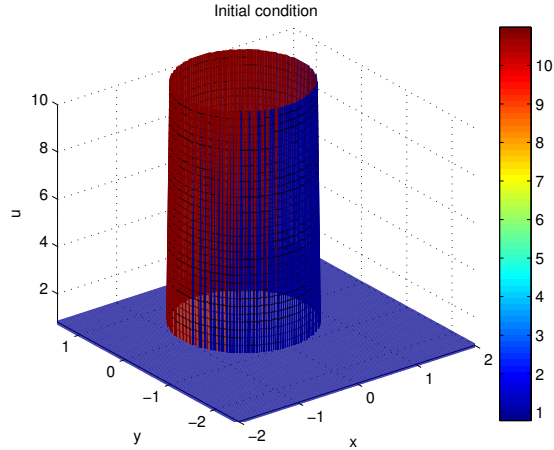
Model Problem 7.2.2. Kurganov, Petrova & Popov, (SIAM SISC), a nonlinear model with nonconvex flow function [98].

In order to address the robustness of the Lagrangian-Eulerian scheme (7.1.25), we consider problem proposed in [98] (see also [39]), whose solution features a composite wave. We numerically solve the following two-dimensional scalar hyperbolic conservation law with nonconvex fluxes (i.e., $f''(u)$ and $g''(u)$ change of sign) given by,

$$\frac{\partial u}{\partial t} + \frac{\partial(\sin(u))}{\partial x} + \frac{\partial(\cos(u))}{\partial y} = 0 \quad (7.2.7)$$

with $(x, y, t) \in [-2, 2] \times [-2.5, 1.5] \times [0, 1]$, and initial condition,

$$u(x, y, 0) = \begin{cases} 3.5\pi, & x^2 + y^2 < 1, \\ 0.25\pi, & \text{otherwise,} \end{cases} \quad (7.2.8)$$



in conjunction with natural (i.e., inflow) boundary condition on all of $\partial\Omega$. For this initial condition, the x -direction flux of (7.2.7) has three inflection points, and the y -direction flux has four. The solution to the Riemann problem is advanced from $T = 0$ to $T = 0.5$ and is shown in the Figure 7.6 and Figure 7.7.

In Figure 7.6 and in Figure 7.7, from top to bottom are shown the numerical solutions computed with the two-dimensional Lagrangian-Eulerian scheme LEH2D (7.1.25) with respect to the nonlinear model with nonconvex flow function described by the Riemann problem (7.2.7)-(7.2.8). From top to bottom are shown of the left (resp. right) column a “3D-plot’s view angle” (resp. contour curves) of numerical approximations. For comparison purposes, we are comparing our two-dimensional numerical approximations with approximations, which in turn were computed with a genuinely multidimensional, non-oscillatory reconstruction the Minimum-Angle Plane Reconstruction (MAPR) proposed in [39].

Our numerical solutions are comparable with the solutions obtained with the central-upwind schemes based on the MM1 proposed in [98] and in [39]. Indeed, we believe that our numerical solutions are better than those obtained with the central-upwind schemes based on the MM2, SB and WENO5 type-reconstructions since such procedure might fail to accurately resolve composite wave structures; see [98] to more details. As before, we also included the time elapsed into a mesh refinement study for a preliminary computational efficiency: 2.3586 segs (64×64 cells), 3.8706 segs (128×128 cells), 12.7589 segs (256×256 cells), 73.2378 segs (512×512 cells), 513.3377 segs (1024×1024 cells) and $3.8385e+003$ segs (2048×2048 cells).

Analogously, in Figures 7.6 and 7.9 are shown the numerical solutions computed with the two-dimensional Lagrangian-Eulerian scheme (7.1.26). From top to bottom are shown on the left (resp. right) column a “3D-plot’s view angle” (resp. contour curves) of numerical approximations with 64×64 cells (top) 0.33 sec, 128×128 cells (middle) 1.92 sec and 256×256 cells

(bottom) in 9.94 sec 512×512 cells (top) 48.61 sec, 1024×1024 cells (middle) 332.81, and 2048×2048 cells (bottom) 2712.30 sec.

Again, we highlight no dependence of mesh orientation, particularly in this example where the flux functions are trigonometric functions with high frequencies and a lot roots. However our numerical method obtained approximations with good resolution despite to be a method of order one. We also mention that in these approximations we observed no spurious oscillations, low diffusion in both schemes and very efficient computationally.

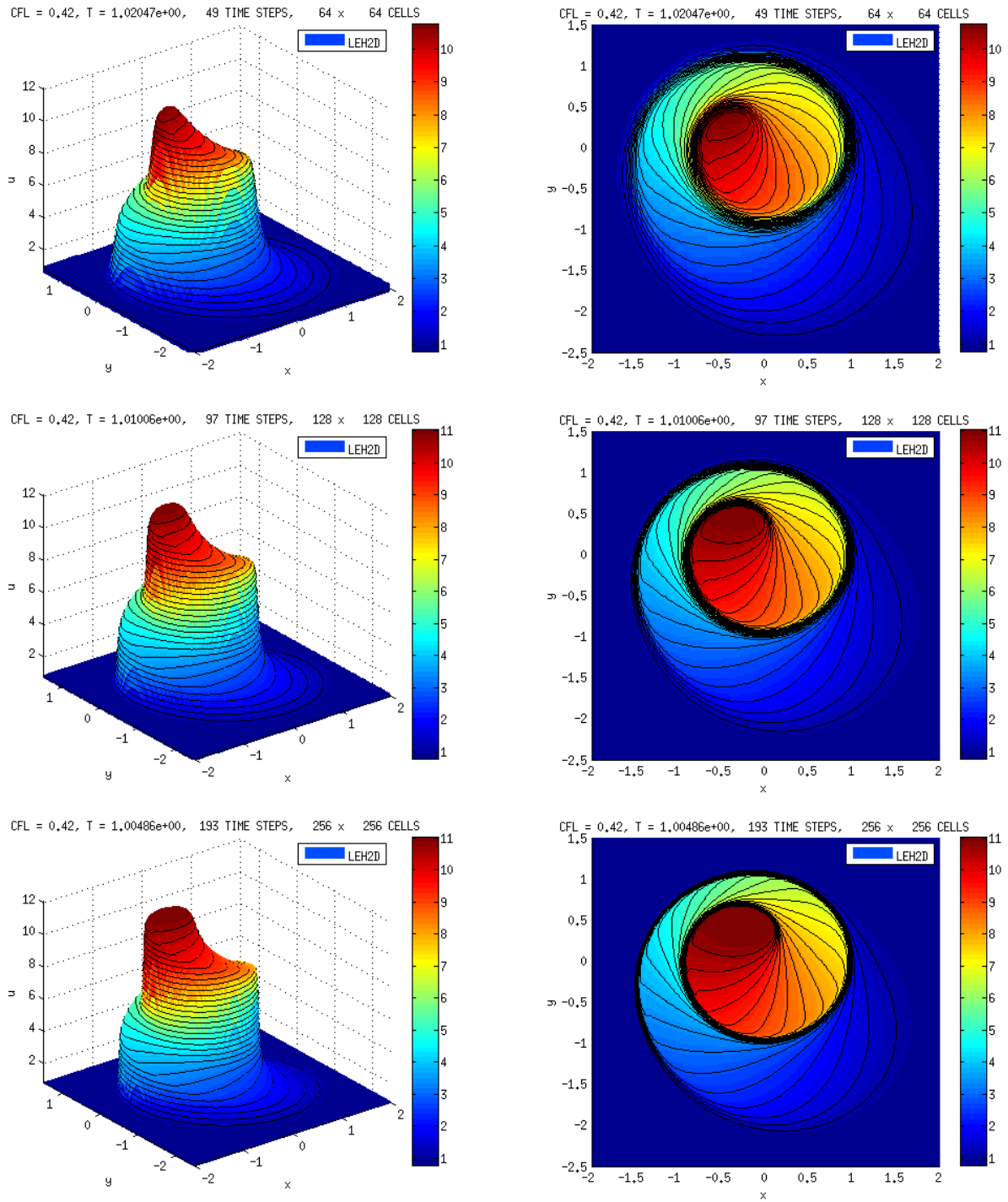


Figure 7.6: From top to bottom are shown the numerical solutions at $T = 1.0$ computed with the two-dimensional Lagrangian-Eulerian scheme LEH2D (7.1.25) with respect to the nonlinear model with nonconvex flow function described by the Riemann problem (7.2.7)-(7.2.8).

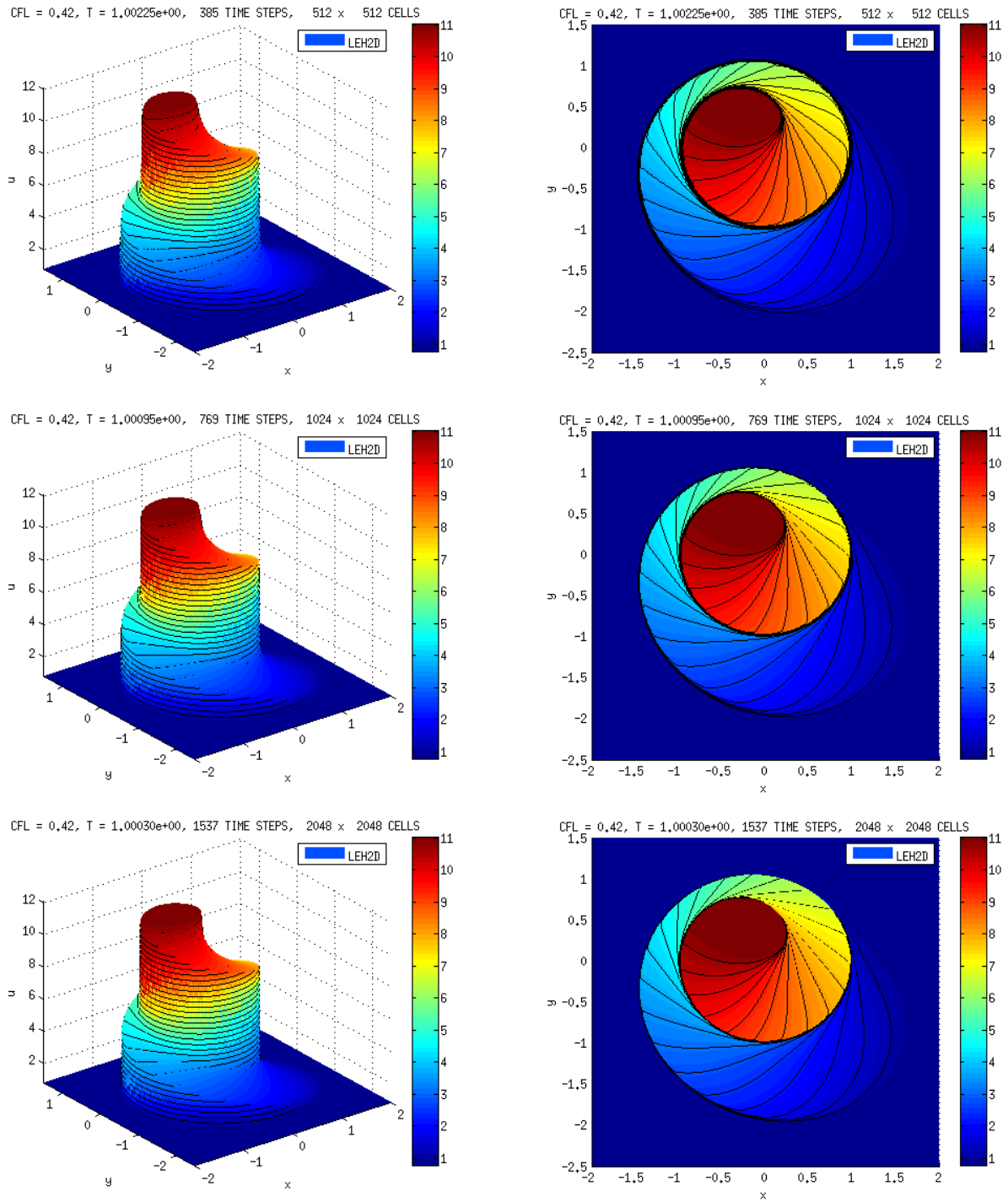


Figure 7.7: From top to bottom are shown the numerical solutions at $T = 1.0$ computed with the two-dimensional Lagrangian-Eulerian scheme LEH2D (7.1.25) with respect to the nonlinear model with nonconvex flow function described by the Riemann problem (7.2.7)-(7.2.8).

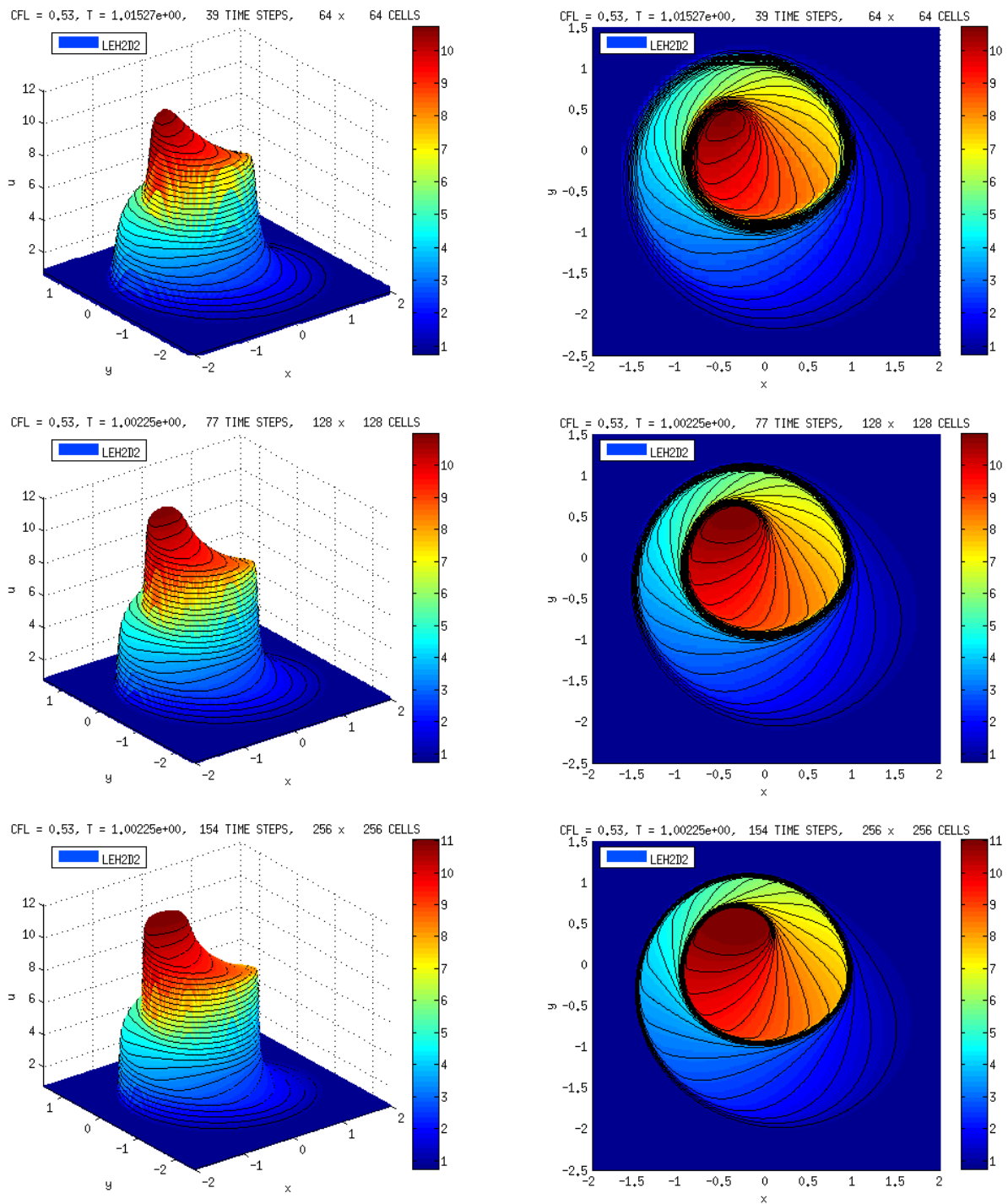


Figure 7.8: From top to bottom are shown the numerical solutions at $T = 1.0$ computed with the two-dimensional Lagrangian-Eulerian scheme LEH2D2 (7.1.26) with respect to the nonlinear model with nonconvex flow function described by the Riemann problem (7.2.7)-(7.2.8).

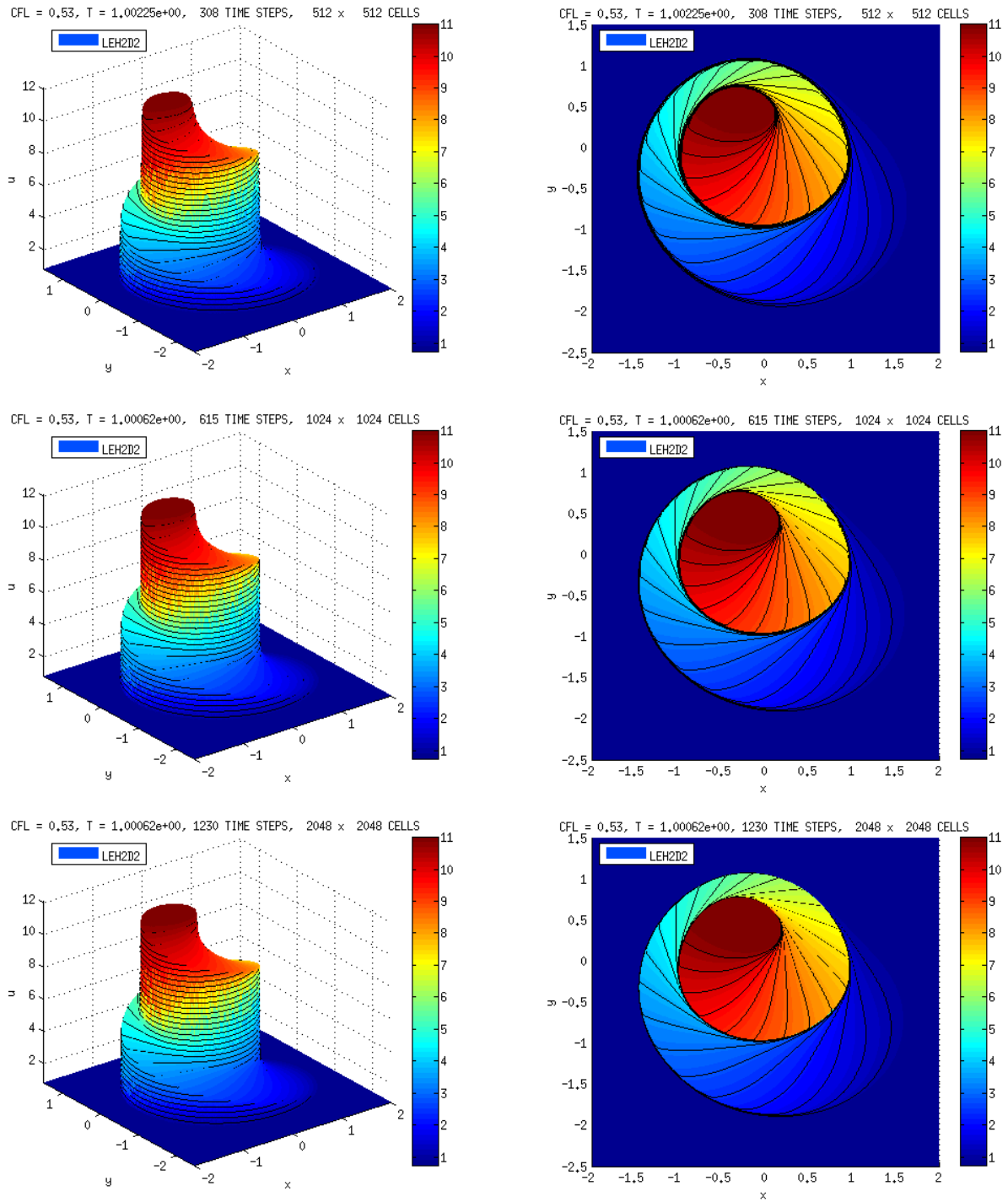


Figure 7.9: From top to bottom are shown the numerical solutions at $T = 1.0$ computed with the two-dimensional Lagrangian-Eulerian scheme LEH2D2 (7.1.26) with respect to the nonlinear model with nonconvex flow function described by the Riemann problem (7.2.7)-(7.2.8).

Model Problem 7.2.3. A like quarter-five spot problem, a two-phase immiscible incompressible Buckley-Leverett problem.

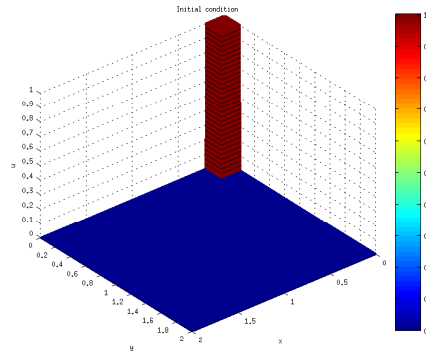
We now turn to the discussion of a set of numerical simulations performed in a like five-spot pattern. In case of a five-spot flood problem, discretized by our two-dimensional Lagrangian-Eulerian scheme LEH2D (7.1.25) with respect to a diagonal grid (from Figure 7.10 to Figure 7.13; see also the right picture of equation 7.2.10), the injection takes place at one corner and production at the diametrically opposite corner; no flow is allowed across the entirety of the boundary.

In our simulations, we consider a similar model problem as (7.2.1)-(7.2.2), with Buckley-Leverett fractional flow function of water along with the following parameters values $\mathbf{u}_{tot} = (u_{tot}; v_{tot}) = (1, 1)$, and different values for the viscosity relation μ_w/μ_o : 0.5 (Figure 7.11), 0.1 (Figure 7.12) and 0.05 (Figure 7.13). The specific problem is as follows,

$$\frac{\partial S_w}{\partial t} + \frac{\partial(f(S_w))}{\partial x} + \frac{\partial(g(S_w))}{\partial y} = 0, \quad (x, y, t) \in [0, 2] \times [0, 2] \times [0, 1] \quad (7.2.9)$$

with initial condition,

$$u(x, y, 0) = \begin{cases} 1, & x < 0.2, \quad y < 0.2, \\ 0, & \text{otherwise} \end{cases} \quad (7.2.10)$$



in conjunction with exact boundary condition on the inflow portions of $\partial\Omega$. For this initial condition, we have one rarefaction and one shock.

Mathematically, the configuration of the moving wave front in the $(x = y)$ -direction corresponds to a shock wave followed by a rarefaction wave (see pictures in Figure 7.10). Indeed, we highlight that such composite Buckley-Leverett solution is respect to the oblique projection over the $(x = y)$ -direction: this projection is a solution of the one scalar hyperbolic problem with a vector flow sum in x -direction as well as in y -direction. In Figure 7.10 are shown a numerical refinement study in order to select a grid mesh resolution to a further numerical simulation study for the quarter-five spot problem related to model (7.2.1)-(7.2.2).

In Figure 7.10 on the left (resp. right) columns are shown 3D-view and projection with respect $x = y$ -plane, respectively. The mesh grids and time computation are: 64×64 cells (0.3347 sec), 128×128 (1.6346 sec), cells and 256×256 cells (8.51 sec), 512×512 cells (56.0134 sec), 1024×1024 (56.0134 sec) and 2048×2048 (2684.8 sec).

The study reported in Figure 7.11 are shown, from top to bottom, the numerical solutions computed with the two-dimensional Lagrangian-Eulerian scheme LEH2D (7.1.25) with respect to the quarter-five spot problem for the Riemann problem (7.2.9)-(7.2.10) with viscosity ratio $\mu_w/\mu_o = 0.5$ and simulation times $T = 0.1$ (top left), $T = 0.3$ (middle left) and $T = 0.6$ (Bottom left). We will use the mesh grid 256×256 with different values for the viscosity relation μ_w/μ_o , described in Figure 7.11 to Figure 7.13. Based in the approximations and on the computational

times we observe that the Lagrangian-Eulerian scheme shown be very efficient computationally and without spurious oscillations in regions with sharp fronts, no mesh orientation dependence and low numerical diffusion.

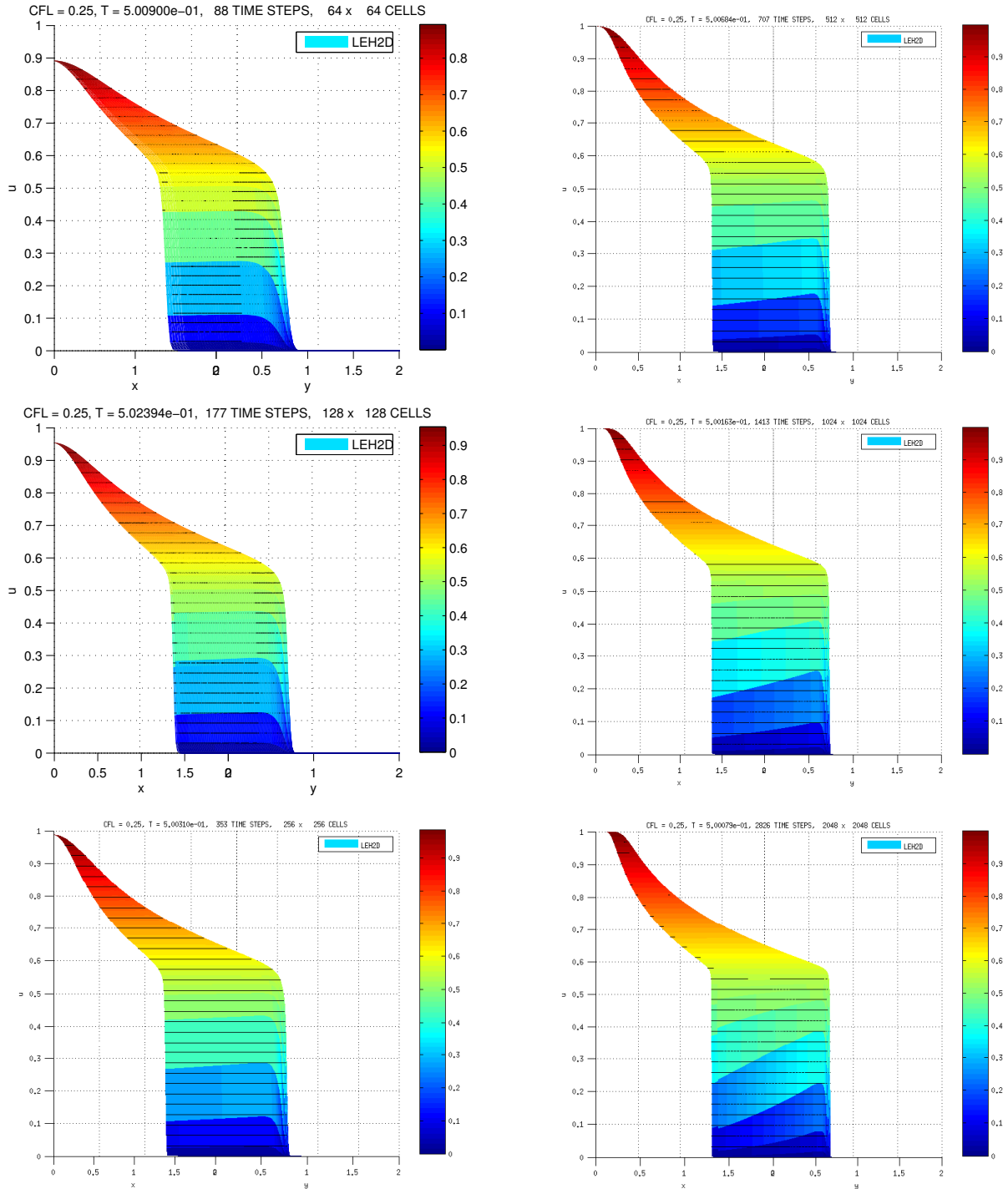


Figure 7.10: From top to bottom are shown a mesh refinement study of scheme LEH2D (7.1.25) for the oblique projection over the $(x = y)$ -direction at time $T = 0.5$ for the quarter-five spot problem, with viscosity ratio $\mu_w/\mu_o = 0.5$.

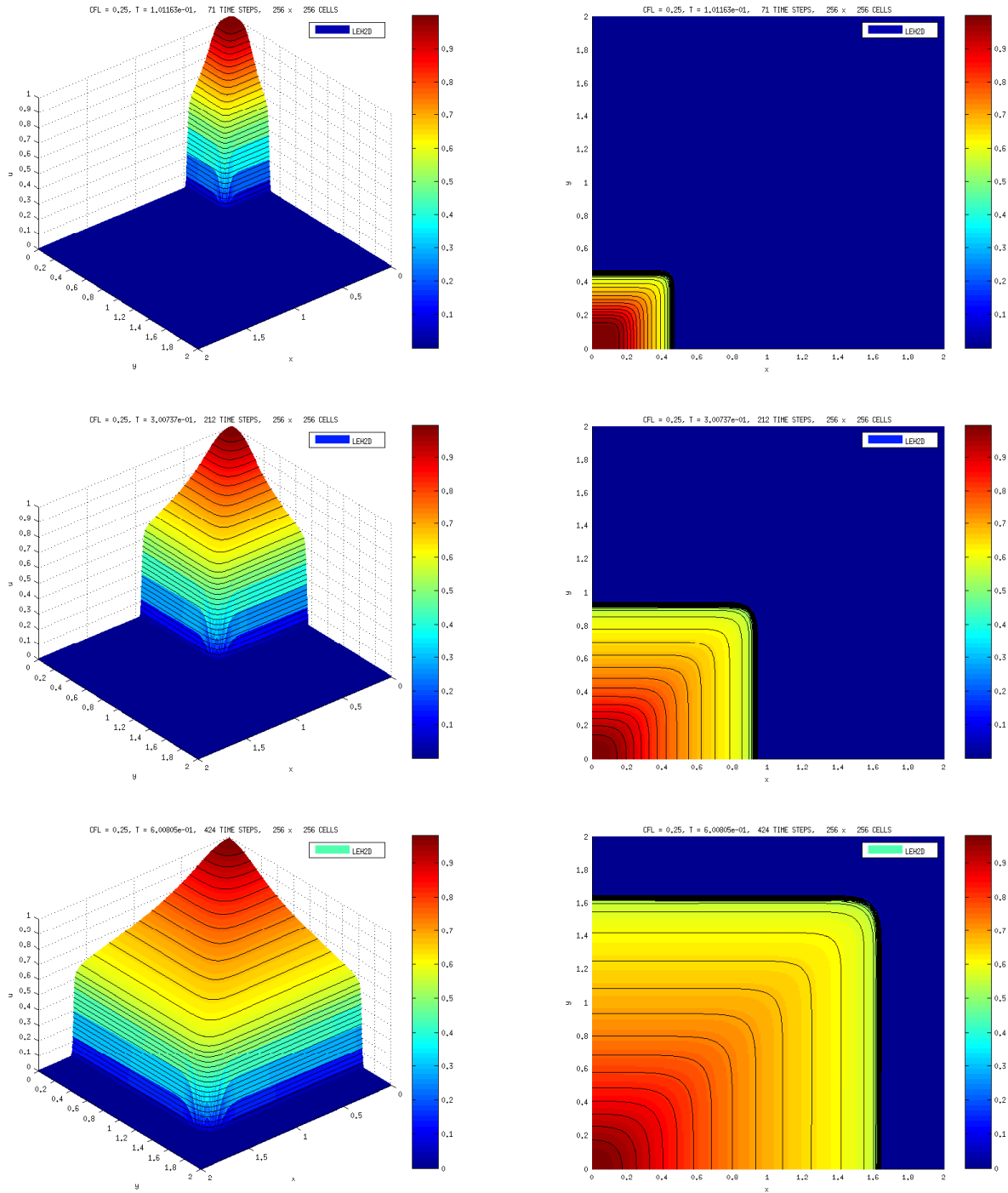


Figure 7.11: From top to bottom are shown the numerical solutions for simulation times $T = 0.1$ (top left), $T = 0.3$ (middle left) and $T = 0.6$ (Bottom left). computed with the two-dimensional Lagrangian-Eulerian scheme LEH2D (7.1.25) with respect to the quarter-five spot problem for Riemann problem (7.2.9)-(7.2.10) with viscosity ratio $\mu_w/\mu_o = 0.5$.

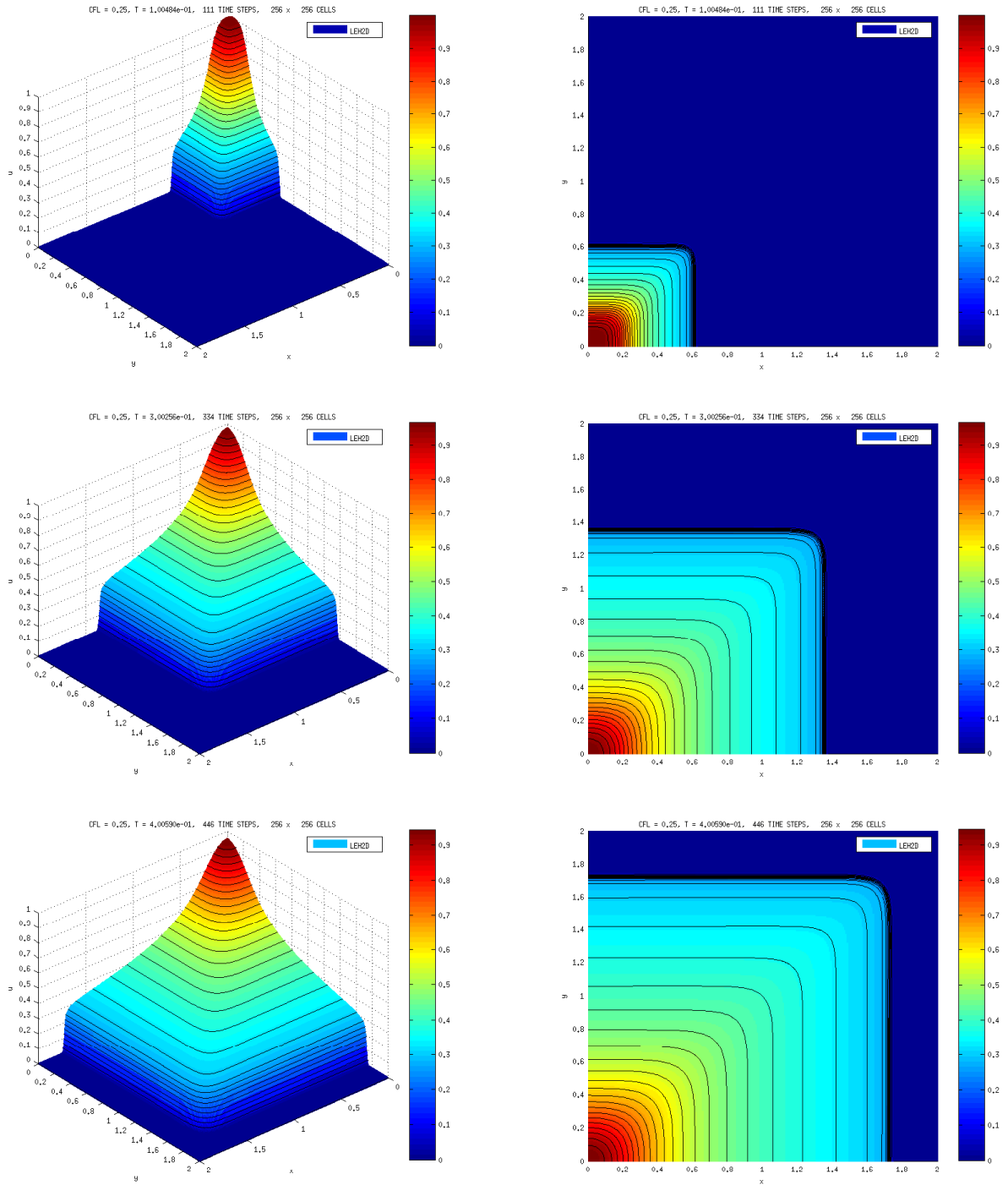


Figure 7.12: From top to bottom are shown the numerical solutions for simulation times $T = 0.1$ (top left), $T = 0.3$ (middle left) and $T = 0.4$ (Bottom left). computed with the two-dimensional Lagrangian-Eulerian scheme LEH2D (7.1.25) with respect to the quarter-five spot problem for Riemann problem (7.2.9)-(7.2.10) with viscosity ratio $\mu_w/\mu_o = 0.1$.

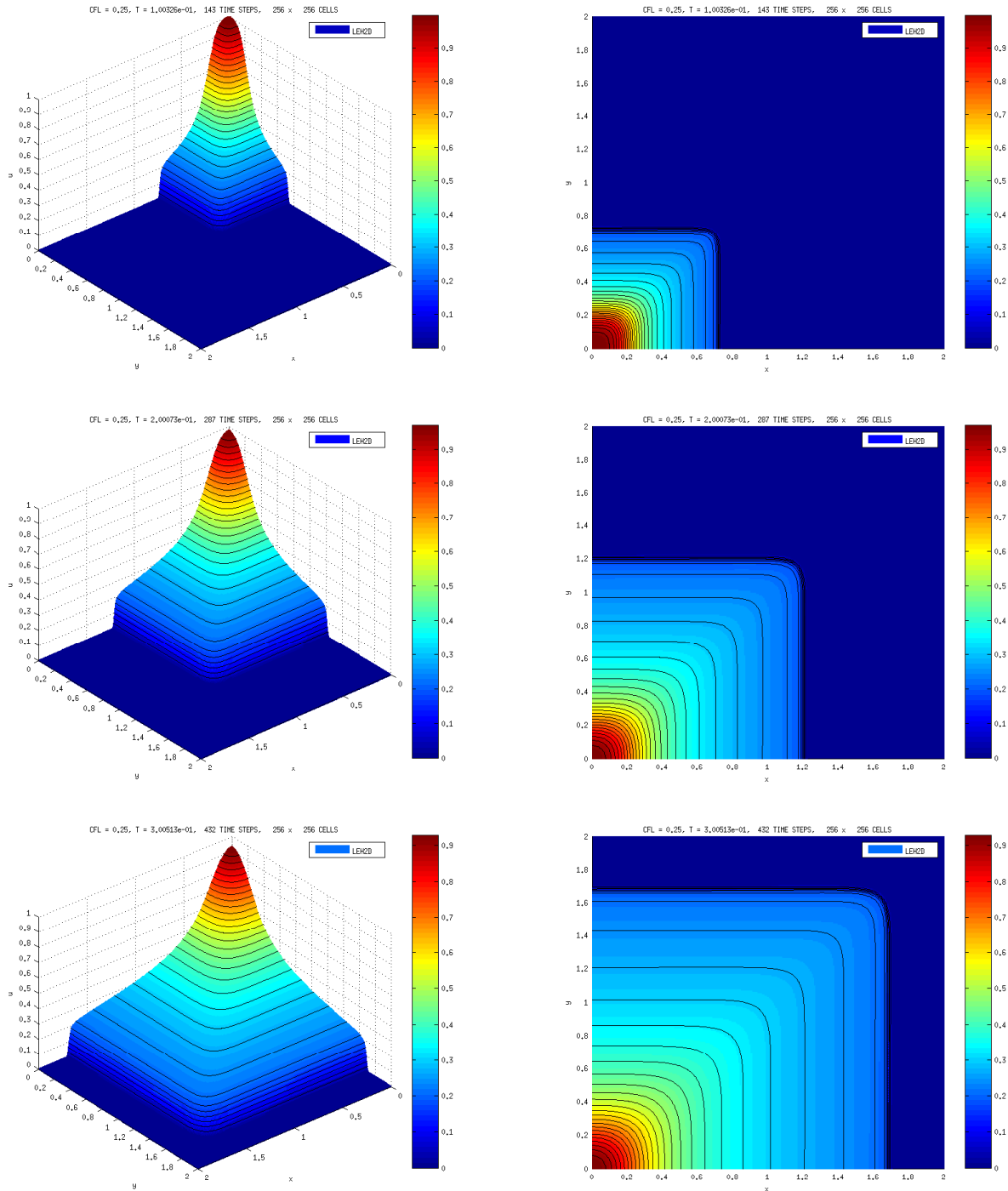


Figure 7.13: From top to bottom are shown the numerical solutions for simulation times $T = 0.1$ (top left), $T = 0.2$ (middle left) and $T = 0.3$ (Bottom left). computed with the two-dimensional Lagrangian-Eulerian scheme LEH2D (7.1.25) with respect to the quarter-five spot problem for Riemann problem (7.2.9)-(7.2.10) with viscosity ratio $\mu_w/\mu_o = 0.05$.

Model Problem 7.2.4. A like quarter-five spot problem, a two-phase immiscible incompressible Buckley-Leverett problem. Validation with scalar projection over xy -plane and x -plane.

In this problem, we consider again the hyperbolic equation in two spatial dimensions,

$$\frac{\partial u}{\partial t} + \frac{\partial(f(S_w))}{\partial x} + \frac{\partial(g(S_w))}{\partial y} = 0, \quad (7.2.11)$$

where $f(S_w) = g(S_w)$ is the Buckley-Leverett fractional flow function of water along with parameters of above problem and with a viscosity ratio of $\mu_w/\mu_o = 0.5$. To make the validation, we will compare numerical approximate solution of r -scalar hyperbolic problems in θ -direction. For this, we will consider the following non-linear transformation: $x = r \cos(\theta)$ and $y = r \sin(\theta)$, with $0 \leq r \leq 2\sqrt{2}$ and $0 \leq \theta \leq \pi/2$. With this, $r^2 = x^2 + y^2$ and $\tan(\theta) = x/y$, then

$$\frac{\partial f(u)}{\partial x} = \frac{\partial f}{\partial u} \frac{\partial u}{\partial r} \frac{\partial r}{\partial x} + \frac{\partial f}{\partial u} \frac{\partial u}{\partial \theta} \frac{\partial \theta}{\partial x} \quad (7.2.12)$$

and

$$\frac{\partial f(u)}{\partial y} = \frac{\partial f}{\partial u} \frac{\partial u}{\partial r} \frac{\partial r}{\partial y} + \frac{\partial f}{\partial u} \frac{\partial u}{\partial \theta} \frac{\partial \theta}{\partial y}. \quad (7.2.13)$$

And note that,

$$\frac{\partial r}{\partial x} = \frac{x}{r} = \frac{r \cos(\theta)}{r} = \cos(\theta), \quad \frac{\partial r}{\partial y} = \frac{y}{r} = \frac{r \sin(\theta)}{r} = \sin(\theta) \quad (7.2.14)$$

$$\frac{\partial \theta}{\partial x} = -\frac{y}{r^2} = -\frac{r \sin(\theta)}{r^2} = -\frac{\sin(\theta)}{r}, \quad \frac{\partial \theta}{\partial y} = \frac{x}{r^2} = \frac{r \cos(\theta)}{r^2} = \frac{\cos(\theta)}{r},$$

with this, and with substitution in (7.2.12) and (7.2.13), give

$$\frac{\partial f(u)}{\partial x} = \frac{\partial f}{\partial u} \frac{\partial u}{\partial r} \cos(\theta) - \frac{\partial f}{\partial u} \frac{\partial u}{\partial \theta} \frac{\sin(\theta)}{r} \quad (7.2.15)$$

and

$$\frac{\partial f(u)}{\partial y} = \frac{\partial f}{\partial u} \frac{\partial u}{\partial r} \sin(\theta) + \frac{\partial f}{\partial u} \frac{\partial u}{\partial \theta} \frac{\cos(\theta)}{r}. \quad (7.2.16)$$

Thus,

$$\begin{aligned} \frac{\partial(f(u))}{\partial x} + \frac{\partial(f(u))}{\partial y} &= \frac{\partial f}{\partial u} \frac{\partial u}{\partial r} \cos(\theta) - \frac{\partial f}{\partial u} \frac{\partial u}{\partial \theta} \frac{\sin(\theta)}{r} \\ &\quad + \frac{\partial f}{\partial u} \frac{\partial u}{\partial r} \sin(\theta) + \frac{\partial f}{\partial u} \frac{\partial u}{\partial \theta} \frac{\cos(\theta)}{r}, \end{aligned} \quad (7.2.17)$$

then,

$$\frac{\partial(f(u))}{\partial x} + \frac{\partial(f(u))}{\partial y} = \frac{\partial f}{\partial r} (\cos(\theta) + \sin(\theta)) + \frac{\partial f}{\partial \theta} \left(\frac{\cos(\theta)}{r} - \frac{\sin(\theta)}{r} \right), \quad (7.2.18)$$

therefore, if $\theta = \pi/4$ then $\cos(\pi/4) = \sin(\pi/4) = \sqrt{2}/2$ and with this,

$$\frac{\partial f(u)}{\partial x} + \frac{\partial g(u)}{\partial y} = 2 \frac{\sqrt{2}}{2} \frac{\partial f(u)}{\partial r} = \sqrt{2} \frac{\partial f(u)}{\partial r}. \quad (7.2.19)$$

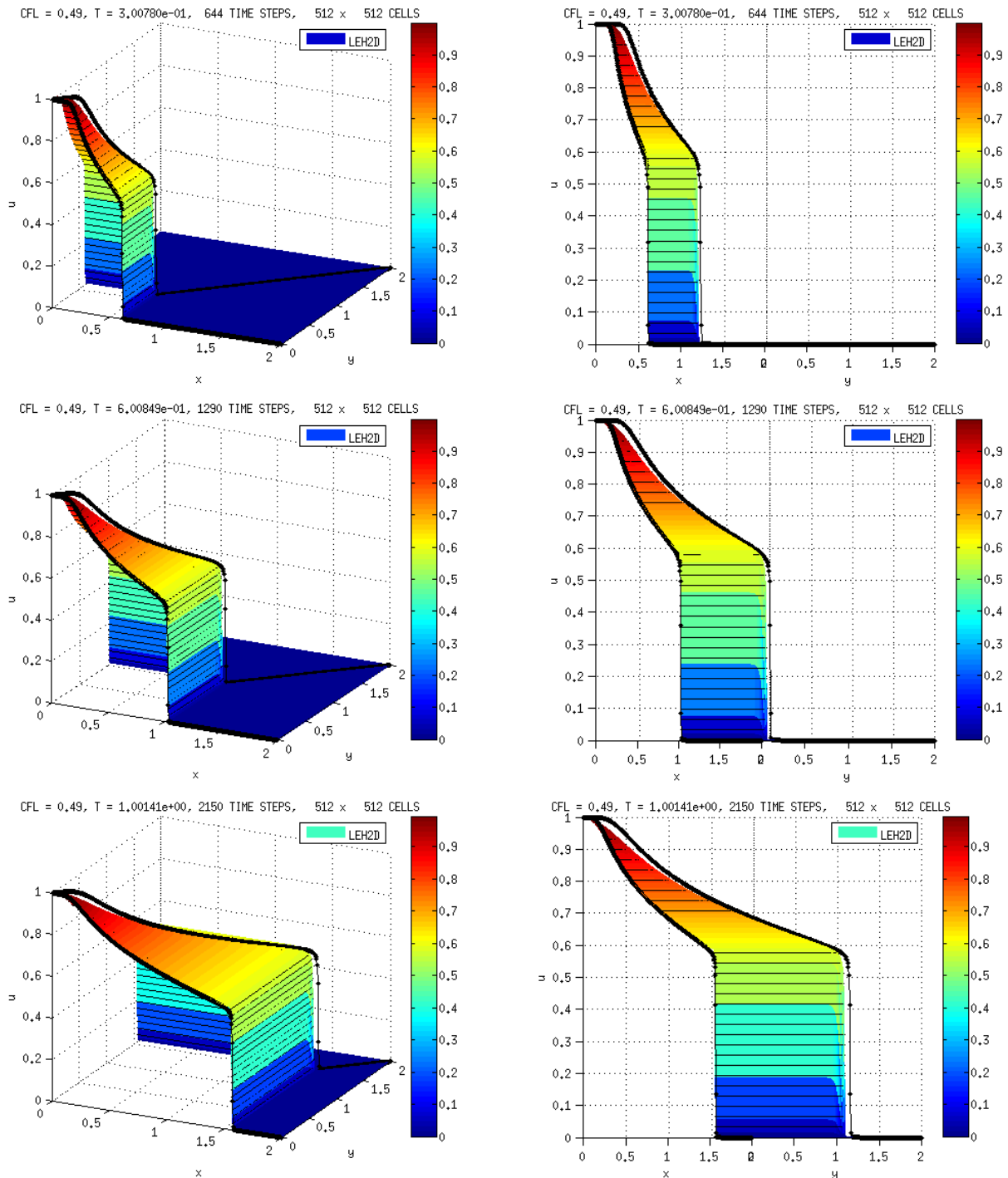


Figure 7.14: Plot of the solution with Lagrangian-Eulerian scheme LEH2D 7.1.25 to the Riemann problem (7.2.9) and (7.2.10) with relation of water viscosity $\frac{\mu_w}{\mu_o} = 0.5$; Approximations by the saturation S_w at different simulation times: at $T = 0.1$ (top), at $T = 0.2$ (middle) and at $T = 0.3$ (Bottom left).

And finally, we get the r -scalar hyperbolic conservation law in θ -direction, with $\theta = \pi/4$, in function of r ,

$$\frac{\partial u}{\partial t} + \sqrt{2} \frac{\partial f(u)}{\partial r} = 0. \quad (7.2.20)$$

Numerical solutions computed with the two-dimensional Lagrangian-Eulerian scheme LEH2D (7.1.25) with 512 cells, respect to the quarter-five spot problem, for the Riemann problem (7.2.9)-(7.2.10) are shown in Figure 7.14. In this example we use a viscosity ratio of $\mu_w/\mu_o = 0.5$ and simulation times of $T = 0.3$ (left), $T = 0.6$ (middle) and $T = 1$ (right). In top figures are shown numerical approximations for “3D”-solution and in bottom figures are shown numerical approximations in a “3D-plot’s view angle”.

In Figure 7.15 are shown the numerical solutions computed with the two-dimensional Lagrangian-Eulerian scheme LEH2D (7.1.25) with respect to the quarter-five spot problem for the Riemann problem (7.2.9)-(7.2.10) with a viscosity ratio of $\mu_w/\mu_o = 0.5$ and simulation times of $T = 1$ with 128 cells (top left), 256 cells (middle) and 512 cells (Bottom). In Figure 7.16 are shown numerical approximations with 512 cells (top left), 1024 cells (middle) and 2048 cells (Bottom). In Figures 7.15 and 7.16 are shown on the left (resp. right) column a “3D-plot”-numerical approximation of the problem (7.2.11), the numerical approximation of the x -scalar problem $\frac{\partial u}{\partial t} + \frac{\partial(f(u))}{\partial x} = 0$ and the numerical approximation of the r -scalar problem (7.2.20) and respectively its “3D-plot’s view angle” on the right. These approximations shown as the “3D”- numerical approximation converges to scalar numerical approximation in x -direction and θ -direction in time simulation $T = 1$.

In Figure 7.17 are shown a refinement of the numerical solution from the problem (7.2.11), where the solution is projected over the plane $y = 0$. Based in approximations quality and on the computational times, we observe that the Lagrangian-Eulerian scheme shows be very efficient computationally, without spurious oscillations in regions with sharp fronts, it don’t has mesh orientation dependence and low numerical diffusion. Yet due to discrepancy in the simulations when they are compared the projection of the solution in two dimension over the plane $y = 0$, with the scalar solution of the problem in x direction (see Figure 7.17), in unrefined mesh, we can not to declare that the Lagrangian_Eulerian scheme 2D is a conservative method.

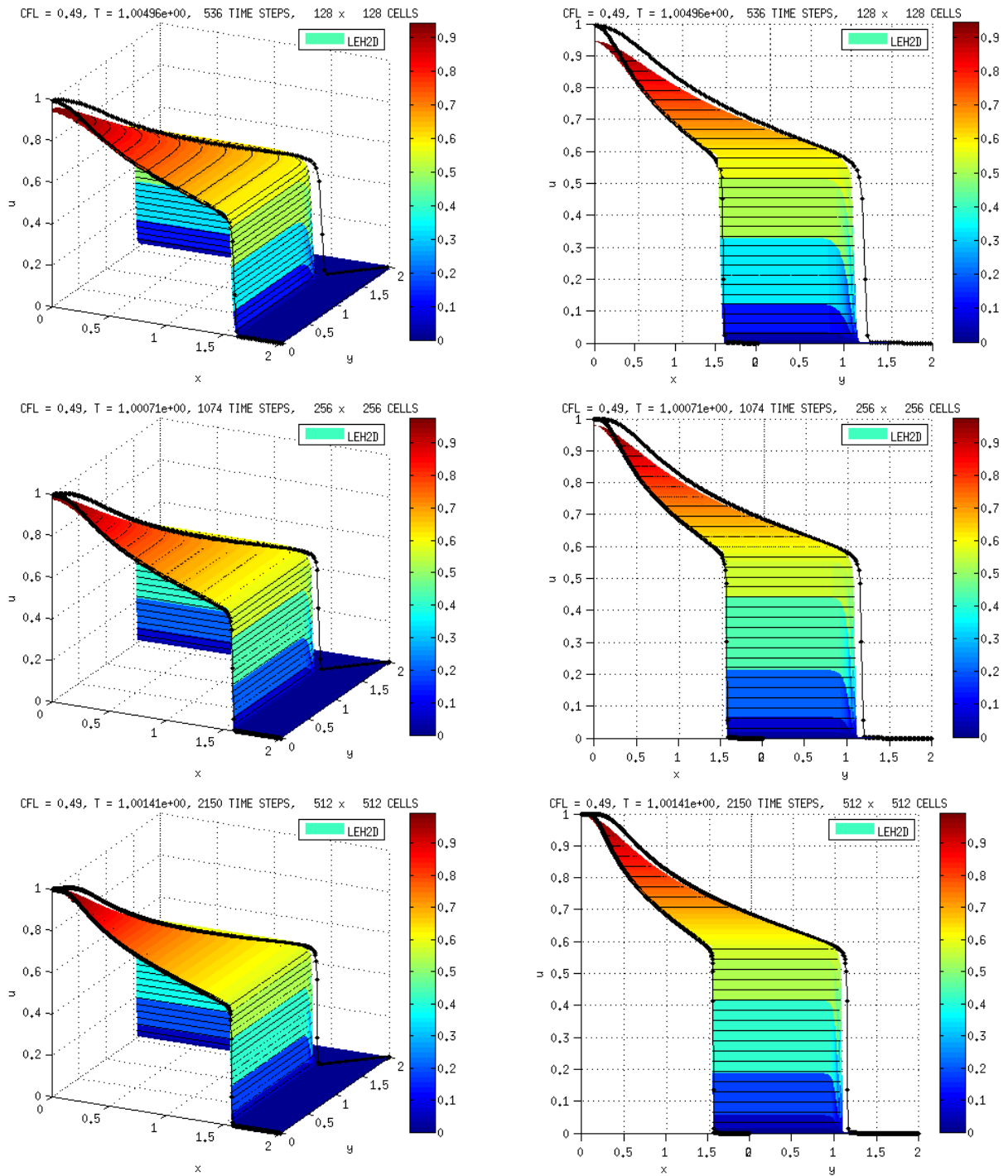


Figure 7.15: Numerical solutions computed with the two-dimensional Lagrangian-Eulerian scheme LEH2D (7.1.25) with respect to the quarter-five spot problem for Riemann problem (7.2.9)-(7.2.10) with viscosity ratio $\mu_w/\mu_o = 0.5$ for simulation time $T = 1$.

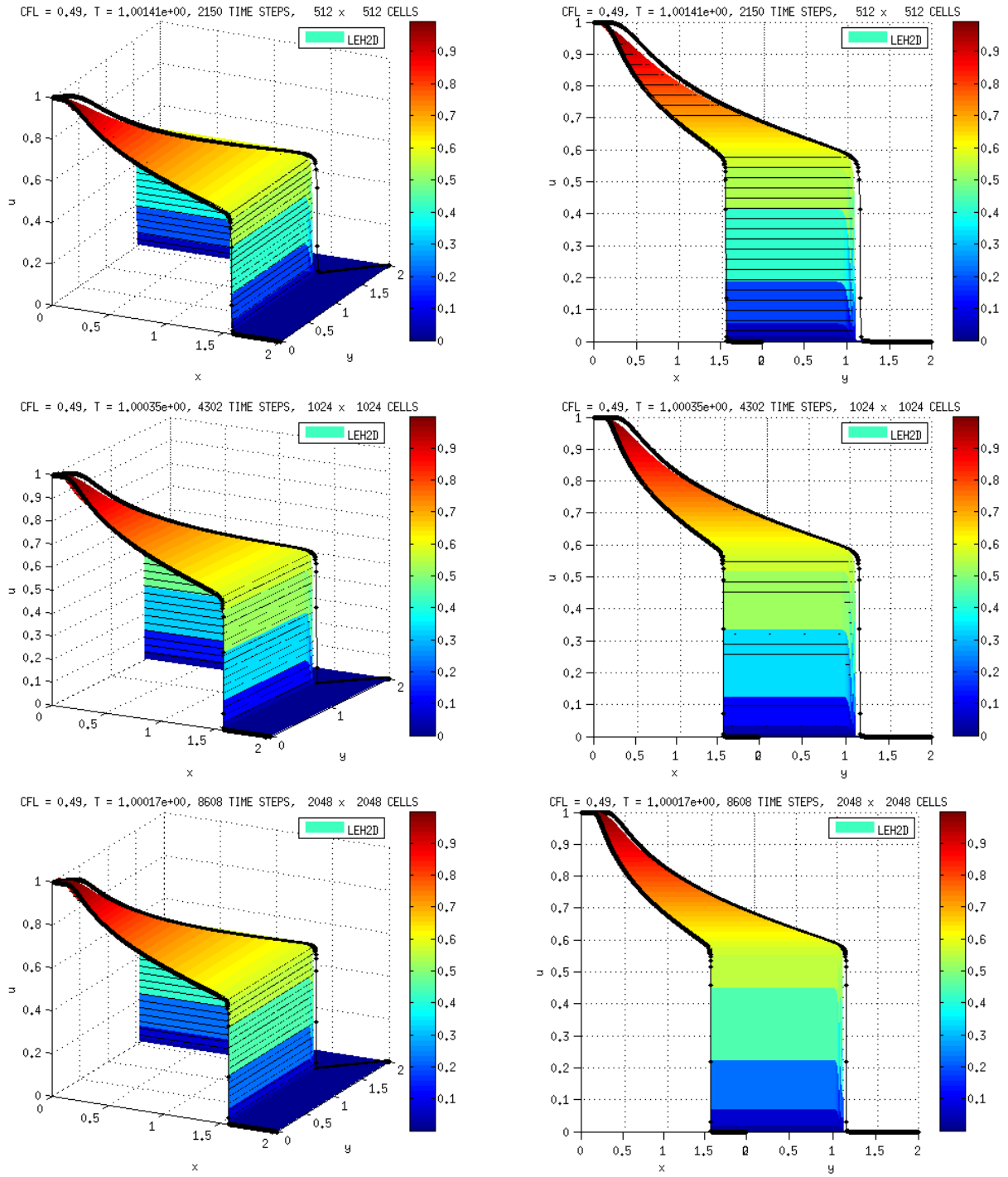


Figure 7.16: Numerical solutions computed with the two-dimensional Lagrangian-Eulerian scheme LEH2D (7.1.25) with respect to the quarter-five spot problem for Riemann problem (7.2.9)-(7.2.10) with viscosity ratio $\mu_w/\mu_o = 0.5$ for simulation times $T = 1$.

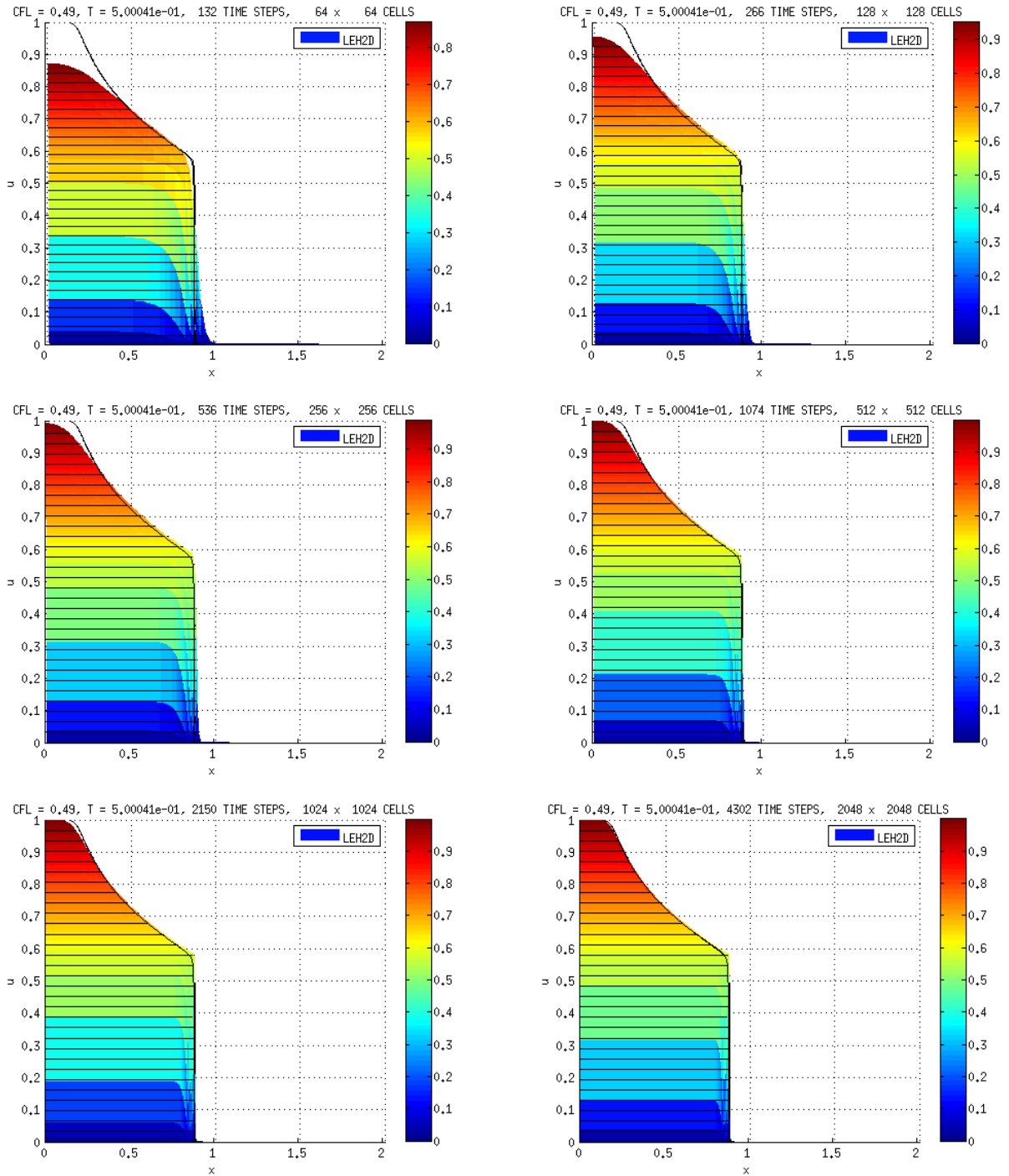


Figure 7.17: Plot of the solution with Lagrangian-Eulerian scheme LEH2D 7.1.25 to the Riemann problem (7.2.9) and (7.2.10) with relation of water viscosity $\frac{\mu_w}{\mu_o} = 0.5$; Approximations by the saturation S_w at time $T = 0.5$ in different mesh size, from 64 cell to 2048 cells.

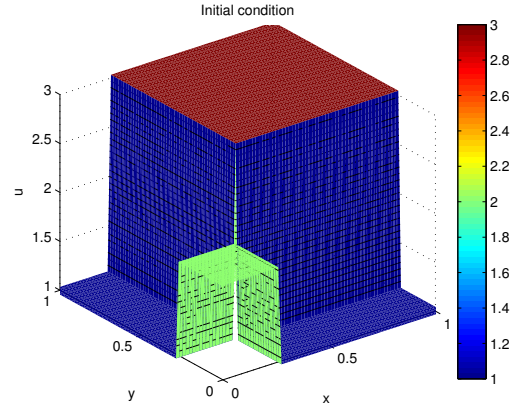
Model Problem 7.2.5. Christov & Popov (JPC), two-dimensional Burgers’s equation [39].

In order to add one more test problem, we will use the two-dimensional Lagrangian-Eulerian scheme (7.1.25) for the two-dimensional Burgers’s equation proposed in [39] (see also [39, 114]). We consider the following two-dimensional initial value problem for associated to the inviscid Burgers’s equation,

$$\frac{\partial u}{\partial t} + \frac{\partial}{\partial x} \left(\frac{u^2}{2} \right) + \frac{\partial}{\partial y} \left(\frac{u^2}{2} \right) = 0, \quad (7.2.21)$$

with $(x, y, t) \in [0, 1] \times [0, 1] \times [0, 0.5]$, and initial condition

$$u(x, y, 0) = \begin{cases} 2.0, & x < 0.25, y < 0.25, \\ 3.0, & x > 0.25, y > 0.25, \\ 1.0, & \text{otherwise,} \end{cases} \quad (7.2.22)$$



in conjunction with exact boundary condition on the inflow portions of $\partial\Omega$. The solution is advanced to $t = 1/12$. The problem consists of two shock waves and two rarefaction that meet towards the middle of the domain to form a cusp. This example is a bit more difficult than the one considered in [156, 100] to study the convergence of the scheme to a discontinuous solution. The approximations are show in Figure 7.18 and in Figure 7.19, where we performed a mesh refinement study for six different mesh grid configurations. For comparison purposes, we compare with approximations of [39], which in turn is shown the exact analytical solution to the Riemann problem (7.2.21)-(7.2.22) at $t = \frac{1}{12}$ computed by the method of characteristics. As before, once more, we also included the time elapsed into a mesh refinement study for a preliminary computational efficiency: 0.3093 secs (64×64 cells), 1.3755 secs (128×128 cells), 7.0047 secs (256×256 cells), 41.2132 secs (512×512 cells), 278.6869 secs (1024×1024 cells) and $2.1970e+03$ secs (2048×2048 cells).

Analogously, in figures 7.20 and 7.21, from top to bottom are shown the numerical solutions computed with the two-dimensional Lagrangian-Eulerian scheme (7.1.26) with respect to the nonlinear model with nonconvex flow function described by the Riemann problem (7.2.21)-(7.2.22). In figure 7.20 from top to bottom are shown on the left (resp. right) column a “3D-plot’s view angle” (resp. contour curves) of numerical approximations with 64×64 cells (top) 0.3342 sec, 128×128 cells (middle) 0.8246 sec and 256×256 cells (bottom) 3.7246 sec. And figure 7.21, from top to bottom, are shown of the left (resp. right) column a “3D-plot’s view angle” (resp. contour curves) of numerical approximations with 512×512 cells (top) 21.885 sec, 1024×1024 cells (middle) 136.77 sec and 2048×2048 cells (bottom) 845.9012 sec.

Based in the approximations and on the computational times we observe that the Lagrangian-Eulerian scheme shown be very efficient computationally and without spurious oscillations in regions with sharp fronts, no mesh orientation dependence and low numerical diffusion.

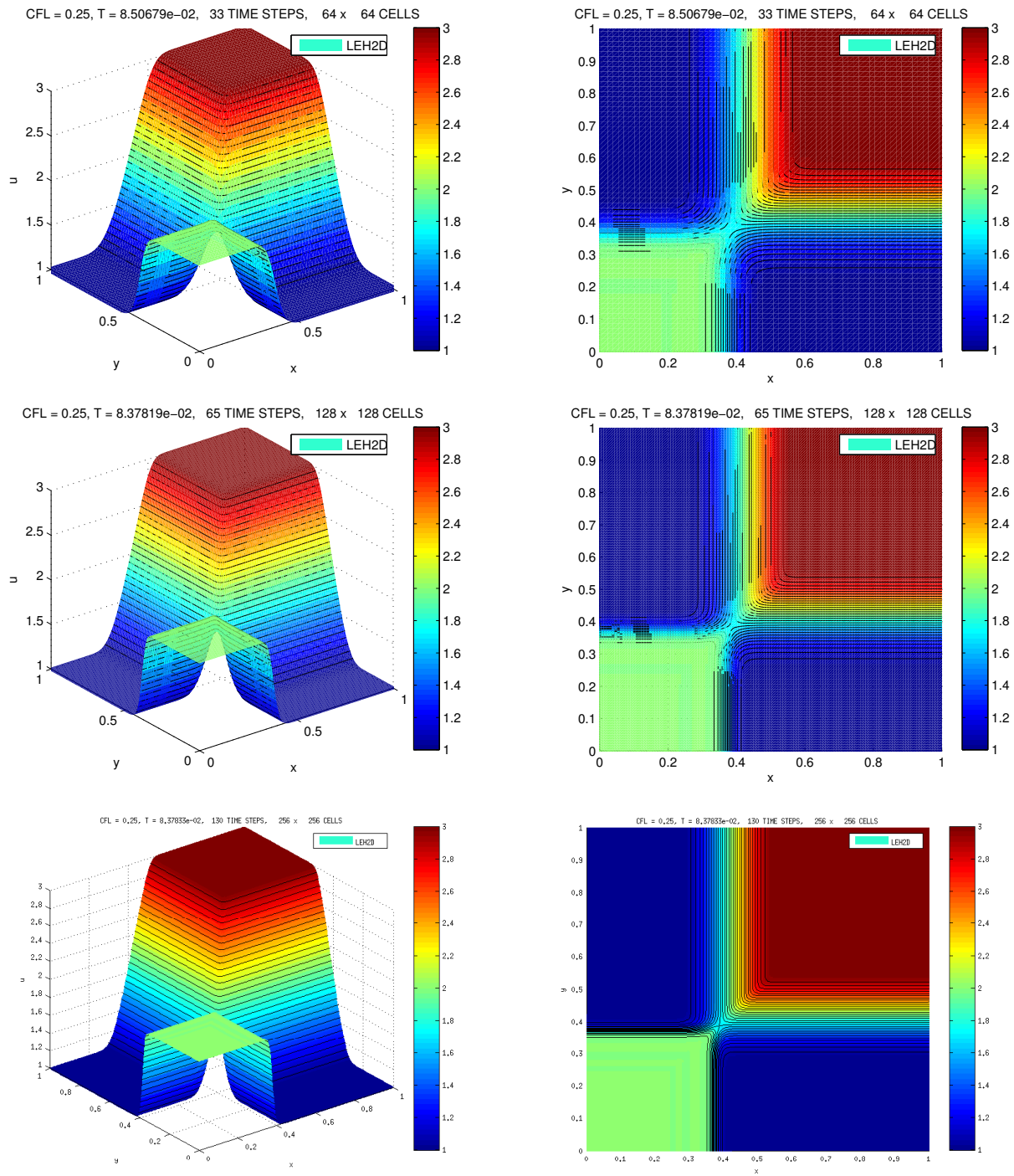


Figure 7.18: From top to bottom are shown the numerical solutions at $T = 1/12$ computed with the two-dimensional Lagrangian-Eulerian scheme (7.1.25) with respect to the nonlinear model with nonconvex flow function described by the Riemann problem (7.2.21)-(7.2.22).

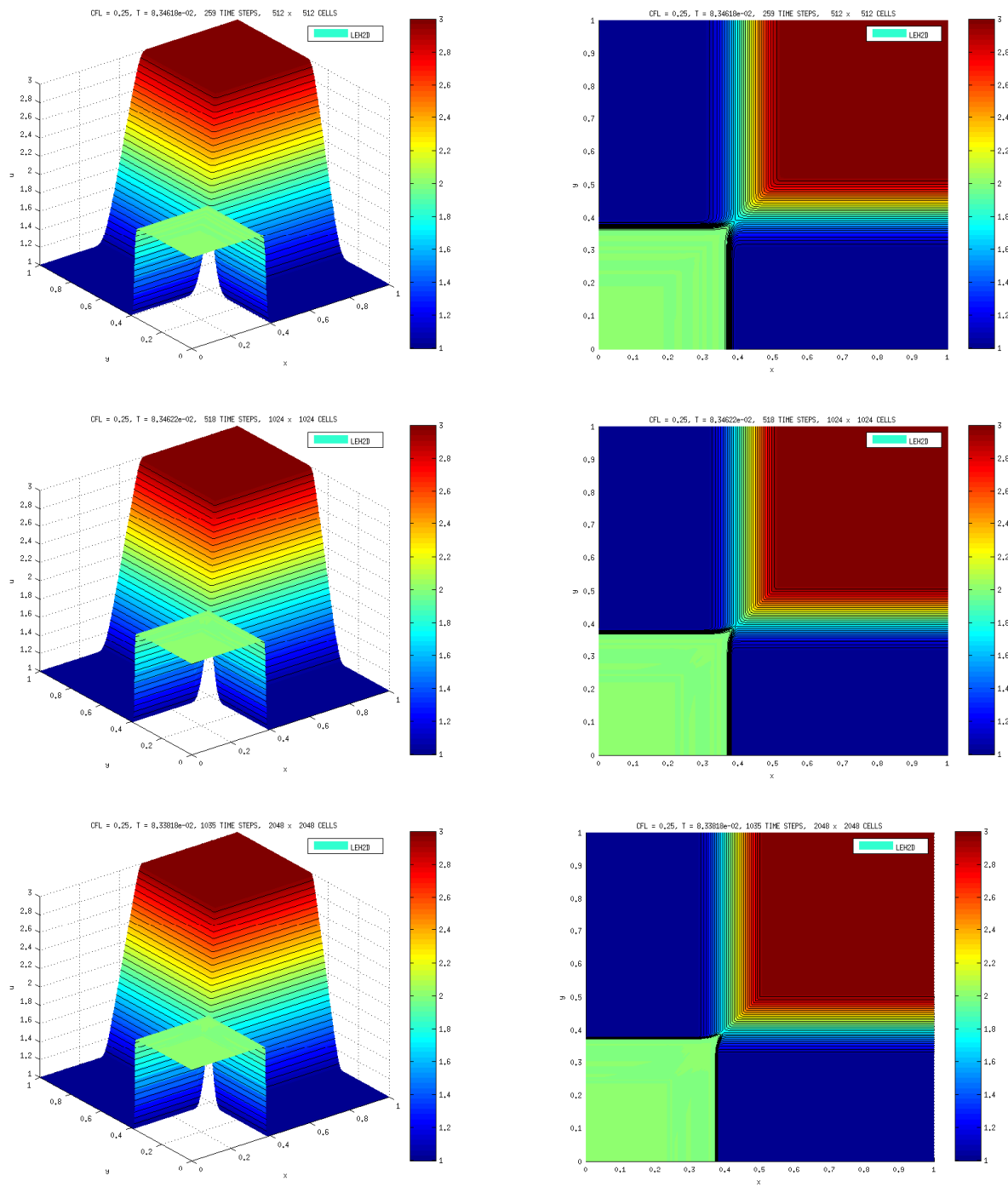


Figure 7.19: From top to bottom are shown the numerical solutions at $T = 1/12$ computed with the two-dimensional Lagrangian-Eulerian scheme LEH2D (7.1.25) with respect to the nonlinear model with nonconvex flow function described by the Riemann problem (7.2.21)-(7.2.22).

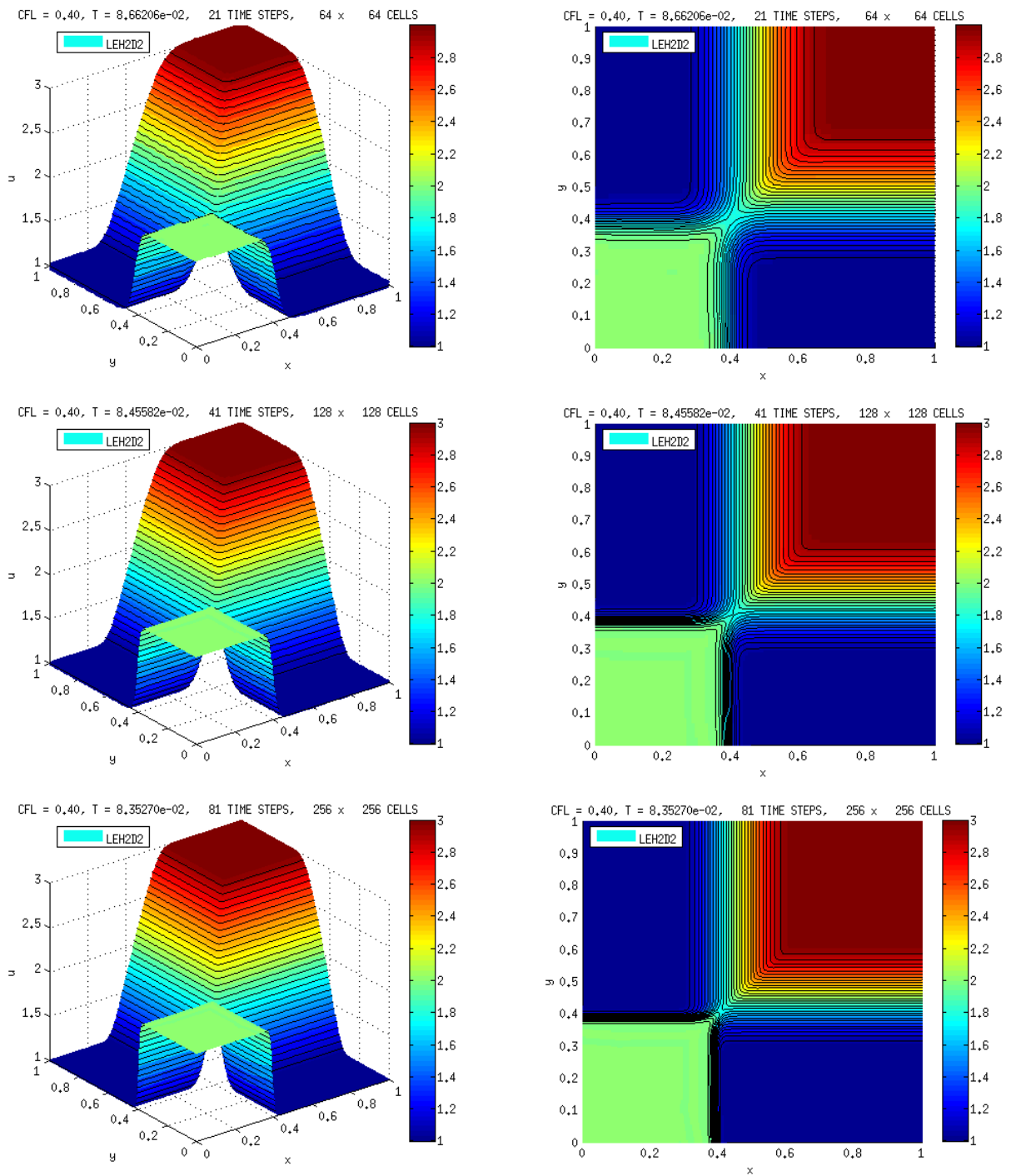


Figure 7.20: From top to bottom are shown the numerical solutions at $T = 1/12$ computed with the two-dimensional Lagrangian-Eulerian scheme LEH2D2 (7.1.26) with respect to the nonlinear model with nonconvex flow function described by the Riemann problem (7.2.21)-(7.2.22).

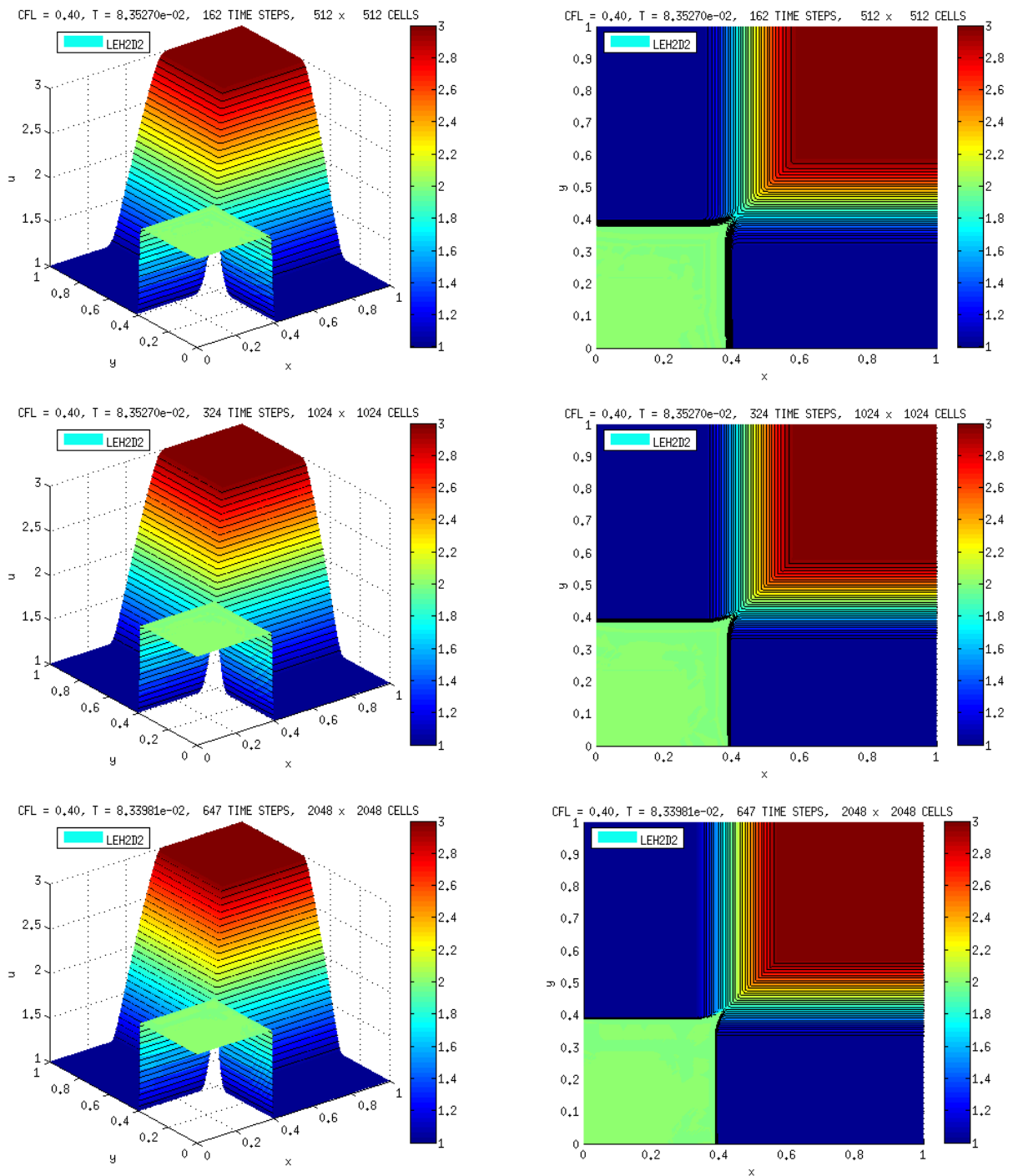


Figure 7.21: From top to bottom are shown the numerical solutions at $T = 1/12$ computed with the two-dimensional Lagrangian-Eulerian scheme LEH2D2 (7.1.26) with respect to the nonlinear model with nonconvex flow function described by the Riemann problem (7.2.21)-(7.2.22).

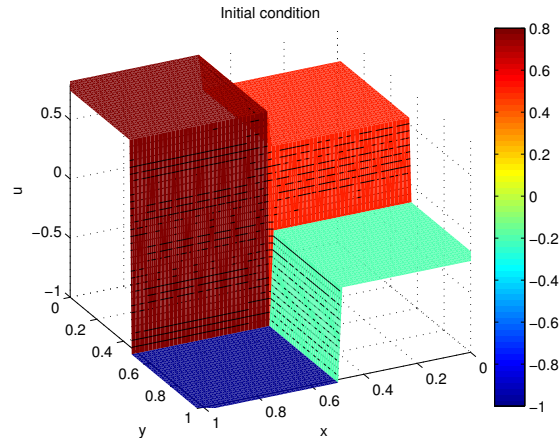
Model Problem 7.2.6. Jiang & Tadmor, (SIAM SISC), An oblique Riemann problem for two-dimensional Burgers's equation [86]

In order to add another test problem, we will use the two-dimensional Lagrangian-Eulerian scheme (7.1.25) for the two-dimensional Burgers's equation discussed in [39, 86]. Consider the following initial value problem for the inviscid Burgers's equation given by,

$$\frac{\partial u}{\partial t} + \frac{\partial}{\partial x} \left(\frac{u^2}{2} \right) + \frac{\partial}{\partial y} \left(\frac{u^2}{2} \right) = 0, \quad (7.2.23)$$

where $(x, y, t) \in [0, 1] \times [0, 1] \times [0, 0.5]$, and with the oblique Riemann problem initial condition,

$$u(x, y, 0) = \begin{cases} -1.0, & x > 0.5, y > 0.5, \\ -0.2, & x < 0.5, y > 0.5, \\ 0.5, & x < 0.5, y < 0.5, \\ 0.8, & x > 0.5, y < 0.5, \end{cases} \quad (7.2.24)$$



in conjunction with exact boundary condition on the inflow portions of $\partial\Omega$. For comparison purposes, we refer the numerical approximation to the solution of the Riemann problem (7.2.21)-(7.2) showed in [39], which was considered the following Friedrichs-Keller triangulation with 12.800 ($80 \times 80 \times 2$) elements, along with the CFL number $\frac{1}{3}$. In Figure (7.22) and in Figure (7.23) we report our approximations computed with our new two-dimensional Lagrangian-Eulerian scheme LEH2D (7.1.25) for the Riemann problem (7.2.21)-(7.2), having performed a mesh grid refinement (along with time elapsed into each simulation): 1.0704 secs (64×64 cells), 4.7941 secs (128×128 cells), 22.7290 secs (256×256 cells), 146.3850 secs (512×256 cells), 937.7651 secs (1024×1024 cells) and $7.5010e+03$ secs (2048×2048 cells). The solution is advanced from $T = 0$ to $T = \frac{1}{12}$ as in [39]. In figure 7.24, from top to bottom, are shown the numerical solutions computed with the 2D Lagrangian-Eulerian scheme LEH2D2 (7.1.26) with respect to the Riemann problem (7.2.23)-(7.2.24). It is shown on the left (resp. right) column a “3D-plot’s view angle” (resp. contour curves) of numerical approximations with 64×64 cells and 0.78 sec (top), 128×128 cells (middle) and 3.29 sec, and 256×256 cells (bottom) and 12.98 sec. And in figure 7.25, are shown of the left (resp. right) column a “3D-plot’s view angle” (resp. contour curves) of numerical approximations with 512×512 cells and 70.92 sec (top), 1024×1024 cells (middle) in 395.97 sec, and 2048×2048 cells (bottom) and 2518.4 sec. Again, we Based in the approximations and on the computational times we observe that the Lagrangian-Eulerian scheme shown be very efficient computationally and without spurious oscillations in regions with sharp fronts, no mesh orientation dependence and low numerical diffusion.

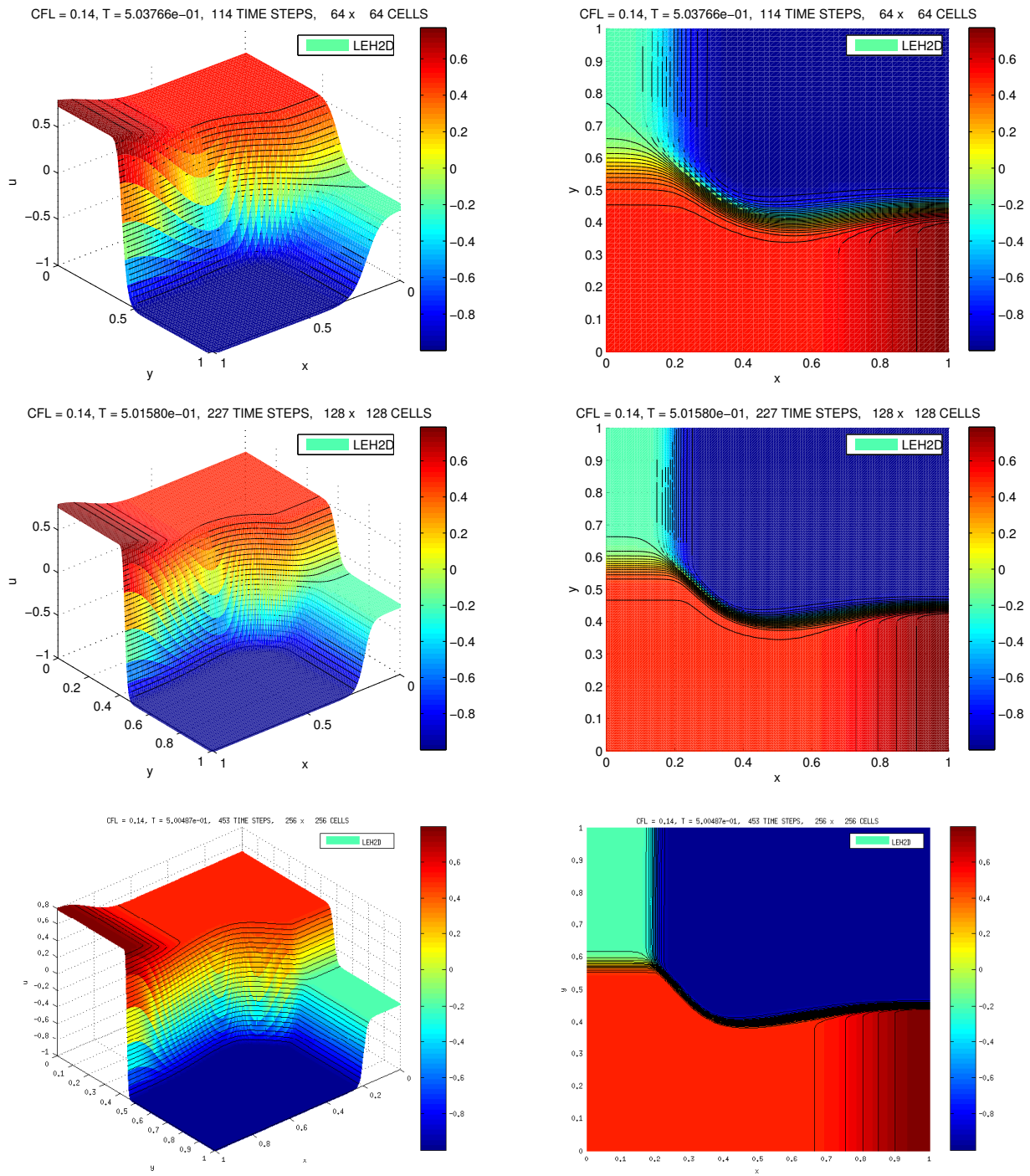


Figure 7.22: From top to bottom are shown the numerical solutions at $T = 1/2$ computed with the 2D Lagrangian-Eulerian scheme LEH2D (7.1.25) with respect to the Riemann problem (7.2.23)-(7.2.24).

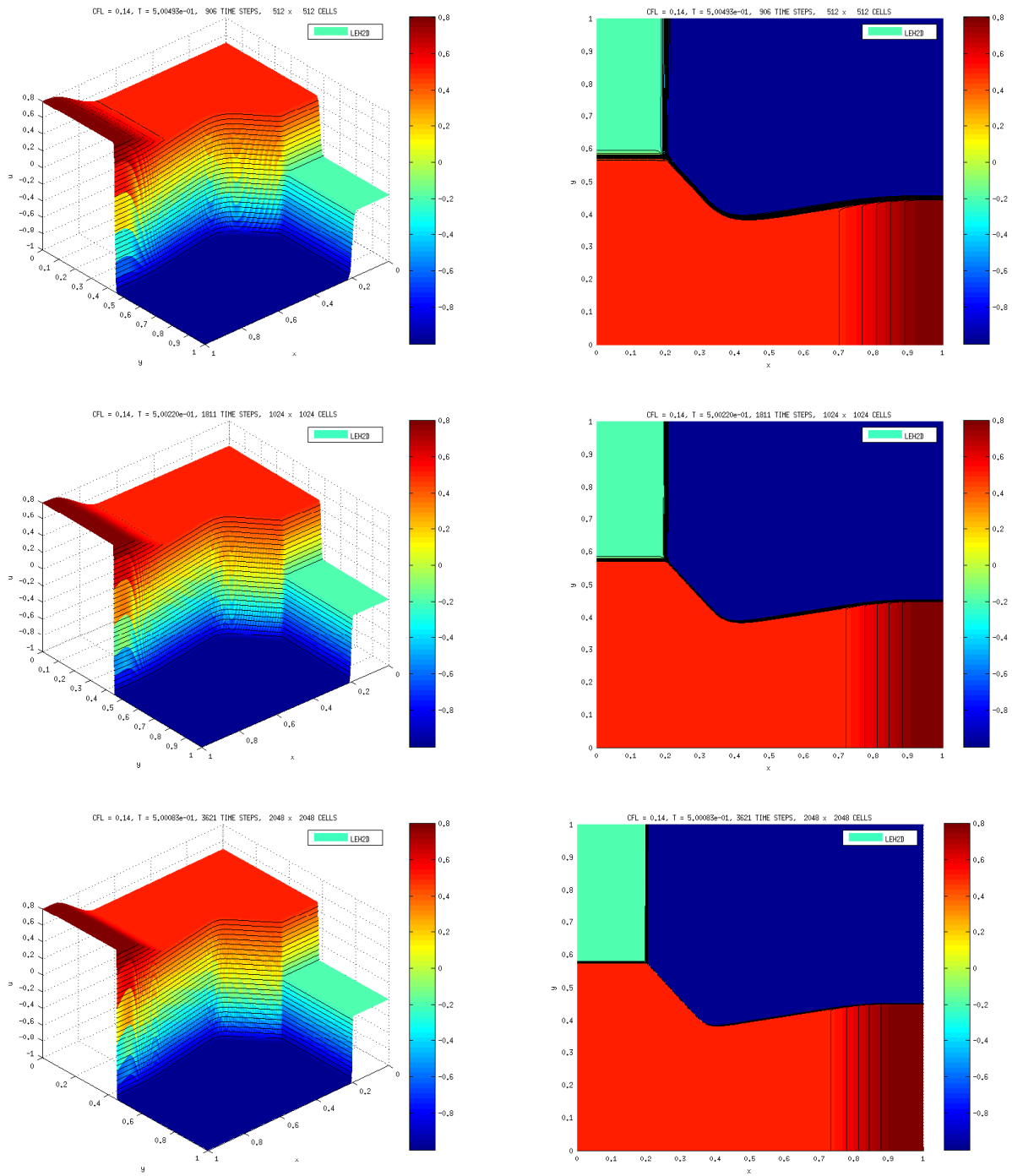


Figure 7.23: From top to bottom are shown the numerical solutions at $T = 1/2$ computed with the 2D Lagrangian-Eulerian scheme LEH2D (7.1.25) with respect to the Riemann problem (7.2.23)-(7.2.24).

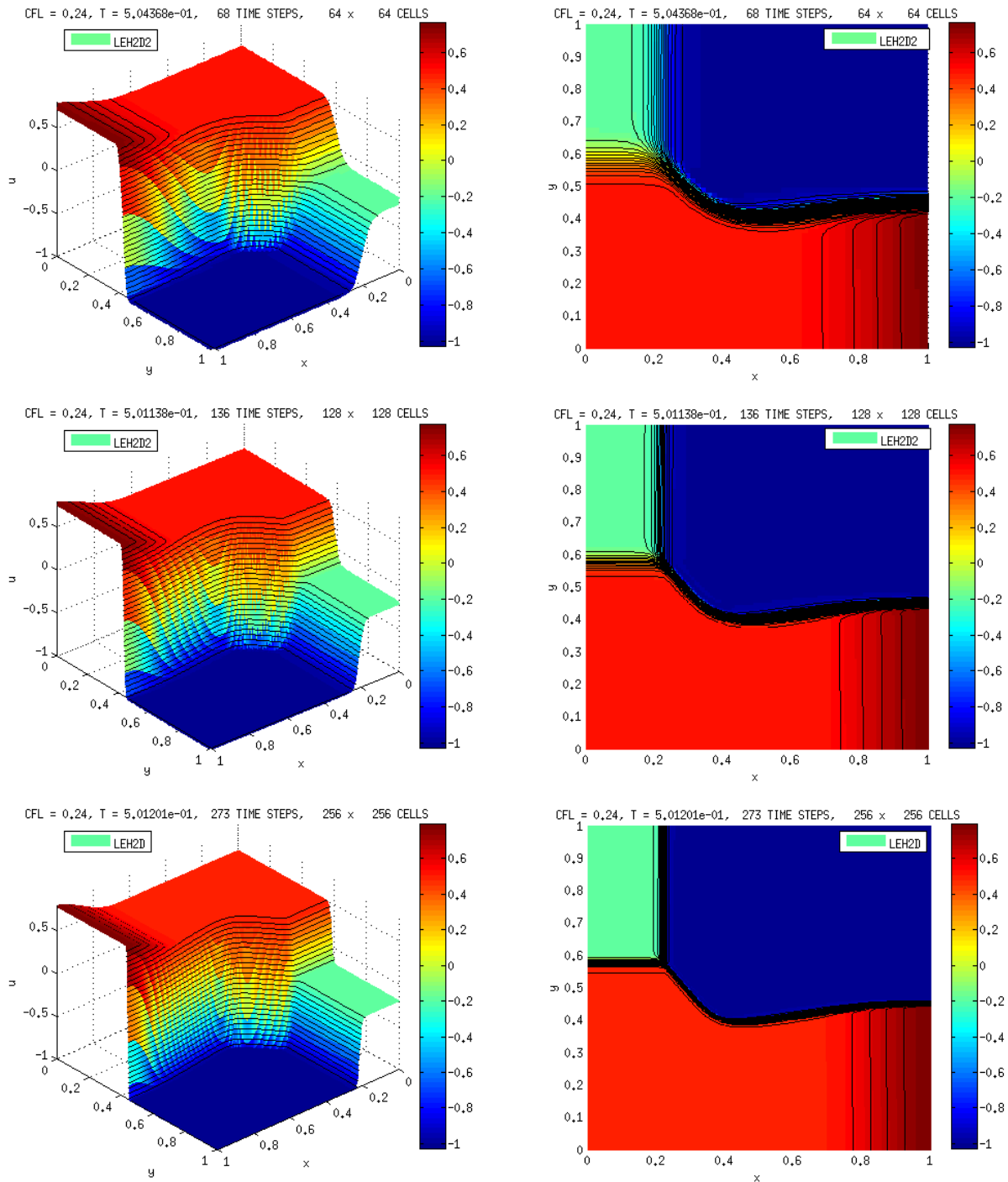


Figure 7.24: From top to bottom are shown the numerical solutions at $T = 1/2$ computed with the 2D Lagrangian-Eulerian scheme LEH2D2 (7.1.26) with respect to the Riemann problem (7.2.23)-(7.2.24).

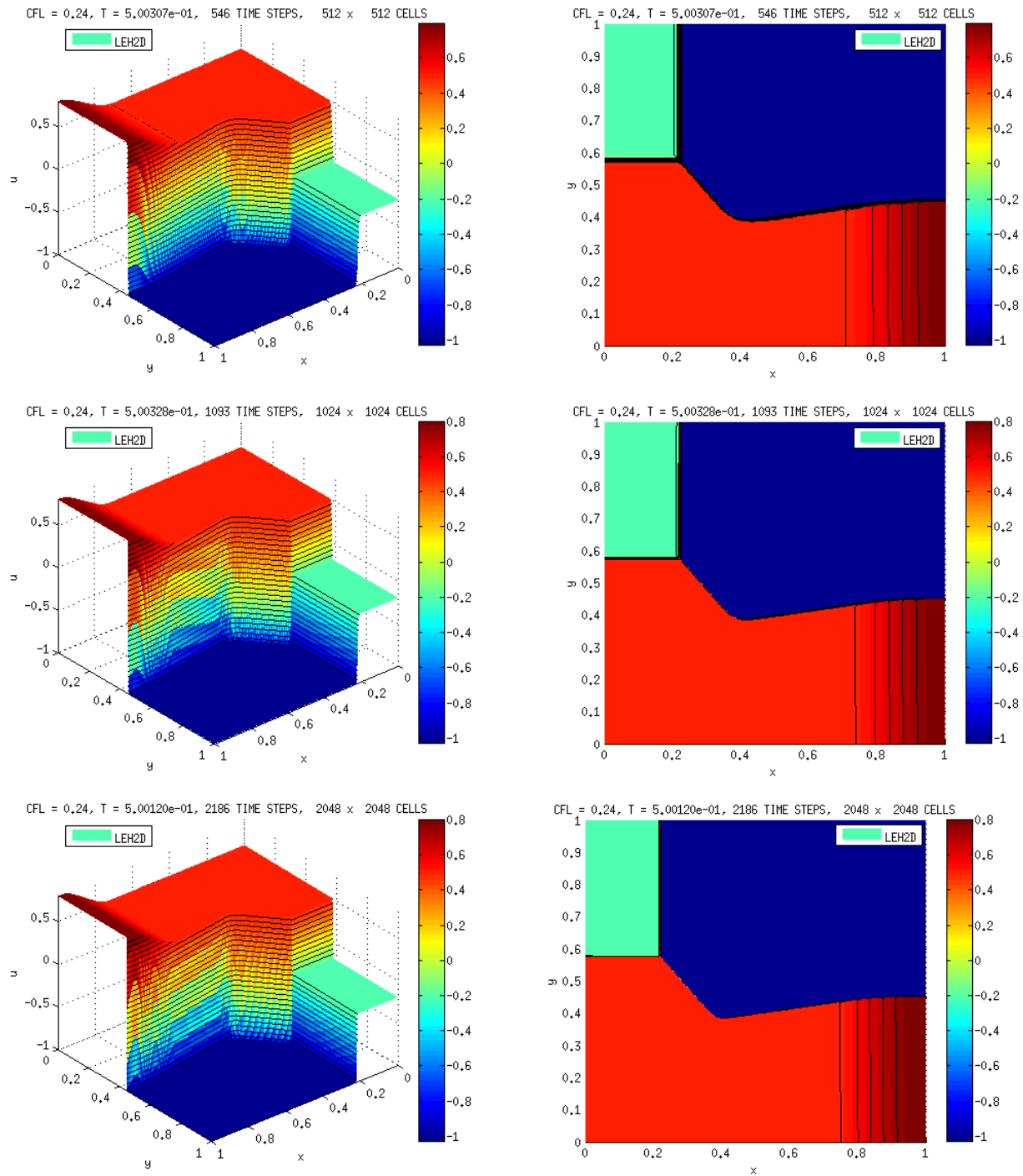


Figure 7.25: From top to bottom are shown the numerical solutions at $T = 1/2$ computed with the 2D Lagrangian-Eulerian scheme LEH2D2 (7.1.26) with respect to the Riemann problem (7.2.23)-(7.2.24).

Model Problem 7.2.7. A numerical convergence study of linear two-dimensional flow problem.

We present a preliminary but comprehensive set of convergence numerical experiments which explore the role of our two-dimensional Lagrangian-Eulerian scheme (7.1.25) to address the issue of the order of convergence rate. At this moment it is worth mentioning that we expect to perform a numerical analysis in ℓ^2 -space two the two-dimensional scheme in a similar fashion as was done to the one-dimensional Lagrangian-Eulerian scheme discussed in details through the preceding text of the current monograph in progress, which is not yet finished. To this aim, we consider the following initial value problem associated to the two-dimensional linear hyperbolic conservation law,

$$\frac{\partial u}{\partial t} + \frac{\partial u}{\partial x} + \frac{\partial u}{\partial y} = 0, \quad \text{in the computational domain } (x, y, t) \in [0, 1] \times [0, 1] \times [0, 1], \quad (7.2.25)$$

and initial condition,

$$u(x, y, 0) = \sin(\pi(x + y)), \quad (7.2.26)$$

subject to exact boundary conditions on the inflow portions of $\partial\Omega$, i.e., along $x = 0$ and $y = 0$ the values of the conserved quantities are prescribed via the exact solution (see also Figure 7.26).

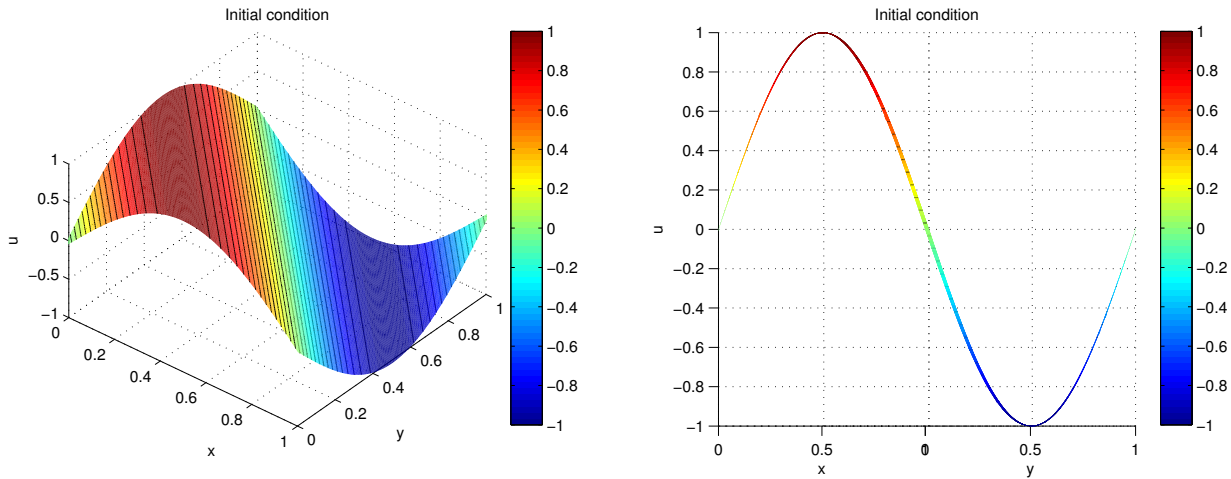


Figure 7.26: Initial condition for problem (7.2.25)-(7.2.26). On the left (resp. right) picture we show a “3D-plot’s view angle” (resp. a oblique projection over the plane $x = y$).

It is easy to show that the exact solution of the problem (7.2.25)-(7.2.26), as previously discussed, is simply $u(x, y, t) = \sin(\pi(x + y - 2t))$. The numerical solution will be advanced from $T = 0$ to $t = 1$ and we notice that at this time the solution is merely translated by one period 2π , with respect to the initial condition in the oblique $x = y$ direction.

Observed numerical convergence rate to (7.2.25) with initial condition $u(x, y, 0) = \sin(\pi(x + y))$ in the l_h^1 -norm (left), in the l_h^2 -norm (middle) and in the l_h^∞ -norm (right). In the tables are shown errors between the numerical approximations (U) and exact solutions (u) in l_h^1 , l_h^2 and l_h^∞ norms to problem (7.2.25) with initial condition $u(x, 0) = \sin(\pi(x + y))$, advanced from $T = 0$ to $T = 1$ along with CFL condition 0.67. From the numerical numbers displayed in this table

as well as from the numerical convergence rate from the linear regression reported in Figure 7.28, we have first order convergence in ℓ^p -spaces, $p=1, 2$ and ∞ . The numerical approximation computed with our two-dimensional Lagrangian-Eulerian scheme (7.1.25) to problem (7.2.25)-(7.2.26) is shown in the Figure 7.27 (left frame) along with the exact solution on the right frame.

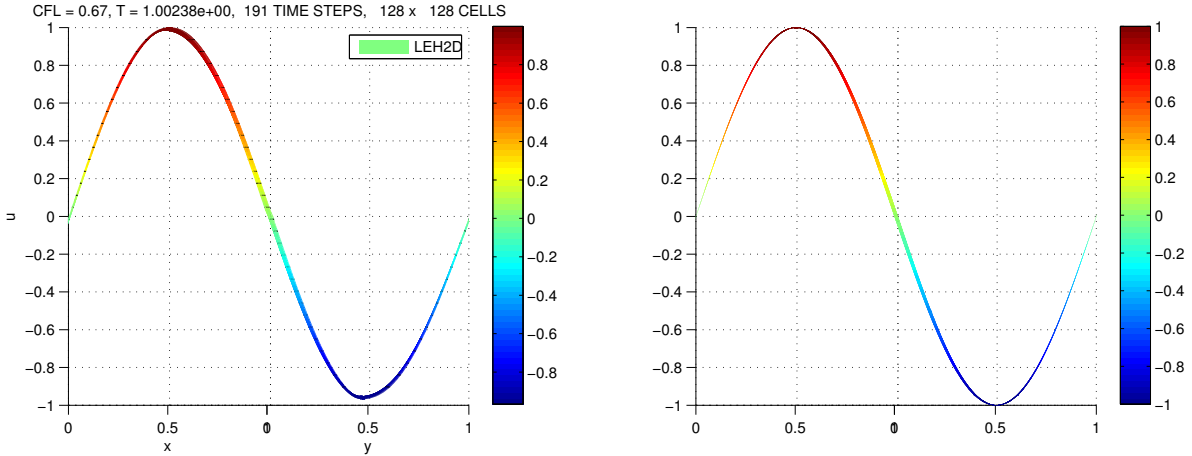


Figure 7.27: Computed solution by our 2D Lagrangian-Eulerian scheme (7.1.25) to problem (7.2.25)-(7.2.26) at simulation time $T = 1$ (left) and exact solution (right) both projected over oblique plane $x = y$.

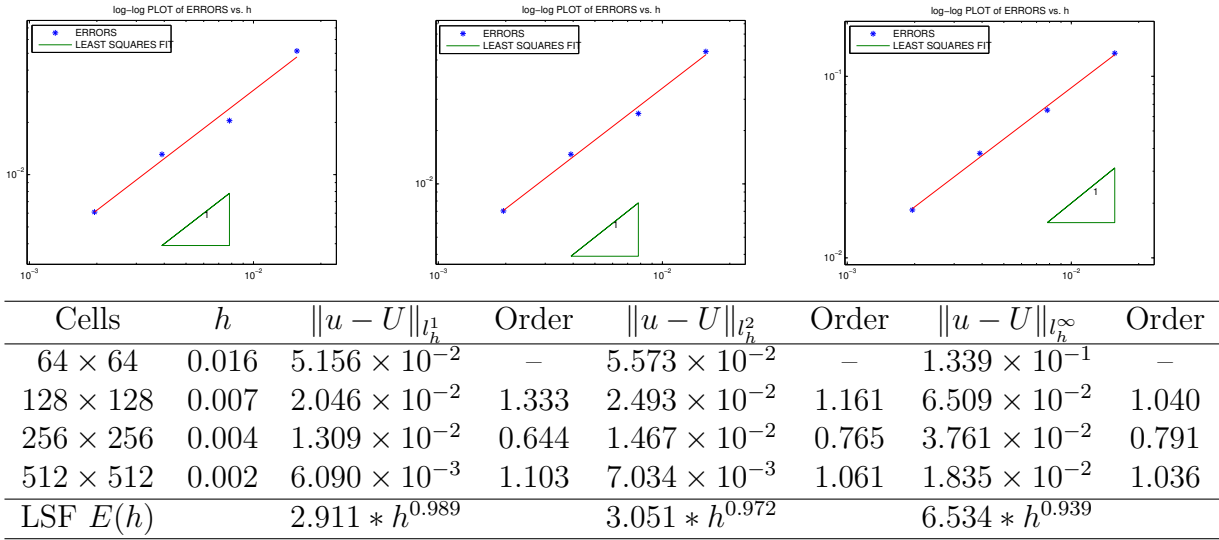


Figure 7.28: In every one of the Figures with different norms, our two-dimensional Lagrangian Eulerian scheme gets approximately first order of accuracy when the mesh is refined.

Chapter 8

Concluding remarks and perspectives for the future

Over the last years, upwind and central (Godunov-type) schemes have gained popularity due to their simplicity and efficiency for solving nonlinear systems of hyperbolic conservation laws in several space dimensions. In particular, the last mentioned methods do not require the solution of a Riemann problem or a characteristic decomposition to compute the inter-cell flux. However, all methods currently in use are derived using the characteristic form of the equations in one space dimension and most of these algorithms used to be extended to several space dimensions using operator splitting of fractional steps [111, 113, 141, 158]. Operator splitting techniques for approximating the solution of partial differential equations systems arise in many fields of application. The idea of splitting sums of complicated operators into simpler operators that are treated separately, is both easy and fundamental, and as such has appeared under various names in different contexts. It has a long history and has been developed with various objectives in mind. One of the first rigorous results is associated with the name of Trotter [149].

The earliest of these procedures were introduced to reduce each time step of a multidimensional transient problem to a cycle of one-dimensional calculations. The first two classes of these procedures were the alternating-direction (*AD*) methods as presented by Douglas, Peaceman, and Rachford [46, 47, 48, 55, 132] and the fractional step methods of D’jakonov, Marchuk, and Yanenko [59, 157]. (Half a century after these methods were defined, it has been shown [54] that a modest modification in any of the splitting produces changes into the others.) These procedures have been applied in numerical simulation of many physically important problems either to obtain a more efficient time-stepping algorithm or, in the case of *AD* methods, to apply an efficient iterator for an elliptic algebraic system. Additionally, in [150], it is described a somewhat hybrid method between a front capturing method there are other relevant publications for this issue [39, 66, 91, 98, 109, 120, 129]. For a front tracking method (see [63, 64, 150]). These articles show a recent survey on the development of such techniques.

It is worth mentioning that adverse effects (ranging from uncontrollable instabilities to difficulties in accurately computing gradients near the interface) might limit the calculation of volume fraction and inter-facial area for dispersed mixing flows in the long-time regimes. This can be a significant drawback over front-tracking methods for the computations of multiphase flow transport problems. Another major drawback of direct front-tracking is complexity. In addition to the obvious question of how the interface grid interacts with the stationary grid, and vice versa, it is generally necessary to restructure the interface grid dynamically as the calcu-

lations proceed. Computational points must be added in regions where the grid stretches, and usually, it is desirable to eliminate points from regions of compression. Additional complications, to be discussed later, arise in three dimensions. Another major problem for front-tracking results come from the interaction of a front with another front (or another part of the same front). Generally, the computational procedure does not recognize more than one front in each cell of the stationary grid, and therefore, double interfaces have to be merged into one interface or eliminated. In other words, when two interfaces are very close to each other, or when an interface folds back on itself, such that two front segments are between the same two fixed grid points; the property value on the fixed grid depends on which interface segment is being considered. Since this situation is fairly common, a more general method is needed.

Only in 1990 a second-order accurate non-oscillatory central Godunov-type scheme was introduced by Nessyahu and Tadmor (NT) [124], whose work generalized the first-order accurate staggered Lax-Friedrichs scheme using a non-oscillatory piecewise-linear reconstruction in the spirit of van Leer's MUSCL [152]. The NT scheme, which is one of the simplest and most versatile Godunov-type numerical methods, has recently been put on solid theoretical ground by the proof of the fully-nonlinear scheme's convergence to the unique entropy solution of the problem in the case of strictly convex nonlinear scalar conservation laws [133]. In addition, over the last decade, the NT scheme has inspired a significant amount of research on the topic of non-oscillatory central schemes. Some of the recent work on central schemes includes, but is not limited to, semi-discrete formulations, less dissipative central-upwind schemes, extensions to multiple spatial dimensions and non-Cartesian meshes (see, e.g., [34, 39, 86, 97, 98, 99, 100] and the references therein).

8.1 Concluding remarks

In this work was explored a locally conservative and divergence space-time finite control volume in a Lagrangian-Eulerian framework, first developed in the context of purely hyperbolic conservation laws, in order to design a locally conservative scheme to account the balance between numerical approximations of the hyperbolic flux function and the source term linked to steady solutions. Our new Lagrangian-Eulerian scheme is aimed to be not dependent of a particular structure of the source term. The designed scheme is also non dependent of Riemann problem solutions, but if available for a particular problem it is somewhat natural to incorporate such information into the procedure and thus yielding flexibility to the development of distinct numerical strategies upon the specific model under consideration. A set of representative numerical experiments for nonlinear problems - scalar and system - of hyperbolic conservation law and balance law types are presented to illustrate the performance of the new method. The numerical results are compared with accurate approximate solutions or exact solutions whenever possible.

We reiterate that, to the best of our knowledge, we have introduced a new approach for construction of new class of approximate solutions for multidimensional hyperbolic conservation laws, thanks to an appropriate reformulation of the original differential governing equation by means of an equivalent system of balance laws. Thus, in order to establish such connection between multidimensional hyperbolic conservation laws and system of balance laws, it was necessary to revisit the Lagrangian-Eulerian in its original setting for linear hyperbolic conservation laws and its extension for scalar and balance laws systems in one-space dimension. Indeed, they were presented, in details, several properties of the the new Lagrangian-Eulerian scheme for

linear hyperbolic conservation laws, namely, consistency, stability and convergence by means of the Lax equivalence theorem. Moreover, we also derived the associated modified equation for the Lagrangian-Eulerian scheme and describe the dispersive-dissipative relation to explain the one-dimensional numerical experiments results. We were able to write the Lagrangian-Eulerian scheme in conservative form for nonlinear hyperbolic conservation laws as well as we construct a Lipschitz continuous consistency condition to the Lagrangian-Eulerian numerical flux function. The Harten theory [75, 76], the Majda and Crandall theory [42] and the ideas in Smoller's book [139] were used to prove the convergence of the approximate solutions, obtained using our Lagrangian-Eulerian scheme for entropic solution of non-linear scalar hyperbolic conservation law in both numerical methods. Furthermore, numerical experiments for hyperbolic conservation laws with convex and non-convex flux functions were also present to illustrate the qualities of the new scheme. In particular, it was discussed the stability and convergence issues of the Lagrangian-Eulerian scheme for linear and nonlinear balance law problems.

We demonstrated the Lagrangian-Eulerian scheme applicability using a standard uniform cartesian discretization to several tests problems, in 1D and 2D, such as:

- two-phase Buckley-Leverett equations.
- Shallow-water flow in an inclined channel
- Rotational flows
- Euler equations based on G A Sod's "Shock Tube" problem Nonequilibrium gas dynamics
- two-dimensional nonlinear inviscid Burgers's equation with an oblique Riemann problem
- Porous media problems with convex
- non-convex and discontinuous flux functions
- LeVeque-Yee's Effect for Riccati source term
- convection-reaction problem with an inhomogeneous N-wave similarity-solution.

We were able to reproduce the expected qualitative behavior with no spurious oscillations nor grid orientation effects. All numerical experiments were performed with the most simple first order version of the Lagrangian-Eulerian scheme.

In Section 6 was discussed a extension of the Lagrangian-Eulerian scheme for systems of balance laws in one-space dimension. Based on the numerical experiments reported in the last part of this Section, we observe that our new Eulerian-Lagrangian approach was able to capture qualitative correct solutions for linear and nonlinear problems as well as for systems in one-dimensional spaces.

For hyperbolic conservation laws in two-space dimensions, the Crandall and Majda theory (see [42]) shown that classic splitting of Godunov type converges to the entropic solution when the numerical method, used in each step of the splitting, converges to the entropic solution, as was proved for our scheme in one space dimension for hyperbolic conservation laws. Furthermore, we proposed an extension to find approximated solutions of hyperbolic conservation laws in two space dimensions. In this case, a balance law system is solved at each step ($\Delta t/2$) aiming the error to be less than in the classic splitting, in this approach the source term couples the system of two equations of balance laws. Along numerical experiments for nonlinear hyperbolic

problems, we observe that our new Eulerian-Lagrangian approach was able to capture qualitative correct solutions for linear and nonlinear problems in two space dimensions, and more important, without any of the sophisticated tools, which makes it easy to be implemented.

8.2 Perspectives for future work

We are working on the extension to higher orders of the Lagrangian-Eulerian scheme for solving one-dimensional and multidimensional problems (conservation laws and balance laws). we are also working on designing other strategies for quadrature rules and nonlinear reconstruction given by slope limiters. We expect to take additional advantage of the similarity between the structure of the Lagrangian-Eulerian scheme and the Lax-Friedrichs and Nessyahu-Tadmor schemes to obtain further convergence proofs based on the milestone works for hyperbolic conservation laws, including discontinuous flux functions.

In Section 6 we discussed a extension of the Lagrangian-Eulerian scheme for systems of balance laws in one-space dimension to hyperbolic conservation laws in two-space dimensions, along with numerical experiments for nonlinear hyperbolic problems. We expect to perform the numerical analysis for the two-dimensional Lagrangian-Eulerian scheme soon. In next future we expect to amplify and clarify our knowledge on the theory of scalar conservation laws, scalar hyperbolic balance laws, system of hyperbolic laws, system of hyperbolic balance laws and hyperbolic conservation laws in two or more space variables; and then we expect to apply all these knowledge to explain and prove the convergence of approximated solutions of the above mentioned problems.

In section 7 was discussed an extension of the Lagrangian-Eulerian scheme to solve a hyperbolic balance law to one scheme to solve a hyperbolic conservation law in two spatial variables by using one system of balance laws that is coupled in the source term. The issue of direct extension of the Lagrangian-Eulerian scheme for approximating solution of scalar nonlinear hyperbolic conservation laws for numerical scheme to solve hyperbolic conservation law in two dimensional variables using integral tubes has not yet been replied, because it seems the surface of the integral tube and the surface normal vector are very difficult to define, as it was discuss in the chapter 7. This extension is also a perspective for a further work.

8.3 Final Considerations

We establish a rigorous convergence proof for the uniqueness of the entropy solution, constructed with the aid of integral tubes by a Lagrangian-Eulerian procedure for hyperbolic conservation laws, in one-space dimension to the case of convex flux. Convergence proofs for linear hyperbolic law problems and linear balance law problems, were also obtained in the context of the Lax equivalence theorem. To the best of our knowledge, this work is the first to establish a rigorous convergence proof for numerical schemes of Lagrangian-Eulerian type for purely nonlinear hyperbolic conservation laws, and thus yielding a novelty approach.

We proposed an extension of the Lagrangian-Eulerian framework to the case of systems of one-dimensional hyperbolic problems, and to the case of balance laws. Furthermore, combing such ideas we also designed a scheme for two-dimensional conservation laws.

We introduced a novel Lagrangian-Eulerian framework for balance laws along with good numerical evidence to be “well-balanced”. In particular, we accurately reproduce numerical

results from those reported in some important journals. The method seems to be promising and further studies will follow to the case of systems of equations in 2D and 3D. In particular, a more rigorous numerical analysis is needed to take into account convergence results in the case of non-linear hyperbolic conservation laws with source terms, which in turn we are interested in finding the space-time domain region where the mass flux takes place for general multi-phase problems in porous media.

Acknowledgements: John Perez thanks CAPES for a graduate fellowship. Eduardo Abreu thanks FAPESP Foundation for financial support through FAPESP grants No. 2014/03204-9 and No. 2011/23628-0, and UNICAMP/FAEPEX through grant No. 519.292-0280/2014 and CNPq through grant No. 445758/2014-7.

Bibliography

- [1] Eduardo Abreu. Numerical modelling of three-phase immiscible flow in heterogeneous porous media with gravitational effects. *Mathematics and Computers in Simulation*, 97:234–259, 2014.
- [2] Eduardo Abreu, Jim Douglas, Frederico Furtado, Dan Marchesin, and Felipe Pereira. Three-phase immiscible displacement in heterogeneous petroleum reservoirs. *Mathematics and computers in simulation*, 73(1):2–20, 2006.
- [3] Eduardo Abreu, Jim Douglas, Frederico Furtado, and Felipe Pereira. Operator splitting based on physics for flow in porous media. *International Journal of Computational Science*, 2(3):315–335, 2008.
- [4] Eduardo Abreu, Jim Douglas, Frederico Furtado, and Felipe Pereira. Operator splitting for three-phase flow in heterogeneous porous media. *Communications in Computational Physics*, 6(1):72, 2009.
- [5] Eduardo Abreu, Wanderson Lambert, John Perez, and Arthur Santo. A lagrangian-eulerian algorithm for solving hyperbolic conservation laws with applications. 6th International Conference on Approximation Methods and Numerical Modelling in Environment and Natural Resources. Pau, France 2015. Editorial Universidad de Granada (2015) 600-617.
- [6] Eduardo Abreu and John Perez. A constructive lagrangian-eulerian method for balance law problems. (In preparation).
- [7] Eduardo Abreu and John Perez. Design, analysis, and implementation of a lagrangian-eulerian approximation scheme for hyperbolic conservation laws and balance laws (apresentação de trabalho). International Congress of Mathematicians, August 13 - 21, 2014 Coex , Seoul , Korea. 2014.
- [8] Eduardo Abreu and John Perez. Design of a well balanced lagrangian approximation scheme for balance laws. (apresentação de trabalho). 29º Colóquio Brasileiro de Matemática IMPA, Rio de Janeiro, 21 de julho a 02 de agosto de 2013.
- [9] Eduardo Abreu and John Perez. Lagrangian approximation schemes for balance laws. (apresentação de trabalho/congresso). VII Encontro Nacional de Matemática e Aplicações (VII ENAMA), 2013, Rio de Janeiro. VII ENAMA, 2013.
- [10] Eduardo Abreu and John Perez. A lagrangian-eulerian algorithm for solving hyperbolic problems and balance laws / um método lagrangiano-euleriano para aproximação de leis

- de balanço e de leis de conservação hiperbólica (apresentação de trabalho). I Brazilian Congress of Young Researchers in Pure and Applied Mathematics (10-12, December 2014); IME/USP. 2014.
- [11] Eduardo Abreu and John Perez. A lagrangian-eulerian algorithm scheme for hyperbolic conservation laws and balance laws (apresentação de trabalho). 15th International Conference: Theory, Numerics and Applications of Hyperbolic Problems 2014, Rio de Janeiro/IMPA.
- [12] Eduardo Abreu and John Perez. Lagrangian-eulerian algorithms for solving balance laws and hyperbolic problems (submitted).
- [13] Eduardo Abreu and John Perez. A new locally conservative lagrangian eulerian method for hyperbolic and balance laws (apresentação de trabalho). VIII Pan-American Workshop Applied and Computational Mathematics, 2014, Barranquilla-Colombia.
- [14] Adimurthi, Jérôme Jaffré, and GD Veerappa Gowda. Godunov-type methods for conservation laws with a flux function discontinuous in space. *SIAM Journal on Numerical Analysis*, 42(1):179–208, 2004.
- [15] Boris Andreianov and Clément Cancès. Vanishing capillarity solutions of buckley–leverett equation with gravity in two-rocks’ medium. *Computational Geosciences*, 17(3):551–572, 2013.
- [16] Boris Andreianov, Kenneth H Karlsen, and Nils Henrik Risebro. A theory of l_1 -dissipative solvers for scalar conservation laws with discontinuous flux. *Archive for rational mechanics and analysis*, 201(1):27–86, 2011.
- [17] José Aquino, AS Francisco, Felipe Pereira, and HP Amaral Souto. An overview of eulerian–lagrangian schemes applied to radionuclide transport in unsaturated porous media. *Progress in Nuclear Energy*, 50(7):774–787, 2008.
- [18] José Aquino, AS Francisco, Felipe Pereira, T Jordem Pereira, and HP Amaral Souto. A lagrangian strategy for the numerical simulation of radionuclide transport problems. *Progress in Nuclear Energy*, 52(3):282–291, 2010.
- [19] José Aquino, Felipe Pereira, HP Amaral Souto, and AS Francisco. A forward tracking scheme for solving radionuclide advective problems in unsaturated porous media. *International Journal of Nuclear Energy Science and Technology*, 3(2):196–205, 2007.
- [20] Todd Arbogast and Chieh-Sen Huang. A fully conservative eulerian–lagrangian method for a convection–diffusion problem in a solenoidal field. *Journal of Computational Physics*, 229(9):3415–3427, 2010.
- [21] Todd Arbogast, Chieh-Sen Huang, and Chen-Hui Hung. A fully conservative eulerian–lagrangian stream-tube method for advection-diffusion problems. *SIAM Journal on Scientific Computing*, 34(4):B447–B478, 2012.
- [22] Todd Arbogast, Chieh-Sen Huang, and Thomas F Russell. A locally conservative eulerian–lagrangian method for a model two-phase flow problem in a one-dimensional porous medium. *SIAM Journal on Scientific Computing*, 34(4):A1950–A1974, 2012.

- [23] Uri M Ascher, Steven J Ruuth, and Brian Wetton. *Implicit-explicit methods for time-dependent PDE's*. University of British Columbia, Department of Computer Science, 1993.
- [24] Arthur V Azevedo, Aparecido J de Souza, Frederico Furtado, Dan Marchesin, and Bradley Plohr. The solution by the wave curve method of three-phase flow in virgin reservoirs. *Transport in porous media*, 83(1):99–125, 2010.
- [25] John B Bell, John A Trangenstein, and Gregory R Shubin. Conservation laws of mixed type describing three-phase flow in porous media. *SIAM Journal on Applied Mathematics*, 46(6):1000–1017, 1986.
- [26] Stefan Berres, R Bürger, and Kenneth H Karlsen. Central schemes and systems of conservation laws with discontinuous coefficients modeling gravity separation of polydisperse suspensions. *Journal of Computational and Applied Mathematics*, 164:53–80, 2004.
- [27] Alberto Bressan and Wen Shen. Optimality conditions for solutions to hyperbolic balance laws. *Contemporary Mathematics*, 426:129–152, 2007.
- [28] Franco Brezzi, L Donatella Marini, and E Süli. Discontinuous galerkin methods for first-order hyperbolic problems. *Mathematical models and methods in applied sciences*, 14(12):1893–1903, 2004.
- [29] Raimund Bürger, Kenneth H Karlsen, and John D Towers. An engquist-osher-type scheme for conservation laws with discontinuous flux adapted to flux connections. *SIAM Journal on Numerical Analysis*, 47(3):1684–1712, 2009.
- [30] Russel E Caflisch, Shi Jin, and Giovanni Russo. Uniformly accurate schemes for hyperbolic systems with relaxation. *SIAM Journal on Numerical Analysis*, 34(1):246–281, 1997.
- [31] Clément Cancès. Asymptotic behavior of two-phase flows in heterogeneous porous media for capillarity depending only on space. ii. nonclassical shocks to model oil-trapping. *SIAM Journal on Mathematical Analysis*, 42(2):972–995, 2010.
- [32] Cristóbal E Castro and Eleuterio F Toro. Solvers for the high-order riemann problem for hyperbolic balance laws. *Journal of Computational Physics*, 227(4):2481–2513, 2008.
- [33] Manuel J Castro, JM Gallardo, ML Munoz, and C Parés. On a general definition of the godunov method for nonconservative hyperbolic systems. application to linear balance laws. In *Numerical mathematics and advanced applications*, pages 662–670. Springer, 2006.
- [34] Manuel J Castro, Philippe G LeFloch, María Luz Muñoz-Ruiz, and Carlos Parés. Why many theories of shock waves are necessary: Convergence error in formally path-consistent schemes. *Journal of Computational Physics*, 227(17):8107–8129, 2008.
- [35] Michael A Celia, Thomas F Russell, Ismael Herrera, and Richard E Ewing. An eulerian-lagrangian localized adjoint method for the advection-diffusion equation. *Advances in Water Resources*, 13(4):187–206, 1990.

- [36] Abdallah Chalabi. On convergence of numerical schemes for hyperbolic conservation laws with stiff source terms. *Mathematics of Computation of the American Mathematical Society*, 66(218):527–545, 1997.
- [37] Sin-Chung Chang. A critical analysis of the modified equation technique of warming and hyett. *Journal of Computational Physics*, 86(1):107–126, 1990.
- [38] Gui-Qiang Chen, C David Levermore, and Tai-Ping Liu. Hyperbolic conservation laws with stiff relaxation terms and entropy. *Communications on Pure and Applied Mathematics*, 47(6):787–830, 1994.
- [39] Ivan Christov and Bojan Popov. New non-oscillatory central schemes on unstructured triangulations for hyperbolic systems of conservation laws. *Journal of Computational Physics*, 227(11):5736–5757, 2008.
- [40] Richard Courant and Kurt Otto Friedrichs. *Supersonic flow and shock waves*, volume 21. Springer Science & Business Media, 1977.
- [41] Michael G Crandall and Andrew Majda. The method of fractional steps for conservation laws. *Numerische Mathematik*, 34(3):285–314, 1980.
- [42] Michael G Crandall and Andrew Majda. Monotone difference approximations for scalar conservation laws. *Mathematics of Computation*, 34(149):1–21, 1980.
- [43] Constantine M Dafermos. *Hyperbolic conservation laws in continuous physics*, volume 227. Springer-Verlag, 2005.
- [44] Gianni Dal Maso, Philippe G Lefloch, and François Murat. Definition and weak stability of nonconservative products. *Journal de mathématiques pures et appliquées*, 74(6):483–548, 1995.
- [45] R Donat, I Higuera, and A Martinez-Gavara. On stability issues for imex schemes applied to 1d scalar hyperbolic equations with stiff reaction terms. *Mathematics of Computation*, 80(276):2097–2126, 2011.
- [46] Jim Douglas. On the numerical integration of $\frac{\partial^2 u}{\partial x^2} + \frac{\partial^2 u}{\partial y^2} = \frac{\partial u}{\partial t}$ by implicit methods. *Journal of the society for industrial and applied mathematics*, pages 42–65, 1955.
- [47] Jim Douglas and Donald W Peaceman. Numerical solution of two-dimensional heat-flow problems. *AIChE Journal*, 1(4):505–512, 1955.
- [48] Jim Douglas and Henry H Rachford. On the numerical solution of heat conduction problems in two and three space variables. *Transactions of the American mathematical Society*, pages 421–439, 1956.
- [49] Jim Douglas, Jr. Finite difference methods for two-phase incompressible flow in porous media. *SIAM Journal on Numerical Analysis*, 20(4):681–696, 1983.
- [50] Jim Douglas, Jr and Thomas F Russell. Numerical methods for convection-dominated diffusion problems based on combining the method of characteristics with finite element or finite difference procedures. *SIAM Journal on Numerical Analysis*, 19(5):871–885, 1982.

- [51] Jim Douglas Jr, Frederico Furtado, and Felipe Pereira. On the numerical simulation of waterflooding of heterogeneous petroleum reservoirs. *Computational Geosciences*, 1(2):155–190, 1997.
- [52] Jim Douglas Jr and Chieh-Sen Huang. A locally conservative eulerian-lagrangian finite difference method for a parabolic equation. *BIT Numerical Mathematics*, 41(3):480–489, 2001.
- [53] Jim Douglas Jr, Chieh-Sen Huang, and Anna M Spagnuolo. The approximation of nuclear contaminant transport in porous media. *J. Comput. Appl. Math*, 21:409–428, 2002.
- [54] Jim Douglas Jr and Seongjai Kim. Improved accuracy for locally one-dimensional methods for parabolic equations. *Mathematical Models and Methods in Applied Sciences*, 11(09):1563–1579, 2001.
- [55] Jim Douglas Jr, Donald W Peaceman, HH Rachford Jr, et al. A method for calculating multi-dimensional immiscible displacement. 1959.
- [56] Jim Douglas Jr, Felipe Pereira, and Li-Ming Yeh. A parallelizable method for two-phase flows in naturally-fractured reservoirs. *Computational Geosciences*, 1(3-4):333–368, 1997.
- [57] Jim Douglas Jr, Felipe Pereira, and Li-Ming Yeh. A locally conservative eulerian-lagrangian numerical method and its application to nonlinear transport in porous media. *Computational Geosciences*, 4(1):1–40, 2000.
- [58] Michael Dumbser, Cedric Enaux, and Eleuterio F Toro. Finite volume schemes of very high order of accuracy for stiff hyperbolic balance laws. *Journal of Computational Physics*, 227(8):3971–4001, 2008.
- [59] E. G. D'yakonov. On an iterative method for the solution of a system of finite-difference equations. *Journal of Computational Physics*, 143(8):522–525, 1961.
- [60] Izrail Moiseevich Gel'fand. Some problems in the theory of quasi-linear equations. *Uspekhi Matematicheskikh Nauk*, 14(2):87–158, 1959.
- [61] Margot G Gerritsen and Louis J Durlofsky. Modeling fluid flow in oil reservoirs. *Annu. Rev. Fluid Mech.*, 37:211–238, 2005.
- [62] T Geveci. The significance of the stability of difference schemes in different l^p -spaces. *SIAM Review*, 24(4):413–426, 1982.
- [63] James Glimm, John W Grove, Xiao Lin Li, Keh-ming Shyue, Yanni Zeng, and Qiang Zhang. Three-dimensional front tracking. *SIAM Journal on Scientific Computing*, 19(3):703–727, 1998.
- [64] James Glimm, John W Grove, XL Li, and De Chun Tan. Robust computational algorithms for dynamic interface tracking in three dimensions. *SIAM Journal on Scientific Computing*, 21(6):2240–2256, 2000.
- [65] James Glimm, Guillermo Marshall, and Bradley Plohr. A generalized riemann problem for quasi-one-dimensional gas flows. *Advances in Applied Mathematics*, 5(1):1–30, 1984.

- [66] Sergei Konstantinovich Godunov. A difference method for numerical calculation of discontinuous solutions of the equations of hydrodynamics. *Matematicheskii Sbornik*, 89(3):271–306, 1959.
- [67] Laurent Gosse. Computing qualitatively correct approximations of balance laws. *SIMAI Springer Series*, 2, 2013.
- [68] Laurent Gosse and Giuseppe Toscani. Asymptotic-preserving & well-balanced schemes for radiative transfer and the rosseland approximation. *Numerische Mathematik*, 98(2):223–250, 2004.
- [69] Sigal Gottlieb, Chi-Wang Shu, and Eitan Tadmor. Strong stability-preserving high-order time discretization methods. *SIAM review*, 43(1):89–112, 2001.
- [70] JM Greenberg, AY Leroux, R Baraille, and A Noussair. Analysis and approximation of conservation laws with source terms. *SIAM Journal on Numerical Analysis*, 34(5):1980–2007, 1997.
- [71] Joshua M Greenberg and Alain-Yves Leroux. A well-balanced scheme for the numerical processing of source terms in hyperbolic equations. *SIAM Journal on Numerical Analysis*, 33(1):1–16, 1996.
- [72] DF Griffiths and JM Sanz-Serna. On the scope of the method of modified equations. *SIAM Journal on Scientific and Statistical Computing*, 7(3):994–1008, 1986.
- [73] Jean-Luc Guermond. A finite element technique for solving first-order pdes in lp. *SIAM Journal on Numerical Analysis*, 42(2):714–737, 2004.
- [74] Youngsoo Ha and Yong Jung Kim. Explicit solutions to a convection-reaction equation and defects of numerical schemes. *Journal of Computational Physics*, 220(1):511–531, 2006.
- [75] Ami Harten. High resolution schemes for hyperbolic conservation laws. *Journal of computational physics*, 49(3):357–393, 1983.
- [76] Amiram Harten, James M Hyman, Peter D Lax, and Barbara Keyfitz. On finite-difference approximations and entropy conditions for shocks. *Communications on pure and applied mathematics*, 29(3):297–322, 1976.
- [77] Helge Holden, Kenneth H Karlsen, Knut-Andreas Lie, and Nils Henrik Risebro. *Splitting methods for partial differential equations with rough solutions*. 2010.
- [78] Helge Holden, Kenneth H Karlsen, Darko Mitrovic, and Evgueni Yu Panov. Strong compactness of approximate solutions to degenerate elliptic-hyperbolic equations with discontinuous flux function. *Acta Mathematica Scientia*, 29(6):1573–1612, 2009.
- [79] Helge Holden and Nils Henrik Risebro. A fractional steps method for scalar conservation laws without the cfl condition. *Preprint series: Pure mathematics <http://urn.nb.no/URN:NBN:no-8076>*, 1991.

- [80] Chieh-Sen Huang, Todd Arbogast, and Jianxian Qiu. An eulerian–lagrangian weno finite volume scheme for advection problems. *Journal of Computational Physics*, 231(11):4028–4052, 2012.
- [81] Chieh-Sen Huang and Anna M Spagnuolo. Implementation of a locally conservative eulerian-lagrangian method applied to nuclear contaminant transport. In *Numerical Treatment of Multiphase Flows in Porous Media*, pages 179–189. Springer, 2000.
- [82] Eli Isaacson, Dan Marchesin, Bradley Plohr, and J Blake Temple. Multiphase flow models with singular riemann problems. *Mat. Apl. Comput*, 11(2):147–166, 1992.
- [83] Eli L Isaacson, Dan Marchesin, and Bradley J Plohr. Transitional waves for conservation laws. *SIAM journal on mathematical analysis*, 21(4):837–866, 1990.
- [84] Matthew D Jackson and Martin J Blunt. Elliptic regions and stable solutions for three-phase flow in porous media. *Transport in porous media*, 48(3):249–269, 2002.
- [85] Bo-Nan Jiang. Non-oscillatory and non-diffusive solution of convection problems by the iteratively reweighted least-squares finite element method. *Journal of Computational Physics*, 105(1):108–121, 1993.
- [86] Guang-Shan Jiang and Eitan Tadmor. Nonoscillatory central schemes for multidimensional hyperbolic conservation laws. *SIAM Journal on Scientific Computing*, 19(6):1892–1917, 1998.
- [87] Shi Jin. Runge-kutta methods for hyperbolic conservation laws with stiff relaxation terms. *Journal of Computational Physics*, 122(1):51–67, 1995.
- [88] Shi Jin and Zhouping Xin. The relaxation schemes for systems of conservation laws in arbitrary space dimensions. *Communications on Pure and Applied Mathematics*, 48(3):235–276, 1995.
- [89] Kenneth H Karlsen, U Koley, and NH Risebro. An error estimate for the finite difference approximation to degenerate convection–diffusion equations. *Numerische Mathematik*, 121(2):367–395, 2012.
- [90] Kenneth H Karlsen, K-A Lie, Jostein Roald Natvig, Hans F Nordhaug, and Helge K Dahle. Operator splitting methods for systems of convection–diffusion equations: nonlinear error mechanisms and correction strategies. *Journal of Computational Physics*, 173(2):636–663, 2001.
- [91] Kenneth H Karlsen, N Risebro, and E Storrøsten. l^1 error estimates for difference approximations of degenerate convection-diffusion equations. *Mathematics of Computation*, 83(290):2717–2762, 2014.
- [92] Kenneth H Karlsen and Nils Henrik Risebro. Corrected operator splitting for nonlinear parabolic equations. *SIAM Journal on Numerical Analysis*, 37(3):980–1003, 2000.
- [93] Kenneth H Karlsen, Nils Henrik Risebro, and John D Towers. L1 stability for entropy solutions of nonlinear degenerate parabolic convection-diffusion equations with discontinuous coefficients. *Preprint series. Pure mathematics <http://urn.nb.no/URN:NBN:no-8076>*, 2003.

- [94] Kenneth H Karlsen and John D Towers. Convergence of the lax-friedrichs scheme and stability for conservation laws with a discontinuous space-time dependent flux. *Chinese Annals of Mathematics*, 25(03):287–318, 2004.
- [95] Tosio Kato. On the trotter-lie product formula. *Proceedings of the Japan Academy*, 50(9):694–698, 1974.
- [96] SN Kružkov. First order quasilinear equations in several independent variables. *Sbornik: Mathematics*, 10(2):217–243, 1970.
- [97] Alexander Kurganov, Sebastian Noelle, and Guergana Petrova. Semidiscrete central-upwind schemes for hyperbolic conservation laws and hamilton–jacobi equations. *SIAM Journal on Scientific Computing*, 23(3):707–740, 2001.
- [98] Alexander Kurganov, Guergana Petrova, and Bojan Popov. Adaptive semidiscrete central-upwind schemes for nonconvex hyperbolic conservation laws. *SIAM Journal on Scientific Computing*, 29(6):2381–2401, 2007.
- [99] Alexander Kurganov and Eitan Tadmor. New high-resolution central schemes for nonlinear conservation laws and convection–diffusion equations. *Journal of Computational Physics*, 160(1):241–282, 2000.
- [100] Marc Küther and Mario Ohlberger. Adaptive second order central schemes on unstructured staggered grids. In *Hyperbolic problems: theory, numerics, applications*, pages 675–684. Springer, 2003.
- [101] NN Kuznetsov. The accuracy of certain approximate methods for the computation of weak solutions of a first order quasilinear equation. *Zhurnal Vychislitel’noi Matematiki i Matematicheskoi Fiziki*, 16(6):1489–1502, 1976.
- [102] Wanderson Lambert and Dan Marchesin. Asymptotic rarefaction waves for balance laws with stiff sources. *Acta Mathematica Scientia*, 29(6):1613–1628, 2009.
- [103] Wanderson Lambert, Dan Marchesin, and Johannes Bruining. The riemann solution for the injection of steam and nitrogen in a porous medium. *Transport in porous media*, 81(3):505–526, 2010.
- [104] JO Langseth, A Tveito, and R Winther. On the convergence of operator splitting applied to conservation laws with source terms. *SIAM journal on numerical analysis*, 33(3):843–863, 1996.
- [105] Peter D Lax. *Hyperbolic systems of conservation laws and the mathematical theory of shock waves*, volume 11. SIAM, 1973.
- [106] Ph Le Floch and Pierre-Arnaud Raviart. An asymptotic expansion for the solution of the generalized riemann problem. part i: general theory. In *Annales de l’institut Henri Poincaré (C) Analyse non linéaire*, volume 5, pages 179–207. Gauthier-Villars, 1988.
- [107] Philippe G LeFloch. *Hyperbolic Systems of Conservation Laws: The theory of classical and nonclassical shock waves*. Springer Science & Business Media, 2002.

- [108] Randall J LeVeque. *Numerical methods for conservation laws*, volume 132. Springer, 1992.
- [109] Randall J LeVeque. *Finite volume methods for hyperbolic problems*, volume 31. Cambridge university press, 2002.
- [110] Randall J LeVeque. *Finite difference methods for ordinary and partial differential equations: steady-state and time-dependent problems*, volume 98. Siam, 2007.
- [111] Randall J LeVeque and Keh-Ming Shyue. One-dimensional front tracking based on high resolution wave propagation methods. *SIAM Journal on Scientific Computing*, 16(2):348–377, 1995.
- [112] Randall J LeVeque and Helen C Yee. A study of numerical methods for hyperbolic conservation laws with stiff source terms. *Journal of computational physics*, 86(1):187–210, 1990.
- [113] K-A Lie and Ruben Juanes. A front-tracking method for the simulation of three-phase flow in porous media. *Computational Geosciences*, 9(1):29–59, 2005.
- [114] Knut-Andreas Lie, VIDAR Haugse, and Kenneth H Karlsen. Dimensional splitting with front tracking and adaptive grid refinement. *Numerical Methods for Partial Differential Equations*, 14(5):627–648, 1998.
- [115] Salvatore Fabio Liotta, Vittorio Romano, and Giovanni Russo. Central schemes for balance laws of relaxation type. *SIAM Journal on Numerical Analysis*, 38(4):1337–1356, 2000.
- [116] Tai Ping Liu. The riemann problem for general 2×2 conservation laws. *Transactions of the American Mathematical Society*, 199:89–112, 1974.
- [117] Tai-Ping Liu. Linear and nonlinear large-time behavior of solutions of general systems of hyperbolic conservation laws. *Communications on Pure and Applied Mathematics*, 30(6):767–796, 1977.
- [118] Tai-Ping Liu. Quasilinear hyperbolic systems. *Communications in Mathematical Physics*, 68(2):141–172, 1979.
- [119] RB Lowrie and JE Morel. Methods for hyperbolic systems with stiff relaxation. *International Journal for Numerical Methods in Fluids*, 40(3-4):413–423, 2002.
- [120] Pierre-Henri Maire. A high-order cell-centered lagrangian scheme for two-dimensional compressible fluid flows on unstructured meshes. *Journal of Computational Physics*, 228(7):2391–2425, 2009.
- [121] Sebastián Mancuso, Felipe Pereira, and Grazione de Souza. Um novo método euleriano-lagrangiano para aproximação de leis de conservação doi: 10.5540/tema. 2007.08. 02.0277. *Trends in Applied and Computational Mathematics*, 8(2):277–286, 2007.
- [122] Guriï Ivanovich Marchuk and Jiri Ruzicka. *Methods of numerical mathematics*, volume 2. Springer-Verlag New York, 1975.

- [123] María Luz Muñoz-Ruiz and Carlos Parés. Godunov method for nonconservative hyperbolic systems. *ESAIM: Mathematical Modelling and Numerical Analysis*, 41(01):169–185, 2007.
- [124] Haim Nessyahu and Eitan Tadmor. Non-oscillatory central differencing for hyperbolic conservation laws. *Journal of computational physics*, 87(2):408–463, 1990.
- [125] Haim Nessyahu and Eitan Tadmor. The convergence rate of approximate solutions for nonlinear scalar conservation laws. *SIAM journal on numerical analysis*, 29(6):1505–1519, 1992.
- [126] Haim Nessyahu, Eitan Tadmor, and Tamir Tassa. The convergence rate of godunov type schemes. *SIAM journal on numerical analysis*, 31(1):1–16, 1994.
- [127] Olga Arsen'evna Oleinik. Discontinuous solutions of non-linear differential equations. *Uspekhi Matematicheskikh Nauk*, 12(3):3–73, 1957.
- [128] Olga Arsen'evna Oleinik. On the uniqueness of the generalized solution of the cauchy problem for a non-linear system of equations occurring in mechanics. *Uspekhi Matematicheskikh Nauk*, 12(6):169–176, 1957.
- [129] MV Papalexandris, Anthony Leonard, and Paul E Dimotakis. Unsplit algorithms for multidimensional systems of hyperbolic conservation laws with source terms. *Computers & Mathematics with Applications*, 44(1):25–49, 2002.
- [130] Lorenzo Pareschi. Central differencing based numerical schemes for hyperbolic conservation laws with relaxation terms. *SIAM Journal on Numerical Analysis*, 39(4):1395–1417, 2001.
- [131] Lorenzo Pareschi and Giovanni Russo. Implicit-explicit runge-kutta schemes and applications to hyperbolic systems with relaxation. *Journal of Scientific computing*, 25(1-2):129–155, 2005.
- [132] Donald W Peaceman and Henry H Rachford, Jr. The numerical solution of parabolic and elliptic differential equations. *Journal of the Society for Industrial & Applied Mathematics*, 3(1):28–41, 1955.
- [133] Bojan Popov and Ognian Trifonov. One-sided stability and convergence of the nessyahu-tadmor scheme. *Numerische Mathematik*, 104(4):539–559, 2006.
- [134] Thomas F Russell and Michael A Celia. An overview of research on eulerian-lagrangian localized adjoint methods (ellam). *Advances in Water Resources*, 25(8):1215–1231, 2002.
- [135] Florin Sabac. The optimal convergence rate of monotone finite difference methods for hyperbolic conservation laws. *SIAM journal on numerical analysis*, 34(6):2306–2318, 1997.
- [136] Aleksandr A Samarskii and Evgenii S Nikolaev. *Numerical methods for grid equations*. Springer, 1989.

- [137] Mancuso Sebastián. Aproximação numérica de leis de conservação leis por esquemas eulerianos-lagrangianos localmente conservativos. Master's thesis, Rio de Janeiro, 2004.
- [138] Joel Smoller. Shock waves and reaction-diffusion equations. In *Research supported by the US Air Force and National Science Foundation. New York and Heidelberg, Springer-Verlag (Grundlehren der Mathematischen Wissenschaften. Volume 258), 1983, 600 p.*, volume 258, 1983.
- [139] Joel Smoller. *Shock waves and reaction—diffusion equations*, volume 258. Springer Science & Business Media, 1994.
- [140] Gary A Sod. A survey of several finite difference methods for systems of nonlinear hyperbolic conservation laws. *Journal of computational physics*, 27(1):1–31, 1978.
- [141] Gilbert Strang. On the construction and comparison of difference schemes. *SIAM Journal on Numerical Analysis*, 5(3):506–517, 1968.
- [142] John C Strikwerda. *Finite difference schemes and partial differential equations*. Siam, 2004.
- [143] Eitan Tadmor and Tao Tang. Pointwise error estimates for relaxation approximations to conservation laws. *SIAM Journal on Mathematical Analysis*, 32(4):870–886, 2000.
- [144] Tao Tang and Zhen-Huan Teng. Error bounds for fractional step methods for conservation laws with source terms. *SIAM journal on numerical analysis*, 32(1):110–127, 1995.
- [145] Tao Tang and Zhen Huan Teng. The sharpness of kuznetsov's $o(\sqrt{\Delta x})$ l^1 -error estimate for monotone difference schemes. *mathematics of computation*, 64(210):581–589, 1995.
- [146] Zhen-Huan Teng. On the accuracy of fractional step methods for conservation laws in two dimensions. *SIAM journal on numerical analysis*, 31(1):43–63, 1994.
- [147] James William Thomas. *Numerical partial differential equations: conservation laws and elliptic equations*, volume 3. Springer Berlin, 1999.
- [148] EF Toro and VA Titarev. Solution of the generalized riemann problem for advection–reaction equations. *Proceedings of the Royal Society of London. Series A: Mathematical, Physical and Engineering Sciences*, 458(2018):271–281, 2002.
- [149] Hale F Trotter. On the product of semi-groups of operators. *Proceedings of the American Mathematical Society*, 10(4):545–551, 1959.
- [150] Grétar Tryggvason, Bernard Bunner, Asghar Esmaeeli, Damir Juric, N Al-Rawahi, W Tauber, J Han, S Nas, and Y-J Jan. A front-tracking method for the computations of multiphase flow. *Journal of Computational Physics*, 169(2):708–759, 2001.
- [151] Aslak Tveito and Ragnar Winther. The solution of nonstrictly hyperbolic conservation laws may be hard to compute. *SIAM Journal on Scientific Computing*, 16(2):320–329, 1995.
- [152] Bram Van Leer. Towards the ultimate conservative difference scheme. v. a second-order sequel to godunov's method. *Journal of computational Physics*, 32(1):101–136, 1979.

- [153] Aleksandr Isaakovich Vol’pert and SI Hudjaev. Cauchy’s problem for degenerate second order quasilinear parabolic equations. *Sbornik: Mathematics*, 7(3):365–387, 1969.
- [154] H Wang, D Liang, RE Ewing, SL Lyons, and G Qin. An ellam approximation for highly compressible multicomponent flows in porous media. *Computational Geosciences*, 6(3-4):227–251, 2002.
- [155] RF Warming and BJ Hyett. The modified equation approach to the stability and accuracy analysis of finite-difference methods. *Journal of computational physics*, 14(2):159–179, 1974.
- [156] Monika Wierse. A new theoretically motivated higher order upwind scheme on unstructured grids of simplices. *Advances in Computational Mathematics*, 7(3):303–335, 1997.
- [157] Nicolay Nicolayevich Yanenko. *Méthode a Pas Fractionnaires*. Librairie Armand Colin, Paris, 1968.
- [158] Nicolay Nicolayevich Yanenko. *The method of fractional steps*. Springer, 1971.
- [159] Son-Young Yi and Jim Douglas Jr. An experimental study of several multidimensional, locally conservative, eulerian-lagrangian finite element methods for a semilinear parabolic equation. *International Journal of Numerical Analysis and Modeling Series B*, 4(3):299–314, 2013.
- [160] Xiaolin Zhong. Additive semi-implicit runge–kutta methods for computing high-speed nonequilibrium reactive flows. *Journal of Computational Physics*, 128(1):19–31, 1996.

‘

Appendix A

Uniqueness of the Entropy Solution

In this section as an important information, we include the uniqueness proof makes by Joel Smoller in [139] in section B of the chapter sixteen that has the same title of this section. It then follows from theorem (3.2.1). We shall show that solution of

$$\frac{\partial u}{\partial t} + \frac{\partial H(u)}{\partial x} = 0, \quad u(x, 0) = \eta(x) \quad (\text{A.0.1})$$

which satisfy the entropy condition (3.2.6) are unique. It then follows from theorem (3.2.1) that the solution which we constructed via the finite-difference, in this case to Lagrangian-Eulerian scheme, is the unique solution of our problem. We call the solution which satisfies (3.2.6), the *the entropy solution*. The method of proof which we shall give is really a non linear version of the Holmgren method (see chapter 5 of [139]). Recall that for linear operators A , since $\eta_A \subset (\mathcal{R}_{A^*})^\perp$ (where η_A and \mathcal{R}_{A^*} are the null space and range of A and A^* respectively), in order to show that $\eta_A = 0$, it suffices to show that \mathcal{R}_{A^*} is everywhere dense. Thus if u and v are solutions of (A.0.1), in order to show $u = v$ almost everywhere in $t > 0$, it suffices to show

$$\iint_{t \geq 0} (u - v)\phi = 0 \quad (\text{A.0.2})$$

for every $\phi \in C_0^1$, we have both

$$\iint_{t \geq 0} (u\psi_t + f(u)\psi_x) + \int_{t=0} u_0 \psi = 0 \quad (\text{A.0.3})$$

and

$$\iint_{t \geq 0} (v\psi_t + f(v)\psi_x) + \int_{t=0} u_0 \psi = 0 \quad (\text{A.0.4})$$

If we subtract these two equations we get

$$\iint_{t \geq 0} ((u - v)\psi_t + [f(u) - f(v)]\psi_x) = 0 \quad (\text{A.0.5})$$

or

$$\iint_{t \geq 0} (u - v) \left[\psi_t + \frac{f(u) - f(v)}{u - v} \psi_x \right] = 0 \quad (\text{A.0.6})$$

next, if we define F by

$$F(x, t) = \frac{f(u) - f(v)}{u - v} \quad (\text{A.0.7})$$

then (A.0.6) can be written as

$$\iint_{t \geq 0} (u - v) [\psi_t + F\psi_x] = 0 \quad (\text{A.0.8})$$

Now if we could solve the linear (adjoint !) equation

$$\psi_t + F\psi_x = \phi, \quad (\text{A.0.9})$$

for arbitrary $\phi \in C_0^1(t > 0)$. then (A.0.8) would imply (A.0.2) and we could conclude that $u = v$, almost everywhere. There is however an obstruction to this approach; namely, F is not smooth (or even continuous) in general, and so it is not clear that (A.0.9) has a solution $\psi \in C_0^1$. The way around this difficulty is to approximate u_m, v_m and solve the corresponding linear equations.

$$\psi_t^m + F_m\psi_x^m = \phi, \quad (\text{A.0.10})$$

with smooth coefficients, for $\psi^m \in C_0^1$, where

$$F_m(x, t) = \frac{f(u_m) - f(v_m)}{u_m - v_m} \quad (\text{A.0.11})$$

Then

$$\begin{aligned} \iint_{t \geq 0} (u - v)\phi &= \iint_{t \geq 0} (u - v)\psi_t^m + \iint_{t \geq 0} (u - v)F_m\psi_x^m \\ &= - \iint_{t \geq 0} (f(u) - f(v))\psi_x^m + \iint_{t \geq 0} (u - v)F_m\psi_x^m \end{aligned} \quad (\text{A.0.12})$$

so that

$$\iint_{t \geq 0} (u - v)\phi = \iint_{t \geq 0} (u - v)(F_m - F)\psi_x^m. \quad (\text{A.0.13})$$

Then if $F_m \rightarrow F$, locally in L_1 , and if ψ_x^m is bounded, independently of m , we could pass to the limit on the right-hand side of this last equation and conclude that (A.0.2) holds. This procedure will be carried out below, whereby the entropy condition (3.2.6) will be used to obtain the uniform bound on ψ_x^m .

Theorem A.0.1. Let $f \in C^2$, $f'' > 0$, and let u and v be two solutions satisfying the entropy condition (3.2.6). Then $u = v$ almost everywhere in $t > 0$.

Proof. For every positive integer m , let

$$u_m = v_m \text{ and } v_m = v * w_m \quad (\text{A.0.14})$$

where w_m is the usual averaging kernel of radius $1/m$, and $*$ denotes convolution product (see chapter 5 of ([139])). We define

$$\begin{aligned} F_m(x, t) &= \int_0^1 f'(\theta u_m + (1 - \theta)v_m) d\theta \\ &= \frac{1}{u_m - v_m} \int_{u_m}^{v_m} f'(s) ds = \frac{f(u_m) - f(v_m)}{u_m - v_m} \end{aligned} \quad (\text{A.0.15})$$

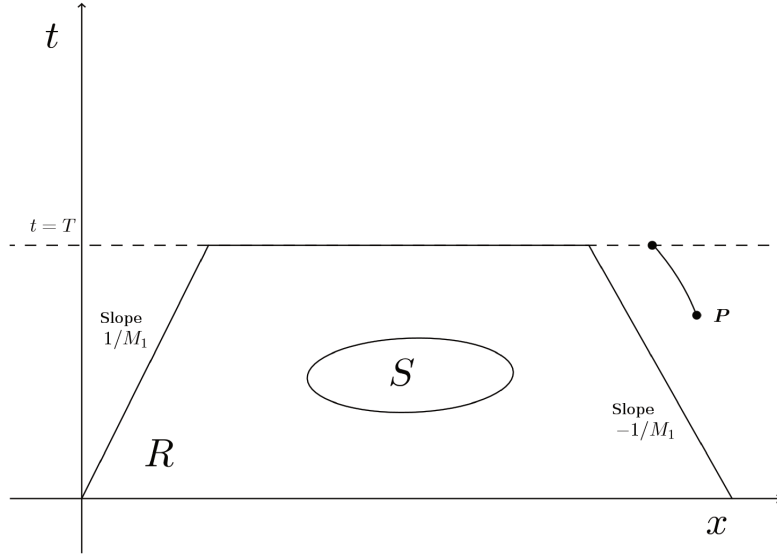


Figure A.1:

and solve (A.0.10) for $\psi^m(x, t)$, subject to the boundary condition $\psi^m(x, T) = 0$, where $T > 0$ is chosen so large that $\phi = 0$ if $t \geq T$. It is not too hard to verify that the solution of this problem is given by

$$\psi^m(x, t) = \int_T^t \phi(x_m(s; x, t), s) ds \tag{A.0.16}$$

where $x_m(s; x, t)$ is the unique solution of the characteristic ordinary differential equation

$$\frac{dx_m}{ds} = F_m(x, s), \text{ with } x_m(t) = x \tag{A.0.17}$$

Now

$$|u_m(x, t)| \leq \int_{\mathbb{R}} |u(x - y)| w_m(y) dy \leq \int_{\mathbb{R}} w_m(y) dy$$

and similarly $|v_m(x, t)| \leq M$. Thus since $f \in C^2$, we see that there is a constant $M_1 > 0$, independent of m , such that

$$|F_m(x, t)| < M_1. \tag{A.0.18}$$

This estimate enables us to show that $\psi^m \in C_0^1(t \geq 0)$. First, it is clear that ψ^m is in C^1 ; to show that $\psi^m \in C_0^1(t \geq 0)$, we proceed as follows. Let $S \subset \{t > 0\}$ denote the support of ϕ ; S being compact. Now consider Figure A.1. R denotes the support a region in $t \geq 0$ which is bounded by the two lines of slope $\pm 1/M_1$, and the lines $t = 0, t = T$, and R contains S in its interior. The claim is that $\text{spt } \psi^m \in R$, for every m . To see this, note that if $t \geq T$, $\phi = 0$ so that $\psi^m = 0$, in view of (A.0.17). furthermore, (A.0.18) shows that if $t \geq T$ must meet the line $t = T$ at point not in R . It follows that all alongs this trajectory, $\phi = 0$. Thus ψ^m satisfies the homogeneous equation $\psi_t^m + F_m \psi_x^m = 0$, so ψ^m is constant along trajectories of (A.0.17). Since the trajectory meets $t = T$. ψ^m is zero at $t = T$, and hence ψ^m is zero on the entire trajectory, and in particular at P . This shows that $\psi^m \in C_0^1$, moreover, that the ψ^m have support lying in the set R , independently of m . It follows, as above, that

$$\iint_{t \geq 0} (u - v) \phi = \iint_{t \geq 0} (u - v) (F_m - F) \psi_x^m. \tag{A.0.19}$$

We shall next show that $F_m \rightarrow F$, locally in L_1 . Let $c = \max\{f''(u) : |u| \geq M\}$. Then

$$\begin{aligned} F(x, t) - F_m(x, t) &= \int_0^1 [f'(\theta u + (1 - \theta)v) - f'(\theta u_m + (1 - \theta)v_m)] d\theta \\ &= \int_0^1 f''(\xi) [\theta(u - u_m) + (1 - \theta)(v - v_m)] d\theta, \end{aligned} \quad (\text{A.0.20})$$

where ξ is between $\theta u + (1 - \theta)v$ and $\theta u_m + (1 - \theta)v_m$, so that $|\xi| \leq M$. Thus

$$\begin{aligned} |F(x, t) - F_m(x, t)| &\leq c \int_0^1 \{\theta|u - u_m| + (1 - \theta)|v - v_m|\} d\theta \\ &= c\{|u - u_m| + |v - v_m|\} \end{aligned} \quad (\text{A.0.21})$$

accordingly, if K is any compact set in $t \geq 0$,

$$\iint_R |F(x, t) - F_m(x, t)| \leq c \iint_K (|u_m - u| + |v_m - v|)$$

and this later integral tends to zero as $m \rightarrow \infty$. It remains to show that we can bound ψ_x^m . It is here where we shall use the entropy condition (3.2.6). Thus, let $\alpha > 0$ be arbitrary. Then for each fixed $t \geq \alpha$, the function $u(x, t) - Ex/\alpha$ is non-increasing in x . This follows from the entropy condition (3.2.6), since if $a > 0$,

$$u(x + a, t) - \frac{E(x + a)}{\alpha} - u(x, t) + \frac{Ex}{\alpha} = Ea \left(\frac{1}{t} - \frac{1}{\alpha} \right) < 0.$$

From this we find that

$$w_n * \left(u - \frac{Ex}{\alpha} \right) = u_m - \frac{E(w_m * x)}{\alpha}$$

is also nonincreasing in x , as one can easily check. Since this latter function is smooth and

$$\frac{\partial}{\partial x} \left[w_m * \left(u - \frac{Ex}{\alpha} \right) \right] = \frac{\partial u_m}{\partial x} - \frac{E}{\alpha},$$

we see that the following are true:

$$\frac{\partial u_m}{\partial x} \leq \frac{E}{\alpha} \quad \text{and} \quad \frac{\partial v_m}{\partial x} \leq \frac{E}{\alpha}. \quad (\text{A.0.22})$$

Next, from (A.0.15),

$$\frac{\partial F_m}{\partial x} = \int_0^1 f''(\theta u_m + (1 - \theta)v_m) \left[\theta \frac{\partial u_m}{\partial x} + (1 - \theta) \frac{\partial v_m}{\partial x} \right] d\theta,$$

and since $f'' > 0$, we get from (A.0.22)

$$\begin{aligned} \frac{\partial F_m}{\partial x} &\leq \int_0^1 f''(\theta u_m + (1 - \theta)v_m) \frac{E}{\alpha} (\theta + 1 - \theta) d\theta \\ &= \frac{E}{\alpha} \int_0^1 f''(\theta u_m + (1 - \theta)v_m) d\theta. \end{aligned}$$

therefore,

$$\frac{\partial F_m}{\partial x} \leq K_\alpha, \quad (\text{A.0.23})$$

where

$$K_\alpha = \frac{E}{\alpha} \max_{|u| \leq M} f''(u),$$

so that K_α is independent of m .

Now let

$$a_m(s) = \frac{\partial x_m}{\partial \bar{x}}(s; \bar{x}, \bar{t}) = 1. \quad (\text{A.0.24})$$

Thus,

$$\begin{aligned} \frac{\partial a_m}{\partial s} &= \frac{\partial}{\partial s} \frac{\partial x_m}{\partial \bar{x}} = \frac{\partial}{\partial \bar{x}} \frac{\partial x_m}{\partial s} = \frac{\partial}{\partial \bar{x}} F_m(x_m, s) \\ &= \frac{\partial}{\partial \bar{x}} F_m(x_m(s; \bar{x}, \bar{t}), s) = \frac{\partial F_m}{\partial x} \frac{\partial x_m}{\partial \bar{x}} = \frac{\partial F_m}{\partial x} a_m. \end{aligned}$$

Then from (A.0.24), we obtain the formula

$$a_m(s) = \exp \left(\int_{\bar{t}}^s \frac{\partial F_m}{\partial x}(x_m(\tau), \tau) d\tau \right).$$

since $\alpha \leq \bar{t} \leq s \leq T$, we have from (A.0.23),

$$a_m(s) = a_m(s) \leq \exp K_\alpha (T - \alpha)$$

But from (A.0.16)

$$\frac{\partial \psi^m}{\partial x} = \int_T^{\bar{t}} \frac{\partial \phi}{\partial x_m} \frac{\partial x_m}{\partial x} ds = \int_T^{\bar{t}} \frac{\partial \phi}{\partial x} a_m ds$$

Thus

$$\left| \frac{\partial \psi^m}{\partial x} \right| \leq \bar{K} \alpha \quad \text{if } t \geq \alpha \quad (\text{A.0.25})$$

where \bar{K}_α is independent of m .

We now must investigate the behavior of ϕ^m in the region $0 \leq t \leq \alpha$. To this end, we define

$$V_t(\psi^m) = \int_{-\infty}^{\infty} \left| \frac{\partial \psi^m}{\partial x} \right| dx,$$

the total variation of ψ^m as a function of x , for each fixed $t > 0$, From (A.0.25), and the fact that the ψ^m are in C_0^1 with their supports being contained in a region independent of m , we have

$$V_t(\psi^m) \leq C_\alpha \quad \text{if } t \geq \alpha \quad (\text{A.0.26})$$

where C_α does not depend on m .

The last estimate we need is

$$\exists N \in \mathbb{Z}_+ \ni: n > N \implies V_t(\psi^m) \leq C_{1/n}, \quad \forall t, \quad 0 < t \leq \frac{1}{n} < \frac{1}{N}. \quad (\text{A.0.27})$$

To prove this, note that since ϕ has compact support in $t > 0$, there is an $N \in \mathbb{Z}_+$ such that $\phi(x, t) = 0$ if $t < 1/N$. Thus from (A.0.10),

$$\frac{\partial \psi^m}{\partial t} + F_m \frac{\partial \psi^m}{\partial x} = 0, \quad \text{if } t < \frac{1}{N} \tag{A.0.28}$$

Now let $n > N$, and let $\sigma_t : \mathbb{R} \rightarrow \mathbb{R}$ be a bijection defined for $t < 1/n$ by the solution of the characteristic equation, (A.0.17); i.e., $\sigma_t(x) = x_m(1/n; x, t)$; see Figure A.2.

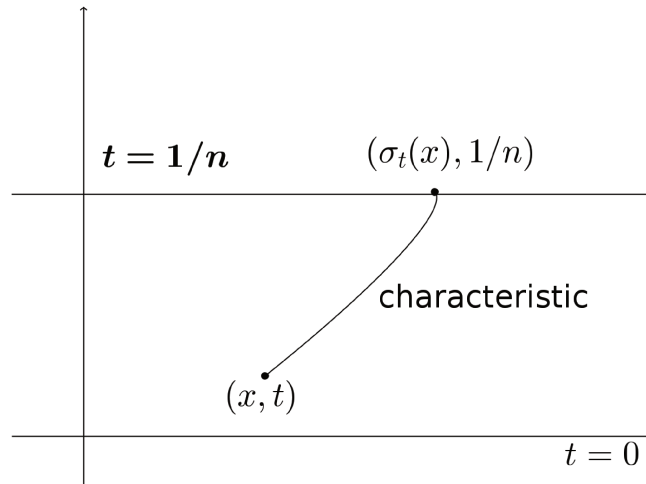


Figure A.2:

Now let t be any number, $0 < t < 1/n < 1/N$. Then for any finite sequence $x_1 < x_2 < \dots < x_p$, we have

$$\sum_{k=1}^{p-1} |\psi^m(x_{k+1}, t) - \psi^m(x_k, t)| = \sum_{k=1}^{p-1} \left| \psi^m \left(\sigma_t(x_{k+1}), \frac{1}{n} \right) - \psi^m \left(\sigma_t(x_k), \frac{1}{n} \right) \right|.$$

This holds since ψ^m is constant along characteristic, in view of (A.0.28). Thus using (A.0.26),

$$\sum_{k=1}^{p-1} |\psi^m(x_{k+1}, t) - \psi^m(x_k, t)| \leq C_{1/n},$$

and this proves (A.0.27).

We can now complete the proof of the theorem. Let $\epsilon > 0$ be arbitrary. With N defined as in (A.0.27), choose $\alpha > 0$ so small that

$$\alpha < \frac{1}{n} \leq \frac{1}{N} \quad \text{and} \quad 4 M M_1 C_1 \alpha < \frac{\epsilon}{2}. \tag{A.0.29}$$

For this α , choose M so large that

$$\iint_{t \geq \alpha} |u - v| |F_m - F| |\psi_x^m| < \frac{\epsilon}{2}, \quad \text{if } m \geq M. \tag{A.0.30}$$

This can be done since $|u - v| \leq 2M$, $F_m \rightarrow F$ locally in L_1 , $\psi^m \in C_0^1(t \geq 0)$ and (A.0.25) holds. Then from (A.0.19)

$$\left| \iint_{t \geq \alpha} (u - v) \phi \right| \leq \iint_{t \geq \alpha} |u - v| |F_m - F| |\psi_x^m| + \iint_{t < \alpha} |u - v| |F_m - F| |\psi_x^m|. \tag{A.0.31}$$

Now since $\alpha < 1/n \leq 1/N$,

$$\begin{aligned}
 \iint_{t < \alpha} |u - v| |F_m - F| |\psi_x^m| &\leq 2M 2M_1 \iint_{t < \alpha} |\psi_x^m| = 4M M_1 \int_0^\infty \int_{-\infty}^\infty |\psi_x^m| \\
 &= 4M M_1 \int_0^\infty \int_{-\infty}^\infty V_t(\psi_x^m) dt \\
 &= 4M M_1 C_{1/n} \alpha \quad (\text{A.0.27})
 \end{aligned}$$

so that

$$\iint_{t < \alpha} |u - v| |F_m - F| |\psi_x^m| < \frac{\epsilon}{2}. \quad (\text{A.0.32})$$

Thus using (A.0.30) and (A.0.32) in (A.0.31), we get

$$\left| \iint_{t \geq 0} (u - v) \phi \right| < \epsilon$$

and from arbitrariness of ϵ ,

$$\int_{t \geq 0} (u - v) \phi = 0$$

for all $\phi \in C_0^1(t > 0)$. Thus $u = v$ almost everywhere in $t > 0$. This completes the uniqueness proof. \square

Appendix B

Licença

Copyright (c) 2015 de John Alexander Perez Sepulveda.

Exceto quando indicado o contrário, esta obra está licenciada sob a licença Creative Commons Atribuição-CompartilhaIgual 3.0 Não Adaptada. Para ver uma cópia desta licença, visite <http://creativecommons.org/licenses/by-sa/3.0/>.



A marca e o logotipo da UNICAMP são propriedade da Universidade Estadual de Campinas. Maiores informações sobre encontram-se disponíveis em <http://www.unicamp.br/unicamp/a-unicamp/logotipo/normas%20oficiais-para-uso-do-logotipo>.

B.1 Sobre a licença dessa obra

A licença Creative Commons Atribuição-CompartilhaIgual 3.0 Não Adaptada utilizada nessa obra diz que:

1. Você tem a liberdade de:

- Compartilhar — copiar, distribuir e transmitir a obra;
- Remixar — criar obras derivadas;
- fazer uso comercial da obra.

2. Sob as seguintes condições:

- Atribuição — Você deve creditar a obra da forma especificada pelo autor ou licenciante (mas não de maneira que sugira que estes concedem qualquer aval a você ou ao seu uso da obra).
- Compartilhamento pela mesma licença — Se você alterar, transformar ou criar em cima desta obra, você poderá distribuir a obra resultante apenas sob a mesma licença, ou sob uma licença similar à presente.